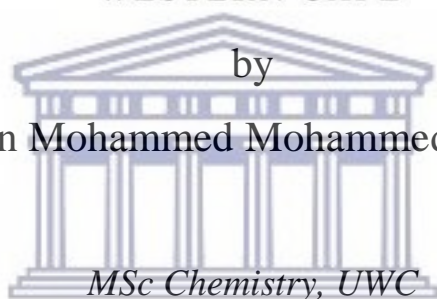

Green synthesis and characterization of gold nanoparticles from South African plants and their biological evaluations



UNIVERSITY of the
WESTERN CAPE

by

Abdulrahman Mohammed Mohammed Nagy Elbagory



MSc Chemistry, UWC

A thesis submitted in the fulfilment of the requirement of the Degree of **Philosophiae Doctor** in the Department of Biotechnology, Faculty of Natural Sciences, University of the Western Cape

Supervisor:
Professor Mervin Meyer

Co-Supervisor:
Professor Ahmed Hussein

August, 2019

ABSTRACT

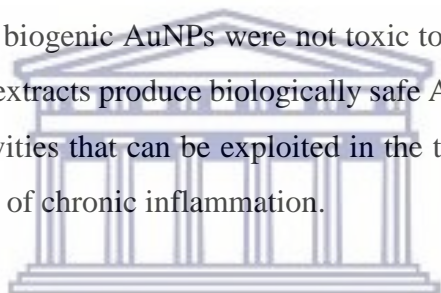
The field of nanotechnology continues to offer solutions for biotechnologists whose target is to improve the quality of life by finding new therapies to combat diseases. Gold nanoparticles (AuNPs) have been showing great potentials in many biomedical applications. The antibacterial activity of the AuNPs presents a therapeutic option for conditions caused by bacterial infections such as chronic wounds. Also, these versatile particles can offer solutions in the treatments of infectious diseases and can also be exploited as “smart” vehicles to carry drugs, such as antibiotics, for improved efficiency. Moreover, the anti-inflammatory activity of AuNPs makes them useful in the management of prolonged inflammation caused by bacterial infections.

The synthesis of AuNPs can be achieved by variety of physical and chemical methods that have been successfully applied in labs and industry. Nonetheless, the drawbacks of these “conventional” methods in terms of high cost, adverse health side effects and incompatibility with the ecosystem cannot be overlooked. Thus, new safer and more cost-effective protocols have been reported for the synthesis of AuNPs. Plants have provided alternate synthesis methods in which the reducing capabilities of the phytochemicals, found in the aqueous plant extracts, can be used to chemically synthesize AuNPs from gold precursors.

The biosynthesis and characterization of AuNPs from the phytochemicals of several South African plants is investigated in this study. The study also reports the optimization of the AuNPs biosynthesis by varying reaction conditions such as temperature and plant extracts’ concentrations. Furthermore, the study highlights the wound healing activity of the AuNPs synthesized from selected plants by investigating their antibacterial activity on bacterial strains known to cause chronic wounds. The ability of these AuNPs to carry ampicillin in order to enhance the antibacterial activity is also described herein. The cytotoxicity of the biosynthesized AuNPs was evaluated

on human normal fibroblasts cells (KMST-6). Additionally, the immunomodulatory effect of the biosynthesized AuNPs on the cytokines production from macrophages and Natural Killer (NK) cells was examined.

The study was successful to produce biocompatible and safe AuNPs synthesized from the tested aqueous plant extracts. The resulted AuNPs showed different physicochemical properties by varying the reaction conditions. The AuNPs exhibited antibacterial activity against several Gram-positive and Gram-negative bacteria. Also, ampicillin was successfully loaded on the biosynthesized AuNPs, which led to the formation of more antibacterial active conjugated AuNPs compared to the free AuNPs. The green synthesized AuNPs were also found to have anti-inflammatory responses as shown by the reduction of pro-inflammatory cytokines from immune cells. *In vitro* assays showed that the biogenic AuNPs were not toxic to KMST-6 cells. Overall, the data suggest that plant extracts produce biologically safe AuNPs with antibacterial and anti-inflammatory activities that can be exploited in the treatment of chronic wounds and in the management of chronic inflammation.



UNIVERSITY of the
WESTERN CAPE

KEYWORDS

Green nanotechnology

Gold nanoparticles

Nanoparticles conjugation

Biosynthesis

Hypoxis hemerocallidea

Galenia africana

Immunomodulation

Antibacterial

Wound healing

High resolution transmission electron microscope

Alamar blue



DECLARATION

I declare that “Green synthesis and characterization of gold nanoparticles from South African plants and their biological evaluations” is my own work that it has not been submitted for any degree or examination in any other university and that all the resources I have used or quoted have been indicated and acknowledged by means of complete references



ACKNOWLEDGMENTS

My sincere gratitude goes to my supervisors: Prof. Mervin Meyer and Prof. Ahmed Hussein. I do not want to thank them only for their encouragement and understanding throughout the past few years, but I feel mostly thankful for their teachings and guidance. I am deeply fortunate to have grown as a researcher under the supervision of such wonderful and supportive mentors. I will always carry what I have learnt from you with deepest appreciation.

I would like to thank the National Research Foundation (NRF) and DST/Mintek Nanotechnology Innovation Centre (NIC) for the financial support.

I also would like to thank Dr. Christopher Cupido, for the collection and identification of the plants used in this study.

I also thank Prof. Abram Madiehe and Prof. Martin Onani for their academic support.

Special thanks to my sister Dr. Nicole Sibuyi, for the amazing assistance in the lab, and for the good company in Rome. Also I thank Phumu, for her assistance during the immunomodulation work.

I would like to thank everyone in the NIC group for the friendly working atmosphere. I think of you as a big family. Thank you, Lauren, Dr. Dorcas, Marius, Boitumelo, Michele, Miche, Yonela, Coraline, Simone, Yam. Also, I thank everyone in Biotechnology and Chemistry Departments (UWC) and the Natural Product Chemistry group (CPUT).

I cannot deny that this journey was going to be harder without the fun, the smiles and the advices I received from good friends who always surrounded me with their care and respect. Thank you Chipa, Wilson, Sketch, Asanda, Carlito, Um sisi, Mischka, Riziki, Leandré, Kenneth and Zebida.

Finally, I would love to thank “soon to be Dr” Luveni Sonka, for the endless support, love and company. I do not know how this would have been possible without you. Your words of confidence and your presence have always lifted me up.

DEDICATION

*To my parents, Mohammed Elbagory and Nadra Elsherief,
to my siblings, Sara, Ali and Salma,
and to the rest of my Family in Egypt.
I owe everything to you.*



LIST OF PUBLICATIONS

1. **Elbagory, A.**, Cupido, C., Meyer, M., & Hussein, A. (2016). Large Scale Screening of Southern African Plant Extracts for the Green Synthesis of Gold Nanoparticles Using Microtitre-Plate Method. *Molecules*, 21(11), 1498.
2. Hussein, A., Meyer, M., **Elbagory, A** (2017). Natural products-nanoparticles interface, a new dimension of South African flora. *South African Journal of Botany*, 109:338.
3. **Elbagory, A.**, Meyer, M., & Hussein, A. (2017). Green synthesis of gold nanoparticles from South African plant extracts for the treatment of skin infection wounds. *Journal of Nanomedicine & Nanotechnology*, 8(4suppl).
4. **Elbagory, A.**, Meyer, M., Cupido, C., & Hussein, A. (2017). Inhibition of Bacteria Associated with Wound Infection by Biocompatible Green Synthesized Gold Nanoparticles from South African Plant Extracts. *Nanomaterials*, 7(12), 417.
5. **Elbagory, A.**, Hussein, A. & Meyer, M., (2019). Plant-derived gold nanoparticles as carriers of ampicillin (**Draft submitted to *Nanoscale Research Letters***)
6. **Elbagory, A.**, Hussein, A. & Meyer, M., (2019). The immunomodulatory effects of gold nanoparticles biosynthesized from *Hypoxis hemerocallidea* and *Hypoxoside* (**Draft submitted to *Journal of Immunology Research***)

LIST OF CONFERENCES

Authors: **Elbagory, A.**, Meyer, M., Cupido, C., & Hussein, A.

Title: “Green synthesis of gold nanoparticles from South African plant extracts for the treatment of skin infections” at the 13th International Conference and Exhibition on Nanomedicine and Pharmaceutical Nanotechnology, Rome, Italy- July 2017



UNIVERSITY *of the*
WESTERN CAPE

LIST OF ABBREVIATIONS

AIDS	Acquired Immune Deficiency Syndrome
ATCC	American Type Culture Collection
AuNPs	Gold Nanoparticles
AuNRs	Gold Nanorods
AuNSPs	Gold Nanospheres
AuNSs	Gold Nanoshells
AuNSTs	Gold Nanostars
BSA	Bovine Serum Albumin
CNTs	Carbon Nanotubes
CRF	Cape Region Flora
CTAB	cetyltrimethylammonium bromide
DCs	Dendrites Cells
DDSs	Drug Delivery Systems
DLS	Dynamic Light Scattering
DMEM	Dulbecco's modified Eagle's medium
DNA	Deoxyribonucleic Acid
ECM	Extracellular Matrix
EDC	1-ethyl-3-(3-dimethylaminopropyl) carbodiimide
EDX	Energy Dispersive X-ray
EGCG	Epigallocatechin gallate
EMT	Epithelial-mesenchymal Transition
EPR	Enhanced Permeability and Retention effect
EUCAST	European Committee for Antimicrobial Susceptibility Testing
fcc	Face Centred Cubic
FGF	Fibroblasts Growth Factor
FRET	Fluorescence Resonance Energy Transfer
FTIR	Fourier Transform Infrared Spectroscopy
h	Hours
HIV	Human Immunodeficiency Virus
HRTEM	High-Resolution Transmission Electron Microscopy
IFN- γ	Interferon-gamma
IL	Interleukin
LPS	Lipopolysaccharide
m	Meter
MEEE	2-(2-(2-mercaptoethoxy)ethoxy)ethanol
MES	2-mercaptoethanesulfonic acid
MHC	Major Histocompatibility Complexes

MIC	Minimum Inhibitory Concentration
min	Minutes
MNPs	Metallic Nanoparticles
MTT	3-[4,5-dimethylthiazol-2-yl]-2,5-diphenyl tetrazolium bromide
MUA	11-mercaptoundecanoic acid MUA
MWNTs	Multi-walled Carbon Nanotubes
NaCl	Sodium Chloride
NIR	Near Infrared Region
NK	Natural Killer
NLCs	Nanostructured Lipid Carriers
nm	Nanometre
NMR	Nuclear Magnetic Resonance
NMs	Nanostructured Materials
NPs	Nanoparticles
OC	Optimum Concentrations
PBMCs	Peripheral Blood Mononuclear Cells
PBP	Penicillin-binding Proteins
PBS	Phosphate Buffered Saline
PDGF	Platelet-derived Growth Factor
Pdi	Polydispersity Index
PDT	Photodynamic Therapy
Penstrep	Penicillin–Streptomycin
PMA	phorbol 12-myristate 13-acetate
PS	Photosensitizers
PTT	Photothermal Therapy
R&D	Research and Development
RES	Reticuloendothelial System
RNA	Ribonucleic Acid
RNS	Reactive Nitrogen Species
ROS	Reactive Oxygen Species
SAED	Selected Area Electron Diffraction
SLNs	Solid Lipid Nanoparticles
SWNTs	Single-walled Carbon Nanotubes
TGA	Thermogravimetric Analysis
TGF	Transforming Growth Factor
Th1	T helper 1
Th2	T helper 2
TLRs	Toll-like receptors
TMAT	N,N,N-trimethylammoniummethanethiol
TNF- α	Tumour Necrosis Factor- α

US
UV-Vis
VEGF

United States
Ultraviolet-visible
Vascular Endothelial Growth Factor



UNIVERSITY *of the*
WESTERN CAPE

LIST OF FIGURES

Figure 1.1 The cup of Lycurgus displayed in the British Museum (Kaushik, 2017).....	10
Figure 1.2 Global public expenditure in nanotechnology R&D in US \$ Billion (Bhushan 2010).	11
Figure 1.3 Nanotechnology market revenue expectation by different (optimistic and pessimistic) market indicator agencies (Inshakova and Inshakov, 2017).	13
Figure 1.4 Different types of nanotechnology systems (Bhatia, 2016).....	14
Figure 1.5 Classification of nanomaterials according to their dimensionally (Malhotra and Ali, 2017).	15
Figure 1.6 Graphene layer rolled into SWCNTs and MWCNTs.	16
Figure 1.7 Schematic illustration showing the several biomedical applications of the CNTs (Alshehri et al., 2016).	17
Figure 1.8 Schematic illustration of different types of fullerenes based on their size (Huy and Li, 2014).....	17
Figure 1.9 Different types of Fullerenes based on their structure (Thakral and Mehta, 2006).	18
Figure 1.10 The nanocapsule and nanosphere structures of the Polymeric NPs (Crucho and Barros, 2017).....	19
Figure 1.11 A diagram of the two types of the lipid-based NPs; SLN and NLC (Yingchoncharoen et al., 2016).....	20
Figure 1.12 A schematic representation of the oscillation of the free electrons around a nanoparticle (Yeh et al., 2012).....	22
Figure 1.13 UV-Vis spectra of 9, 22, 48 and 99 nm AuNPs showing of λ_{\max} values of 517, 521, 533 and 575, respectively (Link and El-Sayed, 1999).....	23
Figure 1.14 The effect of changing the size of the AuNPs on the colour their solutions (Mody et al., 2010).	24
Figure 1.15 The UV-Vis spectra, TEM and aqueous solutions of GNRs with different aspect ratio of; (a) 1.35, (b) 1.95, (c) 3.06, (d) 3.50, (e) 4.42 (Murphy et al., 2005).	25
Figure 1.16 Schematic illustrations and electron microscope images of the different shapes of AuNPs; (A) AuNSs, (B) AuNRs and (C) AuNSPs (Jihyoun Lee et al., 2014).....	27
Figure 1.17 Schematic diagram showing the accumulation of AuNPs in cancer cells through the gaps in the endothelial cells (leaky tumour vasculature) (Lim et al., 2011).	28
Figure 1.18 Schematic diagram of mercaptocarboxylic acids capping a single AuNP (DeLong et al., 2010).	29
Figure 1.19 Schematic diagram showing EDC-mediated functionalization of AuNPs (DeLong et al., 2010).	30
Figure 1.20 Schematic diagram showing different approaches for AuNPs synthesis.....	37
Figure 1.21 Different examples of NPs synthesis techniques (Iravani, 2011).....	38
Figure 1.22 Growth mechanism of the citrate AuNPs.	40
Figure 1.23 Growth mechanism of MNPs using plant extracts (Mittal et al., 2013).	46
Figure 1.24 Map of South Africa showing the Cape Flora Kingdom or Cape Region Flora..	51

Figure 1.25 Photographs of (A) <i>G. africana</i> , (B) leaves and flower of <i>H. hemerocallidea</i> and (C) corms of <i>H. hemerocallidea</i>	52
Figure 1.26 Chemical structures of hypoxoside and rooperol.	54
Figure 1.27 Wound healing stages.	61
Figure 1.28 A diagram illustrating; (A) mechanisms of action for the different classes of antibiotics; (B) mode of bacterial resistance (Slavin et al., 2017).	64
Figure 1.29 Cell wall structure of Gram-positive and Gram-negative bacteria (Slavin et al., 2017).	66
Figure 1.30 Regulation of the DCs, T lymphocytes and macrophages by NK cells. After activating NK cells by DCs and macrophages (green arrows), the activated NK cells in turn activate inactive DCs, T cells and macrophages by secreting IFN- γ and TNF- α (red arrows). The NK cells can also kill the activated T cells and macrophages and inactive DCs cells by inducing cytotoxicity (Vivier et al., 2008).	71
Figure 1.31 The effects of the cytokines on the different immune system cells (Zhang and An, 2007).	72



UNIVERSITY of the
WESTERN CAPE

LIST OF TABLES

Table 1.1 Applications of nanomaterials in industry (Pitkethly, 2004).	12
Table 1.2 The 12 principles of green chemistry (Anastas and Warner, 1998).....	43
Table 1.3 Different examples of biosynthesized AuNPs from plants reported recently in the literature.	45
Table 1.4 The different cytokine promoters for the different macrophages phenotypes and their cytokine productions.....	70



UNIVERSITY *of the*
WESTERN CAPE

TABLE OF CONTENT

Abstract.....	ii
Keywords.....	iv
Declaration.....	v
Acknowledgments.....	vi
Dedication.....	vii
List of Publications.....	viii
List of Conferences.....	ix
List of Abbreviations.....	x
List of Figures.....	xiii
List of Tables.....	xv
Table of Content.....	xvi
Chapter One: Introduction.....	1
1.1 Background.....	1
1.2 Problem statement and rationale.....	4
1.3 Hypothesis.....	6
1.4 Research aim.....	6
1.5 Research objectives.....	6
1.6 Thesis outline.....	7
Chapter Two: Literature review.....	9
2.1 Background on Nanotechnology: “There is plenty of room in the bottom”.....	9
2.2 Nanoparticles: classification and types.....	13
2.2.1 Types of NPs.....	15
2.2.1.1 Carbon-based NPs.....	15
2.2.1.1.1 CNTs.....	15
2.2.1.1.2 Fullerenes.....	17
2.2.1.2 Ceramic NPs.....	18
2.2.1.3 Polymeric NPs.....	19
2.2.1.4 Lipid-based NPs.....	19
2.2.1.5 Semiconductors NPs.....	20
2.2.1.6 MNPs.....	21

2.3	AuNPs	21
2.3.1	The Physicochemical Properties of the AuNPs	22
2.3.1.1	LSPR	22
2.3.1.2	Fluorescence quenching properties of the AuNPs	25
2.3.2	Potential of AuNPs in biomedical applications	25
2.3.2.1	Controllable morphologies.....	26
2.3.2.2	Controllable surface chemistry	28
2.3.2.3	Nanotoxicity and bioavailability of the AuNPs	30
2.3.2.4	Examples of biomedical applications of the AuNPs.....	33
2.3.2.4.1	Photodynamic therapy (PDT)	33
2.3.2.4.2	Photothermal therapy (PTT)	34
2.3.2.4.3	X-ray imaging as contrast agents	34
2.3.2.4.4	Sensors	35
2.3.2.4.5	Drug delivery carriers	35
2.3.3	Synthesis of the AuNPs.....	36
2.3.3.1	Growth mechanism of the AuNPs	39
2.3.3.2	Characterization of the AuNPs	40
2.3.3.3	Green synthesis of AuNPs	41
2.3.3.4	AuNPs biosynthesis from plants	43
2.3.3.4.1	Factors affecting AuNPs reaction with plants' phytochemicals	46
2.3.3.4.1.1	Influence of pH	47
2.3.3.4.1.2	Influence of plant extract concentration	47
2.3.3.4.1.3	Influence of reaction temperature	48
2.3.3.4.1.4	Influence of incubation time	49
2.3.3.4.2	Possible phytochemicals involved in the biosynthesis of the AuNPs... ..	49
2.4	Plant diversity of the Cape Region	50
2.4.1	Background on <i>G. africana</i> and <i>H. hemerocallidea</i> plants	51
2.5	Wound healing	55
2.5.1	Wound healing stages	56
2.5.1.1	Haemostasis stage	56
2.5.1.2	Inflammation stage.....	57
2.5.1.3	Proliferation stage	58
2.5.1.3.1	Angiogenesis.....	58

2.5.1.3.2	Fibroblasts migration and collagen deposition	59
2.5.1.3.3	epithelization.....	60
2.5.1.4	Remodelling stage.....	60
2.5.2	Bacterial infection and wound healing.....	62
2.5.3	AuNPs as antibacterial agents in wound healing	63
2.5.3.1	Antibacterial mechanism of action of AuNPs.....	65
2.5.3.2	Antibiotics conjugation to AuNPs	67
2.6	Immune system and immunomodulation effects of the AuNPs.....	68
2.6.1	Macrophages	68
2.6.2	NK cells	70
2.6.3	Cytokines	71
2.6.3.1	IL-1 β	73
2.6.3.2	TNF- α	74
2.6.3.3	IL-6	74
2.6.4	Immunomodulation of plants' phytochemicals.....	75
2.6.5	AuNPs and immunomodulation.....	76
	Bibliography	79
	Chapter Three: Manuscript "Large Scale Screening of Southern African Plant Extracts for the Green Synthesis of Gold Nanoparticles Using Microtitre-Plate Method"	104
	Chapter Four: Manuscript "Inhibition of Bacteria Associated with Wound Infection by Biocompatible Green Synthesized Gold Nanoparticles from South African Plant Extracts".....	125
	Chapter Five: Manuscript draft "Plant-derived gold nanoparticles as carriers of ampicillin"	148
	Chapter Six: Manuscript draft "The in vitro immunomodulatory effects of gold nanoparticles synthesized from <i>Hypoxis hemerocallidea</i> extract and Hypoxoside"	175
	Chapter Seven: General conclusions and recommendations	203
7.1	General Conclusions	203
7.2	Recommendations.....	205

CHAPTER ONE: INTRODUCTION

1.1 Background

The emerging field of nanotechnology has contributed to different industrial sectors with their many applications in the areas of biotechnology, electronics, drug delivery, cosmetics, material science, engineering, and biosensors (Manke et al., 2013). Metallic nanoparticles (MNPs) have shown potentials in many industrial and biomedical applications for their optical, electrical and photothermal properties (Geethalakshmi and Sarada, 2012). One of the advantages of the MNPs is the ease of their synthesis and modification (Nath and Banerjee, 2013). Among the MNPs, gold nanoparticles (AuNPs) have received considerable attention because of their unique optical properties and biocompatibility (Ahmed et al., 2016). AuNPs are incorporated in many applications in separation science (Sýkora et al., 2010), the food industry as well as space and environmental sciences (Santhoshkumar et al., 2017). AuNPs are also important for different biomedical applications such as drug delivery, diagnosis and treatment of diseases (Abadeer and Murphy, 2016; Huang et al., 2006; Qiu et al., 2016).

The preparation of MNPs involves a variety of chemical and physical methods, such as chemical reduction (Yu, 2007), photochemical reduction (Mallick et al., 2005), electrochemical reduction (Liu and Lin, 2004), laser ablation (Tsuji et al., 2003) and lithography (Jensen et al., 2000). These methods are expensive and involve the use of several toxic and environmentally harmful chemicals (Lukman et al., 2011). Thus, the use of the AuNPs synthesized by these methods can be limited when considered for biomedical applications. Conversely, the green synthesis of AuNPs involves the use of safe biological reagents that produce biocompatible and eco-friendly AuNPs (Khan et al., 2013).

AuNPs have been successfully synthesized from different biological sources such as proteins, flagella, bacteria and fungi (He et al., 2007; Kitching et al., 2015; Wang et al., 2012, 2008). Compared to the aforementioned biological systems, the use of plants is more attractive to researchers as they are readily available, safer and contain a variety of reducing phytochemicals. Also, in contrast to the microbial-derived chemicals, the plant-derived phytochemicals require shorter incubation periods with gold salt to synthesize AuNPs (Nath and Banerjee, 2013). Phytochemicals are not only responsible for the biosynthesis of AuNPs but also they act as capping agents to prevent the aggregation of AuNPs and control their growth (Lukman et al., 2011). Examples of these reducing phytochemicals are proteins, amines, phenols, carboxylic acids, ketones, aldehydes, etc. (Siddiqi and Husen, 2017). Several studies reported the synthesis of AuNPs using plant extracts (Balashanmugam et al., 2016; Dorosti and Jamshidi, 2016; Khan et al., 2013; Rajan et al., 2017; Yuan et al., 2017). These synthesis methods are not only eco-friendly, but also cost-effective and can be easily modified for large-scale synthesis (Geethalakshmi and Sarada, 2012). These plant-derived AuNPs can enhance the bioavailability and biological activity of the phytochemicals responsible for the bioactivity (Jaewook Lee et al., 2014; Park et al., 2011; Rao et al., 2016).

Galenia africana and *Hypoxis hemerocallidea* are two examples of medicinal plants that are indigenous to South Africa. They are widely exploited by local tribes to treat many diseases such as human immunodeficiency virus (HIV), acquired immune deficiency syndrome (AIDS), diabetes and wound infections (Basseyy et al., 2015; Drewes et al., 2008; Lall and Kishore, 2014). The biological activities of *G. africana* and *H. hemerocallidea* were also reported by several studies (Drewes et al., 2008; Mabona and Van Vuuren, 2013; Steenkamp and Gouws, 2006; Vries et al., 2005). Furthermore, the chemical investigations of the two plants have led to the isolation of several phytochemicals that can be incorporated in the biosynthesis of AuNPs (Drewes et al., 2008; Vries et al., 2005). Among those phytochemicals, hypoxoside is a major

secondary metabolite of *H. hemerocallidea* that has shown several biological activities (Katerere, 2013).

The disruption of skin integrity in the wound site renders the host at risk of physiological imbalance, severe disability or, in some cases, death (Wang et al., 2018). The wound healing process is activated immediately upon injury and consists of four stages including haemostasis, inflammation, proliferation stages and remodelling and scar formation (Broughton et al., 2006). Microbial infections can deter the wound healing process. Microbial pathogens can reduce the number of fibroblasts and collagen regeneration *via* the activation of inflammatory mediators as a result of the production of microbial toxins (Su et al., 2017). Therefore, wound-healing agents with antimicrobial activity can contribute towards effective and quicker healing (Machado et al., 2018). Several studies have reported the antimicrobial activities of AuNPs. The antibacterial mechanism of the AuNPs is not yet fully understood, but it is believed that the coating materials surrounding their gold cores play an important role in their antibacterial actions (Nadeem et al., 2017). The extracts of *G. africana* and *H. hemerocallidea* plants contain phytochemicals with antibacterial activity that could aid in the wound healing process (Elbagory et al., 2017). The synthesis of AuNPs using extracts produced from plants with known antibacterial activities can potentially produce nanoparticles (NPs) with significant antibacterial activities.

The antibacterial action of AuNPs can be enhanced by conjugating antibiotics into their surfaces. The use of AuNPs as antibiotics carriers can reduce the side effects of the antibiotics, increase their cellular uptake (Wang et al., 2017) and decrease bacterial resistance to antibiotics (Mühling et al., 2009). Several antibiotics were successfully loaded into AuNPs and showed improved antibacterial effects compared to the free drugs or unconjugated AuNPs (Brown et al., 2012; Nirmala Grace and Pandian, 2007).

Moreover, AuNPs have been found to regulate the immune system that includes a number of different cell types, such as macrophages and Natural Killer (NK) cells that fights infections, diseases or foreign biological invasion (Jiao et al., 2014). Some reports showed that some AuNPs have anti-inflammatory properties (Sumbayev et al.,

2013). Phytochemicals have also been shown proven their immunomodulatory (Ebadi et al., 2014). The anti-inflammatory effect of *H. hemerocallidea* was reported (Ojewole, 2006). It is then believed that phytochemicals can form the basis for new immunomodulatory therapies that can either stimulate immune responses for immunocompromised patients or suppress the immune responses if wanted in case of organ transplant, autoimmune patients or chronic inflammation conditions (Brindha et al., 2016).

Bacterial infections stimulate the macrophages and NK cells to dispatch pro-inflammatory cytokines to orchestrate the immune cells into the infected tissue (Arango Duque and Descoteaux, 2014). In some cases however, persistent inflammation (chronic inflammation) can lead to undesired complications (Rauch et al., 2013). In chronic inflammation, continual recruitment of innate and adaptive immune cells occurs, which leads to the production of high levels of pro-inflammatory modulators (Meirow and Baniyash, 2017). Patients with unmanaged chronic inflammation can be susceptible to several diseases, for example, diabetes, cancer, inflammatory bowel syndrome and rheumatoid arthritis (Pahwa and Jialal, 2018). Anti-inflammatory agents, therefore, can prove useful in the management of bacterial infections (Sheth, 2013).

1.2 Problem statement and rationale

The inorganic chemicals, such as sodium/potassium borohydride, hydrazine and salts of tartrate, or organic chemicals such as sodium citrate, used in the conventional synthesis of AuNPs have drastic effects on the health and the environment (Lukman et al., 2011). Sodium citrate, specifically, is widely used in the literature for AuNPs synthesis yet it has been shown to have extreme toxic effects both *in vivo* and *in vitro* experiments (Freese et al., 2012; Vijayakumar and Ganesan, 2012). The surface modification of the AuNPs, using biocompatible coating materials, could prove useful

in increasing the bioavailability of the AuNPs for biomedical applications (Fraga et al., 2013). Accordingly, the green synthesis of AuNPs using safe phytochemicals found in plant extracts can prove more beneficial compared to the conventionally synthesized AuNPs.

The biosynthesis of AuNPs from plants is governed by several factors such as reaction incubation time, pH, temperature and phytochemical and gold salt concentrations (Ahmed et al., 2016). As such, there is a need to establish an easy and quick method to screen large number of plant extracts with the ability to optimize one or more of the reaction's conditions during the synthesis.

Further, the search of new antibacterial agents has becoming a global priority due to the rapid emergence of bacterial resistance to the current antibiotics (Zhang et al., 2011). It is estimated that by 2050 resistant bacterial infections will cause around 10 million deaths annually worldwide (Lai et al., 2018). Among many health complications, microbial infections can deter the wound healing progress and promote the development of chronic wound infections, which is complicated by the antibiotic resistance (Pîrvănescu et al., 2014). Chronic wound infections place a fiscal burden on both governments and patients. Globally, there are around 20 million cases with chronic wounds that cost around 31 billion US \$ per year for their management (Leaper et al., 2015). Moreover, chronic wound infections reduce patient's quality of life and reproductivity. For instance, in unhealed diabetic foot ulcers, bacterial infections can result in limb amputations in up to 14 of every 1000 diabetic patients (Singh et al., 2005).

Further, bacterial infections can cause persistent inflammation, which can lead to several health complications, including rheumatoid arthritis, inflammatory bowel disease, multiple sclerosis, psoriasis and eczema (Coutinho and Chapman, 2011). Thus, the use of anti-inflammatory agents can be useful in the management of the side effects of the bacterial infections.

MNPs, including AuNPs, have shown potent antibacterial and immunomodulatory activities. MNPs can be form the basis of novel antibiotics to replace the conventional antimicrobial agents (Wang et al., 2017).

1.3 Hypothesis

The phytochemicals present in the plants aqueous extract can reduce the gold precursor into AuNPs. These biogenic AuNPs can provide safer options for the treatment of chronic wound infections and expected to have a role in management of chronic inflammation through their immunomodulatory effects.

1.4 Research aim

The aim of this study is to biosynthesize AuNPs from several South African plant extracts and to evaluate their antibacterial activity against several bacterial strains known to cause wound infections in addition to the investigation of their immunomodulation effect on selected immune cells *in vitro*.

1.5 Research objectives

- 1- Collection of South African plants from the Western Cape province and the preparation of aqueous extracts for each plant collected.
- 2- Synthesis of AuNPs from the collected plants using green methods.
- 3- Optimization of the AuNPs synthesis by varying the reaction temperature and reactants' concentrations.

- 4- Characterization of the biosynthesized AuNPs using different spectroscopic and optical techniques.
- 5- Evaluate the stability of the biosynthesized AuNPs in several biological buffers and media.
- 6- Evaluate the cytotoxicity of the biosynthesized AuNPs on normal human fibroblasts cells (KMST-6).
- 7- Investigate the antibacterial effects of the biosynthesized AuNPs on several Gram-positive and Gram-negative bacteria associated with wound infections.
- 8- Functionalization of the biosynthesized AuNPs with ampicillin and measure their physicochemical properties and their antibacterial effects.
- 9- Isolate hypoxoside from *H. hemerocallidea* and evaluate its ability to produce AuNPs.
- 10- Examine the immunomodulation activity of the biosynthesized AuNPs on the cytokine production from macrophages and NK cells.



1.6 Thesis outline

This thesis is divided into 7 chapters. **Chapter 1** introduces the scope of the study, its aims and objectives. **Chapter 2** presents a literature review on the different aspects about the field of nanotechnology, its background and the different types of nanomaterials. The chapter also describes the potential applications of AuNPs in biomedical research, specifically as antibacterial and immunomodulatory agents, the methods used for their synthesis and the importance of biogenic AuNPs. The chapter also highlights the process of wound healing and its different stages, the role of immune system and its cellular components and their cytokines. **Chapters 3 - 6** describe the results obtained in this study following the established objective. **Chapter 3** and **4** are published research articles and they are included in their journal format. **Chapters 5** and **6** are article drafts and appear according to the required format of their journals. **Chapter 3** describes the collection of different South African plants and the

biosynthesis and characterization of AuNPs from their aqueous extracts using a developed method. **Chapter 4** describes the biosynthesis of AuNPs from *H. hemerocallidea* and *G. africana* and their antibacterial activity against bacterial strains associated with wound infections. **Chapter 5** reports on the conjugation of ampicillin onto biogenic AuNPs from *H. hemerocallidea*. **Chapter 6** is an evaluation of the immunomodulatory effects of the biogenic AuNPs from *H. hemerocallidea* and hypoxoside. Finally **chapter 7** is general conclusions that summarizes the findings of each research chapter and includes also a brief recommendations for future work.



UNIVERSITY *of the*
WESTERN CAPE

CHAPTER TWO: LITERATURE REVIEW

2.1 Background on Nanotechnology: “There is plenty of room in the bottom”

The term “nano”, which refers to one billionth of a unit (10^{-9}), is derived from the Greek word “nanos” that means “very small or dwarf” (B. Ahmad et al., 2017). Thus, one nanometre (nm) equals 10^{-9} meter (m). The nanoscale is widely used to describe the small diameters in which larger scales would be inappropriate or difficult to apply. For instance, the diameter of a human hair is approximately $10\ \mu\text{m}$ (10,000 nm), whereas the diameter of a DNA strand is about a few nm. Atoms have diameters of tenths (10^{-1}) of nm (Vo-Dinh, 2006).

Nanotechnology can be defined as “the design, characterization, production and application of materials, devices and systems by controlling shape and size on the nanoscale” (Ramsden, 2009). The synthesis and the self-assembly of the nanoparticles (NPs) are considered the cornerstone of nanotechnology (Gardea-Torresdey et al., 2002). NPs are defined by the American Society for Testing and Materials as particles that have at least two or more dimensions ranging in size from 1 to 100 nm (B. Ahmad et al., 2017). More recently however, the British Standard Institution defined NPs as particles that have one or more dimensions at the nanoscale ($\leq 100\ \text{nm}$) (Manke et al., 2013). NPs used in the biotechnology field, however, can have a particle size up to 500 nm and seldom exceed 700 nm (Mody et al., 2010).

The use of nanosize particles has been documented in ancient history. Old Roman glassmakers in the 4th century A.D. used nanosized metals to fabricate glasses. An example of these works is the Lycurgus cup, which depicts the death of King Lycurgus from that era. The cup was made of gold and silver NPs and if a light source is placed inside, these NPs can alter the colour of the cup from green to red (Figure 1.1) (Poole,

2003). This optical phenomenon is one of the unique characteristics of the NPs that will be discussed later.



Figure 1.1 The cup of Lycurgus displayed in the British Museum (Kaushik, 2017).

During the annual meeting of the American Physical Society in 1959, Richard Feynman, a Nobel Prize laureate for physics, gave one of the classic science lectures of the 20th century entitled “There is plenty of room in the bottom”. In his speech, he envisioned, for the first time, the potential of manipulating matter of “atomic scale” on different aspects of modern science (Nouailhat, 2008). Several research outputs on “small” metal particles were conducted for the first time during the 1950s and 1960s, yet the term “nanotechnology” was not yet used. For example, porous silicon was first fabricated in 1956 (Poole, 2003). The magnetic fluids (ferrofluids) that contain nanosized magnetic particles suspended in liquids were first synthesized in the 1960s (Poole, 2003). It was not before 1974 when the term “nanotechnology” was first introduced by Dr. Norio Taniguchi of Tokyo Science University after attempting to design nanosized materials (Sharon et al., 2012). The numerous inventions in the development of NPs since the 1980s have been testaments to Feynman’s vision in 1959 (Bhushan, 2010).

The potential of nanotechnology is reflected by the global expenditure towards the research and development (R&D) of nanosized materials. The USA announced the National Nanotechnology Initiative (NNI) in the fiscal 2001 budget. Through this initiative, a coalition between the government, private and research sectors would work together to achieve economic and social benefits by supporting different aspects of nanotechnology science (Bhushan, 2010). In 2002, a three years plan, called the Sixth Framework Program or FP6, was set by the European Union prioritizing the funding of nanotechnologies (Bhushan, 2010). By 2003, the total global public expenditure towards nanotechnology was around 3.5 billion US \$ contributed mainly by the EU, Japan and USA (Figure 1.2) (Bhushan, 2010).

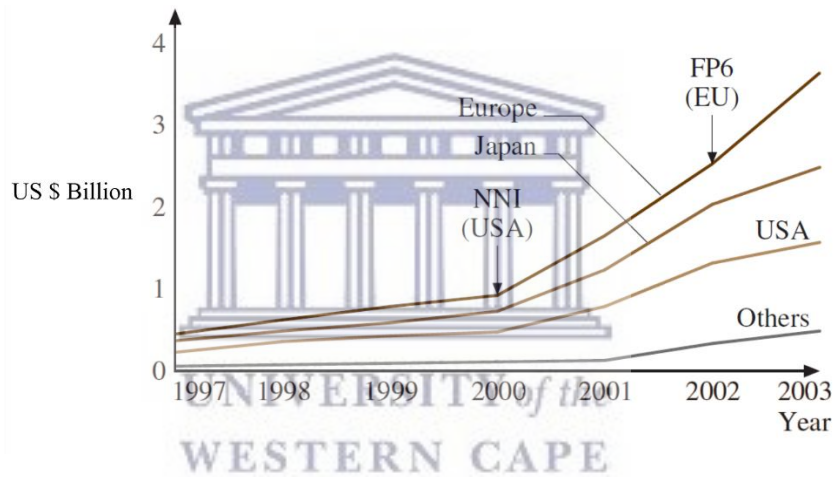


Figure 1.2 Global public expenditure in nanotechnology R&D in US \$ Billion (Bhushan 2010).

The financial support for the nanotechnologies R&D led to the development of several nanomaterials-based products that incorporated in a myriad of industrial applications. Table 1.1 shows some of these applications of the nanomaterials that on the market or under development.

Table 1.1 Applications of nanomaterials in industry (Pitkethly, 2004).

Field	Under development	In use
Energy	<ul style="list-style-type: none"> • Dye-sensitized solar cells using TiO₂ • H₂ storage using metal hydrides • Improved anode and cathode materials for fuel cells • Thermal control fluids using Cu 	<ul style="list-style-type: none"> • Automotive catalysts • Nanocrystalline Ni and metal hydrides for batteries • Environmental catalysts, ceria in diesel
Healthcare/biomedical	<ul style="list-style-type: none"> • Nanocrystalline drugs for easier absorption • Inhalable insulin • Anticancer treatments • Antioxidant drugs based on fullerenes 	<ul style="list-style-type: none"> • Ag-based antibacterial wound dots dressings, ZnO fungicide • Drug carriers for drugs with low water solubility • Au for biolabeling and detection • Magnetic resonance imaging contrast agents using superparamagnetic Fe₂O₃ • Sunscreens using ZnO and TiO₂
Engineering	<ul style="list-style-type: none"> • More efficient Thermal barrier coatings • Spark plugs • Delivery of herbicides 	<ul style="list-style-type: none"> • Thermal spray coatings • Cutting tools • Automotive tires
Consumer goods		<ul style="list-style-type: none"> • Packaging using silicates • Glass coatings for antiglare mirrors using TiO₂ • Ski wax • Sports goods: tennis balls, rackets using nanoclays • Water/stain-repellent textiles
Environmental	<ul style="list-style-type: none"> • Environmentally friendly antifouling paints and coatings • Soil remediation using Fe 	<ul style="list-style-type: none"> • Self-cleaning glass • Antireflection coatings
Electronics	<ul style="list-style-type: none"> • EMI shielding using conducting and magnetic materials • Electrically conductive plastics • Light-emitting Si LED nanoparticles for displays 	<ul style="list-style-type: none"> • Chemical-mechanical planarization alumina • Computer chips • Optical fibres based on Si

The impact of nanomaterials-based products on the nanotechnology market proved highly profitable. Data from several market indicators showed that the nanomaterial market has been thriving since the new millennium. A report from Mordor Intelligence suggests that the value of global nanomaterials market was at about US \$4.1 billion in 2015, and this value will continue to grow to US \$11.3 billion by 2020. A more optimistic report by Allied Market Research estimated the nanotechnology market in 2015 at about US \$14.7 billion and to reach US \$55.0 billion by 2022 (Figure 1.3) (Inshakova and Inshakov, 2017).

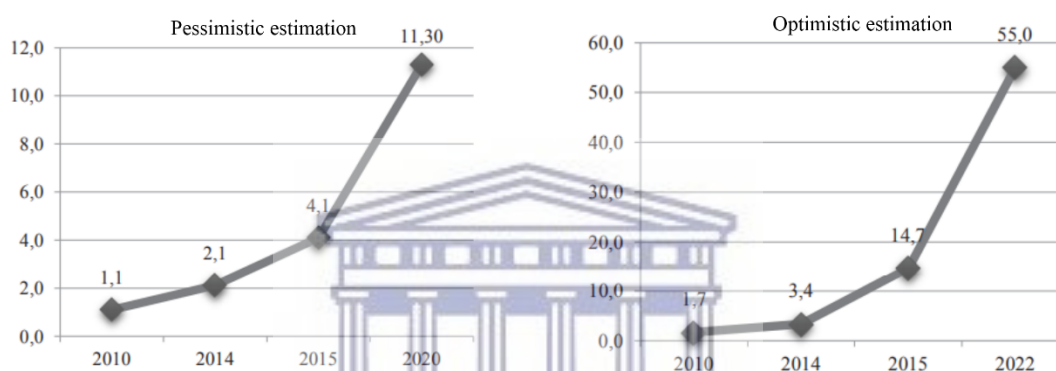


Figure 1.3 Nanotechnology market revenue expectation by different (optimistic and pessimistic) market indicator agencies (Inshakova and Inshakov, 2017).

UNIVERSITY of the
WESTERN CAPE

2.2 Nanoparticles: classification and types

The size reduction of the bulk materials gives rise to NPs, which are dictated by the quantum physics and have unique physicochemical properties that can be utilized in many applications. Hence, the key aspect of nanotechnology, its potential in different industries and the unique properties of its NPs revolve around a major and simple platform: “The miniaturization of bulk materials”. NPs are considered nanostructured materials (NMs) according to the classification of nanotechnology systems (Figure 1.4). MNPs, including AuNPs, are nonpolymeric nanostructures that also include several other nonpolymeric nanostructures e.g. Silica NPs and carbon nanotubes (CNTs) (Figure 1.4) (Bhatia, 2016).

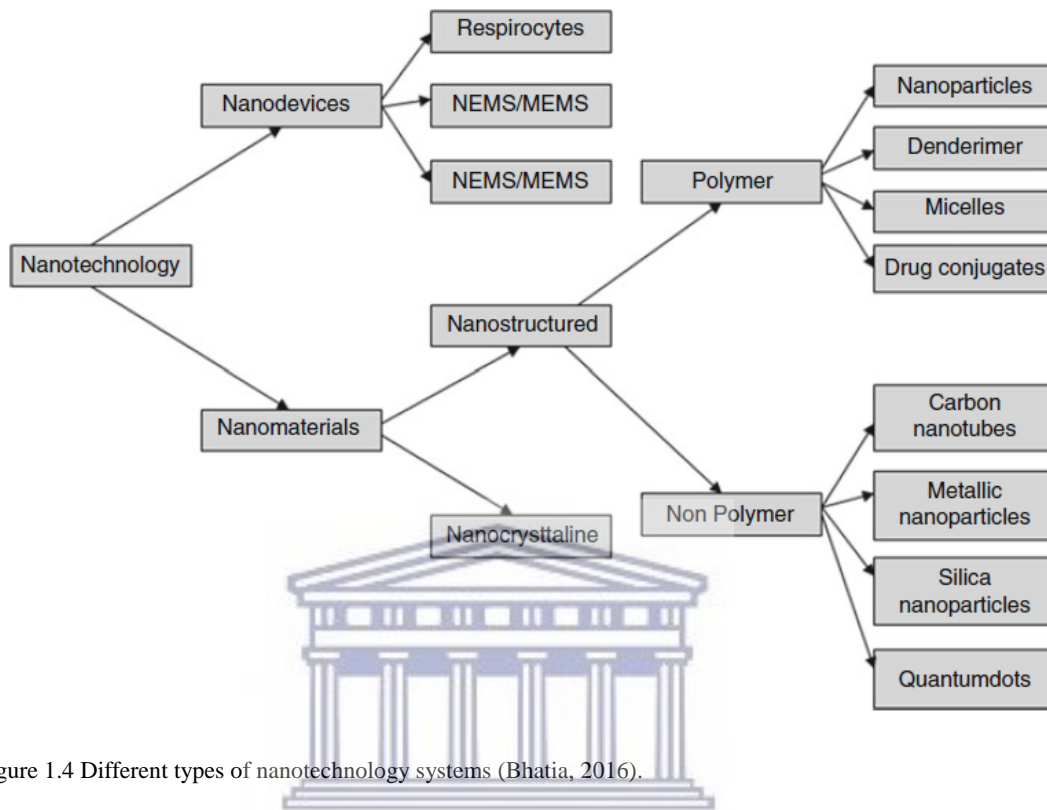


Figure 1.4 Different types of nanotechnology systems (Bhatia, 2016).

There are hundreds of NMs that were manufactured in the past few decades, and thus there is a need to classify them. Pokropivny and Skorokhod (2007) reported a classification of the NMs based on their dimensionality (Pokropivny and Skorokhod, 2007). In their classification, NMs can be divided into four categories; zero-dimension (0D), one-dimension (1D), two-dimension (2D) and three-dimension NMs (3D) (Figure 1.5).

- 1- 0D NMs have all their dimensions at nanoscale. Examples of the 0D NMs are MNPs such as spherical and some cubes and polygons of AuNPs (Malhotra and Ali, 2017).
- 2- 1D NMs have two dimensions at the nanoscale and one at the macroscale. Nanowires and nanofibers are two examples of the 1D NMs (Malhotra and Ali, 2017).

- 3- 2D NMs, such as nano thin-films and nanosheets, have only one dimension in nanoscale of their three sides (Malhotra and Ali, 2017).
- 4- 3D NMs possess no nanoscale dimensions, yet they contain building units of nanoscale materials, which are confined in their 3D macrostructure (Malhotra and Ali, 2017).

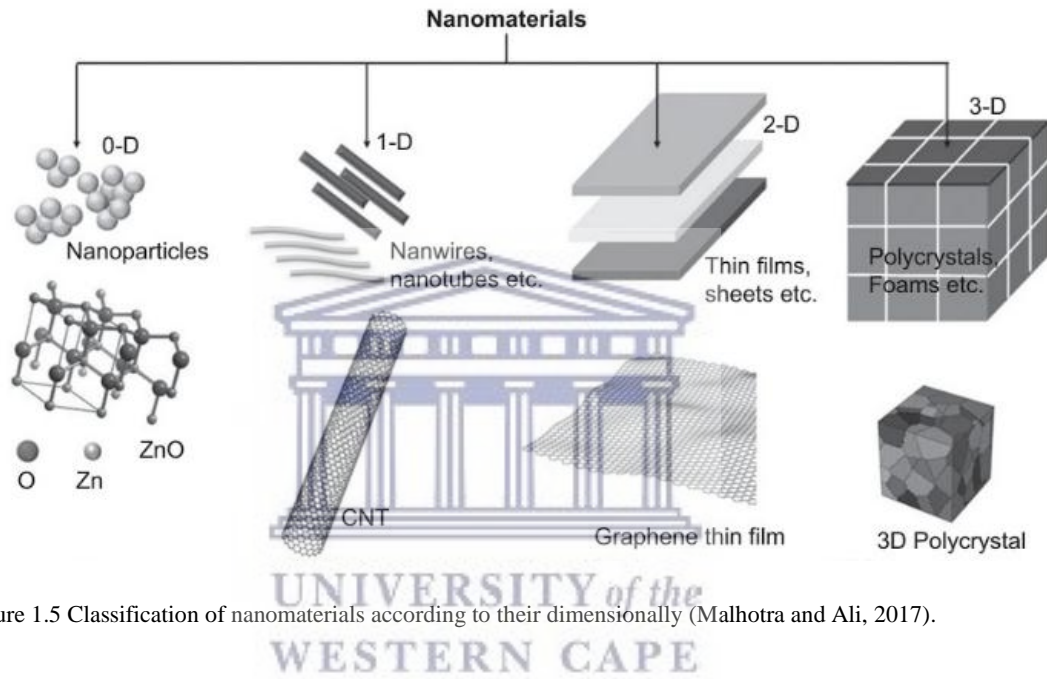


Figure 1.5 Classification of nanomaterials according to their dimensionally (Malhotra and Ali, 2017).

2.2.1 Types of NPs

NPs can also be classified depending on their physical and chemical properties, particle size and morphology. Below are examples of these NPs:

2.2.1.1 Carbon-based NPs

2.2.1.1.1 CNTs

CNTs are graphene sheets composed primarily of hexagonal carbon units that are rolled up to form seamless cylinders (Figure 1.6) (Bhatia, 2016). CNTs can be configured to have one or multiple graphene layers (single-walled carbon nanotubes, SWCNTs, or multi-walled carbon nanotubes, MWCNTs) (Khan et al., 2017). MWCNTs can be more than 100 nm in diameter, while SWCNTs are only 0.8 to 2 nm in diameter. The lengths of CNTs can range from less than 100 nm to several centimetres (De Volder et al., 2013). Thus, CNTs merge both nano and macro scales together. These tubular structures are used as filters, gas adsorbents for environmental remediation and supporting medium for organic and inorganic catalysts (Khan et al., 2017).

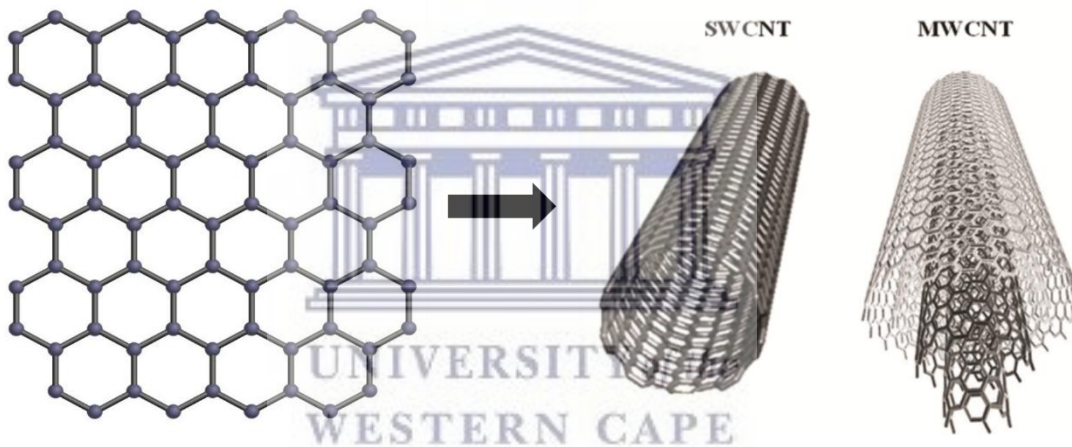


Figure 1.6 Graphene layer rolled into SWCNTs and MWCNTs.

The surface of the CNTs can be easily be functionalized to accommodate different biological, organic and inorganic structures that can render them useful in several biomedical applications such as; biosensors, gene and drug delivery, diagnostics, drug delivery and biomedical imaging (Figure 1.7) (Alshehri et al., 2016).

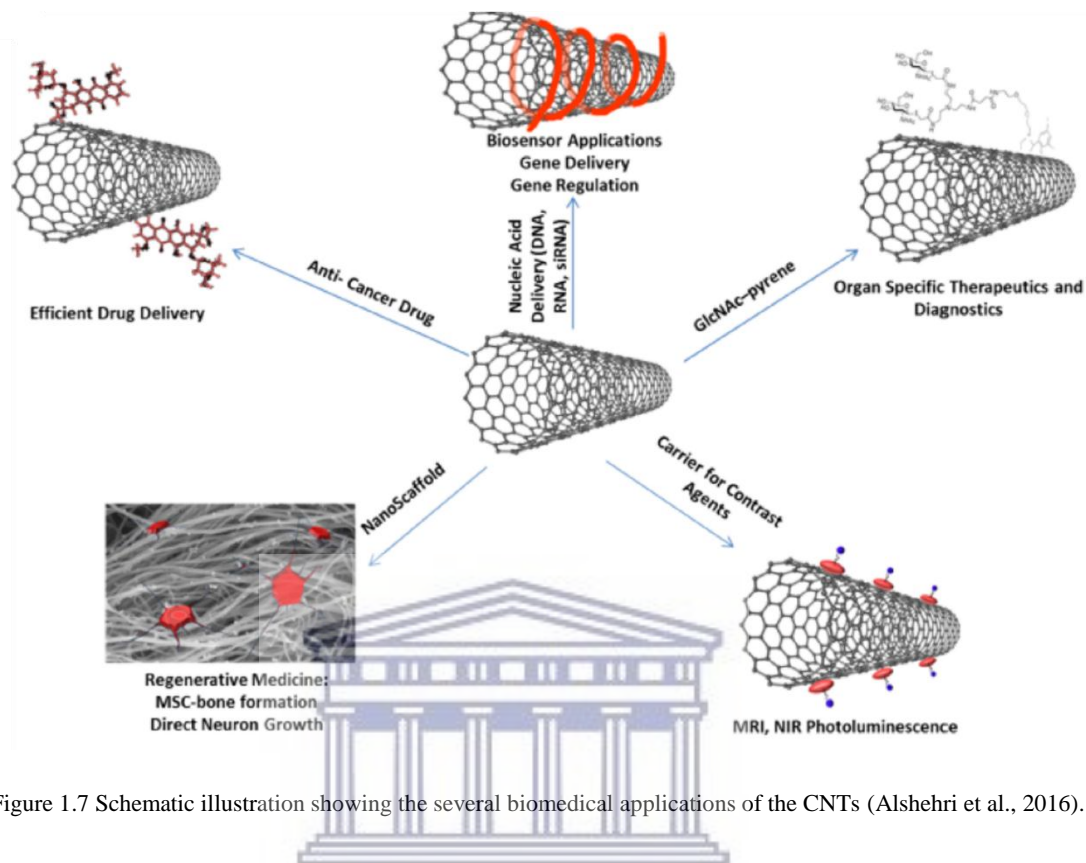


Figure 1.7 Schematic illustration showing the several biomedical applications of the CNTs (Alshehri et al., 2016).

UNIVERSITY of the
WESTERN CAPE

2.2.1.1.2 Fullerenes

Known as buckyballs, fullerenes are hollow nanosized spherical structures whose surface has 20 or more carbon atoms arranged in pentagonal and hexagonal formation (Figure 1.8) (Bhatia, 2016).

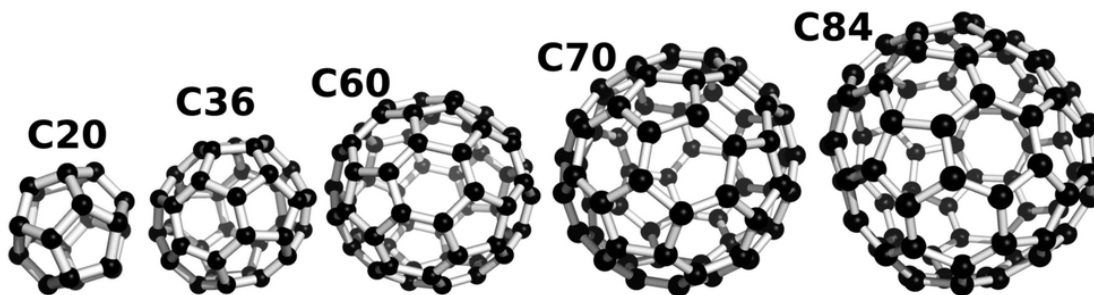


Figure 1.8 Schematic illustration of different types of fullerenes based on their size (Huy and Li, 2014).

The inclusion of one or more atoms to the buckyball gives rise to different types of fullerenes. For instance, endohedral fullerenes have another atom enclosed within the buckyball structure. In contrast to endohedral fullerenes, exohedral fullerenes (or fullerenes derivatives) have another chemical group attached to the buckyball surface. Heterofullerenes, on the other hand, have one or more of carbon atoms in their buckyball structure replaced by hetero-atoms such as, Nitrogen or Boron (Figure 1.9) (Thakral and Mehta, 2006).

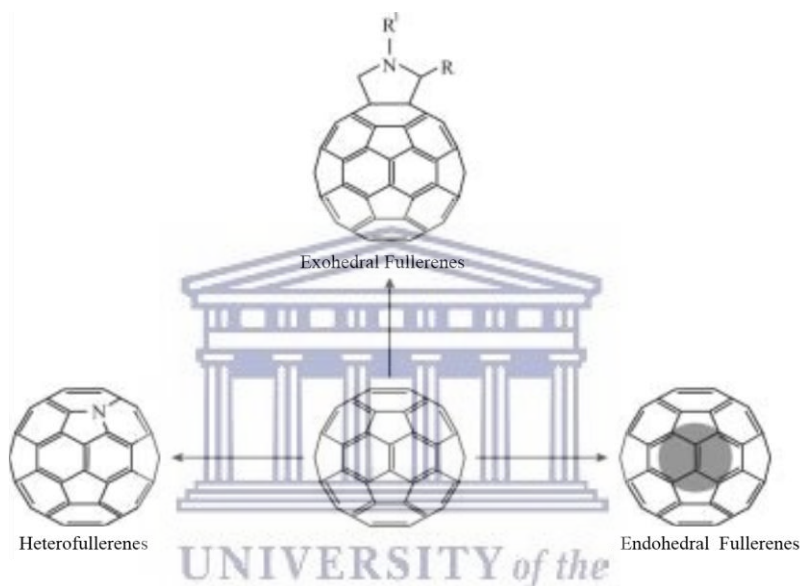


Figure 1.9 Different types of Fullerenes based on their structure (Thakral and Mehta, 2006).

Like CNTs, Fullerenes can be also easily functionalized for different biomedical applications. Fullerenes have been found to have free radical scavenging properties, anti-HIV and anticancer activities (Thakral and Mehta, 2006).

2.2.1.2 Ceramic NPs

Ceramic NPs are the oxides, carbides, phosphates and carbonates of different metals and metalloids such as, calcium, titanium, silicon, etc. (Thomas et al., 2015). They can be synthesized in amorphous, polycrystalline, dense, porous or hollow forms (Khan et

al., 2017). For that reason, these NPs can be applied in different applications such as catalysis, photocatalysis and photodegradation of dyes (Khan et al., 2017). For biomedical applications, ceramic NPs are also regarded as excellent carriers for drugs, genes, proteins and imaging agents (Thomas et al., 2015).

2.2.1.3 Polymeric NPs

Polymeric NPs composed of macromolecules (or polymers) that comprise many repeating units attached together to form chain-like molecules. Polymeric NPs are mainly used for drug delivery, although some other biomedical applications have been reported such as bioimaging and biosensing (Moreno-Vega et al., 2012). Polymeric NPs are mostly nanocapsule or nanosphere in shape. The nanocapsule particles have their carried drug in an aqueous or oily cavity encapsulated in a polymeric shell. The drug in the nanosphere systems, however, is uniformly dispersed along with the polymer in a matrix-like structure (Figure 1.10) (Crucho and Barros, 2017).

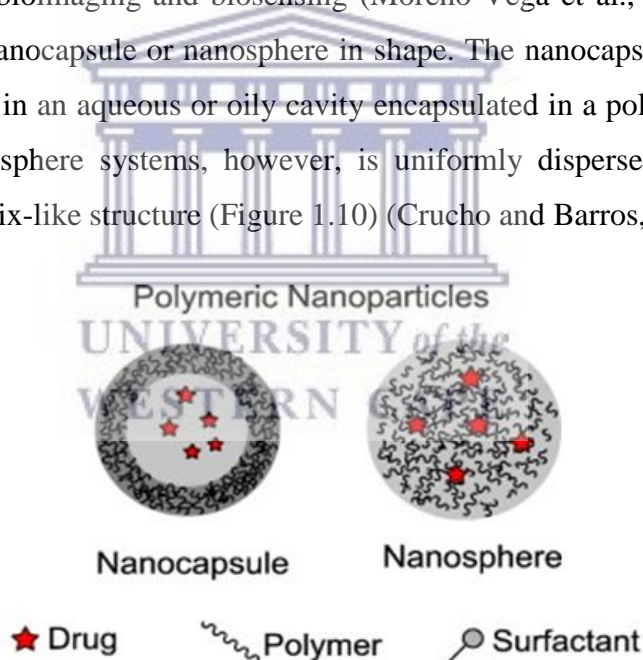


Figure 1.10 The nanocapsule and nanosphere structures of the Polymeric NPs (Crucho and Barros, 2017).

2.2.1.4 Lipid-based NPs

Similar to the polymeric NPs, the lipid-based NPs contain a solid inner matrix of soluble lipophilic matter encapsulated with surfactants or emulsifiers (Rawat et al.,

2011). However, the synthesis of the lipid-based NPs involves the use of physiological lipids (Kaur et al., 2015), which are more biocompatible and biodegradable than the polymers used in the synthesis of the polymeric NPs. The lipid-based NPs are therefore used to develop biocompatible nanosized drug, deoxyribonucleic acid (DNA) and ribonucleic acid (RNA) carrier systems (Ganesan and Narayanasamy, 2017). Ranging in size between 50 to 100 nm, the solid lipid nanoparticles (SLNs) are the first generation of the lipid-based NPs, which are prepared from lipids that remain solid at both room and body temperatures (Figure 1.11) (Wong et al., 2007). However, the nanostructured lipid carriers (NLCs) are improved generation of the SLNs in which the drug is immobilized by a mixture of solid lipid and liquid lipid phases resulting in the increase in the drug loading capacity (Figure 1.11) (Yingchoncharoen et al., 2016).

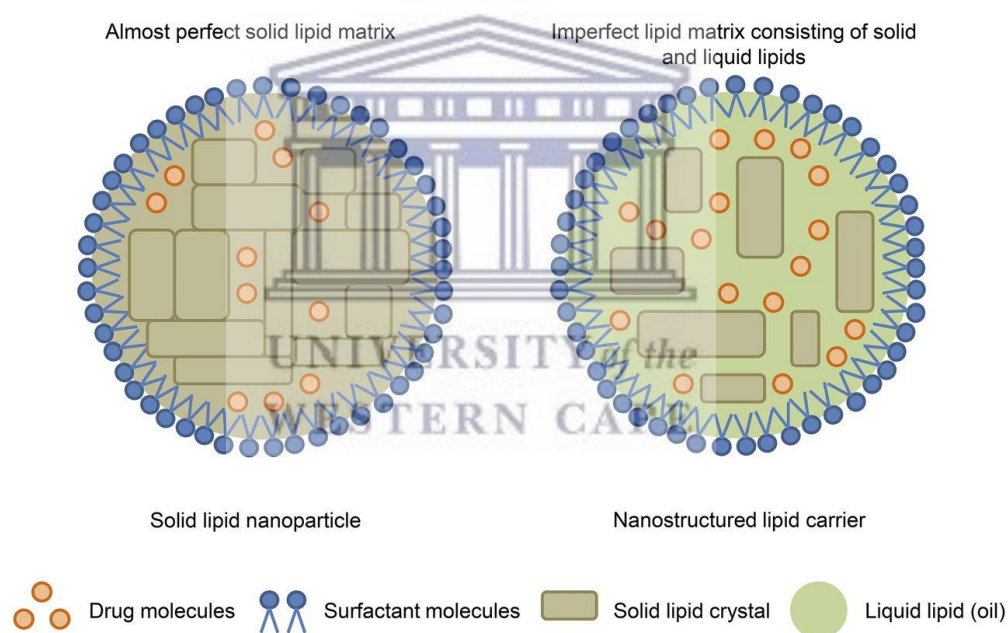


Figure 1.11 A diagram of the two types of the lipid-based NPs; SLN and NLC (Yingchoncharoen et al., 2016).

2.2.1.5 *Semiconductors NPs*

The semiconductors NPs have the properties of conductors and insulators (Suresh, 2013). The semiconductors NPs play an important role in photocatalysis, photo optics

and electronic devices. They are also effective in water splitting applications (Khan et al., 2017). Semiconductors NPs are synthesized from different atoms, which are, based on their periodic table position, denoted II-VI, III-V or IV-VI. For instance, semiconductors NPs made from ZnO, ZnS, CdS, CdSe and CdTe are known as II-VI semiconductors NPs (Suresh, 2013).

2.2.1.6 MNPs

MNPs have attracted researchers for over a century and are utilized in various fields including, physics, chemistry, electronics, optics, material and biomedical sciences (Shankar et al., 2016). These particles can be easily fabricated and functionalized with antibodies, ligands, drugs, etc. and hence they provide a plethora of potential applications in biomedicine, targeted drug delivery, magnetic separation, gene delivery and diagnostic imaging (Mody et al., 2010).

Made of metal precursors, MNPs can be synthesized from gold (B. Ahmad et al., 2017; Arunachalam et al., 2013; Ayaz Ahmed et al., 2014; Rouhana et al., 2007), silver (Ajitha et al., 2015; Khan et al., 2013), titanium (Prasad et al., 2007), zirconium (Eshed et al., 2011), strontium (Frasnelli et al., 2017), copper (Umer et al., 2014), etc. These MNPs have unique optical properties because of their famous localized surface plasmon resonance (LSPR) (Khan et al., 2017). These optical properties play a key factor in determining the potential of MNPs in the biomedical applications (Khan et al., 2017).

2.3 AuNPs

AuNPs, sometimes referred to as colloidal gold, are suspended nanosized gold particles (Mody et al., 2010). In the 1850s the scientific study of AuNPs was first conducted by Michael Faraday, who observed differences between the colloidal and bulk gold in

terms of their physical and chemical (physicochemical) properties (Mody et al., 2010). Now, the AuNPs are the one of most reported MNPs in the literature (Shankar et al., 2016).

2.3.1 *The Physicochemical Properties of the AuNPs*

2.3.1.1 *LSPR*

The reduction in size of the bulk materials into NPs provides materials with a large surface-to-volume ratio leading to an increased number of surface atoms and gives rise to the quantum size effect (Raikar et al., 2011). NPs, therefore, have unique physicochemical properties different from their bulk forms. These properties include higher electrical and heat conductivity, improved catalytic activity, optoelectronic properties, enhanced or hindered particles aggregation and enhanced photoemission (Abdelhalim et al., 2012).

The optical properties of the AuNPs result from the interaction of their free electrons with light. This interaction is known as the LSPR effect in which the free electrons of the AuNPs undergo a collective coherent oscillation with respect to the gold lattice in the presence of the electromagnetic field of the photons (light) (Figure 1.12) (Jain et al., 2008).

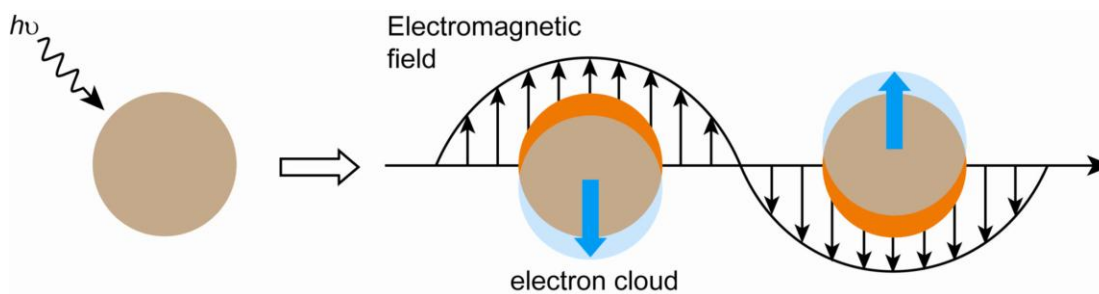


Figure 1.12 A schematic representation of the oscillation of the free electrons around a nanoparticle (Yeh et al., 2012).

The LSPR effect of the MNPs produce absorption bands in the visible-light region between 500 to 600 nm (Rastogi and Arunachalam, 2012). These bands are unique to MNPs and are not visible in the bulk gold or tiny particles (particle diameter < 2 nm) (Yeh et al., 2012). Depending on LSPR position in the visible spectrum, the aqueous solutions of AuNPs show a range of colours such as brown, orange and red, etc. (Jain et al., 2008). Several factors affect the position of LSPR bands such as size, shape and surface charge of the AuNPs, the solvent used, the surface ligand, temperature and the distance between the neighbouring NPs (Yeh et al., 2012). To illustrate, spherical AuNPs with 10 nm particle diameter exhibit a strong absorption maximum (λ_{\max}) around 520 nm, which give these particles their famous red colour (Jain et al., 2008). However, a red-shift of the bands from the blue to the red end of the visible light spectrum is observed with NPs of bigger sizes (Jain et al., 2008). For example, 40 nm spherical AuNPs produce λ_{\max} around 530 nm (Jain et al., 2008). Also, a study by Link and El-Sayed showed λ_{\max} values of 517, 521, 533 and 575 nm corresponding to AuNPs of different particle sizes (9, 22, 48 and 99 nm, respectively) (Figure 1.13) (Link and El-Sayed, 1999).

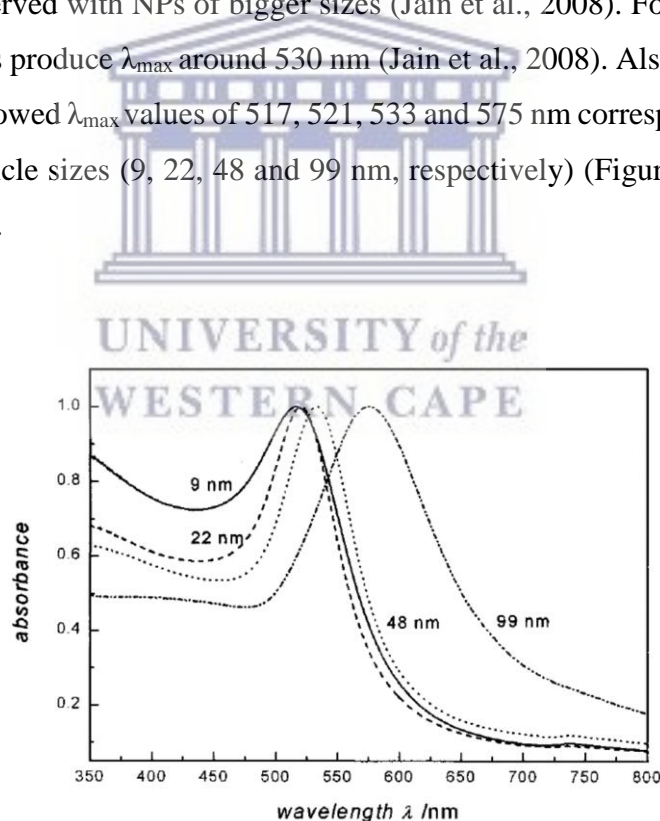


Figure 1.13 UV-Vis spectra of 9, 22, 48 and 99 nm AuNPs showing of λ_{\max} values of 517, 521, 533 and 575, respectively (Link and El-Sayed, 1999).

This red-shift is accompanied by a change of the AuNPs solutions to a blue colour. Figure 1.14 shows the effect of different size of AuNPs on the colour of their solutions.

The solution of the smallest AuNPs appears bright red, while the solutions of AuNPs of bigger size appear bluish red (Mody et al., 2010).

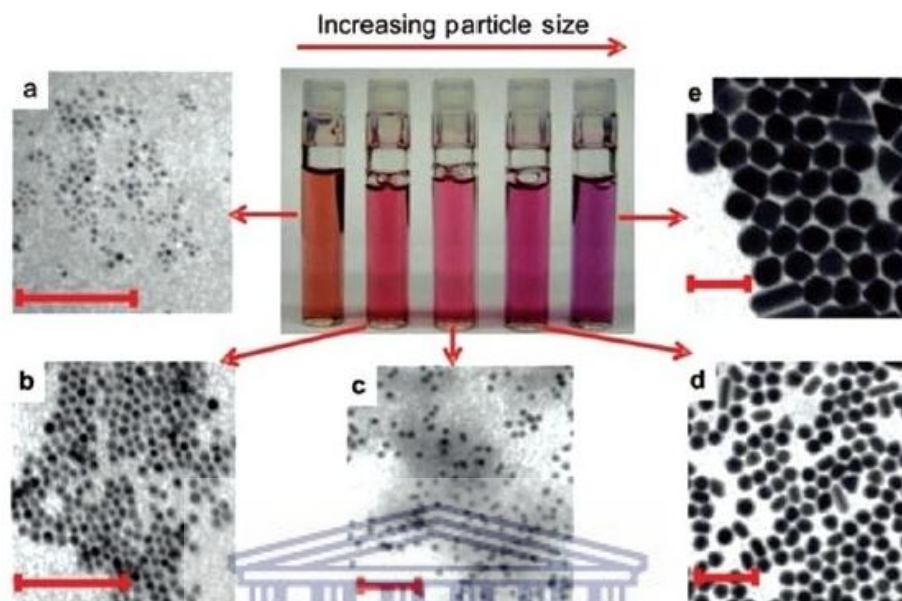


Figure 1.14 The effect of changing the size of the AuNPs on the colour their solutions (Mody et al., 2010).

The shape of the AuNPs also plays an important role in determining the position of their LSPR bands. Gold nanorods (AuNRs), for instance, exhibit extra absorption bands at the near infrared region (NIR) (650-900 nm). The appearance of such bands is because nanorods have two resonances: one from the plasmon oscillation along the nanorod short axis and another from their long axis (Murphy et al., 2005). This “double oscillation property” depends on the nanorod’s aspect ratio (length-to-width ration) in which the LSPR band undergoes a red-shift from the visible region to the NIR of the light spectrum, with the increase in the aspect ratio of the AuNPs (Jain et al., 2008). Figure 1.15 illustrates the effect of changing the aspect ratio of the AuNPs on their solutions’ colours and their Ultraviolet-Visible (UV-Vis) spectra (Murphy et al., 2005). The AuNPs showed a shift in their LSPR bands towards the NIR with the increase of their aspect ratios from 1.35 to 4.42 (Figure 1.15).

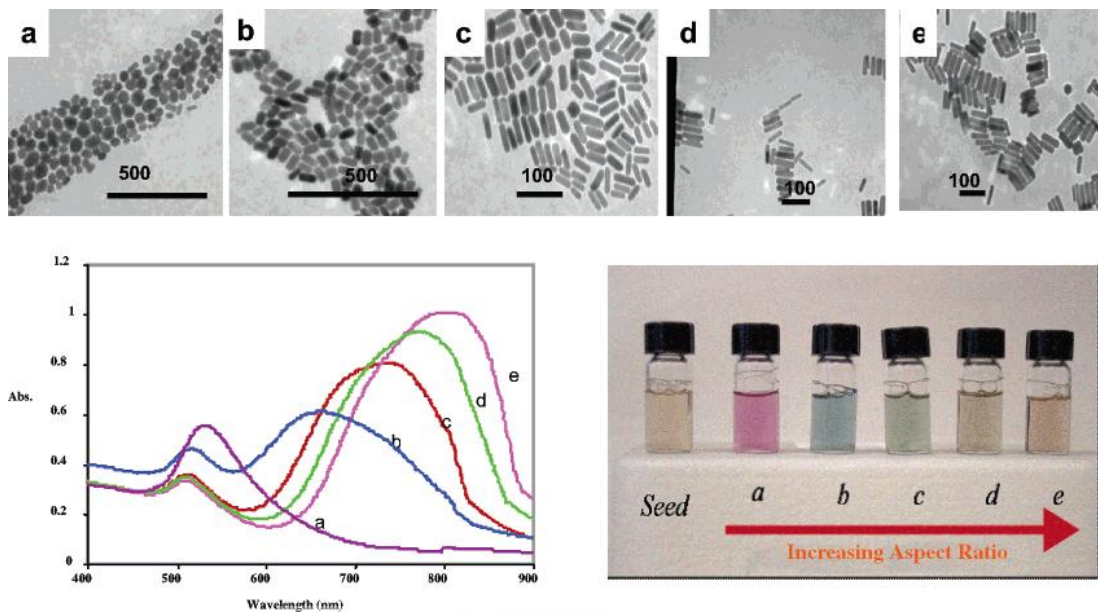


Figure 1.15 The UV-Vis spectra, TEM and aqueous solutions of GNRs with different aspect ratio of: (a) 1.35, (b) 1.95, (c) 3.06, (d) 3.50, (e) 4.42 (Murphy et al., 2005).

2.3.1.2 Fluorescence quenching properties of the AuNPs

AuNPs can also quench the fluorescence of nearby fluorophores. This property results from the overlap between the emission spectrum of excited fluorophores and the LSPR band of the AuNPs, also known as the fluorescence resonance energy transfer (FRET) phenomenon (Yeh et al., 2012). Xue and co-workers (2013) investigated the quenching effect of AuNPs of different shapes and sizes. The AuNPs studied quenched the fluorescence of the fluorophore perylene diimide. The authors concluded that the quenching ability was dependent on both the shape and the size of the AuNPs, in which the smallest spherical AuNPs had the strongest quenching effects (Xue et al., 2013).

2.3.2 Potential of AuNPs in biomedical applications

The wide use of AuNPs in biomedical applications is attributed to their versatility. In addition to the physicochemical properties of the AuNPs, which hugely dictate their

biomedical use, the ability to modify or control other features of the AuNPs can also have an impact in determining their role in biological systems.

2.3.2.1 Controllable morphologies

AuNPs can be fabricated in different sizes, shapes and structures that make them useful for a specific biomedical application (Zhang, 2015) (Figure 1.16). Because of the position LSPR of the AuNRs near the NIR for example, they are considered excellent materials for *in vivo* biomedical imaging and drug delivery applications (Ma et al., 2013). Gold nanoshells (AuNSs) have spherical structures and comprised of a silica core surrounded by a thin layer of gold (Zhang, 2015). AuNSs can have their optical properties adjusted by controlling the core diameter and shell thickness and thus included in microscopy and biomedical imaging (Jihyoun Lee et al., 2014). Another form of AuNPs that are included in many biomedical applications, such as cancer treatment and as antibacterial agents, are the gold nanospheres (AuNSPs). AuNSPs are solid balls of gold synthesized by the chemical reduction of chloroauric acid (Zhang, 2015). Other types of the AuNPs include hollow gold nanospheres and nanocages, which have photothermal properties (Zhang, 2015). Because of their facile synthesis compared to other morphologies, spherical AuNPs have received more attention from researchers in the literature (Zeng et al., 2011).

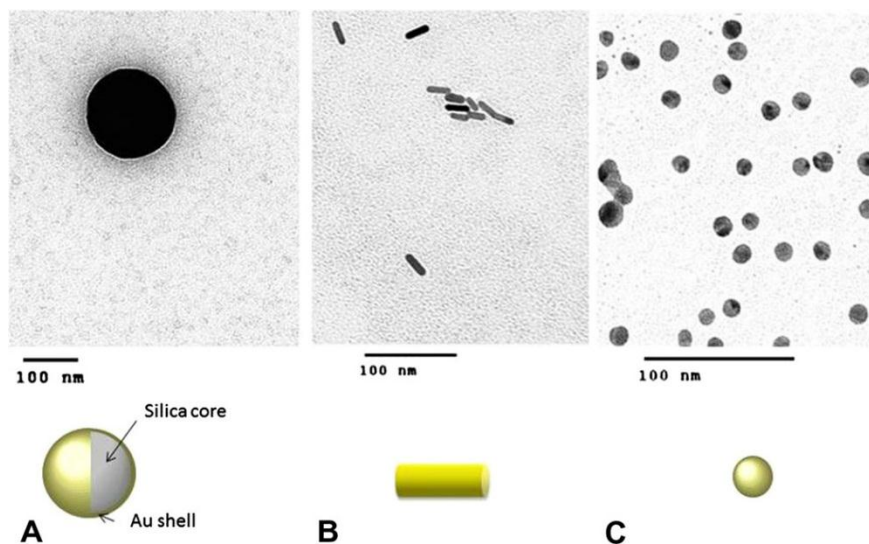


Figure 1.16 Schematic illustrations and electron microscope images of the different shapes of AuNPs; (A) AuNSs, (B) AuNRs and (C) AuNSPs (Jihyoun Lee et al., 2014).

Further, the size of the AuNPs can determine their role in biomedical applications. The size of the AuNPs can influence their cellular uptake, *in vivo* distribution and pharmacokinetics (Au et al., 2010a; Li and Huang, 2008). The blood circulation duration of the AuNPs and their accumulation location and the ability of the body to excrete them are also affected by their sizes (Cobley et al., 2011). The size of the AuNPs can also control their interaction with the biomolecules located extra- or intracellularly (Zhang, 2015). A study by Jiang et al. (2008) showed that AuNPs of 40 and 50 nm coated with antibodies caused membrane receptor internalization and induced cell responses more than other AuNPs of other sizes (Jiang et al., 2008).

The size of the AuNPs also plays an important role in their passive targeting to tumour cells. As the spaces in the tumour capillaries are larger (100 nm to 2 μ m) than those in the endothelial lining of normal vessels, AuNPs can easily gain access to the tumour mass through the damaged surfaces of the blood vessels that supply nutrients to the tumour cells (Yuan et al., 1995). Moreover, AuNPs can be retained in the tumour cells because of the absence of lymphatic system in the tumour mass (Zhang, 2015) and also because of low diffusivity of the AuNPs (Pluen et al., 2001). This ability of the AuNPs

to target the tumour cells is referred to as the enhanced permeability and retention (EPR) effect (Figure 1.17).

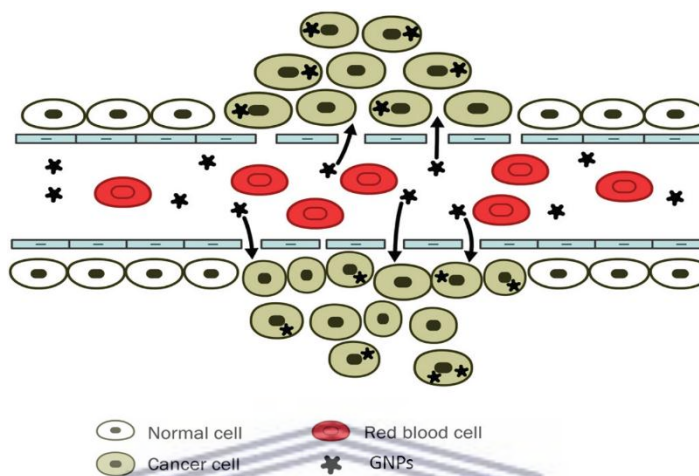


Figure 1.17 Schematic diagram showing the accumulation of AuNPs in cancer cells through the gaps in the endothelial cells (leaky tumour vasculature) (Lim et al., 2011).

2.3.2.2 *Controllable surface chemistry*

AuNPs can provide an excellent platform by which biomolecules are delivered to a certain location in the body. Through functionalization (or conjugation) of the AuNPs, biomolecules can be attached on their surface. This process can be done chemically using chemical functional groups or by means of electrostatic interaction between the biological molecules and the AuNPs (DeLong et al., 2010).

Despite being mostly non-reactive, the surface of gold can establish stable gold-thiolate bonds to molecules with thiol ($-SH$) or disulphide ($S-S$) groups (Cobley et al., 2011). Long hydrocarbon chains ligands (capping agents) with thiol or disulphide groups can protect the colloidal gold from aggregation and increase their stability in different biological conditions (DeLong et al., 2010). For example, Mercaptocarboxylic acids are commonly used NPs ligands that can be adsorbed on the surface of the AuNPs with their ($-SH$) inner end (Figure 1.18). The outer end of these ligands ($-COOH$) provides

an electrostatic repulsions that maintain the stability of the AuNPs (DeLong et al., 2010). Another example of a stabilizing ligand is Polyethylene glycol (PEG), which can provide stability to the AuNPs by increasing the steric bulk effect (Kanaras et al., 2002). PEG can also prevent the uptake of the AuNPs by the reticuloendothelial system (RES), which provides longer blood circulation for the AuNPs (Cobley et al., 2011). It is also possible to replace a bounded capping agent with another for surface modification. For instance, PEG can replace other capping agents by mixing with AuNPs for few hours (Au et al., 2010b).

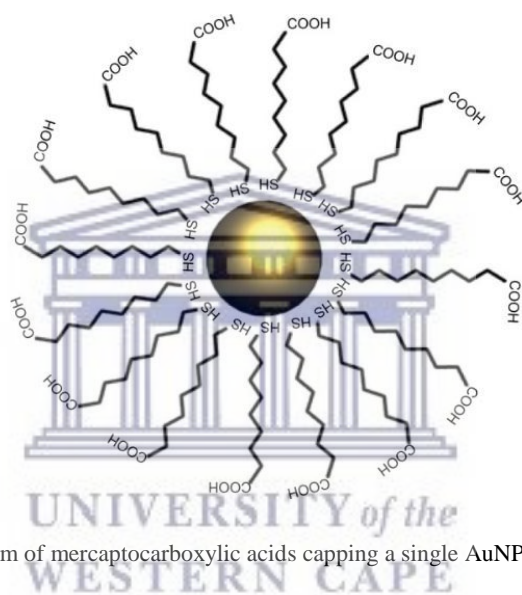


Figure 1.18 Schematic diagram of mercaptocarboxylic acids capping a single AuNP (DeLong et al., 2010).

Biomolecules can also be attached onto the surface of AuNPs through electrostatic interactions (DeLong et al., 2010). For instance, positively charged AuNPs can bind with the phosphate ester backbone of nucleic acids, or the negatively charged carboxylate groups (DeLong et al., 2010).

Thiolated biomolecules can bind with the AuNPs via thiol-thiol interactions. One example of this is the conjugation of thiolated aptamers with AuNPs for sensitive and selective detection of cancer cells by utilizing the optical properties of the AuNPs and the selectivity of aptamers (Medley et al., 2008)

Moreover, biomolecules can be attached to AuNPs by conjugate chemistries (click chemistry) (Cobley et al., 2011). One of the common protocols used to achieve this is the binding of (–COOH) of a capping agent (in mercaptocarboxylic acids for example) with an amino group of a biomolecule using 1-ethyl-3-(3-dimethylaminopropyl) carbodiimide (EDC) HCl-mediated reaction as shown in Figure 1.19 (Sperling et al., 2006).

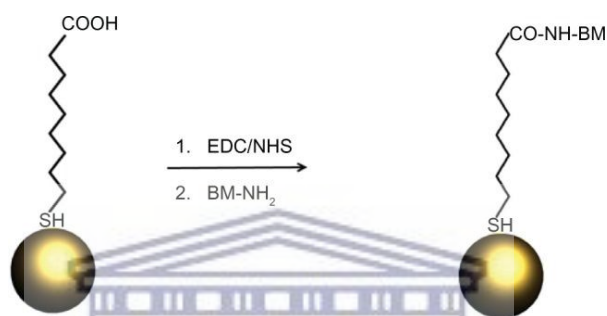


Figure 1.19 Schematic diagram showing EDC-mediated functionalization of AuNPs (DeLong et al., 2010).

Abbreviations: BM, biomolecules; NHS, N-hydroxysuccinimide

2.3.2.3 *Nanotoxicity and bioavailability of the AuNPs*

There is a high concern regarding the toxicity of the AuNPs considered for any biomedical application, and hence it is important to evaluate their potential toxicity both *in vitro* and *in vivo* (Fraga et al., 2013; Kagan et al., 2005). Large number of studies evaluated the toxicity of AuNPs by investigating their cellular uptake, intracellular localization, apoptotic effects, DNA damage, bio-distribution, organ accumulation and elimination and their effect on the immune system (Jia et al., 2017). Interestingly, there have been conflicting reports regarding the toxic effects of the AuNPs (Mukherjee et al., 2016; Patra et al., 2007; Peng et al., 2009; Zhang et al., 2009), possibly because of the variations in the experimental conditions among the published literature that usually entail different cell lines, tissues, organs and the use of animal models with different administrative routes, doses and exposure time. Also, the use of

AuNPs of different physicochemical properties can play a part in the variation of the results from the different studies (Alkilany and Murphy, 2010). Pan et al. evaluated the toxicity of AuNPs of different sizes (0.8 to 15 nm) on different normal and cancerous cell lines. They found that AuNPs with particles size of 1.4 nm induced the highest toxicity with IC_{50} value ranging from 30 to 56 μ M. Conversely, 15 nm AuNPs were nontoxic up to 100-fold higher concentrations than the smaller particles. In their study, not only different sizes of AuNPs induced different cell toxicity but also different cellular responses. 1.4 nm AuNPs were found to induce rapid cell death *via* necrosis after 12 h of incubation, whereas the 1.2 nm AuNPs caused programmed cell death by apoptosis (Pan et al., 2007). Another study by Favi et al. investigated the cytotoxicity of gold nanostars (AuNSTs) and AuNSPs on human skin fibroblast and rat fat pad endothelial cells. The AuNSPs in their study exhibited lethal concentration at 40 μ g/mL for both cell lines. In comparison, the AuNSTs only showed lethal dose at 400 μ g/mL. The authors concluded that AuNSTs may prove safer material for biomedical applications (Favi et al., 2015).

The coating material also determines the toxicity of the AuNPs. Fraga et al. tested the cytotoxicity of 20 nm AuNPs in human liver HepG2 cells with two surface coatings, citrate and 11-mercaptopundecanoic acid (MUA). Although both AuNPs did not show cytotoxicity, yet the citrate AuNPs induced genotoxicity in contrast to the MUA-AuNPs. The authors highlighted the impact of the surface coating on the safety of the AuNPs (Fraga et al., 2013). Further, the cytotoxicity of AuNPs stabilized with citrate and two natural stabilizers (starch and gum arabic) was evaluated by Vijayakumar and Ganesan. The citrate AuNPs showed high toxicity on the cell lines used in their study, and the author highlighted the role of high acidity of the citrate for such toxicity (Vijayakumar and Ganesan, 2012). Another study by Freese et al. measured the cytotoxicity of different sizes of AuNPs stabilized with different concentrations of sodium citrate. The authors reported increased cell death with the increase in the amount of citrate coating the AuNPs. The authors recommended that the amount of

sodium citrate should be monitored to ensure the biosafety of the citrate AuNPs (Freese et al., 2012).

While it is generally accepted that AuNPs are toxic both *in vitro* and *in vivo* at a certain range of concentrations, yet the toxicity can be reduced or eliminated with proper surface modifications (Jia et al., 2017). A report by Truong et al. studied the influence of the AuNPs surface functionalization *in vivo* on dechorionated embryonic zebrafishes. The AuNPs used were functionalized with three ligands: 2-mercaptoethanesulfonic acid (MES), N,N,N-trimethylammoniummethanethiol (TMAT), or 2-(2-(2-mercaptoethoxy)ethoxy)ethanol (MEEE). TMAT-AuNPs were toxic to the embryos, while MES-AuNPs exhibited sublethal malformations. In the molecular level, both TMAT and MES-AuNPs caused inflammation, immune response and misregulation of transport mechanisms to the exposed embryonic zebrafishes. In contrast, the MEEE-AuNPs showed no biological response. The authors concluded that the surface functionalization of the AuNPs can influence the biological response (Truong et al., 2013).

Ultimately, in order to include the AuNPs in biomedical applications, they will be administered into living systems at either the cellular or organismal levels. These systems contain a variety of electrolytes, proteins, nutrients, metabolites, etc. Therefore, it is expected that these AuNPs will interact with these biomolecules, which can lead to changes in their physicochemical properties such as hydrodynamic size, surface charge and colloidal stability, and thus it is important to measure the chemical and physical changes that occur to the AuNPs after introducing them to such living systems (Alkilany and Murphy, 2010).

Similarly, the growth media for any cell line (for *in vitro* studies) consist of serum proteins, essential amino acids, vitamins, electrolytes and other chemicals such as antibiotics. These components could interact and alter the physicochemical properties of the AuNPs (Alkilany and Murphy, 2010). For instance, aggregation of the AuNPs *via* electrostatic forces can occur after mixing with biological media that contain electrolytes with high ionic strength (Vesaratchanon et al., 2007). The aggregation of

the AuNPs can change their interactions with the cells, leading to difficulties in interpreting the data concerning their uptake and bio-distribution (Alkilany and Murphy, 2010). The protein contents found in biological media can undergo non-specific binding on the surface of the AuNPs resulting in changes in both surface charge and chemistry and the formation of protein “corona” around the AuNPs (Nel et al., 2009). Cationic and anionic AuNRs were found, for example, to adsorb proteins, e.g. bovine serum albumin (BSA), from the growth medium after only 5 min of mixing. This interaction resulted in an increase in the particles’ diameters and a change in their surface charge to a value equal to the charge of the serum proteins (Alkilany et al., 2009). The investigation of the AuNPs’ stability and biocompatibility can be done by observing the changes in their LSPR bands, sizes or surface charges after the incubation with different biological media (Elbagory et al., 2017) or buffer solutions with different pH values (Wagers et al., 2014).

2.3.2.4 Examples of biomedical applications of the AuNPs

2.3.2.4.1 Photodynamic therapy (PDT)

PDT is an alternative therapy that aims to treat cancer with less side effects associated with the conventional cancer therapy such as chemo and radiotherapy (Lucky et al., 2015). PDT uses photosensitizers (PS) that can be activated using laser of a specific wavelength at the tumour site. The activation of the PS leads to the generation of energy that can be transferred to the molecular oxygen resulting in the production of reactive oxygen species (ROS) that can oxidize cellular molecules causing tumour cell death (Elahi et al., 2018; Lucky et al., 2015). Besides treating oncological diseases, PDT is considered in the treatment of skin and infectious diseases (Elahi et al., 2018). AuNPs are excellent carrier system for the PS for improved targeting to the tumour site. Wieder et al. (2006) showed, for example, that the AuNPs conjugates with the PS,

phthalocyanines, were taken up by HeLa cells, which resulted in more than twice the cell death compared to the free phthalocyanines (Wieder et al., 2006).

2.3.2.4.2 Photothermal therapy (PTT)

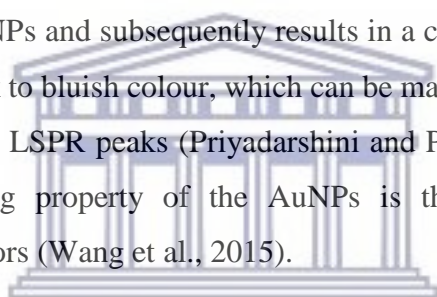
PTT, also known as thermal ablation or optical hyperthermia, is well recognized in the treatment of cancer (Riley and Day, 2017). AuNPs induce heat when exposed to light energy at the targeted tumour cells leading to cell death (Riley and Day, 2017). This phenomenon is a result of the unique optical properties of the AuNPs. The amount of the heat generated by the AuNPs is, therefore, highly dependent on their shape and size (Kim and Lee, 2017).

2.3.2.4.3 X-ray imaging as contrast agents

In medical x-ray imaging, a contrast agent is used to increase the contrast between tissues with similar and/or low x-ray attenuation without the need to increase the radiation dose to the patient (Cole et al., 2015). Recently, a clinical study reported the risk of developing thyroid dysfunction after the sudden exposure to high levels of iodinated contrast agents (Rhee et al., 2012). AuNPs represent a high x-ray absorption coefficient compared to the recognized x-ray contrast agents such as barium sulphate or iodinated compounds, and hence AuNPs can be employed as a safer x-ray contrast agent for enhanced images' resolutions (Elahi et al., 2018). AuNPs can also overcome the limitations of some x-ray contrast agents. For instance, as opposed to the tri-iodobenzenes, an iodinated x-ray contrast agents, AuNPs can deliver longer imaging window for their longer vascular retention time (Hainfeld et al., 2006). AuNPs can be also considered a safer alternative without posing the risk of developing side effects by administering higher doses of the tri-iodobenzenes to overcome their rapid systemic elimination (Elahi et al., 2018; Hainfeld et al., 2006).

2.3.2.4.4 Sensors

Sensors are devices that produce detectable responses to physical alterations or changed chemical concentrations (Li et al., 2010). Sensors consist of a sensing element to provide selective binding to an analyte (such as metal ions, small molecules, proteins and nucleic acids, etc.), and a signal transducer for signalling the binding event (Saha et al., 2012). The detection of chemical and biological agents using sensors has many applications in biomedical, forensic and environmental sciences in addition to anti-bioterrorism applications (Saha et al., 2012). AuNPs are considered important materials in the fabrication of novel sensors (Saha et al., 2012). For instance, in colorimetric-based sensors, the binding of the target analyte to AuNPs' surface leads to the aggregation of the AuNPs and subsequently results in a change in the colloidal gold's colour from red or pink to bluish colour, which can be manifested with the broadening and the red-shift in the LSPR peaks (Priyadarshini and Pradhan, 2017). Utilizing the fluorescence quenching property of the AuNPs is the basis for fabrication of fluorescent-based sensors (Wang et al., 2015).



UNIVERSITY of the
WESTERN CAPE

2.3.2.4.5 Drug delivery carriers

Drug delivery is a process by which the biologically active molecules (drugs) can be released at a certain rate in a specific location in the body (Kong et al., 2017). The concentration of the drugs is therefore increased at the target site (*via* passive and active targeting) without the exposure to the healthy tissue leading to reduced toxicity of the drug (Peer et al., 2007). Drug delivery can also improve the drugs' solubility, *in vivo* stability and pharmacokinetics (Ghosh et al., 2008). The different properties of the AuNPs make them excellent carriers in the drug delivery systems (DDSs). The high surface-to-volume ratio of the AuNPs allows the loading of large drug payload on their surfaces (Elahi et al., 2018). Also, the ERP effect of the AuNPs provides the basis for the selective targeting to the action site (Peer et al., 2007). AuNPs can carry multiple

drugs, proteins, vaccines, genes or nucleotides. They can also control their load release by internal biological triggers or externally by light activation (Kong et al., 2017).

2.3.3 Synthesis of the AuNPs

Generally there are two approaches for AuNPs synthesis; the top-down and bottom-up approaches (Figure 1.20). The top-down approach aims to fabricate nanoscale materials by physically breaking down bulk materials using externally controlled tools to cut, grind, mill and shape materials into a desired shape and size (Nath and Banerjee, 2013). This approach includes, ball milling, lithography and laser ablation (Elahi et al., 2018; Eustis and El-Sayed, 2006). In laser ablation for example, colloidal NPs solutions with tunable properties can be synthesized by reducing gold salt by the photo-induced effects of a 532 nm laser beam (Elahi et al., 2018). Although this synthesis method is considered a green approach to synthesize AuNPs, yet its main drawbacks is the high energy required per unit of AuNPs produced and the limited control over the growth rate of the AuNPs (Nath and Banerjee, 2013). Ball milling is another physical approach for the synthesis of AuNPs in which moving balls apply their kinetic energy to the crushed material leading to the breakage of the chemical bonds and the reduction in size of the crushed material (Xing et al., 2013). Ball milling can create high pressure and temperatures (above 1000 °C) (James et al., 2012), which limits its use for research purposes. Generally, the top-down method is limited due to the difficulty in controlling the size and shape of NPs (Nguyen et al., 2011).

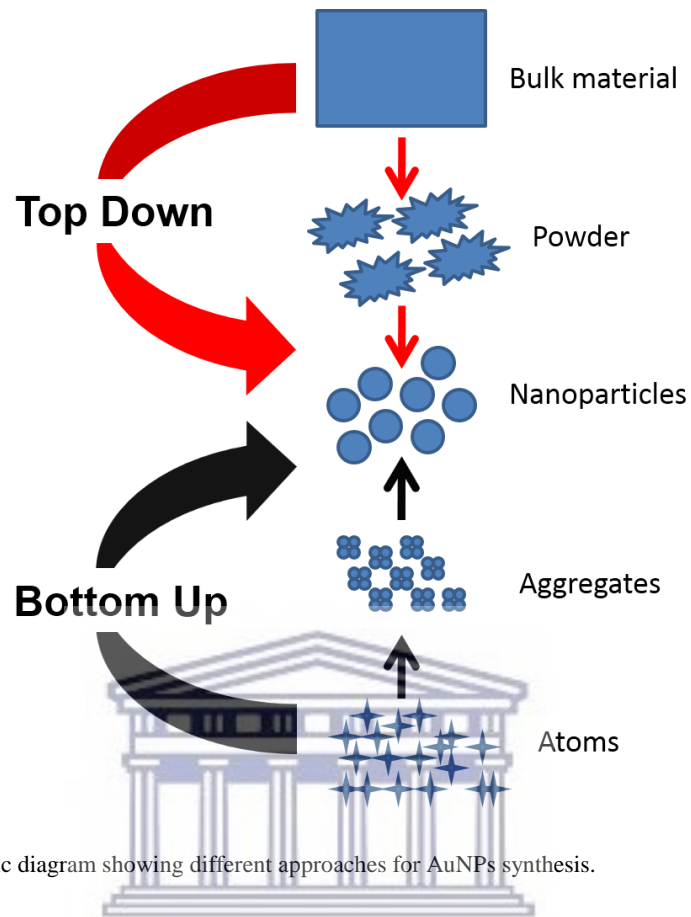


Figure 1.20 Schematic diagram showing different approaches for AuNPs synthesis.

On the other hand, the bottom-up approach is based on the self-assembly of atoms into nanoscale structures (Figure 1.20) (B. Ahmad et al., 2017). Sedimentation and reduction techniques, including sol gel, chemical reduction, green synthesis and spinning are examples of the bottom-up approach (Iravani, 2011) (Figure 1.21).

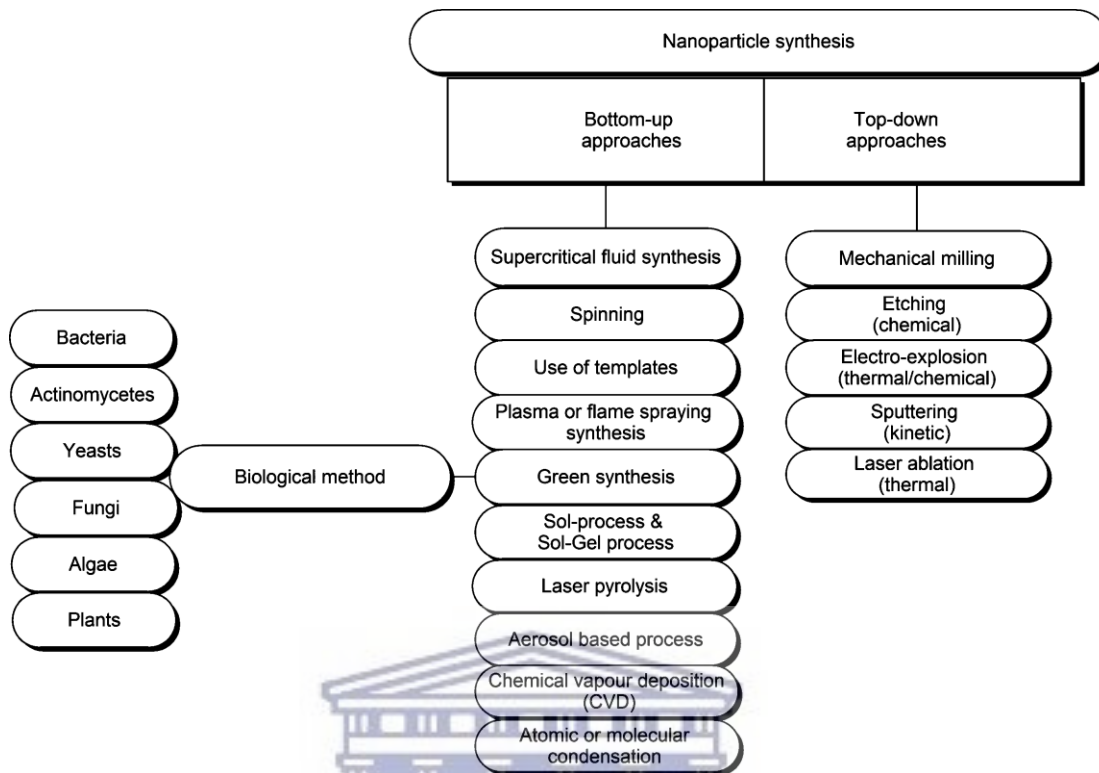


Figure 1.21 Different examples of NPs synthesis techniques (Iravani, 2011).

The AuNPs can be chemically synthesized by reducing the gold precursor (gold (III) tetrachloroaurate) using reducing agents in an aqueous medium. Sodium citrate is a commonly used reducing and anionic stabilizing agent that was first used by Turkevitch et al. to synthesize 15 nm spherical AuNPs (Turkevitch et al., 1951). The Turkevitch method has been modified by several studies to fabricate spherical AuNPs with different diameters ranging from 15 to 150 nm by manipulating different reaction parameters, such as changing the ratio of sodium citrate to the gold salt or altering the reaction's temperature (Tran et al., 2016). The reduction method by sodium borohydride is also used in the synthesis of the AuNPs, which, unlike sodium citrate, is rapid and performed in room temperature (Male et al., 2008). Furthermore, capping agents can be employed to avoid aggregation or further growth of the AuNPs (Zhao et al., 2013). Examples of these capping agents include, sodium citrate, oxygen-based

ligands, phosphorus ligands, sulphur ligands (e.g. thiolates), nitrogen-based ligands, polymers and surfactants (e.g. CTAB) (Zhao et al., 2013).

2.3.3.1 Growth mechanism of the AuNPs

The classical citrate method (reduction of the gold precursor with sodium citrate ($\text{Na}_3\text{C}_6\text{H}_5\text{O}_7$) in aqueous solution near the boiling point) is adapted as a model reaction to understand the mechanism of AuNPs formation, mainly because of its simplicity (among other conventional chemical methods) and its reliability in producing monodispersed AuNPs (Polte et al., 2010).

Polte's research group described the growth mechanism of the citrate AuNPs as a seed-mediated growth (Figure 1.22) (Kettemann et al., 2016). After a few seconds of starting the reaction (addition of sodium citrate to the gold precursor (containing Au^3) at high temperature) around 1–2 % of the gold precursor is reduced (step 1). This is followed by the particle growth by the coalescence of the reduced seeds (nuclei) of the Au^0 leading to the formation of stable seed particles with a diameter of 3 nm (step 2). Afterwards, the remaining precursor is attached and undergo autocatalytic reduction reaction on the surface of these seeds particles (steps 3 and 4), in a step that determines the final particle size. As such, when a higher number of seed particles are formed in the first two steps, which can be influenced by a change of reaction conditions, the remaining precursor is attached on more seed particles (steps 3 and 4) leading to a high number and smaller particles and vice versa (Kettemann et al., 2016). Several studies, however, reported that the growth mechanism of the AuNPs is mediated by the Ostwald ripening of the seed particles rather than their coalescence (Jang et al., 2012; Liebig et al., 2016). In both pathways the particles number decreases with the increase of particle size, and hence it is experimentally difficult to distinguish between the growth due to coalescence and growth due to Ostwald ripening. Thus, a scientifically accepted

mechanism is unattainable and the growth mechanism of AuNPs remains speculative (Polte, 2015).

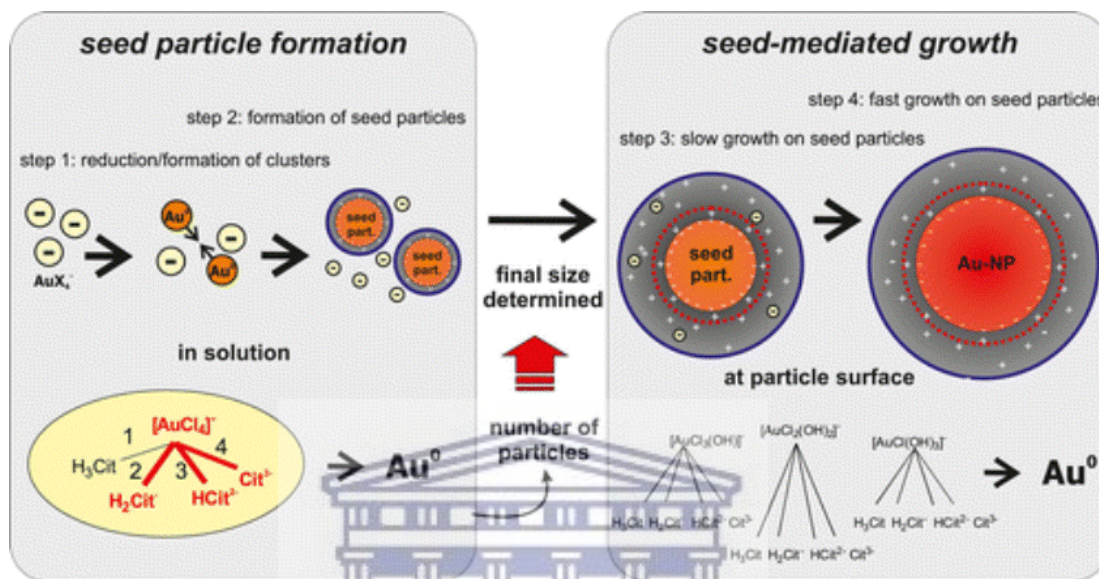


Figure 1.22 Growth mechanism of the citrate AuNPs.

2.3.3.2 Characterization of the AuNPs

The interdisciplinary field of nanotechnology have many characterization techniques that are utilized to measure the morphologies, size, particle size distribution and physicochemical characters of the synthesized NPs. Monitoring the different AuNPs properties is important to determine their stability and their biomedical application.

The LSPR bands of the AuNPs are detected in the visible region using UV-Vis spectroscopy in which an UV-Vis spectrum of a sample is recorded after the exposure to an ultraviolet light beam of different wavelengths. The light beam can promote, at a certain wavelength, the free electrons of the AuNPs to a higher orbital level, which is accompanied by energy absorption by the sample. A computer can then calculate the wavelength (λ_{max}) that caused the highest energy absorption by the sample (Joshi et al., 2008).

In contrast to ordinary optical microscopy, which is limited by the wavelength range of light, the High-Resolution Transmission Electron Microscopy (HRTEM) can investigate the morphology of the AuNPs at the atomic scale whereby a beam of electrons instead of light is used (Bhatia, 2016). This technique when coupled with Energy Dispersive X-ray (EDX) spectroscopy can provide more information on the surface elements of the NPs and estimate their quantities (Joshi et al., 2008).

Further, the particle size of the NPs can be determined by the Dynamic Light Scattering (DLS) technique. This technique detects the Brownian motion phenomenon of the NPs in a solution to estimate their size as smaller particles move quicker than bigger particles (Joshi et al., 2008).

Finally, the Fourier transform infrared spectroscopy (FTIR) can be utilized to determine the surface chemistry of the AuNPs, such as carbonyls and hydroxyls moieties that adhere on the surface during the biosynthesis of the AuNPs (Shah et al., 2015)

2.3.3.3 *Green synthesis of AuNPs*

Most of the chemicals involved in the chemical synthesis of AuNPs are not only flammable and bio-toxic but also hazardous to the environment. Additionally, the conventional chemical methods use high energy and expensive organic chemicals with limited production rate (B. Ahmad et al., 2017). For example, the use of conventional reducing agents, such as hydrazine hydrate, sodium borohydride, dimethylformamide and ethylene glycol, may cause the absorption of harmful chemicals on the surfaces of NPs resulting in adverse effects on the human body (Iravani, 2011). The toxicity of sodium citrate was also studied (Section 2.3.2.3). Hence, there is a growing need for clean, green, biocompatible, cost effective and eco-friendly approach for fabricating AuNPs (B. Ahmad et al., 2017). Using reducing microbial enzymes (from bacteria, fungi, yeast and algae) or the plant phytochemicals set the basis for the green synthesis

(biosynthesis) to reduce the metal salts into their respective NPs (Durán et al., 2011). The biosynthesis of biogenic AuNPs is promising because it is a single-step in nature and can be easily scaled up for large scale synthesis (Ramajo et al., 2009). This approach follows the 12 principles of green chemistry (Table 1.2), which were published in 1998 by Anastas and Werner in the first textbook on green chemistry (Anastas and Warner, 1998). Based on those principles, the biosynthesis of AuNPs involves three main steps: (1) the selection of bio-friendly and nontoxic solvent medium, (2) the use of environmentally benign reducing agent, and (3) the incorporation of safe stabilizing agent (Nath and Banerjee, 2013). Applying these rules through the field of green nanotechnology can lead to the production of inherently safer NPs with reduced hazardous waste generation (Dahl et al., 2007).



UNIVERSITY *of the*
WESTERN CAPE

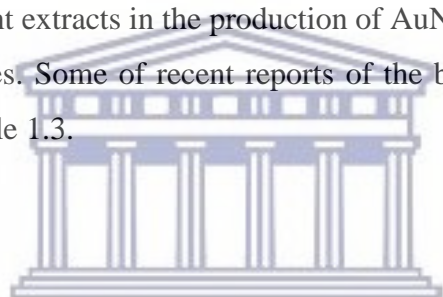
Table 1.2 The 12 principles of green chemistry (Anastas and Warner, 1998).

-
1. It is better to prevent waste than to treat or clean up waste after it is formed
 2. Synthetic methods should be designed to maximize the incorporation of all materials used in the process into the final product
 3. Wherever practicable, synthetic methodologies should be designed to use and generate substances that possess little or no toxicity to human health and the environment
 4. Chemical products should be designed to preserve efficacy of function while reducing toxicity
 5. The use of auxiliary substances (e.g. solvents, separation agents, etc.) should be made unnecessary wherever possible and innocuous when used
 6. Energy requirements should be recognized for their environmental and economic impacts and should be minimized. Synthetic methods should be conducted at ambient temperature and pressure
 7. A raw material or feedstock should be renewable rather than depleting wherever technically and economically practicable
 8. Unnecessary derivatization (blocking group, protection/deprotection, temporary modification of physical/chemical processes) should be avoided whenever possible
 9. Catalytic reagents (as selective as possible) are superior to stoichiometric reagents
 10. Chemical products should be designed so that at the end of their function they do not persist in the environment and break down into innocuous degradation products
 11. Analytical methodologies need to be further developed to allow for real-time, in process monitoring and control prior to the formation of hazardous substances
 12. Substances and the form of a substance used in a chemical process should be chosen so as to minimize the potential for chemical accidents, including releases, explosions, and fires
-

2.3.3.4 AuNPs biosynthesis from plants

The biosynthesis of AuNPs using plants is preferable than the use of microbes. The handling of plant materials is easier, inexpensive and safer compared to microorganisms (Malik et al., 2014). The use of plants to fabricate NPs incorporates the use of several phytochemicals present in extracts e.g. terpenes, carbohydrates, eugenols, polyphenols that contain chemical functional groups like carboxyl, hydroxyl

and aldehydes that undergo the chemical reduction of gold salt into AuNPs (Singh et al., 2010). Similar guidelines are usually adapted by researchers to fabricate AuNPs from plant extracts. First, different plant parts (leaf, bark, stem, root, etc.) are washed, cut into small pieces and mixed with distilled water to obtain their extracts. Secondly, the extracts are filtered and centrifuged to remove undissolved materials. The gold salt can then be mixed in different ratios with the extracts in which the synthesis of the AuNPs can be done using one pot and single step method. The addition of external capping agents may not be needed as the plant phytochemicals act as reducing and capping agents. The change in colour of the mixture to a characteristic red colour of the AuNPs can visually monitor the reaction. Finally, the biosynthesized AuNPs are centrifuged and kept for further characterization. To date, several research groups reported the use of plant extracts in the production of AuNPs of different sizes, shapes and biological activities. Some of recent reports of the biosynthesis of AuNPs from plants are listed in Table 1.3.



UNIVERSITY *of the*
WESTERN CAPE

Table 1.3 Different examples of biosynthesized AuNPs from plants reported recently in the literature.

Plant species	Part of the plant	Size of AuNPs (nm)	Shape of AuNPs	Activity tested	Reference
<i>Abelmoschus esculentus</i>	Seeds	45–75	Spherical	Antifungal	(Jayaseelan et al., 2013)
<i>Actinidia deliciosa</i>	Fruit	7–20	Mostly spherical	Anticancer, antibacterial, catalytic activities	(Naraginti and Li, 2017)
<i>Anemarrhena asphodeloides</i>	Rhizome	190 and 258	Spherical	Anticancer	(Lee et al., 2018)
<i>Citrus maxima</i>	Fruit	25.7±10	Rod and spherical	Catalytic activity	(Yu et al., 2016)
<i>Couropita guianensis</i>	Flower	25–45	Mixed	Anticancer	(Geetha et al., 2013)
<i>Cymbopogon citratus</i>	Leaves	20–50	Mixed	Mosquitocidal	(Murugan et al., 2015)
<i>Kalopanax Cortex</i>	Stem bark	41.07±3.05	Mixed	Anti-ischemic therapy	(Park et al., 2017)
<i>Mentha piperita</i>	Leaves	78	Hexagonal	Anticancer	(N. Ahmad et al., 2017)
<i>Mussaenda glabrata</i>	Leaves	10.59	Mixed	Antibacterial, dye degradation	(Francis et al., 2017)
<i>Nigella arvensis</i>	Leaves	3–37	Spherical	Anticancer, antibacterial	(Chahardoli et al., 2018)
<i>Phoenix dactylifera</i>	Pollen	95	Spherical	Anticancer	(Banu et al., 2018)
<i>Platycodon grandiflorum</i>	Root	14.94 ± 2.14	Mostly spherical	Catalytic activity	(Choi et al., 2018)
<i>Pleuropterus multiflorus</i>	Root	104.8	Spherical	Anticancer	(Castro-Aceituno et al., 2017)
<i>Plumeria alba</i>	Flower	28–15	Spherical	Antibacterial, catalytic activity	(Mata et al., 2016)
<i>Prunus domestica</i>	Gum	5–30	Mostly spherical	Anticancer, antibacterial	(Islam et al., 2017)
<i>Rhaphidophora aurea</i>	Aerial roots	10–35	Spherical	Anticancer	(Jannathul Firdhouse and Lalitha, 2017)
<i>Sphaeranthus indicus</i>	Leaves	25	Spherical	Potential in growth media	(Balalakshmi et al., 2017)
<i>Stereospermum suaveolens</i>	Root bark	27.19 ± 5.96	Spherical	Anticancer, antibacterial	(Francis et al., 2018)
<i>Trianthema decandra L.</i>	Leaves	37.7–79.9	Mixed	Antibacterial	(Geethalakshmi and Sarada, 2013)

2.3.3.4.1 Factors affecting AuNPs reaction with plants' phytochemicals

In addition to the biosynthesis of AuNPs, plant extracts were also used to biosynthesize other metal NPs such as silver, copper, titanium, palladium, platinum, etc. (Chung et al., 2017; Logeswari et al., 2015; Nasrollahzadeh et al., 2015; Siddiqi and Husen, 2016). During the biosynthesis of AuNPs, and MNPs in general, the reducing phytochemicals first convert the metal ions (e.g. gold ions) from their mono or divalent oxidation states to their zero-valent states and then the nucleation of the reduced metal ions takes place (Shah et al., 2015). This is followed by a growth period during which small NPs aggregate to form NPs of different morphologies and sizes (Akhtar et al., 2013). Finally, the phytochemicals surround (cap) the growing NPs and stop their growth at the most energetically favourable morphology (Figure 1.23) (Shah et al., 2015).

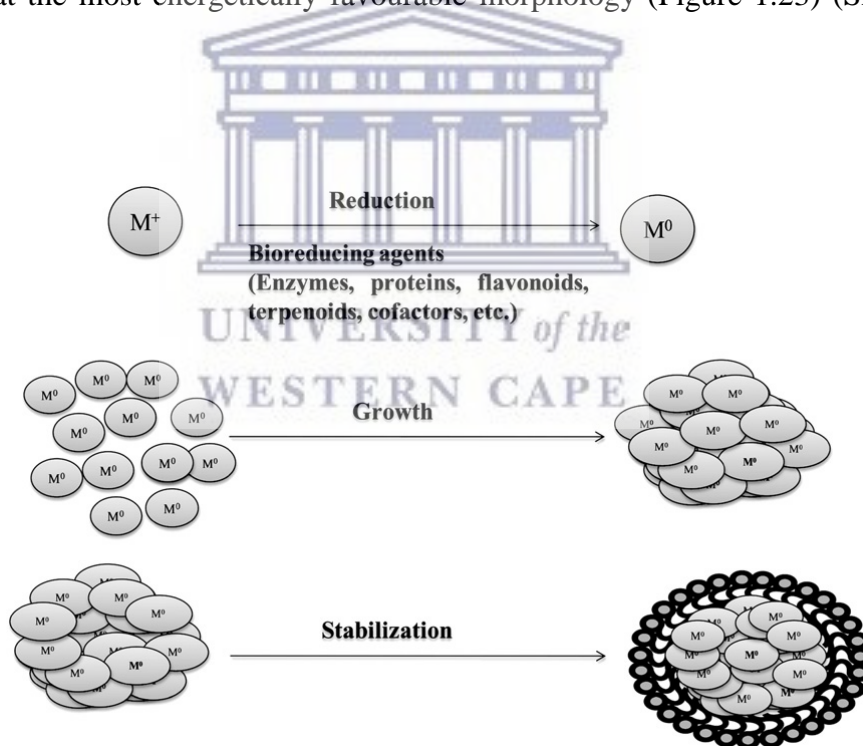


Figure 1.23 Growth mechanism of MNPs using plant extracts (Mittal et al., 2013).

The quality, size and morphology of the produced AuNPs can be significantly influenced by the concentration and type of phytochemicals found in the plant extracts, the pH of the reaction medium, reaction time and temperature.

2.3.3.4.1.1 Influence of pH

Studies have shown that changing the pH value of the reaction medium can influence the morphology and the size of the biogenic AuNPs. Specifically, high pH values can produce smaller particles compared to lower acidic pH values (Dubey et al., 2010). Armendariz and colleagues found that larger (25 to 85 nm) AuNRs can be obtained, using *Avena sativa* (Oat) biomass, at pH 2.0, whereas smaller (5.0 to 20 nm) AuNRs were synthesized at pH values of 3.0 and 4.0. The authors suggested that more functional groups were less accessible at low pH value in contrast to higher pH values (Armendariz et al., 2004). This inaccessibility of the functional groups at low pH would allow the AuNRs to aggregate to form larger particles rather than to nucleate new AuNRs seeds to have smaller sizes (Armendariz et al., 2004).

UNIVERSITY of the
WESTERN CAPE

2.3.3.4.1.2 Influence of plant extract concentration

The concentration of the phytochemicals can also manipulate the biosynthesis of the AuNPs. For example, Chandran et al. showed that varying the volume of the *Aloe vera* extract added to the gold salt dictated the shape of the biosynthesized AuNPs. In their study, the synthesis of triangular AuNPs with large edge lengths was achieved after the addition of 0.5 mL of the *Aloe vera* extract, whereas the addition of 4.0 mL of the extract to the reaction medium led to the reduction of the average edge lengths of the synthesized AuNPs triangles and the formation of more spherical AuNPs (Chandran et al., 2006). Another study by Haung et al. reported the formation of different shapes of AuNPs with varying the amount of *Cinnamomum camphora* (camphor) leaf extract

mixed with the gold precursor (Huang et al., 2007). The authors concluded that a stronger interaction between the phytochemicals and the nascent AuNPs takes place with the increase in biomass. This strong interaction produce spherical AuNPs by preventing the addition of gold atoms to the surface of the AuNPs, which stop the formation (growing) of the AuNPs into other different shapes (Huang et al., 2007).

2.3.3.4.1.3 Influence of reaction temperature

It is generally accepted that any reaction is influenced by changing the temperature. Changes in size, shape and the yield of the AuNPs were observed with varying the reaction temperature (Shah et al., 2015). It was also found that higher temperatures increases the formation rate of the AuNPs (Gericke and Pinches, 2006). In a study by Gericke and Pinches, the formation of AuNRs was favoured at high temperature, while AuNSPs were synthesized at low temperature (Gericke and Pinches, 2006). Further, an increase in the sharpness of the LSPR bands was observed with the increase of the temperature from 25 °C to 150 °C during the biosynthesis of the AuNPs from *Tanacetum vulgare* fruit extract (Dubey et al., 2010). This observation was also reported for the AuNPs synthesized from *Chenopodium album* leaf extract (Dwivedi and Gopal, 2010). As the shape of LSPR bands is dependent on the characteristics of the AuNPs, such as their size, this sharpness of the bands might indicate the production of smaller AuNPs with the increase of temperature (Akhtar et al., 2013). Other studies, however, reported a broadening of the LSPR bands with an increase in the size of the AuNPs at high temperature (Tsi Ndeh et al., 2017). This variation might be because of different heat response from the different phytochemicals found in each plant extract (Dzimitrowicz et al., 2016).

2.3.3.4.1.4 Influence of incubation time

The incubation time, or the time given for the reactants to complete their reaction's steps, is too another factor that can affect the biosynthesis of the AuNPs. Many reports discussed the effect of incubation time and its effect on of the LSPR bands. For instance, the *Chenopodium* leaf extract mediated AuNPs showed sharper absorption peaks with the increase in contact time with the precursor. The LSPR of the *Chenopodium* AuNPs appeared after 15 min citing the formation of the AuNPs in the reaction medium. The reaction continued until 2.0 h at which no more significant changes in the LSPR bands could be detected, which was considered a sign of the absence of newly formed AuNPs (Dwivedi and Gopal, 2010). A similar observation was also reported by Dubey et al. with the AuNPs biosynthesized from Tansy fruit (Dubey et al., 2010). To ensure that the AuNPs are stable after the reaction, it is recommended to have an optimum duration to complete the nucleation phase followed by the encapsulation by the acting capping agents (Veerasingam et al., 2011). A constant λ_{\max} value of the LSPR band over time can also be indication of complete reaction. For instance, Ahmad et al. observed initial increase in the λ_{\max} value after 5.0 min during the biosynthesis of AuNPs from palm seed oil. The authors attributed such observation to the reduction of the gold salt and the increase in the number of the AuNPs. On the other hand, a constant value was reached after 60 min as a result of a complete reduction of the available gold ions (Ahmad et al., 2016).

2.3.3.4.2 Possible phytochemicals involved in the biosynthesis of the AuNPs.

As mentioned in Section 2.3.3.4, the bio-reduction of AuNPs using plants is mediated through the phytochemicals occluded within their aqueous extracts mainly free sugars (polysaccharides) and/or glycosidic containing derivatives (e.g. saponins), proteins, alkaloids and polyphenolic compounds (e.g. tannins and flavonoid derivatives) in

addition to low percentage of lipophilic compounds coming to the solution by cosolvation. These phytochemicals provide polyfunctional matrix that can initiate the reduction of the gold ions and the stabilization of the AuNPs. Moreover, it appears that the reducing action of the plant extracts is not induced by one type of phytochemical, but it differs from plant to another depending on the major contents in each plant. For instance, polyphenols and flavonoids contents were found to be responsible for the formation of AuNPs from black tea (Begum et al., 2009). The AuNPs synthesis from *Memecylon umbellatum* was attributed to the saponin content of the plant (Arunachalam et al., 2013). Organo-sulphur compounds were suggested to be the reducing agents to synthesize AuNPs from *Allium sativum* (garlic) (Rastogi and Arunachalam, 2013). AuNPs were also successfully synthesized from the aldehyde containing cinnamon essential oils (Chanda et al., 2011). The formation of AuNPs from *Cinnamomum camphora* was associated with the presence of terpenoids (Huang et al., 2007). Dzimitrowicz and co-workers concluded that phenolic compounds play essential role in the synthesis of AuNPs from some of Lamiaceae plants (Dzimitrowicz et al., 2016). On the other hand, pure phytochemicals were reported to have dual actions (as reducer and stabilizer) like Epigallocatechin gallate (EGCG) (Nune et al., 2009), apiin (apigenin-7-O-apioglucoside) (Kasthuri et al., 2009), and guavanoic acid (Kasthuri et al., 2009).

2.4 Plant diversity of the Cape Region

The Cape region is located at the southwestern tip of Africa (Figure 1.24) and has a unique flora (plant life occurring in a specific region) that is contrast to the flora of the immediately adjacent lands (Goldblatt and Manning, 2002). The characteristics of the Cape Region Flora (CRF), which is commonly referred to as the Cape Flora or the Core Cape Sub-region of the Greater Cape Floristic Region, are so distinct and unusual that is has been regarded as one of the world's six floral kingdoms. With a total area of 90,000 km² (less than 5% of the total area of the southern African continent), the CRF

has one of the world's botanical diverse flora with estimate 9300 species of plants grow in the region, nearly 70% of which are occurring nowhere else in the world (Manning and Goldblatt, 2012). Among the several plant species that were collected for this study from this region, both *G. africana* and *H. hemerocallidea* are two famous medicinal plants in the South African folk medicine that are discussed further below.

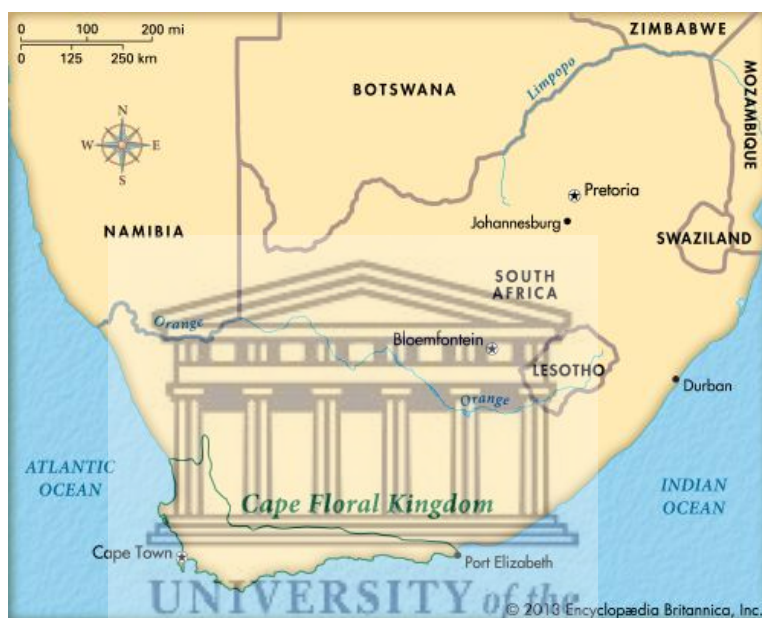


Figure 1.24 Map of South Africa showing the Cape Flora Kingdom or Cape Region Flora.

2.4.1 Background on *G. africana* and *H. hemerocallidea* plants

Of the investigated plants in this study, both *G. africana* and *H. hemerocallidea* are two famous South African medicinal plants. *G. africana* (family: Aizoaceae), also known as “kraalbos” or “geelbos”, is aromatic, woody perennial sub-shrub (Figure 1.25 A). The plant can be found in the area from Northern Cape and Namaqualand to the Karoo and Eastern Cape, South Africa. Kraalbos is active invader and can be spotted around kraals (enclosures for livestock) and along the roads. This plant can grow up to

1 m in height and has small oppositely arranged green leaves that turn yellow with age (Van Der Lugt et al., 1992).

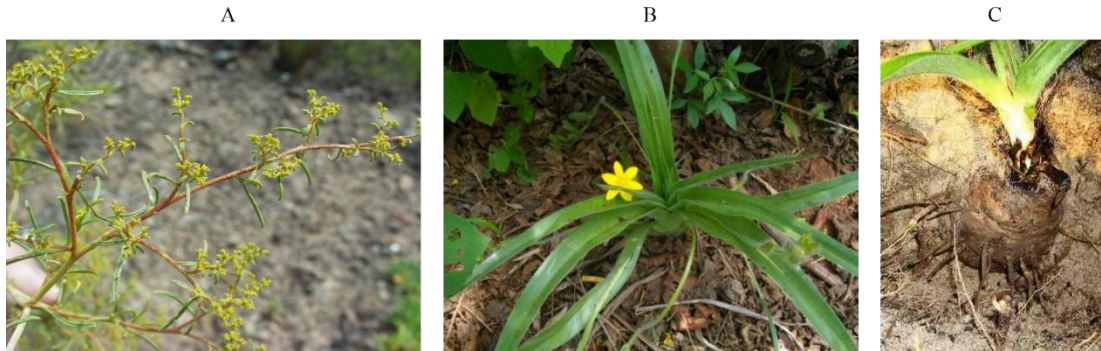


Figure 1.25 Photographs of (A) *G. africana*, (B) leaves and flower of *H. hemerocallidea* and (C) corms of *H. hemerocallidea*.

H. hemerocallidea (Family: Hypoxidaceae) is a geophytic plant that survives winter conditions with the aid of its underground rootstock “the corm”. Figure 1.25 B shows the characteristic “star-like” yellow flower of *H. hemerocallidea*, while Figure 1.25 C shows its corm that can reach a diameter of 10 to 15 cm. When the corms are cut a resinous substance oozes out to seal the wound and prevent infections (Nair, 2006). The genus *Hypoxis* has approximately 90 species, the largest in the family Hypoxidaceae (Bassey et al., 2015). 29 of these species are endemic to South Africa (Singh, 2009). The plant grows in a vast area stretching from the Eastern Cape province to KwaZulu-Natal, to Lesotho, Gauteng, Limpopo and north to Mozambique, Zimbabwe and further north into East Africa (Drewes et al., 2008). The plant has many names in local African languages, but is famous for its English name (African Potato) (Drewes et al., 2008).

Kraalbos is used to treat venereal sores, asthma, coughs and eye infections. Indigenous tribes use the leaves from this plant to relieve toothache (Mativandlela et al., 2009). The corms of *H. hemerocallidea*, on the other hand, are used traditionally to treat psychiatric disturbances and as a diuretic. It is also used to kill small vermin and to treat gall sickness in cattle (Hutchings et al., 1996). The infusion of this plant is widely

exploited by the Zulu tribe to cure impotency (Bryant, 1916). Moreover, the extracts of *H. hemerocallidea* are used to treat many diseases including diabetes, urinary infections, cancer and in the management of HIV/AIDS (Drewes et al., 2008). In addition to these medicinal uses, both *G. africana* and *H. hemerocallidea* plants are also known for their wound healing properties. A lotion from *G. africana* decoction is used to alleviate inflammation and to treat skin diseases (Lall and Kishore, 2014). *H. hemerocallidea* extracts can be applied topically to relieve skin wounds and rashes (Bassey et al., 2015).

Many researchers sought to validate the medicinal importance of *G. africana* and *H. hemerocallidea*. Indeed, many reports illustrated several activities for the two plants as anticancer, antioxidant, antidiabetic, antibacterial, antifungal and in treatment of skin diseases (Drewes et al., 2008; Mabona and Van Vuuren, 2013; Steenkamp and Gouws, 2006; Vries et al., 2005). *G. africana*, for instance, was found to have anti-tuberculosis activity with a Minimum Inhibitory Concentration (MIC) of 0.78 and 1.20 mg/mL against *Mycobacterium smegmatis* and *Mycobacterium tuberculosis*, respectively (McGaw et al., 2008). The 5,7,2-trihydroxyflavanone isolated from *G. africana* has been found to have antibacterial activity against *Mycobacterium smegmatis* and *Mycobacterium tuberculosis* (McGaw et al., 2008). The acetone and the ethanolic extracts of *H. hemerocallidea* have been shown antibacterial activities against *Staphylococcus aureus*. Also, different extracts of *H. hemerocallidea* exhibited efficient antibacterial activity against several bacterial strains. This activity was enhanced when the extracts of *H. hemerocallidea* were combined with other medicinal plant extracts (Ncube et al., 2012).

Little is known about the chemical composition of *G. africana*. Yet, the few chemical reports of *G. africana* revealed that the plant is rich in flavonoids. Three flavanones and two chalcones were isolated from the ethanolic extract of *G. africana*, whose fractions showed also antifungal activity (Vries et al., 2005). Another phytochemical study of the ethanolic leaves extract of *G. africana* led to the isolation of three known flavonoids; (2*S*)-5,7,2'-trihydroxyflavanone, (*E*)-3,2',4'-trihydroxychalcone and (*E*)-

2',4'-dihydroxychalcone, and the new (*E*)-3,2',4'-trihydroxy-3'-methoxychalcone. The 3,2',4'-trihydroxychalcone, in particular, was found to be most active against *M. smegmatis* (MIC = 174.8 μ M) (Mativandlela et al., 2009).

In contrast to *G. africana*, the phytochemical contents of *H. hemerocallidea* are well investigated. The major constituent of *H. hemerocallidea*'s corms was found to be a di-glycoside norlignan called "hypoxoside" (Figure 1.26) (Drewes et al., 1984). Several pharmacological studies reported the activity of the hypoxoside and it is suggested that hypoxoside is mainly responsible for the biological activity of *H. hemerocallidea*. This activity, however, was shown to be increased upon the enzymatic removal of the two glucose units of this compound by β -glucosidase to yield the active aglycone derivative "rooperol" (Figure 1.26) (Drewes et al., 2008).

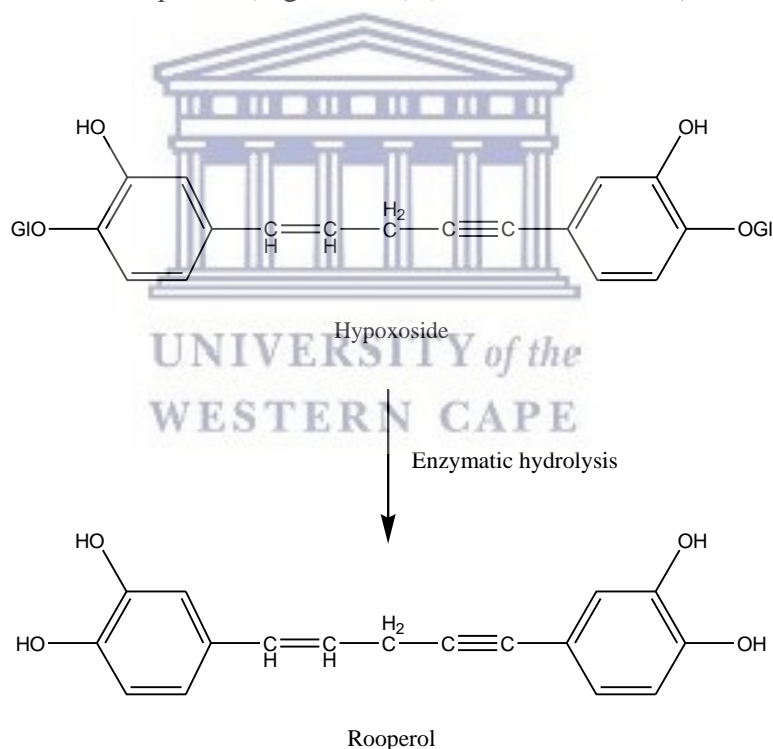


Figure 1.26 Chemical structures of hypoxoside and rooperol.

Further, the gas chromatographic analysis of *H. hemerocallidea* led to the detection of the phytosterol " β -sitosterol" (Boukes et al., 2008). The immune boosting effect of

phytosterols and β -sitosterol is known (Bouic, 2001) and hence might be responsible for the immune modulation activity of *H. hemerocallidea* in the treatment of HIV/AIDS.

2.5 *Wound healing*

Being the largest organ in mammals, the skin covers the entire body surface and serves as a physical barrier against harmful mechanical, chemical and biological damages. Additionally, the skin maintains the physiological homeostasis of the mammalian body (Wang et al., 2018). Skin consists of two layers; a superficial thin or thick epidermis layer and a deeper connective tissue of the dermis layer composed mainly of collagen-rich Extracellular Matrix (ECM). The epidermis is composed of several layers of keratinocytes and separated from the dermis by the basement membrane. The keratinized water-impermeable epidermis layer is mainly responsible for the physical defence of the body, a role shared also by the dermis layer besides its function in supporting the underlying blood vessels, lymphatic system and sensory nerves and in providing flexibility to the skin (Zhong et al., 2010).

Wounds induced by physical, chemical or thermal injuries can disrupt the integrity of the skin and, in other cases, can also cause unwanted anatomical and physiological effects on underlying living tissues (Agyare et al., 2016). The disturbance in the skin integrity can render an individual vulnerable to physiological imbalance, severe disability or death (Wang et al., 2018). When an injury occurs, several cellular and extracellular pathways are activated to restore tissue integrity in a process known as wound healing. These pathways are orchestrated through four synchronized processes of the wound healing starting from the haemostasis (coagulating) response, followed by the inflammation and proliferation stages and finally the remodelling and scar formation (Figure 1.27) (Broughton et al., 2006).

There are two types of wounds; acute and chronic. In the acute wounds, which are usually a result of cuts or surgical incisions, full restoration of the anatomical and physiological features of the injured tissue is completed within the expected timeframe, leading to efficient wound healing (Menke et al., 2007). On the other hand, chronic wounds do not progress through the different stages of wound healing and remain in recurring and prolonged pathological inflammation stage. Factors that can lead to the development of chronic wounds include, bacterial infection, hypoxia, foreign bodies in addition to systemic health issues such as, diabetes mellitus, malnutrition and immunodeficiency (Agyare et al., 2016). The cost of managing chronic wounds related health problems is significant. In the united states, the annual expenditure on such problems exceeds one billion dollars (Ueno et al., 2006).

2.5.1 Wound healing stages

2.5.1.1 Haemostasis stage

At the beginning of the injury, the first response of the body is to halt any bleeding induced by the insult (Broughton et al., 2006). This leads to the vasoconstriction of the blood vessels in the wounded area. The first mechanism of the wound healing is to enforce a balance to the vasoconstriction response of the body through haemostasis (Pool, 1977). Lack of the blood supply to the wound results in hypoxia and acidosis to the affected tissue, which promotes the production of nitric oxide and adenosine along with other vasodilator metabolites that can relax the arteries (Velnar et al., 2009). Vasodilation is also achieved through the release of histamine from mast cells. The relaxation of the blood veins can facilitate the entry of the inflammatory cells to the wound site to initiate the inflammation stage (Singh et al., 2017).

The formation of the blood clot during the haemostasis stage is also an important step to stop blood loss. Blood clot formation is initiated by several intrinsic and extrinsic

pathways to activate the thrombin action and in return leads to the formation of the fibrin plug (Jespersen, 1988). Thrombin also activates platelets to form a platelet plug and trigger the production of critical growth factors that are involved in the regulation of the wound healing process (Singh et al., 2017). The following inflammatory stage is triggered through the production of several inflammatory signalling molecules such as, prostaglandins, leukotrienes and thromboxanes by breaking down of arachidonic acid, which is released as a response to the injured cell membranes (Toy, 2005).

2.5.1.2 Inflammation stage

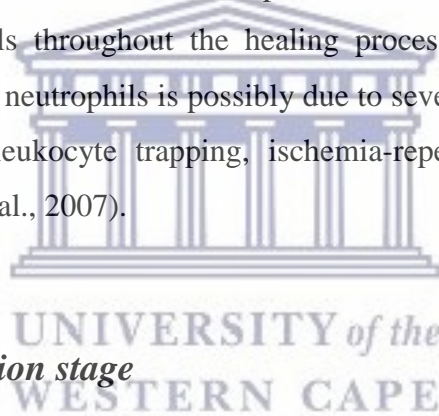
The loss of the physical barrier in wounds renders the body susceptible to the invasion by microorganisms. The main aim of the inflammatory stage is to prevent infections (Broughton et al., 2006). This stage is orchestrated by several immune cells that are activated in the wound site at different time frames. The “first immune responders” are the highly motile neutrophils that infiltrate the wound within an hour (Singh et al., 2017). The release of these phagocytic cells is mediated through several chemical signalling mechanisms including, complement cascade, interleukin (IL) activation and transforming growth factor (TGF) signalling, specifically TGF- β (Singh et al., 2017). Neutrophils can kill bacteria through different mechanisms such as, phagocytosis, the release of toxic molecules and the production of chromatin and proteases “traps” that can capture and destroy bacteria (Broughton et al., 2006; Singh et al., 2017).

Within 48 to 72 h, the larger phagocytic cells, macrophages, arrive to the wound site. Unlike neutrophils, macrophages have a longer life span and can survive the high acidic environment present in the wound site at this stage (Larson et al., 2010). The infiltration of macrophages is triggered by the release of IL-4 from several granulocytes (Mosser and Edwards, 2008). In addition to their role in subsiding infections, macrophages also carry growth factors e.g. epidermal growth factor (EGF) and TGF- β that can initiate the production of different important cells in wound healing process such as,

keratinocytes, fibroblast and endothelial cells (Broughton et al., 2006), promote angiogenesis and stimulate the formation of granulation tissue (Singh et al., 2017). The absence of macrophages in this stage can lead to critical disturbances in wound healing resulting in delayed wound healing (Velnar et al., 2009).

The last immune cells that enter the wound are the lymphocytes, which are incorporated in the production of extracellular matrix scaffold and collagen remodelling (Singh et al., 2017). The inhibition of T-lymphocytes was found to decrease the wound strength and weaken the collagen deposition (Peterson et al., 1987).

The inflammation stage is also critical in determining the final fate of the wound healing. Indeed, the only difference between acute and chronic wounds is in the occurrence of prolonged inflammation response in chronic wounds marked by the presence of neutrophils throughout the healing process (Diegelmann, 2003). The persistent activation of neutrophils is possibly due to several reasons including, tissue trauma by pressure, leukocyte trapping, ischemia-reperfusion injury or bacterial overgrowth (Menke et al., 2007).



2.5.1.3 Proliferation stage

The proliferation stage marks the beginning of a complicated healing cascade, which aims to repair the defected wounded tissues. The different processes of this stage include, angiogenesis, fibroblasts migration and collagen deposition, and epithelization (Singh et al., 2017).

2.5.1.3.1 Angiogenesis

The development of new blood vessels is important in wound healing process and takes place simultaneously during all stages of the repairing process. The angiogenic factors

are secreted during the haemostasis stage to promote angiogenesis (Pierce et al., 1991). Local vascular endothelial cells respond to various angiogenic factors such as fibroblasts growth factor (FGF), vascular endothelial growth factor (VEGF), platelet derived growth factor (PDGF), angiogenin, TGF- α and TGF- β (Velnar et al., 2009). The mixed Metalloproteinases (MMP) secreted from the neutrophils also assist in triggering angiogenesis (Singh et al., 2017). This promotes the proliferation of the vascular endothelial cells in four steps: (1) Release of proteases by endothelial cells to degenerate the basal lamina in the damaged vessels to allow their migration to the ECM; (2) chemotaxis; (3) proliferation; and finally (4) remodelling (Velnar et al., 2009). As the angiogenesis stage continues, the initial avascular wound site develops new capillaries from the offshoots of the intact vessels, which contributes to the tissue oedema and the formation of granulation tissue (Singh et al., 2017).



2.5.1.3.2 Fibroblasts migration and collagen deposition

The haemostatic clot stimulates the proliferation of fibroblasts through the production of growth factors (mainly TGF- β and PDGF) following the wound insult (Goldman, 2004). By the third day, the fibroblasts fill the wound site and produce collagen and fibronectin resulting in the formation of the granulation tissue that replaces the clot (Singh et al., 2017). Considered a key player in the proliferation and remodelling stages of wound healing, collagens are proteins that lay down the foundation of the intracellular matrix within the wound and give unity and strength to all tissues (Velnar et al., 2009). By the end of first week of the insult, the fibroblasts change into myofibroblasts, which attach to fibronectin and collagen in the ECM and assist in contracting the wound and bringing its edges closer (Singh et al., 2017).

2.5.1.3.3 epithelization

The process of epithelial-mesenchymal transition (EMT) allows the epithelial cells to gain motility and move across the wound surface (Yang and Weinberg, 2008). This allows the epithelial cells to migrate from the edges of the wound and cover the wound surface and attach to the underlying matrix. Afterwards, the motile epithelial cells switch to proliferative phenotypes as a result of changes in cytokines concentrations leading to a complete the wound repair (De Donatis et al., 2010).

2.5.1.4 Remodelling stage

The remodelling stage is the final stage of the wound healing process in which the new epithelium is developed and the scare tissue is formed (Velnar et al., 2009). This stage involves a balanced equilibration between the synthesis and degradation of cells with the collagens are deposited in the wound and become more organized (Singh et al., 2017). As the wound healing progresses, the density of fibroblasts and macrophages is reduced by apoptosis (Greenhalgh, 1998). The angiogenesis of new capillaries also stops, the blood flow decreases and the metabolic activity at the wound site declines (Baum and Arpey, 2005). Eventually, the scar matures and its colour changes from red to pink to grey over time (Singh et al., 2017). Figure 1.27 summarizes the whole wound healing stages and the cells involved.

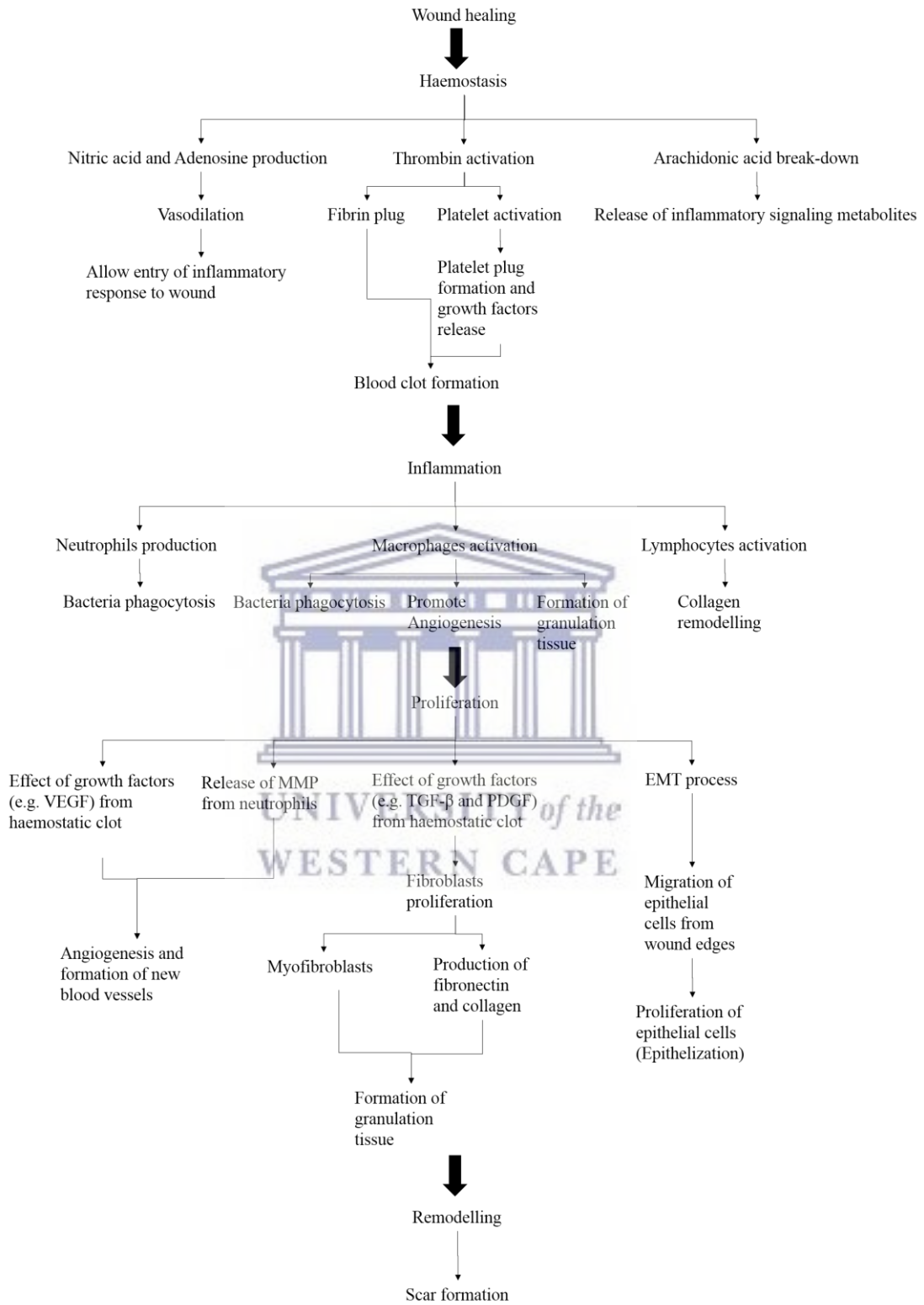


Figure 1.27 Wound healing stages.

2.5.2 Bacterial infection and wound healing

Bacterial overgrowth has been found to affect the wound healing by inducing prolonged pathogenic inflammation (Section 2.5.1.2). This inflammation results from the production of bacterial endotoxin, which leads to the increase of proinflammatory cytokines e.g. IL-1 and tumour necrosis factor- α (TNF- α) (Power et al., 2001). Bacterial infection was also found to decrease platelets number (Robson et al., 1990). Wounds with bacterial infection can undergo severe tissue necrosis accelerated by the production of cytotoxic enzymes and free oxygen radicals (Edwards and Harding, 2004). Additionally, the release of vasoconstrictive metabolites from bacteria aggravates the tissue hypoxia and increase bacterial proliferation (Robson et al., 1990).

Furthermore, the interruption of wound healing process by the bacterial overgrowth is not limited to the inflammation stage. An oedematous, haemorrhagic and fragile granulation tissue and excessive scar formation can occur because of bacterial enzymes (Power et al., 2001). Also, the migration of epithelial cells can be stopped by bacteria (Lawrence, 1987), which can also increase the production of neutrophils proteases that can kill epithelial cells (Orgill and Demling, 1988). Moreover, bacteria associated with wound infections were found to reduce the proliferation of fibroblasts and delay the production of collagen (Robson et al., 1990).

Gram-positive bacteria, such as *S. aureus* and *Streptococcus pyogenes* are commonly found in the initial stage of the skin infection process, whereas Gram-negative microorganisms, such as *Escherichia coli* and *Pseudomonas aeruginosa*, are only detected at a later stage when wound chronicity develops (Cardona and Wilson, 2015).

2.5.3 AuNPs as antibacterial agents in wound healing

There are several *in vitro* assays that can be performed to assess the wound healing ability of any potential wound healing agent. These assays investigate the ability of these agents to affect one or more stages of the wound healing stages to promote effective wound healing. For instance, the overproduction of ROS and proteases secreted by an abnormal high number of neutrophils can overcome the action of proteases inhibitors that protect the normal tissue (Yager and Nwomeh, 1999). Hence, testing the antioxidant activities can be useful in the search for a new wound healing agent that can suppress the effect of neutrophils' oxidants. Measuring the effect of a potential wound healing agent on the proliferation of fibroblasts is another method to assess its efficiency in wound healing during the proliferation stage (Houghton et al., 2005). Furthermore, as bacterial infections are a major cause of chronic wounds (Section 2.5.2), the investigation of the antibacterial activity is also another aspect that can be considered for any potential wound healing agent. Several MNPs, among them AuNPs, have been found to have both bactericidal and bacteriostatic activities (Mohamed et al., 2017) and thus they can also be incorporated in the treatment of wound infections.

Investigating the antibacterial activity of NPs is also important to find new antibacterial therapies against the emerging antibiotic-resistant bacteria (Slavin et al., 2017). This resistance results from several reasons including, the overuse or the inappropriate prescribing of antibiotics, which has led the emergence of untreatable bacterial infections causing significant economic and clinical burdens globally (Ventola, 2015). Figure 1.28 illustrates the different mechanisms of different classes of antibiotics: β -lactams (e.g. penicillin, carbapenems, cephalosporins), aminoglycosides (e.g. amikacin, kanamycin, gentamicin), glycopeptides (e.g. vancomycin, teicoplanin, decaplanin), macrolides (e.g. azithromycin, erythromycin, clarithromycin), tetracyclines (e.g. tetracycline, doxycycline, minocycline), and quinolones (e.g. ciprofloxacin, levofloxacin, moxifloxacin) and the mode of bacterial resistance. β -

lactams, for instance, are four-membered β -lactam ring agents, which kill bacteria by targeting the bacterial enzymes responsible of cell wall biosynthesis (penicillin-binding proteins(PBP)) (Essack, 2001). Several Gram-positive (Bell et al., 2002) and Gram-negative bacteria (Clark et al., 2003) have developed resistance to β -lactams through drug inactivation by β -lactamases, target site alterations of PBP, decreased permeability and efflux (Essack, 2001).

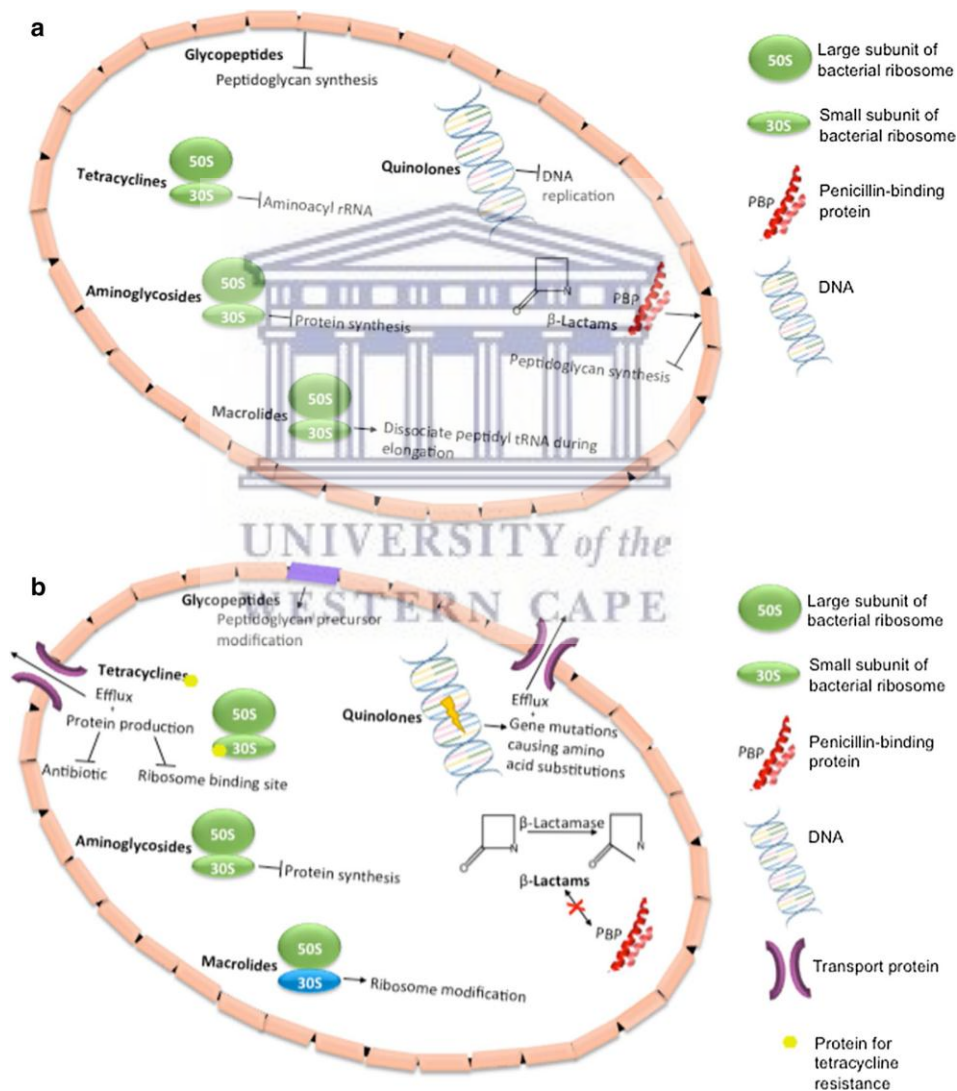


Figure 1.28 A diagram illustrating; (A) mechanisms of action for the different classes of antibiotics; (B) mode of bacterial resistance (Slavin et al., 2017).

2.5.3.1 Antibacterial mechanism of action of AuNPs

There is still uncertainty on how AuNPs, and MNPs in general, undergo their antibacterial action (Wang et al., 2017). Generally, NPs are thought to kill bacteria by: (1) disruption of cell wall; (2) release of ROS (Gurunathan et al., 2012), metal ions (Dutta et al., 2011) or perform non-oxidative mechanisms (Leung et al., 2014); (3) penetration of cell wall; (4) interaction with DNA or proteins to induce the antibacterial effects (Wang et al., 2017). As opposed to the mode of action of the current antibiotics, MNPs act on different bacterial biomolecules at once and exert their antibacterial action by becoming in contact with the bacterial cell wall. It is thus hypothesized that it would be difficult for bacteria to develop resistance against MNPs (Slavin et al., 2017; Wang et al., 2017). It was also found that MNPs can induce their antibacterial effect physically on the cell wall. For example, MNPs with high aspect ratio surfaces, spikes or pillars could rupture bacterial cell wall by applying high local stresses (Sjöström et al., 2016). Penders and co-workers investigated the antibacterial action of the citrate AuNPs of different shapes (spheres, stars and flowers). The authors found that nanoflowers, which has numerous protrusions on their surfaces compared to the other two types were more toxic to the bacteria presumably because of their rough surface (Penders et al., 2017).

MNPs were found to be more active against Gram-negative compared to Gram-positive bacteria (Shamaila et al., 2016). This observation was attributed to the difference in the cell wall structure of different Gram stained bacteria (Shamaila et al., 2016). The cell wall of Gram-positive bacteria have a thick layer of peptidoglycan (e.g. 80 nm in *S. aureus*), whereas Gram-negative bacteria only have a thin layer of peptidoglycan (e.g. 8 nm in *E. coli*) with an extra layer of lipopolysaccharide on their outer layer (Figure 1.29) (Slavin et al., 2017). The thick peptidoglycan is thus may act as a protective layer for the Gram-positive bacteria against the action of the MNPs.

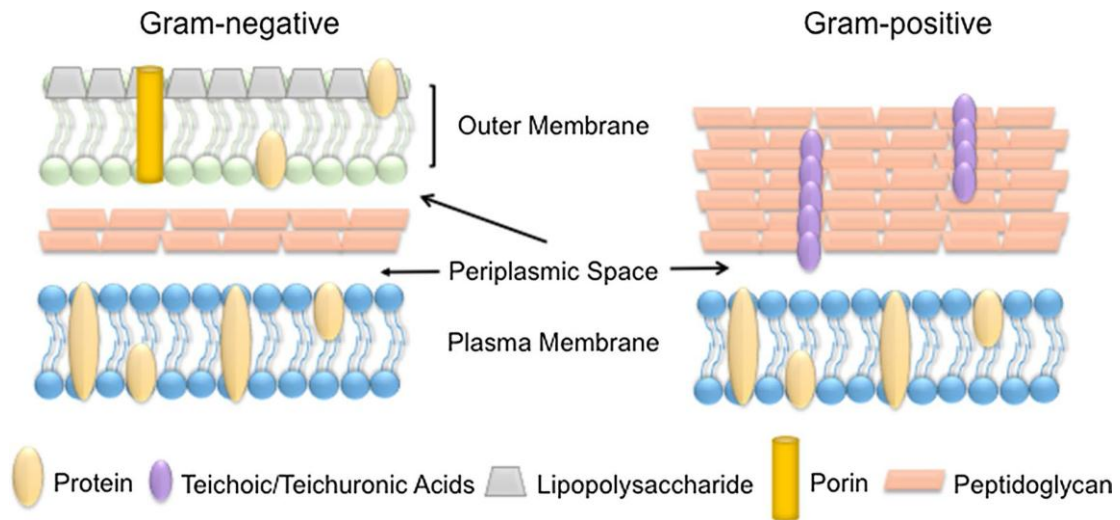


Figure 1.29 Cell wall structure of Gram-positive and Gram-negative bacteria (Slavin et al., 2017).

The electrostatic attraction is another suggested physical interaction between MNPs and bacteria. The negatively charged lipopolysaccharide layer of Gram-negative bacteria can facilitate the biosorption of the positive ions released by most MNPs, which leads to the accumulation and uptake of such ions causing intracellular stress (Slavin et al., 2017). Although Gram-positive bacteria also carry negative charge on their surface, yet it was demonstrated that Gram-negative bacteria are more negatively charged (Sonohara et al., 1995), which may cause stronger attraction between the bacteria and the MNPs (if positively charged) or their released positive ions. Hayden and colleagues illustrated the deposition of cationic AuNPs on the surface of the *E. coli* and *Bacillus subtilis* and concluded that the cationic AuNPs either coalesce on the hydrophobic spots on the cell membrane or the AuNPs aggregate on the anionic regions already present on the bacteria surface (Hayden et al., 2012).

The antibacterial activities of the biosynthesized AuNPs from plants are well established in the literature. The AuNPs from the Chinese *A. deliciosa* showed antibacterial activity against the β -lactam resistant *P. aeruginosa* as determined by their maximum zone of inhibition (Naraginti and Li, 2017). In another study, the zone of inhibition also showed that AuNPs from the Indian *M. glabrata* were toxic to both

Gram-positive and Gram-negative bacteria including *S. aureus*, *P. aeruginosa* and *E. coli* (Francis et al., 2017). *E. coli* was also susceptible to the biosynthesized AuNPs from *Ziziphus zizyphus* (Ennab leaves) (Aljabali et al., 2018).

2.5.3.2 Antibiotics conjugation to AuNPs

MNPs are extensively incorporated in DDSs studies to improve the therapeutic actions of the drugs (Section 2.3.2.4.5). Using MNPs as antibiotics carriers may also prove useful in the management of bacterial resistance or improve the antibiotics' efficiency. For instance, the small size MNPs, which can easily penetrate bacteria, facilitates the cell uptake of antibiotics of poor membrane transport (Wang et al., 2017). Also, as they can avoid bacterial extrusion mechanisms such as efflux, MNPs can assist in avoiding bacterial resistance to antibiotics (Mühling et al., 2009). The side effects of some antibiotics, such as ear and kidney toxicity of vancomycin, can be decreased with the enhanced targeting effect of the MNPs towards infection site (Wang et al., 2017). A controlled (sustained) release of an antibiotic can also be achieved by activating the MNPs through stimulatory responses (e.g. chemical compounds, magnetic field, pH, heat and light) (Lv et al., 2016; Wang et al., 2017; Wu et al., 2016).

Brown et al. used the thioether moiety of ampicillin to conjugate the antibiotic to citrate AuNPs by simple mixing for 24 hr. Intriguingly, the functionalized AuNPs showed bactericidal effect against several bacterial strains, among them β -lactamase gene carrier *E. coli* strain. A similar bactericidal effect was not, however, attainable by the unconjugated AuNPs against any of the tested bacterial strains (Brown et al., 2012). In another study, the citrate AuNPs was also used as a drug carrier for different aminoglycosidic antibiotics. The functionalized AuNPs exhibited higher inhibition zones more than the corresponding pure drugs against different Gram-positive and Gram-negative bacteria (Nirmala Grace and Pandian, 2007).

Further, antibiotics also possess reducing capabilities that enable them to reduce gold ions into AuNPs. The combined reduction power of ampicillin, kanamycin and streptomycin and sodium borohydride was utilized to synthesize AuNPs that demonstrated higher antibacterial activity more than the free antibiotics (Bhattacharya et al., 2012). Kanamycin alone was found to formulate kanamycin-capped AuNPs after 5 min of incubation with gold salt at 80 °C. The antibiotic capped AuNPs were able to kill bacteria including kanamycin resistant strains (Payne et al., 2016).

2.6 Immune system and immunomodulation effects of the AuNPs

A healthy immune system help in fighting infections, diseases or foreign biological invasion without targeting the body's healthy cells to avoid allergies and autoimmune diseases. This system is regulated by several cells, cell products, tissues and organs (Brindha et al., 2016). The immune response, against infections or malignant cells, is controlled by the interaction between an innate (natural and non-specific) and an acquired (adaptive and specific) components of the immune system. The innate immune cells (e.g. macrophages, NK cells, neutrophils and dendritic cells (DCs)) are the first responders against foreign particles. These phagocytic cells kill invading microbes by using a combination of degrading enzymes (e.g. proteases in neutrophils), antimicrobial enzymes and ROS and reactive nitrogen species (RNS) production (Brindha et al., 2016; Hancock and Scott, 2000). The acquired immune cells (B and T lymphocytes) are triggered by the innate cells and use specific antigens, usually small fragments of the pathogen, to identify their targets.

2.6.1 Macrophages

Since their discovery by the Russian zoologist Elie Metchnikoff early last century, macrophages have been long considered a major immune effector cells (Gordon, 2016).

Beside their role in the innate immune response, macrophages also trigger the acquired immune response by expressing fingerprint antigens (histocompatibility complexes (MHC) class II) on their surface in order for the T lymphocytes to recognize the microbes. The T lymphocytes would then activate B lymphocytes to produce antibodies “specific” to the antigens for the microbes to form antibody-bound complexes, which in return increases the activity of the macrophages towards the identified microbes (Arango Duque and Descoteaux, 2014). Yet, these cells have also been shown to contribute in body haemostasis and development (Sieweke and Allen, 2013). Macrophages can clear up to 2×10^{11} erythrocytes in a single day that enable the body to recycle and reuse around 3 kg of iron each year. Additionally, macrophages take part in tissue remodelling by removing cell debris, and can effectively clear apoptotic cells (Mosser and Edwards, 2008). These cells can be found in all body tissues and are differentiated from the CD14⁺ monocytes that are part of the peripheral blood mononuclear cells (PBMCs) (Hopper et al., 2015).

Macrophages are usually at rest and they can be activated by a variety of external stimuli including cytokines (Edwards et al., 2006), microbial components, which can be recognized by Toll-like receptors (TLRs) present on the surfaces of the macrophages (Akira et al., 2006), and a group of host-cell derived “danger signals” (Oppenheim and Yang, 2005). Interestingly, different stimuli give rise to different populations of macrophages. The classically activated macrophages (M1) is activated from monocytes by the action of the cytokines produced from T helper 1 (Th1) cells including, TNF- α and Interferon-gamma (IFN- γ) or lipopolysaccharide (LPS) (Arango Duque and Descoteaux, 2014). The M1 population produce pro-inflammatory cytokines, which induce Th1 immune response (Edwards et al., 2006). M1 macrophages are also known to have microbicidal and cytotoxic activities by releasing ROS and RNS (Nathan and Shiloh, 2000). On the other hand, the M2 populations (M2a, M2b and M2c) include different types of macrophages that vary in their biochemistry and physiological properties (Edwards et al., 2006). Contrary to M1, the different M2 phenotypes increase the immune responses of the T helper 2 (Th2) cells and induce immunosuppression

activities, promote tumour growth and aid in wound healing (Arango Duque and Descoteaux, 2014). For example, M2a macrophages, originally termed alternatively activated macrophages, can stimulate the collagen production during the granulation tissue formation (Mosser and Edwards, 2008). Table 1.4 summarizes the cytokines and other biomolecules responsible for the differentiation of the different macrophages populations and their secretions.

Table 1.4 The different cytokine promoters for the different macrophages phenotypes and their cytokine productions

Macrophage phenotype	Promoters	Cytokines secretions
M1	TNF- α , IFN- γ , LPS	TNF- α , IL-1 β , IL-6, IL-12, IL-23,
M2a	IL-4, IL-13	IL-10, TGF- β , IL-1Ra
M2b	IL-1Ra, LPS, immune complexes, apoptotic cells.	TNF- α , IL-1 β , IL-6, IL-10
M2c	IL-10, TGF- β , glucocorticoids.	IL-10, TGF- β

2.6.2 NK cells

NK cells can be described as lymphocytes with natural cytotoxicity towards cancer cells with cytokines-producing effector functions (Trinchieri, 1989). NK cells are activated through the binding of their NKG2D receptors with activating ligands (such as UL-16 binding proteins and MICA/B), which are expressed in the viral or tumor cells but downregulated in normal cells (Molfetta et al., 2017). NK cells can also be regulated by the action of cytokines. For instance, it was found that IFN- α and - β , IL-12, IL-18 and IL-15 secreted by the DCs can promote the cytotoxicity of NK cells (Walzer et al., 2005). It was also found that IL-2 enhance the proliferation and cytotoxicity of the NK cells (Trinchieri, 1989).

Upon activation, NK cells can kill their targets by one of two pathways. First, activated NK cells can promote apoptosis of target cells by releasing a cell membrane-lysing protein known as perforin and a group of serine proteases-like enzymes (granzymes) (Smyth et al., 2005). The second pathway incorporates the activation of death receptors

(e.g. Fas/CD95) on the target cells by their associated ligands (e.g. FasL) found on NK cells (Smyth et al., 2005). Also, NK cells are a major source of IFN- γ , which promotes macrophages (M1) differentiation (Table 1.4) leading to the production of the pro-inflammatory cytokines and the deployment of more macrophages to counteract the biological stress (Mosser and Edwards, 2008). A similar immune regulatory role by the NK cells is also established with activating DCs and T lymphocytes (Figure 1.30).

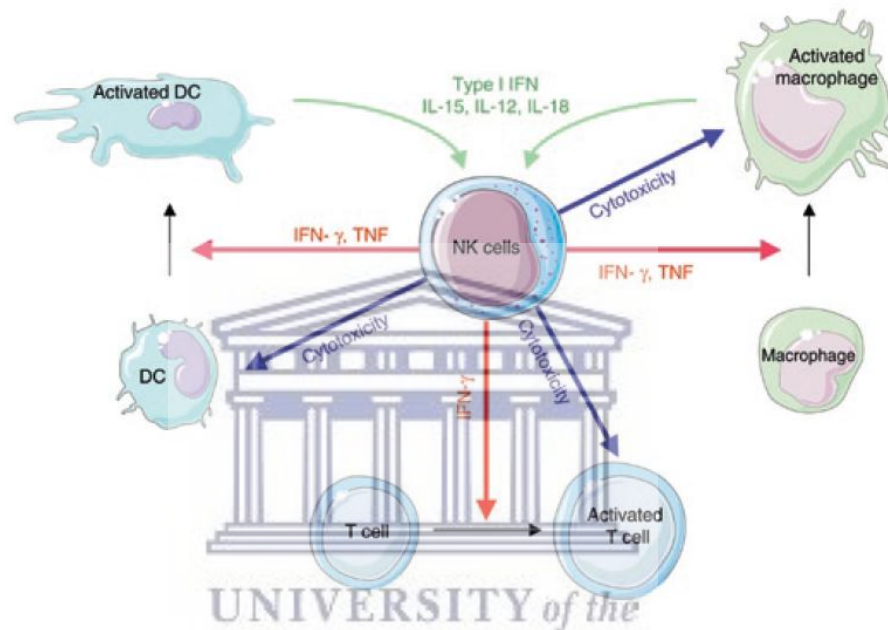


Figure 1.30 Regulation of the DCs, T lymphocytes and macrophages by NK cells. After activating NK cells by DCs and macrophages (green arrows), the activated NK cells in turn activate inactive DCs, T cells and macrophages by secreting IFN- γ and TNF- α (red arrows). The NK cells can also kill the activated T cells and macrophages and inactive DCs cells by inducing cytotoxicity (Vivier et al., 2008).

2.6.3 Cytokines

Cytokines are low molecular weight proteins that control intercellular communication, regulate systemic inflammation, cell proliferation and chemotaxis (Arango Duque and Descoteaux, 2014). When cytokines are produced from lymphocytes (e.g. NK cells) they are called lymphokines. Other names for cytokines include monokines (cytokines from monocytes) and chemokines (cytokines intended for chemotaxis). ILs are also cytokines that are produced by one leukocyte to act on another leukocyte (Zhang and

An, 2007). Since their discovery, there are over 100 types of cytokines identified in the literature, 33 of which are ILs (Dinarelo, 2007). Cytokines can have an autocrine action when acting on the cells that secrete them or paracrine action when acting on nearby cells and in some situations they can have an endocrine action on distant cells (Zhang and An, 2007). It is common to have different cytokines that induce a similar action in a cascade fashion. Additionally, cytokines are pleiotropic, meaning that one cytokine can act on different cells (Arango Duque and Descoteaux, 2014). The combination and individual effect of the cytokines on the immune cells (Figure 1.31) controls the activation and regulation of both the innate and the antigen-specific immune cells, and with their redundant behavior, cytokines present a challenge for immunology researchers to identify a specific role for each cytokine.

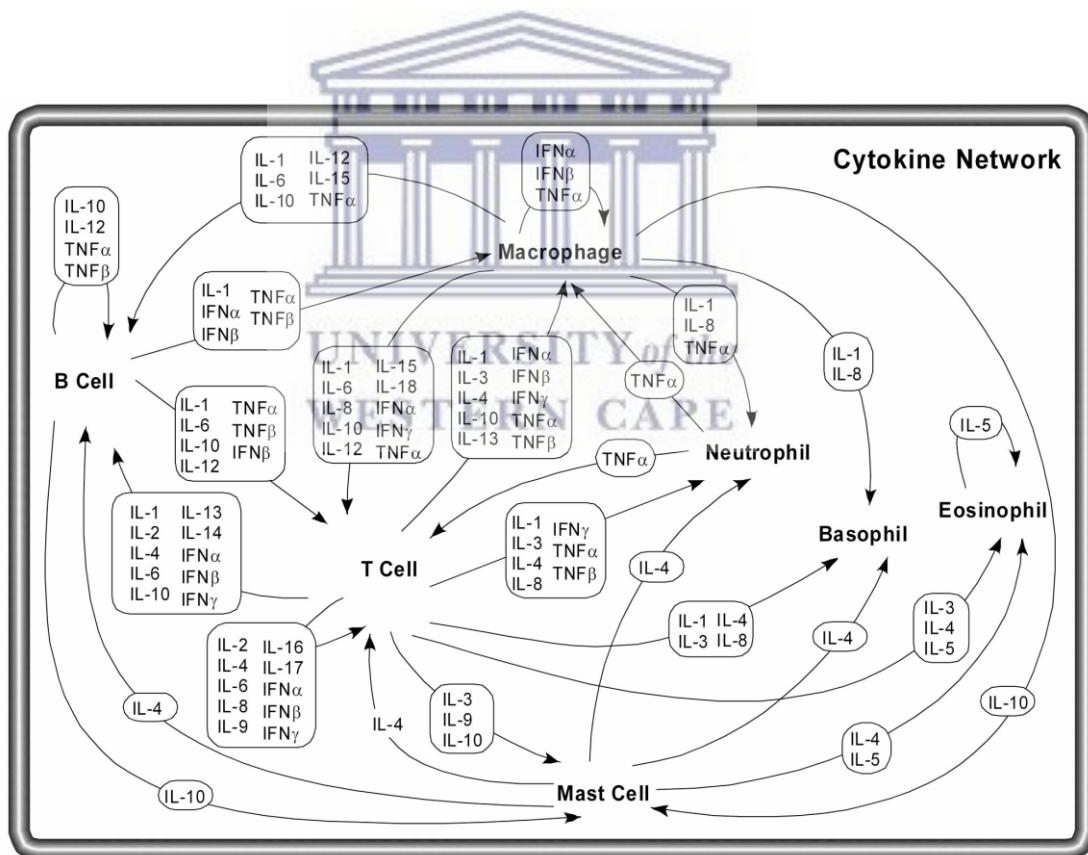


Figure 1.31 The effects of the cytokines on the different immune system cells (Zhang and An, 2007).

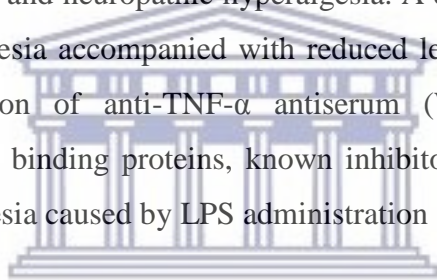
The main function of cytokines is to regulate inflammation, and thus can be grouped into pro- and anti-inflammatory cytokines. The pro-inflammatory cytokines, such as TNF- α , IL-1, IL-8 and IL-12, are mainly produced by monocytes and macrophages, although they can also be secreted by active lymphocytes, endothelial and fibroblast cells (Arango Duque and Descoteaux, 2014). When released because of an inflammatory stimuli, the pro-inflammatory cytokines increase the vascular permeability and rally the inflammatory cells (Arango Duque and Descoteaux, 2014). Although the inflammatory action of the pro-inflammatory cytokines is beneficial to the host, yet the excessive release of these cytokines can be harmful. IL-1 β and TNF- α can cause an acute inflammatory response characteristic to septic shock and multi-organ failure (Beutler, 1999). Thus, the main biological role of the anti-inflammatory cytokines, such as IL-4, IL-10, IL-11 and IL-13, is to establish immunoregulatory effects by regulating the response and secretions of the pro-inflammatory cytokines (Zhang and An, 2007).

2.6.3.1 IL-1 β

IL-1 has three forms; IL-1 α , IL-1 β and IL-1Ra, with the former two being stronger proinflammatory ILs. Monocytes and macrophages are the main producers of IL-1 β in addition to specific lymphocytes, DCs, epithelial and fibroblast cells (Arango Duque and Descoteaux, 2014). IL-1 β is expressed in the host following the occurrence of inflammation stimulus, cell injury, infection or invasion leading to the promotion of both vasodilation and inflammation. This action might be due to the induction of prostaglandin secretion by IL-1 β (Schweizer et al., 1988), which is a principal hormone in acute immune reaction and inflammation (Ricciotti and FitzGerald, 2011). IL-1 β is also involved in histamine secretion from mast cells, which induces vasodilation and localized inflammation (Arango Duque and Descoteaux, 2014).

2.6.3.2 *TNF- α*

Also known as cachectin, TNF- α is another pro-inflammatory cytokine that was initially identified for its necrotic effects on some tumours (Carswell et al., 1975). TNF- α is a pyrogenic (induce fever) cytokine that is dispatched in response to a pathogenic stimulus (Beutler, 1999). TNF- α induces vasodilation and increase the vascular permeability, which is important in the infiltration of immune cells to the action site (Arango Duque and Descoteaux, 2014). TNF- α is one of the main cytokines that cause inflammatory hyperalgesia (pain) (Cunha et al., 1992). Elevated levels of TNF- α and other pro-inflammatory cytokines, such as IL-1 β , were detected upon the interplanar injection of the inflammation inducing Freund's adjuvant in adult rats leading to localized inflammation and neuropathic hyperalgesia. A delayed onset of the induced inflammation hyperalgesia accompanied with reduced levels of IL-1 β was achieved after the administration of anti-TNF- α antiserum (Woolf et al., 1997). The administration of TNF binding proteins, known inhibitors of TNF- α , was found to eliminate the hyperalgesia caused by LPS administration (Watkins et al., 1994).



UNIVERSITY of the
WESTERN CAPE

2.6.3.3 *IL-6*

Being a pleiotropic cytokine, IL-6, which is predominantly secreted by M1 macrophages, can have both pro- and anti-inflammatory functions that are incorporated in several processes ranging from immune regulation to tissue repair and metabolism (Kishimoto, 2010). There is evidence that IL-6 dictates the activation and proliferation of microglia (macrophages of the central nervous system) (Klein et al., 1997). IL-6 was also found to stimulate the effector T-cell development. IL-6 also acts as a warning signal in the event of tissue damage or microbial invasion (Tanaka et al., 2014). Further, the transgenic mice constitutively expressing both IL-6 and its receptor, IL-6R, were found to have accelerated nerve tissue regeneration compared to nontransgenic mice, which highlight the role of IL-6 in tissue repair (Hirota et al., 1996). The contribution

of IL-6 in hepatic tissue regeneration was also established. For instance, high levels of IL-6 secretion were measured after partial hepatectomy in rats (Trautwein et al., 1996), while impaired liver regeneration was observed in IL-6 deficient mice (Cressman et al., 1996). On the other hand, abnormal levels of IL-6 have been found to exert pathological roles in various health conditions, including chronic inflammation and autoimmune diseases (Tanaka et al., 2014). Interestingly for example, IL-6 is a detrimental factor in cancer development as it accelerates tumour growth in liver and colon tissues. Elevated IL-6 levels are observed in deteriorating cancer patients (Sansone et al., 2007).

2.6.4 Immunomodulation of plants' phytochemicals

The importance of the immune system in fighting diseases promoted interest from researchers to provide new therapies for immunologically mediated diseases such as cancer, AIDS, infections and diabetes (Dacoba et al., 2017). An immunomodulation effect can alter the immune responses through the induction or inhibition of the immune responses. New immunomodulatory therapies, of synthetic or natural origins, can stimulate immune responses for immunocompromised patients for example, or can be used to suppress the immune responses in organ transplant recipients, autoimmune patients or chronic inflammation conditions (Brindha et al., 2016). Plants are a major source of phytochemicals that have proven their potential as immunomodulatory agents to regulate the functions of several immune cells, including macrophages and NK cells (Ebadi et al., 2014).

Experiments have shown that the naturally occurring alkaloid, berberine, can decrease mortality rate of LPS induced organ damage in mice. Berberine was found to counteract the inflammatory responses of LPS administration by reducing the pro-inflammatory cytokines such as TNF- α and IFN- γ (Li et al., 2006). Moreover, the immunomodulation evaluation of several natural compounds of different chemical classes from *plantago*

genus was investigated. The results showed that these compounds namely aucubin, chlorogenic acid, ferulic acid, *p*-coumaric acid and vanillic acid can enhance the proliferation of human lymphocytes and the IFN- γ production (Chiang et al., 2003). In another study, curcumin, a yellow pigment found in spice turmeric, was also found to augment the IFN- γ induced NK cells cytotoxicity against erythroleukemic cells *in vitro* (Yadav et al., 2005). This compound also increased the pro-inflammatory cytokine production resulting in improved tumoricidal activity of NK cells against solid tumours in rats (Bhaumik et al., 2000). Further, the naturally occurring antioxidant, chebulagic acid, demonstrated potent anti-inflammatory effects in mouse macrophages *via* the downregulation of several pro-inflammatory cytokines including IL-6 and TNF- α (Reddy and Reddanna, 2009).

H. hemerocallidea is famous for its immunostimulatory effects. The corms of *H. hemerocallidea* are extensively used in a wide range of immune-related conditions such as arthritis, cancer, common cold and flu (Mills et al., 2005). Indirect evidence has showed that sterols and sterolins of *H. hemerocallidea* may have immunostimulatory effects (Section 2.4.1). The south African media is advocating the use of *H. hemerocallidea* preparations in the management of HIV (Mills et al., 2005). On the whole, it can be speculated that *H. hemerocallidea* and its contents, chosen in this study, may have an immunomodulation activity and the incorporation of its phytochemicals with AuNPs as immunomodulatory agents may further add another dimension (the combined effect of the phytochemicals and their NPs) to this activity.

2.6.5 AuNPs and immunomodulation

The unique physicochemical properties of the NPs facilitate their internalization in the immune cells to regulate their responses. NPs can infiltrate the immune cells assisted by their small size, NPs can be also functionalized with targeting moieties that can favour their selective access to certain immune cells (Dacoba et al., 2017). Moreover,

NPs are expected to interact with the immune cells upon administration inside the body. Indeed, the early bio-distribution studies showed that AuNPs are captured in the liver by Kupffer cells (liver macrophages) before they excreted from the body in the faeces (Dykman and Khlebtsov, 2017). Inspecting the interaction of the AuNPs with immune cells is therefore of an utmost importance, not only to document the immunomodulation effect of the AuNPs on the immune system but also to understand the effect of the immune barrier on the AuNPs before reaching their target sites. The immunomodulation activity of the AuNPs is well documented in the literature with several studies reporting contrasting data. For instance, AuNPs were reported to activate the immune response of the macrophages and upregulated the production of several pro-inflammatory cytokines including TNF- α , IL-1 and IL-6 (Yen et al., 2009). AuNPs were also found to increase the proliferation of lymphocytes and NK cells accompanied with an increase of IL-2 production (Dykman and Khlebtsov, 2017). Other studies, however, showed no immunomodulatory action of AuNPs on the production of the pro-inflammatory despite their internalization inside the macrophages (Shukla et al., 2005).

The immunomodulation effects of the AuNPs start by infiltration the immune cells and hence their activity is dependent on their physicochemical properties and the type of coating material (Getts et al., 2015). For example, Fallarini and colleagues showed that 5 nm AuNPs conjugated with disaccharide showed immunoactivity on macrophages than the 2 nm ones (Fallarini et al., 2013). Wei et al. also used two different sizes of AuNPs (15 and 30 nm) conjugated with cytosine-phosphate-guanosine oligodeoxynucleotides, which mimic the macrophage activating microbial DNA. The authors found that the 15 nm AuNPs activated the macrophages and stimulated the production of pro-inflammatory cytokines (TNF- α and IL-6) more than the 30 nm AuNPs (Wei et al., 2012).

The shape of the AuNPs also determines the immune response of the AuNPs. Indeed, the geometry of any foreign particles is critical for their internalization in phagocytic cells. It was found that AuNSPs tend to infiltrate macrophages more readily than any

other shapes (Champion and Mitragotri, 2006). A study by Xie et al. showed that different shapes of AuNPs exhibited different degrees of internalization with the macrophages regardless of their coating material, in which triangular AuNPs were easily taken by the macrophages more than AuNRs or AuNSTs (Xie et al., 2017).

The type of the coating material of the AuNPs can also influence their immunomodulatory actions. For instance, replacing CATB coating of the AuNPs by poly(ethylene oxide) significantly reduced the uptake of the AuNPs by several immune cells among them macrophages (Bartneck et al., 2010). The effect of the phytochemicals as coating material could hence prove critical for the immune response of the green synthesized AuNPs.



BIBLIOGRAPHY

- Abadeer, N.S., Murphy, C.J., 2016. Recent Progress in Cancer Thermal Therapy Using Gold Nanoparticles. *J. Phys. Chem. C* 120, 4691–4716.
<https://doi.org/10.1021/acs.jpcc.5b11232>
- Abdelhalim, M.A.K., Mohsen, M.M., Ghannam, M.M., 2012. Physical Properties of Different Gold Nanoparticles: Ultraviolet-Visible and Fluorescence Measurements. *J. Nanomed. Nanotechnol.* 3. <https://doi.org/10.4172/2157-7439.1000133>
- Agyare, C., Boakye, Y.D., Bekoe, E.O., Hensel, A., Dapaah, S.O., Appiah, T., 2016. Review: African medicinal plants with wound healing properties. *J. Ethnopharmacol.* 177, 85–100. <https://doi.org/10.1016/j.jep.2015.11.008>
- Ahmad, B., Hafeez, N., Bashir, S., Rauf, A., Mujeeb-ur-Rehman, 2017. Phytofabricated gold nanoparticles and their biomedical applications. *Biomed. Pharmacother.* 89, 414–425.
<https://doi.org/10.1016/j.biopha.2017.02.058>
- Ahmad, N., Bhatnagar, S., Saxena, R., Iqbal, D., Ghosh, A.K., Dutta, R., 2017. Biosynthesis and characterization of gold nanoparticles: Kinetics, in vitro and in vivo study. *Mater. Sci. Eng. C* 78, 553–564. <https://doi.org/10.1016/j.msec.2017.03.282>
- Ahmad, T., Irfan, M., Bhattacharjee, S., 2016. Effect of Reaction Time on Green Synthesis of Gold Nanoparticles by Using Aqueous Extract of Elaise Guineensis (Oil Palm Leaves). *Procedia Eng.* 148, 467–472. <https://doi.org/10.1016/J.PROENG.2016.06.465>
- Ahmed, S., Annu, Ikram, S., Yudha, S., 2016. Biosynthesis of gold nanoparticles: A green approach. *J. Photochem. Photobiol. B Biol.* 161, 141–153.
<https://doi.org/10.1016/j.jphotobiol.2016.04.034>
- Ajitha, B., Ashok Kumar Reddy, Y., Sreedhara Reddy, P., 2015. Green synthesis and characterization of silver nanoparticles using Lantana camara leaf extract. *Mater. Sci. Eng. C* 49, 373–381. <https://doi.org/10.1016/j.msec.2015.01.035>
- Akhtar, M.S., Panwar, J., Yun, Y.-S., 2013. Synthesis of metallic nanoparticles using plant extracts. *ACS Sustain. Chem. Eng.* 1, 591–602.
<https://doi.org/10.1016/j.biotechadv.2013.01.003>
- Akira, S., Uematsu, S., Takeuchi, O., 2006. Pathogen Recognition and Innate Immunity. *Cell* 124, 783–801. <https://doi.org/10.1016/J.CELL.2006.02.015>
- Aljabali, A., Akkam, Y., Al Zoubi, M., Al-Batayneh, K., Al-Trad, B., Abo Alrob, O., Alkilany, A., Benamara, M., Evans, D., 2018. Synthesis of Gold Nanoparticles Using Leaf Extract of Ziziphus zizyphus and their Antimicrobial Activity. *Nanomaterials* 8, 174. <https://doi.org/10.3390/nano8030174>
- Alkilany, A.M., Murphy, C.J., 2010. Toxicity and cellular uptake of gold nanoparticles: What we have learned so far? *J. Nanoparticle Res.* 12, 2313–2333.
<https://doi.org/10.1007/s11051-010-9911-8>
- Alkilany, A.M., Nagaria, P.K., Hexel, C.R., Shaw, T.J., Murphy, C.J., Wyatt, M.D., 2009.

- Cellular Uptake and Cytotoxicity of Gold Nanorods: Molecular Origin of Cytotoxicity and Surface Effects. *Small* 5, 701–708. <https://doi.org/10.1002/smll.200801546>
- Alshehri, R., Ilyas, A.M., Hasan, A., Arnaout, A., Ahmed, F., Memic, A., 2016. Carbon Nanotubes in Biomedical Applications: Factors, Mechanisms, and Remedies of Toxicity. *J. Med. Chem.* 59, 8149–8167. <https://doi.org/10.1021/acs.jmedchem.5b01770>
- Anastas, P.T., Warner, J.C., 1998. *Green chemistry : theory and practice*. Oxford University Press.
- Arango Duque, G., Descoteaux, A., 2014. Macrophage Cytokines: Involvement in Immunity and Infectious Diseases. *Front. Immunol.* 5, 491. <https://doi.org/10.3389/fimmu.2014.00491>
- Armendariz, V., Herrera, I., peralta-vidua, J.R., Jose-yacaman, M., Troiani, H., Santiago, P., Gardea-Torresdey, J.L., 2004. Size controlled gold nanoparticle formation by *Avena sativa* biomass: use of plants in nanobiotechnology. *J. Nanoparticle Res.* 6, 377–382. <https://doi.org/10.1007/s11051-004-0741-4>
- Arunachalam, K.D., Annamalai, S.K., Hari, S., 2013. One-step green synthesis and characterization of leaf extract-mediated biocompatible silver and gold nanoparticles from *Memecylon umbellatum*. *Int. J. Nanomedicine* 8, 1307–1315. <https://doi.org/10.2147/IJN.S36670>
- Au, L., Zhang, Q., Cobley, C.M., Gidding, M., Schwartz, A.G., Chen, J., Xia, Y., 2010a. Quantifying the Cellular Uptake of Antibody-Conjugated Au Nanocages by Two-Photon Microscopy and Inductively Coupled Plasma Mass Spectrometry. *ACS Nano* 4, 35–42. <https://doi.org/10.1021/nn901392m>
- Au, L., Zhang, Q., Cobley, C.M., Gidding, M., Schwartz, A.G., Chen, J., Xia, Y., 2010b. Quantifying the Cellular Uptake of Antibody-Conjugated Au Nanocages by Two-Photon Microscopy and Inductively Coupled Plasma Mass Spectrometry. *ACS Nano* 4, 35–42. <https://doi.org/10.1021/nn901392m>
- Ayaz Ahmed, K.B., Subramanian, S., Sivasubramanian, A., Veerappan, G., Veerappan, A., 2014. Preparation of gold nanoparticles using *Salicornia brachiata* plant extract and evaluation of catalytic and antibacterial activity. *Spectrochim. Acta - Part A Mol. Biomol. Spectrosc.* 130, 54–58. <https://doi.org/10.1016/j.saa.2014.03.070>
- Balalakshmi, C., Gopinath, K., Govindarajan, M., Lokesh, R., Arumugam, A., Alharbi, N.S., Kadaikunnan, S., Khaled, J.M., Benelli, G., 2017. Green synthesis of gold nanoparticles using a cheap *Sphaeranthus indicus* extract: Impact on plant cells and the aquatic crustacean *Artemia nauplii*. *J. Photochem. Photobiol. B Biol.* 173, 598–605. <https://doi.org/10.1016/j.jphotobiol.2017.06.040>
- Balashanmugam, P., Durai, P., Balakumaran, M.D., Kalaichelvan, P.T., 2016. Phytosynthesized gold nanoparticles from *C. roxburghii* DC. leaf and their toxic effects on normal and cancer cell lines. *J. Photochem. Photobiol. B Biol.* 165, 163–173. <https://doi.org/10.1016/j.jphotobiol.2016.10.013>
- Banu, H., Renuka, N., Faheem, S.M., Ismail, R., Singh, V., Saadatmand, Z., Khan, S.S., Narayanan, K., Raheem, A., Premkumar, K., Vasanthakumar, G., 2018. Gold and Silver Nanoparticles Biomimetically Synthesized Using Date Palm Pollen Extract-Induce

- Apoptosis and Regulate p53 and Bcl-2 Expression in Human Breast Adenocarcinoma Cells. *Biol. Trace Elem. Res.* 1–13. <https://doi.org/10.1007/s12011-018-1287-0>
- Bartneck, M., Keul, H.A., Zwadlo-Klarwasser, G., Groll, J., 2010. Phagocytosis Independent Extracellular Nanoparticle Clearance by Human Immune Cells. *Nano Lett.* 10, 59–63. <https://doi.org/10.1021/nl902830x>
- Bassey, K., Viljoen, A., Combrinck, S., Choi, Y.H., 2015. New phytochemicals from the corms of medicinally important South African Hypoxis species. *Phytochem. Lett.* 10, lxix–lxxv. <https://doi.org/10.1016/j.phytol.2014.09.014>
- Baum, C.L., Arpey, C.J., 2005. Normal cutaneous wound healing: clinical correlation with cellular and molecular events. *Dermatol. Surg.* 31, 674–86; discussion 686.
- Begum, N.A., Mondal, S., Basu, S., Laskar, R.A., Mandal, D., 2009. Biogenic synthesis of Au and Ag nanoparticles using aqueous solutions of Black Tea leaf extracts. *Colloids Surfaces B Biointerfaces* 71, 113–118. <https://doi.org/10.1016/J.COLSURFB.2009.01.012>
- Bell, J.M., Turnidge, J.D., SENTRY APAC, 2002. High prevalence of oxacillin-resistant *Staphylococcus aureus* isolates from hospitalized patients in Asia-Pacific and South Africa: results from SENTRY antimicrobial surveillance program, 1998-1999. *Antimicrob. Agents Chemother.* 46, 879–881.
- Beutler, B.A., 1999. The role of tumor necrosis factor in health and disease. *J. Rheumatol. Suppl.* 57, 16–21.
- Bhatia, S., 2016. Nanoparticles Types, Classification, Characterization, Fabrication Methods and Drug Delivery Applications, in: *Natural Polymer Drug Delivery Systems: Nanoparticles, Plants, and Algae*. Springer International Publishing, pp. 33–93.
- Bhattacharya, D., Saha, B., Mukherjee, A., Ranjan Santra, C., Karmakar, P., 2012. Gold Nanoparticles Conjugated Antibiotics: Stability and Functional Evaluation. *Nanosci. Nanotechnol.* 2, 14–21. <https://doi.org/10.5923/j.nm.20120202.04>
- Bhaumik, S., Jyothi, M.D., Khar, A., 2000. Differential modulation of nitric oxide production by curcumin in host macrophages and NK cells. *FEBS Lett.* 483, 78–82.
- Bhushan, B., 2010. *Springer Handbook of Nanotechnology*. Springer.
- Bouic, P.J., 2001. The role of phytosterols and phytosterolins in immune modulation: a review of the past 10 years. *Curr. Opin. Clin. Nutr. Metab. Care* 4, 471–475.
- Boukes, G.J., van de Venter, M., Oosthuizen, V., 2008. Quantitative and qualitative analysis of sterols/sterolins and hypoxoside contents of three *Hypoxis* (African potato) spp. *African J. Biotechnol.* 7, 1624–1629. <https://doi.org/10.5897/AJB08.218>
- Brindha, P., Venkatalakshmi, P., Vadivel, V., 2016. Role of phytochemicals as immunomodulatory agents: A review. *Int. J. Green Pharm.* 10.
- Broughton, G., Janis, J.E., Attinger, C.E., 2006. The basic science of wound healing. *Plast. Reconstr. Surg.* 117, 12S–34S. <https://doi.org/10.1097/01.prs.0000225430.42531.c2>
- Brown, A.N., Smith, K., Samuels, T.A., Lu, J., Obare, S.O., Scott, M.E., 2012. Nanoparticles

functionalized with ampicillin destroy multiple-antibiotic-resistant isolates of *Pseudomonas aeruginosa* and *Enterobacter aerogenes* and methicillin-resistant *Staphylococcus aureus*. *Appl. Environ. Microbiol.* 78, 2768–2774.
<https://doi.org/10.1128/AEM.06513-11>

- Bryant, A.T., 1916. Zulu Medicine and medicine-men, in: *Annals of the Natal Museum*. Natal Museum, Pietermaritzburg, South Africa, pp. 1–103.
- Cardona, A.F., Wilson, S.E., 2015. Skin and Soft-Tissue Infections: A Critical Review and the Role of Telavancin in Their Treatment. *Clin. Infect. Dis.* 61, S69–S78.
<https://doi.org/10.1093/cid/civ528>
- Carswell, E.A., Old, L.J., Kassel, R.L., Green, S., Fiore, N., Williamson, B., 1975. An endotoxin-induced serum factor that causes necrosis of tumors. *Proc. Natl. Acad. Sci. U. S. A.* 72, 3666–3670.
- Castro-Aceituno, V., Abbai, R., Moon, S.S., Ahn, S., Mathiyalagan, R., Kim, Y.-J., Kim, Y.-J., Yang, D.C., 2017. *Pleuropterus multiflorus* (Hasuo) mediated straightforward eco-friendly synthesis of silver, gold nanoparticles and evaluation of their anti-cancer activity on A549 lung cancer cell line. *Biomed. Pharmacother.* 93, 995–1003.
<https://doi.org/10.1016/J.BIOPHA.2017.07.040>
- Chahardoli, A., Karimi, N., Sadeghi, F., Fattahi, A., 2018. Green approach for synthesis of gold nanoparticles from *Nigella arvensis* leaf extract and evaluation of their antibacterial, antioxidant, cytotoxicity and catalytic activities. *Artif. Cells, Nanomedicine, Biotechnol.* 46, 579–588.
<https://doi.org/10.1080/21691401.2017.1332634>
- Champion, J.A., Mitragotri, S., 2006. Role of target geometry in phagocytosis. *Proc. Natl. Acad. Sci. U. S. A.* 103, 4930–4934. <https://doi.org/10.1073/pnas.0600997103>
- Chanda, N., Shukla, R., Zambre, A., Mekapothula, S., Kulkarni, R.R., Katti, K., Bhattacharyya, K., Fent, G.M., Casteel, S.W., Boote, E.J., Viator, J.A., Upendran, A., Kannan, R., Katti, K. V., 2011. An Effective Strategy for the Synthesis of Biocompatible Gold Nanoparticles Using Cinnamon Phytochemicals for Phantom CT Imaging and Photoacoustic Detection of Cancerous Cells. *Pharm. Res.* 28, 279–291.
<https://doi.org/10.1007/s11095-010-0276-6>
- Chandran, S.P., Chaudhary, M., Pasricha, R., Ahmad, A., Sastry, M., 2006. Synthesis of Gold Nanotriangles and Silver Nanoparticles Using Aloe vera Plant Extract. *Biotechnol. Prog.* 22, 577–583. <https://doi.org/10.1021/bp0501423>
- Chiang, L.-C., Ng, L.T., Chiang, W., Chang, M.-Y., Lin, C.-C., 2003. Immunomodulatory Activities of Flavonoids, Monoterpenoids, Triterpenoids, Iridoid Glycosides and Phenolic Compounds of *Plantago* Species. *Planta Med.* 69, 600–604.
<https://doi.org/10.1055/s-2003-41113>
- Choi, Y., Kang, S., Cha, S.-H., Kim, H.-S., Song, K., Lee, Y.J., Kim, K., Kim, Y.S., Cho, S., Park, Y., 2018. Platycodon saponins from *Platycodi Radix* (*Platycodon grandiflorum*) for the Green Synthesis of Gold and Silver Nanoparticles. *Nanoscale Res. Lett.* 13, 23.
<https://doi.org/10.1186/s11671-018-2436-2>
- Chung, I.-M., Abdul Rahuman, A., Marimuthu, S., Kirthi, A.V., Anbarasan, K., Padmini, P.,

- Rajakumar, G., 2017. Green synthesis of copper nanoparticles using *Eclipta prostrata* leaves extract and their antioxidant and cytotoxic activities. *Exp. Ther. Med.* 14, 18–24. <https://doi.org/10.3892/etm.2017.4466>
- Clark, N.M., Patterson, J., Lynch, J.P., 2003. Antimicrobial resistance among gram-negative organisms in the intensive care unit. *Curr. Opin. Crit. Care* 9, 413–423.
- Cobley, C.M., Chen, J., Cho, E.C., Wang, L. V., Xia, Y., 2011. Gold nanostructures: a class of multifunctional materials for biomedical applications. *Chem. Soc. Rev.* 40, 44–56. <https://doi.org/10.1039/B821763G>
- Cole, L.E., Ross, R.D., Tilley, J.M., Vargo-Gogola, T., Roeder, R.K., 2015. Gold nanoparticles as contrast agents in x-ray imaging and computed tomography. *Nanomedicine* 10, 321–341. <https://doi.org/10.2217/nnm.14.171>
- Coutinho, A.E., Chapman, K.E., 2011. The anti-inflammatory and immunosuppressive effects of glucocorticoids, recent developments and mechanistic insights. *Mol. Cell. Endocrinol.* 335, 2–13. <https://doi.org/10.1016/j.mce.2010.04.005>
- Cressman, D.E., Greenbaum, L.E., DeAngelis, R.A., Ciliberto, G., Furth, E.E., Poli, V., Taub, R., 1996. Liver failure and defective hepatocyte regeneration in interleukin-6-deficient mice. *Science* 274, 1379–1383.
- Crucho, C.I.C., Barros, M.T., 2017. Polymeric nanoparticles: A study on the preparation variables and characterization methods. *Mater. Sci. Eng. C* 80, 771–784. <https://doi.org/10.1016/j.msec.2017.06.004>
- Cunha, F.Q., Poole, S., Lorenzetti, B.B., Ferreira, S.H., 1992. The pivotal role of tumour necrosis factor alpha in the development of inflammatory hyperalgesia. *Br. J. Pharmacol.* 107, 660–4.
- Dacoba, T.G., Olivera, A., Torres, D., Crecente-Campo, J., Alonso, M.J., 2017. Modulating the immune system through nanotechnology. *Semin. Immunol.* 34, 78–102. <https://doi.org/10.1016/j.smim.2017.09.007>
- Dahl, J.A., Maddux, B.L.S., Hutchison, J.E., 2007. Toward Greener Nanosynthesis. *Chem. Rev.* 107, 2228–2269. <https://doi.org/10.1021/CR050943K>
- De Donatis, A., Ranaldi, F., Cirri, P., 2010. Reciprocal control of cell proliferation and migration. *Cell Commun. Signal.* 8, 20. <https://doi.org/10.1186/1478-811X-8-20>
- De Volder, M., Tawfick, S., Baughman, R., Hart, A., 2013. Carbon nanotubes: present and future commercial applications. *Science* (80-.). 339, 535–539. <https://doi.org/10.1126/science.1222453>
- DeLong, R.K., Reynolds, C.M., Malcolm, Y., Schaeffer, A., Severs, T., Wanekaya, A., 2010. Functionalized gold nanoparticles for the binding, stabilization, and delivery of therapeutic DNA, RNA, and other biological macromolecules. *Nanotechnol. Sci. Appl.* 3, 53–63. <https://doi.org/10.2147/NSA.S8984>
- Diegelmann, R.F., 2003. Excessive neutrophils characterize chronic pressure ulcers. *Wound repair Regen.* 11, 490–5.
- Dinarello, C.A., 2007. Historical insights into cytokines. *Eur. J. Immunol.* 37, S34–S45.

<https://doi.org/10.1002/eji.200737772>

- Dorosti, N., Jamshidi, F., 2016. Plant-mediated gold nanoparticles by *Dracocephalum kotschyi* as anticholinesterase agent: Synthesis, characterization, and evaluation of anticancer and antibacterial activity. *J. Appl. Biomed.* 14, 235–245.
<https://doi.org/10.1016/j.jab.2016.03.001>
- Drewes, S.E., Elliot, E., Khan, F., Dhlamini, J.T.B., Gcumisa, M.S.S., 2008. Hypoxis hemerocallidea—Not merely a cure for benign prostate hyperplasia. *J. Ethnopharmacol.* 119, 593–598. <https://doi.org/10.1016/j.jep.2008.05.027>
- Drewes, S.E., Hall, A.J., Learmonth, R.A., Upfold, U.J., 1984. Isolation of hypoxoside from hypoxis rooperi and synthesis of (E)-1,5-bis(3',4'-dimethoxyphenyl)pent-4-en-1-yne. *Phytochemistry* 23, 1313–1316. [https://doi.org/10.1016/S0031-9422\(00\)80449-5](https://doi.org/10.1016/S0031-9422(00)80449-5)
- Dubey, S.P., Lahtinen, M., Sillanpää, M., 2010. Tansy fruit mediated greener synthesis of silver and gold nanoparticles. *Process Biochem.* 45, 1065–1071.
<https://doi.org/10.1016/J.PROCBIO.2010.03.024>
- Durán, N., Marcato, P.D., Durán, M., Yadav, A., Gade, A., Rai, M., 2011. Mechanistic aspects in the biogenic synthesis of extracellular metal nanoparticles by peptides, bacteria, fungi, and plants. *Appl. Microbiol. Biotechnol.* 90, 1609–1624.
<https://doi.org/10.1007/s00253-011-3249-8>
- Dutta, P., Harrison, A., Sabbani, S., Munson, R.S., Dutta, P.K., Waldman, W.J., 2011. Silver nanoparticles embedded in zeolite membranes: release of silver ions and mechanism of antibacterial action. *Int. J. Nanomedicine* 6, 1833–1852.
<https://doi.org/10.2147/IJN.S24019>
- Dwivedi, A.D., Gopal, K., 2010. Biosynthesis of silver and gold nanoparticles using *Chenopodium album* leaf extract. *Colloids Surfaces A Physicochem. Eng. Asp.* 369, 27–33. <https://doi.org/10.1016/J.COLSURFA.2010.07.020>
- Dykman, L.A., Khlebtsov, N.G., 2017. Immunological properties of gold nanoparticles. *Chem. Sci.* 8, 1719–1735. <https://doi.org/10.1039/C6SC03631G>
- Dzimitrowicz, A., Jamróz, P., diCenzo, G.C., Sergiel, I., Kozlecki, T., Pohl, P., 2016. Preparation and characterization of gold nanoparticles prepared with aqueous extracts of Lamiaceae plants and the effect of follow-up treatment with atmospheric pressure glow microdischarge. *Arab. J. Chem.* <https://doi.org/10.1016/J.ARABJC.2016.04.004>
- Ebadi, P., Karimi, M.H., Amirghofran, Z., 2014. Plant components for immune modulation targeting dendritic cells: implication for therapy. *Immunotherapy* 6, 1037–1053.
<https://doi.org/10.2217/imt.14.77>
- Edwards, J.P., Zhang, X., Frauwirth, K.A., Mosser, D.M., 2006. Biochemical and functional characterization of three activated macrophage populations. *J. Leukoc. Biol.* 80, 1298–1307. <https://doi.org/10.1189/jlb.0406249>
- Edwards, R., Harding, K.G., 2004. Bacteria and wound healing Colonisation Contamination. *Curr. Opin. Infect. Dis.* 17, 91–96.
<https://doi.org/10.1097/01.qco.0000124361.27345.d4>

- Elahi, N., Kamali, M., Baghersad, M.H., 2018. Recent biomedical applications of gold nanoparticles: A review. *Talanta* 184, 537–556. <https://doi.org/10.1016/j.talanta.2018.02.088>
- Elbagory, A., Meyer, M., Cupido, C., Hussein, A., 2017. Inhibition of Bacteria Associated with Wound Infection by Biocompatible Green Synthesized Gold Nanoparticles from South African Plant Extracts. *Nanomaterials* 7, 417. <https://doi.org/10.3390/nano7120417>
- Eshed, M., Pol, S., Gedanken, A., Balasubramanian, M., 2011. Zirconium nanoparticles prepared by the reduction of zirconium oxide using the RAPET method. *Beilstein J. Nanotechnol.* 2, 198–203. <https://doi.org/10.3762/bjnano.2.23>
- Essack, S.Y., 2001. The Development of β -Lactam Antibiotics in Response to the Evolution of β -Lactamases. *Pharm. Res.* 18, 1391–1399. <https://doi.org/10.1023/A:1012272403776>
- Eustis, S., El-Sayed, M.A., 2006. Why gold nanoparticles are more precious than pretty gold: Noble metal surface plasmon resonance and its enhancement of the radiative and nonradiative properties of nanocrystals of different shapes. *Chem. Soc. Rev.* 35, 209–217. <https://doi.org/10.1039/B514191E>
- Fallarini, S., Paoletti, T., Battaglini, C.O., Ronchi, P., Lay, L., Bonomi, R., Jha, S., Mancin, F., Scrimin, P., Lombardi, G., 2013. Factors affecting T cell responses induced by fully synthetic glyco-gold-nanoparticles. *Nanoscale* 5, 390–400. <https://doi.org/10.1039/C2NR32338A>
- Favi, P.M., Gao, M., Johana Sepúlveda Arango, L., Ospina, S.P., Morales, M., Pavon, J.J., Webster, T.J., 2015. Shape and surface effects on the cytotoxicity of nanoparticles: Gold nanospheres versus gold nanostars. *J. Biomed. Mater. Res. Part A* 103, 3449–3462. <https://doi.org/10.1002/jbm.a.35491>
- Fraga, S., Faria, H., Soares, M.E., Duarte, J.A., Soares, L., Pereira, E., Costa-Pereira, C., Teixeira, J.P., de Lourdes Bastos, M., Carmo, H., 2013. Influence of the surface coating on the cytotoxicity, genotoxicity and uptake of gold nanoparticles in human HepG2 cells. *J. Appl. Toxicol.* 33, 1111–1119. <https://doi.org/10.1002/jat.2865>
- Francis, S., Joseph, S., Koshy, E.P., Mathew, B., 2017. Green synthesis and characterization of gold and silver nanoparticles using *Mussaenda glabrata* leaf extract and their environmental applications to dye degradation. *Environ. Sci. Pollut. Res.* 24, 17347–17357. <https://doi.org/10.1007/s11356-017-9329-2>
- Francis, S., Koshy, E.P., Mathew, B., 2018. Green synthesis of *Stereospermum suaveolens* capped silver and gold nanoparticles and assessment of their innate antioxidant, antimicrobial and antiproliferative activities. *Bioprocess Biosyst. Eng.* 1–13. <https://doi.org/10.1007/s00449-018-1925-0>
- Frasnelli, M., Cristofaro, F., Sglavo, V.M., Dirè, S., Callone, E., Ceccato, R., Bruni, G., Cornaglia, A.I., Visai, L., 2017. Synthesis and characterization of strontium-substituted hydroxyapatite nanoparticles for bone regeneration. *Mater. Sci. Eng. C* 71, 653–662. <https://doi.org/10.1016/J.MSEC.2016.10.047>
- Freese, C., Uboldi, C., Gibson, M.I., Unger, R.E., Weksler, B.B., Romero, I.A., Couraud, P.-

- O., Kirkpatrick, C., 2012. Uptake and cytotoxicity of citrate-coated gold nanospheres: Comparative studies on human endothelial and epithelial cells. Part. Fibre Toxicol. 9, 23. <https://doi.org/10.1186/1743-8977-9-23>
- Ganesan, P., Narayanasamy, D., 2017. Lipid nanoparticles: Different preparation techniques, characterization, hurdles, and strategies for the production of solid lipid nanoparticles and nanostructured lipid carriers for oral drug delivery. Sustain. Chem. Pharm. 6, 37–56. <https://doi.org/10.1016/j.scp.2017.07.002>
- Gardea-Torresdey, J.L., Parson, J.G., Gomez, E., Peralta-Videa, J., Troiani, H.E., Santiago, P., Yacarman, M.J., 2002. Formation and Growth of Au Nanoparticles in live side Live Alfalfa Plants. Nano Lett. 2, 397–401. <https://doi.org/10.1021/nl015673+>
- Geetha, R., Ashokkumar, T., Tamilselvan, S., Govindaraju, K., Sadiq, M., Singaravelu, G., 2013. Green synthesis of gold nanoparticles and their anticancer activity. Cancer Nanotechnol. 4, 91–98. <https://doi.org/10.1007/s12645-013-0040-9>
- Geethalakshmi, R., Sarada, 2012. Gold and silver nanoparticles from *Trianthema decandra*: synthesis, characterization, and antimicrobial properties. Int. J. Nanomedicine 7, 5375–5384. <https://doi.org/10.2147/IJN.S36516>
- Geethalakshmi, R., Sarada, D.V., 2013. Characterization and antimicrobial activity of gold and silver nanoparticles synthesized using saponin isolated from *Trianthema decandra* L. Ind. Crops Prod. 51, 107–115. <https://doi.org/10.1016/J.INDCROP.2013.08.055>
- Gericke, M., Pinches, A., 2006. Biological synthesis of metal nanoparticles. Hydrometallurgy 83, 132–140. <https://doi.org/10.1016/J.HYDROMET.2006.03.019>
- Getts, D.R., Shea, L.D., Miller, S.D., King, N.J.C., 2015. Harnessing nanoparticles for immune modulation. Trends Immunol. 36, 419–427. <https://doi.org/10.1016/j.it.2015.05.007>
- Ghosh, P., Han, G., De, M., Kim, C.K., 2008. Gold nanoparticles in delivery applications. Adv. Drug Deliv. Rev. 60, 1307–1315. <https://doi.org/10.1016/J.ADDR.2008.03.016>
- Goldblatt, P., Manning, J.C., 2002. Plant Diversity of the Cape Region of Southern Africa. Ann. Missouri Bot. Gard. 89, 281. <https://doi.org/10.2307/3298566>
- Goldman, R., 2004. Growth factors and chronic wound healing: past, present, and future. Adv. Skin Wound Care 17, 24–35.
- Gordon, S., 2016. Phagocytosis: The Legacy of Metchnikoff. Cell 166, 1065–1068. <https://doi.org/10.1016/J.CELL.2016.08.017>
- Greenhalgh, D.G., 1998. The role of apoptosis in wound healing. Int. J. Biochem. Cell Biol. 30, 1019–1030.
- Gurunathan, S., Woong Han, J., Abdal Daye, A., Eppakayala, V., Kim, J., 2012. Oxidative stress-mediated antibacterial activity of graphene oxide and reduced graphene oxide in *Pseudomonas aeruginosa*. Int. J. Nanomedicine 7, 5901–5914. <https://doi.org/10.2147/IJN.S37397>
- Hainfeld, J.F., Slatkin, D.N., Focella, T.M., Smilowitz, H.M., 2006. Gold nanoparticles: a new X-ray contrast agent. Br. J. Radiol. 79, 248–253.

<https://doi.org/10.1259/bjr/13169882>

- Hancock, R.E., Scott, M.G., 2000. The role of antimicrobial peptides in animal defenses. *Proc. Natl. Acad. Sci. U. S. A.* 97, 8856–8861.
- Hayden, S.C., Zhao, G., Saha, K., Phillips, R.L., Li, X., Miranda, O.R., Rotello, V.M., El-Sayed, M.A., Schmidt-Krey, I., Bunz, U.H.F., 2012. Aggregation and Interaction of Cationic Nanoparticles on Bacterial Surfaces. *J. Am. Chem. Soc.* 134, 6920–6923. <https://doi.org/10.1021/ja301167y>
- He, S., Guo, Z., Zhang, Y., Zhang, S., Wang, J., Gu, N., 2007. Biosynthesis of gold nanoparticles using the bacteria *Rhodospseudomonas capsulata*. *Mater. Lett.* 61, 3984–3987. <https://doi.org/10.1016/j.matlet.2007.01.018>
- Hirota, H., Kiyama, H., Kishimoto, T., Taga, T., 1996. Accelerated Nerve Regeneration in Mice by upregulated expression of interleukin (IL) 6 and IL-6 receptor after trauma. *J. Exp. Med.* 183, 2627–2634.
- Hopper, N., Wardale, J., Brooks, R., Power, J., Rushton, N., Henson, F., 2015. Peripheral Blood Mononuclear Cells Enhance Cartilage Repair in in vivo Osteochondral Defect Model. *PLoS One* 10, e0133937. <https://doi.org/10.1371/journal.pone.0133937>
- Houghton, P.J., Hylands, P.J., Mensah, A.Y., Hensel, A., Deters, A.M., 2005. In vitro tests and ethnopharmacological investigations: Wound healing as an example. *J. Ethnopharmacol.* 100, 100–107. <https://doi.org/10.1016/j.jep.2005.07.001>
- Huang, J., Li, Q., Sun, D., Lu, Y., Su, Y., Yang, X., Wang, H., Wang, Y., Shao, W., He, N., Hong, J., Chen, C., 2007. Biosynthesis of silver and gold nanoparticles by novel sundried *Cinnamomum camphora* leaf. *Nanotechnology* 18, 105104. <https://doi.org/10.1088/0957-4484/18/10/105104>
- Huang, X., El-Sayed, I.H., Qian, W., El-Sayed, M.A., 2006. Cancer cell imaging and photothermal therapy in the near-infrared region by using gold nanorods. *TL - 128. J. Am. Chem. Soc.* 128, 2115–2120. <https://doi.org/10.1021/ja057254a>
- Hutchings, A., Scott, A., Lewis, G., Cunningham, A., 1996. *Zulu Medicinal Plants: An Inventory, illustrate.* ed. University of Natal Press, Pietermaritzburg.
- Huy, P.D.Q., Li, M.S., 2014. Binding of fullerenes to amyloid beta fibrils: size matters. *Phys. Chem. Chem. Phys.* 16, 20030. <https://doi.org/10.1039/C4CP02348J>
- Inshakova, E., Inshakov, O., 2017. World market for nanomaterials: structure and trends. *MATEC Web Conf.* 129, 2013. <https://doi.org/10.1051/mateconf/201712902013>
- Iravani, S., 2011. Green synthesis of metal nanoparticles using plants. *Green Chem.* 13, 2638. <https://doi.org/10.1039/c1gc15386b>
- Islam, N.U., Amin, R., Shahid, M., Amin, M., Zaib, S., Iqbal, J., 2017. A multi-target therapeutic potential of *Prunus domestica* gum stabilized nanoparticles exhibited prospective anticancer, antibacterial, urease-inhibition, anti-inflammatory and analgesic properties. *BMC Complement. Altern. Med.* 17, 276. <https://doi.org/10.1186/s12906-017-1791-3>
- Jain, P.K., Huang, X., El-Sayed, I.H., El-Sayed, M.A., 2008. Noble Metals on the Nanoscale:

Optical and Photothermal Properties and Some Applications in Imaging, Sensing, Biology, and Medicine. *Acc. Chem. Res.* 41, 1578–1586.
<https://doi.org/10.1002/chin.200914223>

- James, S.L., Adams, C.J., Bolm, C., Braga, D., Collier, P., Friščić, T., Grepioni, F., Harris, K.D.M., Hyett, G., Jones, W., Krebs, A., Mack, J., Maini, L., Orpen, A.G., Parkin, I.P., Shearouse, W.C., Steed, J.W., Waddell, D.C., 2012. Mechanochemistry: opportunities for new and cleaner synthesis. *Chem. Soc. Rev.* 41, 413–447.
<https://doi.org/10.1039/C1CS15171A>
- Jang, E., Lim, E.-K., Choi, J., Park, J., Huh, Y.-J., Suh, J.-S., Huh, Y.-M., Haam, S., 2012. Br-Assisted Ostwald Ripening of Au Nanoparticles under H₂O₂ Redox. *Cryst. Growth Des.* 12, 37–39. <https://doi.org/10.1021/cg201243n>
- Jannathul Firdhouse, M., Lalitha, P., 2017. Cytotoxicity of spherical gold nanoparticles synthesised using aqueous extracts of aerial roots of *Rhaphidophora aurea* (Linden ex Andre) intertwined over *Lawsonia inermis* and *Areca catechu* on MCF-7 cell line. *IET Nanobiotechnology* 11, 2–11. <https://doi.org/10.1049/iet-nbt.2016.0076>
- Jayaseelan, C., Ramkumar, R., Rahuman, A.A., Perumal, P., 2013. Green synthesis of gold nanoparticles using seed aqueous extract of *Abelmoschus esculentus* and its antifungal activity. *Ind. Crops Prod.* 45, 423–429.
<https://doi.org/10.1016/J.INDCROP.2012.12.019>
- Jensen, T.R., Malinsky, M.D., Haynes, C.L., Van Duyne, R.P., 2000. Nanosphere Lithography: Tunable Localized Surface Plasmon Resonance Spectra of Silver Nanoparticles. *J. Phys. Chem. B* 104, 10549–10556. <https://doi.org/10.1021/jp002435e>
- Jespersen, J., 1988. Pathophysiology and clinical aspects of fibrinolysis and inhibition of coagulation. Experimental and clinical studies with special reference to women on oral contraceptives and selected groups of thrombosis prone patients. *Dan. Med. Bull.* 35, 1–33.
- Jia, Y.P., Ma, B.Y., Wei, X.W., Qian, Z.Y., 2017. The in vitro and in vivo toxicity of gold nanoparticles. *Chinese Chem. Lett.* 28, 691–702.
<https://doi.org/10.1016/j.ccllet.2017.01.021>
- Jiang, W., Kim, B.Y.S., Rutka, J.T., Chan, W.C.W., 2008. Nanoparticle-mediated cellular response is size-dependent. *Nat. Nanotechnol.* 3, 145–150.
<https://doi.org/10.1038/nnano.2008.30>
- Jiao, Q., Li, L., Mu, Q., Zhang, Q., 2014. Immunomodulation of nanoparticles in nanomedicine applications. *Biomed Res. Int.* 2014, 426028.
<https://doi.org/10.1155/2014/426028>
- Joshi, M., Bhattacharyya, A., Ali, S.W., 2008. Characterization techniques for nanotechnology applications in textiles. *Indian J. Fibre Text. Res.* 33, 304–317.
- Kagan, V.E., Bayir, H., Shvedova, A.A., 2005. Nanomedicine and nanotoxicology: two sides of the same coin. *Nanomedicine Nanotechnology, Biol. Med.* 1, 313–316.
<https://doi.org/10.1016/J.NANO.2005.10.003>
- Kanaras, A.G., Kamounah, F.S., Schaumburg, K., Kiely, C.J., Brust, M., 2002. Thioalkylated

- tetraethylene glycol: a new ligand for water soluble monolayer protected gold clusters. *Chem. Commun.* 2294–2295. <https://doi.org/10.1039/b207838b>
- Kasthuri, J., Veerapandian, S., Rajendiran, N., 2009. Biological synthesis of silver and gold nanoparticles using apiin as reducing agent. *Colloids Surfaces B Biointerfaces* 68, 55–60. <https://doi.org/10.1016/j.colsurfb.2008.09.021>
- Katerere, D.R., 2013. Hypoxis hemerocallidea (African potato): A Botanical Whose Time Has Come?, in: Juliani, H.R., Simon, J.E., Ho, C.-T. (Eds.), *African Natural Plant Products Volume II: New Discoveries and Challenges in Chemistry and Quality*. American Chemical Society, Washington, pp. 51–61. <https://doi.org/10.1021/bk-2013-1127.ch004>
- Kaur, S., Nautyal, U., Singh, R., Singh, S., Devi, A., 2015. Nanostructure Lipid Carrier (NLC): the new generation of lipid nanoparticles. *Asian Pacific J. Heal. Sci.* 2, 76–93.
- Kaushik, 2017. Lycurgus Cup: A Piece of Ancient Roman Nanotechnology [WWW Document]. URL <http://www.amusingplanet.com/2016/12/lycurgus-cup-piece-of-ancient-roman.html>
- Kettemann, F., Birnbaum, A., Witte, S., Wuithschick, M., Pinna, N., Kraehnert, R., Rademann, K., Polte, J., 2016. Missing Piece of the Mechanism of the Turkevich Method: The Critical Role of Citrate Protonation. *Chem. Mater.* 28, 4072–4081. <https://doi.org/10.1021/acs.chemmater.6b01796>
- Khan, I., Saeed, K., Khan, I., 2017. Nanoparticles : Properties , applications and toxicities. *Arab. J. Chem.* <https://doi.org/10.1016/j.arabjc.2017.05.011>
- Khan, M., Khan, M., Adil, S.F., Tahir, N.M., Tremel, W., Alkhatlan, H.Z., Al-Warthan, A., Siddiqui, M.R.H., 2013. Green synthesis of silver nanoparticles mediated by *Pulicaria glutinosa* extract. *Int. J. Nanomedicine* 8, 1507. <https://doi.org/10.2147/IJN.S43309>
- Kim, H.S., Lee, D.Y., 2017. Photothermal therapy with gold nanoparticles as an anticancer medication. *J. Pharm. Investig.* 47, 19–26. <https://doi.org/10.1007/s40005-016-0292-6>
- Kishimoto, T., 2010. IL-6: from its discovery to clinical applications. *Int. Immunol.* 22, 347–352. <https://doi.org/10.1093/intimm/dxq030>
- Kitching, M., Ramani, M., Marsili, E., 2015. Fungal biosynthesis of gold nanoparticles: Mechanism and scale up. *Microb. Biotechnol.* 8, 904–917. <https://doi.org/10.1111/1751-7915.12151>
- Klein, M.A., Möller, J.C., Jones, L.L., Bluethmann, H., Kreutzberg, G.W., Raivich, G., 1997. Impaired neuroglial activation in interleukin-6 deficient mice. *Glia* 19, 227–33.
- Kong, F.-Y., Zhang, J.-W., Li, R.-F., Wang, Z.-X., Wang, W.-J., Wang, W., 2017. Unique Roles of Gold Nanoparticles in Drug Delivery, Targeting and Imaging Applications. *Molecules* 22, 1445. <https://doi.org/10.3390/molecules22091445>
- Konturek, P., Brzozowski, T., Konturek, S., Kwiecien, S., Dembinski, A., Hahn, E., 2001. Influence of Bacterial Lipopolysaccharide on Healing of Chronic Experimental Ulcer in Rat. *Scand. J. Gastroenterol.* 36, 1239–1247. <https://doi.org/10.1080/003655201317097065>

- Lai, P.S., Bebell, L.M., Meney, C., Valeri, L., White, M.C., 2018. Epidemiology of antibiotic-resistant wound infections from six countries in Africa. *BMJ Glob. Heal.* 2, e000475. <https://doi.org/10.1136/bmjgh-2017-000475>
- Lall, N., Kishore, N., 2014. Are plants used for skin care in South Africa fully explored? *J. Ethnopharmacol.* 153, 61–84. <https://doi.org/10.1016/j.jep.2014.02.021>
- Larson, B.J., Longaker, M.T., Lorenz, H.P., 2010. Scarless Fetal Wound Healing: A Basic Science Review. *Plast. Reconstr. Surg.* 126, 1172–1180. <https://doi.org/10.1097/prs.0b013e3181eae781>
- Lawrence, J.C., 1987. The aetiology of scars. *Burns* 13, S3–S14. [https://doi.org/10.1016/0305-4179\(87\)90086-6](https://doi.org/10.1016/0305-4179(87)90086-6)
- Leeper, D., Assadian, O., Edmiston, C.E., 2015. Approach to chronic wound infections. *Br. J. Dermatol.* 173, 351–358. <https://doi.org/10.1111/bjd.13677>
- Lee, H.A., Castro-Aceituno, V., Abbai, R., Moon, S.S., Kim, Y.-J., Simu, S.Y., Yang, D.C., 2018. Rhizome of *Anemarrhena asphodeloides* as mediators of the eco-friendly synthesis of silver and gold spherical, face-centred cubic nanocrystals and its anti-migratory and cytotoxic potential in normal and cancer cell lines. *Artif. Cells, Nanomedicine, Biotechnol.* 1–10. <https://doi.org/10.1080/21691401.2018.1457038>
- Lee, J., Chatterjee, D.K., Lee, M.H., Krishnan, S., 2014. Gold nanoparticles in breast cancer treatment: promise and potential pitfalls. *Cancer Lett.* 347, 46–53. <https://doi.org/10.1016/j.canlet.2014.02.006>
- Lee, J., Park, E.Y., Lee, J., 2014. Non-toxic nanoparticles from phytochemicals: Preparation and biomedical application. *Bioprocess Biosyst. Eng.* 37, 983–989. <https://doi.org/10.1007/s00449-013-1091-3>
- Leung, Y.H., Ng, A.M.C., Xu, X., Shen, Z., Gethings, L.A., Wong, M.T., Chan, C.M.N., Guo, M.Y., Ng, Y.H., Djurišić, A.B., Lee, P.K.H., Chan, W.K., Yu, L.H., Phillips, D.L., Ma, A.P.Y., Leung, F.C.C., 2014. Mechanisms of Antibacterial Activity of MgO: Non-ROS Mediated Toxicity of MgO Nanoparticles Towards *Escherichia coli*. *Small* 10, 1171–1183. <https://doi.org/10.1002/sml.201302434>
- Li, F., Wang, H., Lu, D., Wang, Y., Qi, R., Fu, Y., Li, C., 2006. Neutral sulfate berberine modulates cytokine secretion and increases survival in endotoxemic mice. *Acta Pharmacol. Sin.* 27, 1199–1205. <https://doi.org/10.1111/j.1745-7254.2006.00368.x>
- Li, S.-D., Huang, L., 2008. Pharmacokinetics and Biodistribution of Nanoparticles. *Mol. Pharm.* 5, 496–504. <https://doi.org/10.1021/mp800049w>
- Li, Y., Schluesener, H.J., Xu, S., 2010. Gold nanoparticle-based biosensors. *Gold Bull.* 43, 29–41.
- Liebig, F., Thünemann, A.F., Koetz, J., 2016. Ostwald Ripening Growth Mechanism of Gold Nanotriangles in Vesicular Template Phases. *Langmuir* 32, 10928–10935. <https://doi.org/10.1021/acs.langmuir.6b02662>
- Lim, Z.-Z.J., Li, J.-E.J., Ng, C.-T., Yung, L.-Y.L., Bay, B.-H., 2011. Gold nanoparticles in cancer therapy. *Acta Pharmacol. Sin.* 32, 983–990. <https://doi.org/10.1038/aps.2011.82>

- Link, S., El-Sayed, M.A., 1999. Size and Temperature Dependence of the Plasmon Absorption of Colloidal Gold Nanoparticles. *J. Phys. Chem. B* 103, 4212–4217. <https://doi.org/10.1021/jp984796o>
- Liu, Y.C., Lin, L.H., 2004. New pathway for the synthesis of ultrafine silver nanoparticles from bulk silver substrates in aqueous solutions by sonoelectrochemical methods. *Electrochem. commun.* 6, 1163–1168. <https://doi.org/10.1016/j.elecom.2004.09.010>
- Logeswari, P., Silambarasan, S., Abraham, J., 2015. Synthesis of silver nanoparticles using plants extract and analysis of their antimicrobial property. *J. Saudi Chem. Soc.* 19, 311–317. <https://doi.org/10.1016/J.JSCS.2012.04.007>
- Lucky, S.S., Soo, K.C., Zhang, Y., 2015. Nanoparticles in photodynamic therapy. *Chem. Rev.* 115, 1990–2042. <https://doi.org/10.1021/cr5004198>
- Lukman, A.I., Gong, B., Marjo, C.E., Roessner, U., Harris, A.T., 2011. Facile synthesis, stabilization, and anti-bacterial performance of discrete Ag nanoparticles using *Medicago sativa* seed exudates. *J. Colloid Interface Sci.* 353, 433–444. <https://doi.org/10.1016/j.jcis.2010.09.088>
- Lv, Y., Hao, L., Hu, W., Ran, Y., Bai, Y., Zhang, L., 2016. Novel multifunctional pH-sensitive nanoparticles loaded into microbubbles as drug delivery vehicles for enhanced tumor targeting. *Sci. Rep.* 6, 29321. <https://doi.org/10.1038/srep29321>
- Ma, Z.Y., Xia, H.X., Liu, Y.P., Liu, B., Chen, W., Zhao, Y., Di, 2013. Applications of gold nanorods in biomedical imaging and related fields. *Chinese Sci. Bull.* 58, 2530–2536. <https://doi.org/10.1007/s11434-013-5720-7>
- Mabona, U., Van Vuuren, S.F., 2013. Southern African medicinal plants used to treat skin diseases. *South African J. Bot.* 87, 175–193. <https://doi.org/10.1016/J.SAJB.2013.04.002>
- Machado, G.H.A., Marques, T.R., de Carvalho, T.C.L., Duarte, A.C., de Oliveira, F.C., Gonçalves, M.C., Piccoli, R.H., Corrêa, A.D., 2018. Antibacterial activity and in vivo wound healing potential of phenolic extracts from jaboticaba skin. *Chem. Biol. Drug Des.* 92, 1333–1343. <https://doi.org/10.1111/cbdd.13198>
- Male, K.B., Li, J., Buh, C.C., Ng, S.C., Luong, J.H.T., 2008. Synthesis and stability of fluorescent gold nanoparticles by sodium borohydride in the presence of mono-6-deoxy-6-pyridinium- β -cyclodextrin chloride. *J. Phys. Chem. C* 112, 443–451. <https://doi.org/10.1021/jp7099515>
- Malhotra, B., Ali, A., 2017. *Nanomaterials for Biosensors Fundamentals and Applications*. Elsevier, Amsterdam, Netherlands.
- Malik, P., Shankar, R., Malik, V., Sharma, N., Mukherjee, T.K., 2014. Green Chemistry Based Benign Routes for Nanoparticle Synthesis. *J. Nanoparticles* 2014. <https://doi.org/10.1155/2014/302429>
- Mallick, K., Witcomb, M.J., Scurrall, M.S., 2005. Self-assembly of silver nanoparticles in a polymer solvent : formation of a nanochain through nanoscale soldering. *Mater. Chem. Phys.* 90, 221–224. <https://doi.org/10.1016/j.matchemphys.2004.10.030>

- Manke, A., Wang, L., Rojanasakul, Y., 2013. Mechanisms of nanoparticle-induced oxidative stress and toxicity. *Biomed Res. Int.* 2013, 15. <https://doi.org/10.1155/2013/942916>
- Manning, J.C., Goldblatt, P., 2012. *Plants of the Greater Cape Floristic Region : The Core Cape flora.* South African National Biodiversity Institute, SANBI, Pretoria, South Africa.
- Mata, R., Bhaskaran, A., Sadras, S.R., 2016. Green-synthesized gold nanoparticles from *Plumeria alba* flower extract to augment catalytic degradation of organic dyes and inhibit bacterial growth. *Particuology* 24, 78–86. <https://doi.org/10.1016/J.PARTIC.2014.12.014>
- Mativandlela, S.P.N., Muthivhi, T., Kikuchi, H., Oshima, Y., Hamilton, C., Hussein, A.A., van der Walt, M.L., Houghton, P.J., Lall, N., 2009. Antimycobacterial flavonoids from the leaf extract of *Galenia africana*. *J. Nat. Prod.* 72, 2169–2171. <https://doi.org/10.1021/np800778b>
- McGaw, L.J., Lall, N., Meyer, J.J.M., Eloff, J.N., 2008. The potential of South African plants against *Mycobacterium* infections. *J. Ethnopharmacol.* 119, 482–500. <https://doi.org/10.1016/j.jep.2008.08.022>
- Medley, C.D., Smith, J.E., Tang, Z., Yanrong, W., Bamrungsap, S., Weihong, T., 2008. Gold Nanoparticle-Based Colorimetric Assay for the Direct Detection of Cancerous Cells. *Anal. Chem.* 80, 1067–1072. <https://doi.org/10.1021/AC702037Y>
- Meirow, Y., Baniyash, M., 2017. Immune biomarkers for chronic inflammation related complications in non-cancerous and cancerous diseases. *Cancer Immunol. Immunother.* 66, 1089–1101. <https://doi.org/10.1007/s00262-017-2035-6>
- Menke, N.B., Ward, K.R., Witten, T.M., Bonchev, D.G., Diegelmann, R.F., 2007. Impaired wound healing. *Clin. Dermatol.* 25, 19–25. <https://doi.org/10.1016/j.clindermatol.2006.12.005>
- Mills, E., Cooper, C., Seely, D., Kanfer, I., 2005. African herbal medicines in the treatment of HIV: Hypoxis and *Sutherlandia*. An overview of evidence and pharmacology. *Nutr. J.* 4. <https://doi.org/10.1186/1475-2891-4-19>
- Mittal, A.K., Chisti, Y., Banerjee, U.C., 2013. Synthesis of metallic nanoparticles using plant extracts. *Biotechnol. Adv.* 31, 346–356. <https://doi.org/10.1016/j.biotechadv.2013.01.003>
- Mody, V. V., Siwale, R., Singh, A., Mody, H.R., 2010. Introduction to metallic nanoparticles. *J. Pharm. Bioallied Sci.* 2, 282–9. <https://doi.org/10.4103/0975-7406.72127>
- Mohamed, M.M., Fouad, S.A., Elshoky, H.A., Mohammed, G.M., Salaheldin, T.A., 2017. Antibacterial effect of gold nanoparticles against *Corynebacterium pseudotuberculosis*. *Int. J. Vet. Sci. Med.* 5, 23–29. <https://doi.org/10.1016/J.IJVSM.2017.02.003>
- Molfetta, R., Quatrini, L., Santoni, A., Paolini, R., 2017. Regulation of NKG2D-Dependent NK Cell Functions: The Yin and the Yang of Receptor Endocytosis. *Int. J. Mol. Sci.* 18. <https://doi.org/10.3390/ijms18081677>
- Moreno-Vega, A.I., Gómez-Quintero, T., Nuñez-Anita, R.E., Acosta-Torres, L.S., Castaño,

- V., 2012. Polymeric and ceramic nanoparticles in biomedical applications. *J. Nanotechnol.* 2012. <https://doi.org/10.1155/2012/936041>
- Mosser, D.M., Edwards, J.P., 2008. Exploring the full spectrum of macrophage activation. *Nat. Rev. Immunol.* 8, 958–969. <https://doi.org/10.1038/nri2448>
- Mühling, M., Bradford, A., Readman, J.W., Somerfield, P.J., Handy, R.D., 2009. An investigation into the effects of silver nanoparticles on antibiotic resistance of naturally occurring bacteria in an estuarine sediment. *Mar. Environ. Res.* 68, 278–283. <https://doi.org/10.1016/j.marenvres.2009.07.001>
- Mukherjee, S., Sau, S., Madhuri, D., Bollu, V.S., Madhusudana, K., Sreedhar, B., Banerjee, R., Patra, C.R., 2016. Green Synthesis and Characterization of Monodispersed Gold Nanoparticles: Toxicity Study, Delivery of Doxorubicin and Its Bio-Distribution in Mouse Model. *J. Biomed. Nanotechnol.* 12, 165–181.
- Murphy, C.J., San, T.K., Gole, A.M., Orendorff, C.J., Gao, J.X., Gou, L., Hunyadi, S.E., Li, T., 2005. Anisotropic metal nanoparticles: Synthesis, assembly, and optical applications. *J. Phys. Chem. B* 109, 13857–13870. <https://doi.org/10.1021/jp0516846>
- Murugan, K., Benelli, G., Panneerselvam, C., Subramaniam, J., Jeyalalitha, T., Dinesh, D., Nicoletti, M., Hwang, J.-S., Suresh, U., Madhiyazhagan, P., 2015. Cymbopogon citratus-synthesized gold nanoparticles boost the predation efficiency of copepod *Mesocyclops aspericornis* against malaria and dengue mosquitoes. *Exp. Parasitol.* 153, 129–138. <https://doi.org/10.1016/j.exppara.2015.03.017>
- Nadeem, M., Abbasi, B.H., Younas, M., Ahmad, W., Khan, T., 2017. A review of the green syntheses and anti-microbial applications of gold nanoparticles. *Green Chem. Lett. Rev.* 10, 216–227. <https://doi.org/10.1080/17518253.2017.1349192>
- Nair, V., 2006. Pharmaceutical analysis and drug interaction studies : African potato (*Hypoxis hemerocallidea*). Rhodes University.
- Naraginti, S., Li, Y., 2017. Preliminary investigation of catalytic, antioxidant, anticancer and bactericidal activity of green synthesized silver and gold nanoparticles using *Actinidia deliciosa*. *J. Photochem. Photobiol. B Biol.* 170, 225–234. <https://doi.org/10.1016/j.jphotobiol.2017.03.023>
- Nasrollahzadeh, M., Sajadi, S.M., Maham, M., 2015. Green synthesis of palladium nanoparticles using *Hippophae rhamnoides* Linn leaf extract and their catalytic activity for the Suzuki–Miyaura coupling in water. *J. Mol. Catal. A Chem.* 396, 297–303. <https://doi.org/10.1016/J.MOLCATA.2014.10.019>
- Nath, D., Banerjee, P., 2013. Green nanotechnology - A new hope for medical biology. *Environ. Toxicol. Pharmacol.* 36, 997–1014. <https://doi.org/10.1016/j.etap.2013.09.002>
- Nathan, C., Shiloh, M.U., 2000. Reactive oxygen and nitrogen intermediates in the relationship between mammalian hosts and microbial pathogens. *Proc. Natl. Acad. Sci. U. S. A.* 97, 8841–8848.
- Ncube, B., Finnie, J.F., Van Staden, J., 2012. In vitro antimicrobial synergism within plant extract combinations from three South African medicinal bulbs. *J. Ethnopharmacol.* 139, 81–89. <https://doi.org/10.1016/j.jep.2011.10.025>

- Nel, A.E., Mädler, L., Velegol, D., Xia, T., Hoek, E.M. V., Somasundaran, P., Klaessig, F., Castranova, V., Thompson, M., 2009. Understanding biophysicochemical interactions at the nano–bio interface. *Nat. Mater.* 8, 543–557. <https://doi.org/10.1038/nmat2442>
- Nguyen, D.T., Kim, D.-J., Kim, K.-S., 2011. Controlled synthesis and biomolecular probe application of gold nanoparticles. *Micron* 42, 207–227. <https://doi.org/10.1016/J.MICRON.2010.09.008>
- Nirmala Grace, A., Pandian, K., 2007. Antibacterial efficacy of aminoglycosidic antibiotics protected gold nanoparticles-A brief study. *Colloids Surfaces A Physicochem. Eng. Asp.* 297, 63–70. <https://doi.org/10.1016/j.colsurfa.2006.10.024>
- Nouailhat, A., 2008. *An Introduction to Nanoscience and Nanotechnology - Nouailhat - Wiley Online Library.* ISTE Ltd and John Wiley & Sons, Inc. <https://doi.org/10.1002/9780470610954>
- Nune, S.K., Chanda, N., Shukla, R., Katti, K., Kulkarni, R.R., Thilakavathi, S., Mekapothula, S., Kannan, R., Katti, K. V, 2009. Green Nanotechnology from Tea: Phytochemicals in Tea as Building Blocks for Production of Biocompatible Gold Nanoparticles. *J. Mater. Chem.* 19, 2912–2920. <https://doi.org/10.1039/b822015h>
- Ojewole, J.A.O., 2006. Antinociceptive, anti-inflammatory and antidiabetic properties of *Hypoxis hemerocallidea* Fisch. & C.A. Mey. (Hypoxidaceae) corm [“African Potato”] aqueous extract in mice and rats. *J. Ethnopharmacol.* 103, 126–134. <https://doi.org/10.1016/J.JEP.2005.07.012>
- Oppenheim, J.J., Yang, D., 2005. Alarmins: chemotactic activators of immune responses. *Curr. Opin. Immunol.* 17, 359–365. <https://doi.org/10.1016/j.coi.2005.06.002>
- Orgill, D., Demling, R.H., 1988. Current concepts and approaches to wound healing. *Crit. Care Med.* 16, 899–908.
- Pahwa, R., Jialal, I., 2018. *Chronic Inflammation, StatPearls.* StatPearls Publishing.
- Pan, Y., Neuss, S., Leifert, A., Fischler, M., Wen, F., Simon, U., Schmid, G., Brandau, W., Jahnen-Dechent, W., 2007. Size-Dependent Cytotoxicity of Gold Nanoparticles. *Small* 3, 1941–1949. <https://doi.org/10.1002/sml.200700378>
- Park, S.Y., Chae, S.Y., Park, J.O., Lee, K.J., Park, G., 2017. Kalopanax Cortex extract-capped gold nanoparticles activate NRF2 signaling and ameliorate damage in human neuronal SH-SY5Y cells exposed to oxygen–glucose deprivation and reoxygenation. *Int. J. Nanomedicine* 12, 4563–4578. <https://doi.org/10.2147/IJN.S138178>
- Park, Y., Hong, Y.N., Weyers, A., Kim, Y.S., Linhardt, R.J., 2011. Polysaccharides and phytochemicals: a natural reservoir for the green synthesis of gold and silver nanoparticles. *IET Nanobiotechnology* 5, 69–78. <https://doi.org/10.1049/iet-nbt.2010.0033>
- Patra, H.K., Banerjee, S., Chaudhuri, U., Lahiri, P., Dasgupta, A.K., 2007. Cell selective response to gold nanoparticles. *Nanomedicine Nanotechnology, Biol. Med.* 3, 111–119. <https://doi.org/10.1016/j.nano.2007.03.005>
- Payne, J.N., Waghwani, H.K., Connor, M.G., Hamilton, W., Tockstein, S., Moolani, H.,

- Chavda, F., Badwaik, V., Lawrenz, M.B., Dakshinamurthy, R., 2016. Novel synthesis of kanamycin conjugated gold nanoparticles with potent antibacterial activity. *Front. Microbiol.* 7. <https://doi.org/10.3389/fmicb.2016.00607>
- Peer, D., Karp, J.M., Hong, S., Farokhzad, O.C., Margalit, R., Langer, R., 2007. Nanocarriers as an emerging platform for cancer therapy. *Nat. Nanotechnol.* 2, 751–760. <https://doi.org/10.1038/nnano.2007.387>
- Penders, J., Stolzoff, M., Hickey, D.J., Andersson, M., Webster, T.J., 2017. Shape-dependent antibacterial effects of non-cytotoxic gold nanoparticles. *Int. J. Nanomedicine* 12, 2457–2468. <https://doi.org/10.2147/IJN.S124442>
- Peng, G., Tisch, U., Adams, O., Hakim, M., Shehada, N., Broza, Y.Y., Billan, S., Abdah-Bortnyak, R., Kuten, A., Haick, H., 2009. Diagnosing lung cancer in exhaled breath using gold nanoparticles. *Nat. Nanotechnol.* 4, 669–673. <https://doi.org/10.1038/nnano.2009.235>
- Peterson, J.M., Barbul, A., Breslin, R.J., Wasserkrug, H.L., Efron, G., 1987. Significance of T-lymphocytes in wound healing. *Surgery* 102, 300–305.
- Pierce, G.F., Vande Berg, J., Rudolph, R., Tarpley, J., Mustoe, T.A., 1991. Platelet-derived growth factor-BB and transforming growth factor beta 1 selectively modulate glycosaminoglycans, collagen, and myofibroblasts in excisional wounds. *Am. J. Pathol.* 138, 629–646.
- Pîrvănescu, H., Bălăşoiu, M., Ciurea, M.E., Bălăşoiu, A.T., Mănescu, R., 2014. Wound infections with multi-drug resistant bacteria. *Chirurgia (Bucur)*. 109, 73–79.
- Pitkethly, M., 2004. Nanomaterials – the Driving Force. *materialstoday* 7, 20–29.
- Pluen, A., Boucher, Y., Ramanujan, S., McKee, T.D., Gohongi, T., di Tomaso, E., Brown, E.B., Izumi, Y., Campbell, R.B., Berk, D.A., Jain, R.K., 2001. Role of tumor-host interactions in interstitial diffusion of macromolecules: Cranial vs. subcutaneous tumors. *Proc. Natl. Acad. Sci.* 98, 4628–4633. <https://doi.org/10.1073/pnas.081626898>
- Pokropivny, V. V., Skorokhod, V. V., 2007. Classification of nanostructures by dimensionality and concept of surface forms engineering in nanomaterial science. *Mater. Sci. Eng. C* 27, 990–993. <https://doi.org/10.1016/j.msec.2006.09.023>
- Polte, J., 2015. Fundamental growth principles of colloidal metal nanoparticles – a new perspective. *CrystEngComm* 17, 6809–6830. <https://doi.org/10.1039/C5CE01014D>
- Polte, J., Ahner, T.T., Delissen, F., Sokolov, S., Emmerling, F., Thünemann, A.F., Kraehnert, R., 2010. Mechanism of Gold Nanoparticle Formation in the Classical Citrate Synthesis Method Derived from Coupled In Situ XANES and SAXS Evaluation. *J. Am. Chem. Soc.* 132, 1296–1301. <https://doi.org/10.1021/ja906506j>
- Pool, J.G., 1977. Normal hemostatic mechanisms: a review. *Am. J. Med. Technol.* 43, 776–80.
- Poole, C., 2003. *Introduction to Nanotechnology*. John Wiley & Sons, Inc., Hoboken, New Jersey.
- Power, C., Wang, J.H., Sookhai, S., Street, J.T., Redmond, H.P., 2001. Bacterial Wall

- Products Induce Downregulation of Vascular Endothelial Growth Factor Receptors on Endothelial Cells via a CD14-Dependent Mechanism: Implications for Surgical Wound Healing. *J. Surg. Res.* 101, 138–145. <https://doi.org/10.1006/JSRE.2001.6270>
- Prasad, K., Jha, A.K., Kulkarni, A.R., 2007. Lactobacillus assisted synthesis of titanium nanoparticles. *Nanoscale Res. Lett.* 2, 248–250. <https://doi.org/10.1007/s11671-007-9060-x>
- Priyadarshini, E., Pradhan, N., 2017. Gold nanoparticles as efficient sensors in colorimetric detection of toxic metal ions: A review. *Sensors Actuators B Chem.* 238, 888–902. <https://doi.org/10.1016/J.SNB.2016.06.081>
- Qiu, P., Yang, M., Qu, X., Huai, Y., Zhu, Y., Mao, C., 2016. Tuning photothermal properties of gold nanodendrites for in vivo cancer therapy within a wide near infrared range by simply controlling their degree of branching. *Biomaterials* 104, 138–144. <https://doi.org/10.1016/j.biomaterials.2016.06.033>
- Raikar, U.S., Tangod, V.B., Mastiholi, B.M., Fulari, V.J., 2011. Fluorescence quenching using plasmonic gold nanoparticles. *Opt. Commun.* 284, 4761–4765. <https://doi.org/10.1016/J.OPTCOM.2011.05.038>
- Rajan, A., Rajan, A.R., Philip, D., 2017. Elettaria cardamomum seed mediated rapid synthesis of gold nanoparticles and its biological activities. *OpenNano* 2, 1–8. <https://doi.org/10.1016/j.onano.2016.11.002>
- Ramajo, L., Parra, R., Reboredo, M., Castro, M., 2009. Preparation of amine coated silver nanoparticles using triethylenetetramine. *J. Chem. Sci.* 121, 83–87. <https://doi.org/10.1007/s12039-009-0009-8>
- Ramsden, J., 2009. *Essentials of Nanotechnology*. Ventus Publishing ApS.
- Rao, P.V., Nallappan, D., Madhavi, K., Rahman, S., Jun Wei, L., Gan, S.H., 2016. Phytochemicals and Biogenic Metallic Nanoparticles as Anticancer Agents. *Oxid. Med. Cell. Longev.* 2016, 3685671. <https://doi.org/10.1155/2016/3685671>
- Rastogi, L., Arunachalam, J., 2013. Green Synthesis Route for the Size Controlled Synthesis of Biocompatible Gold Nanoparticles Using Aqueous Extract of Garlic (*Allium sativum*). *Adv. Materials Lett.* 4, 548–555.
- Rastogi, L., Arunachalam, J., 2012. Microwave-Assisted Green Synthesis of Small Gold Nanoparticles Using Aqueous Garlic (*Allium sativum*) Extract: Their Application as Antibiotic Carriers. *Int. J. Green Nanotechnol.* 4, 163–173. <https://doi.org/10.1080/19430892.2012.676926>
- Rauch, I., Müller, M., Decker, T., 2013. The regulation of inflammation by interferons and their STATs. *JAK-STAT* 2, e23820. <https://doi.org/10.4161/jkst.23820>
- Rawat, M.K., Jain, A., Singh, S., 2011. Studies on Binary Lipid Matrix Based Solid Lipid Nanoparticles of Repaglinide: in Vitro and in Vivo Evaluation. *J. Pharm. Sci.* 100, 2366–2378. <https://doi.org/10.1002/JPS.22435>
- Reddy, D.B., Reddanna, P., 2009. Chebulagic acid (CA) attenuates LPS-induced inflammation by suppressing NF- κ B and MAPK activation in RAW 264.7

- macrophages. *Biochem. Biophys. Res. Commun.* 381, 112–117.
<https://doi.org/10.1016/j.bbrc.2009.02.022>
- Rhee, C.M., Bhan, I., Alexander, E.K., Brunelli, S.M., 2012. Association Between Iodinated Contrast Media Exposure and Incident Hyperthyroidism and Hypothyroidism. *Arch. Intern. Med.* 172, 153–159. <https://doi.org/10.1001/archinternmed.2011.677>
- Ricciotti, E., FitzGerald, G.A., 2011. Prostaglandins and inflammation. *Arterioscler. Thromb. Vasc. Biol.* 31, 986–1000. <https://doi.org/10.1161/ATVBAHA.110.207449>
- Riley, R.S., Day, E.S., 2017. Gold nanoparticle-mediated photothermal therapy: applications and opportunities for multimodal cancer treatment. *Wiley Interdiscip. Rev. Nanomedicine Nanobiotechnology* 9, e1449. <https://doi.org/10.1002/wnan.1449>
- Robson, M.C., Stenberg, B.D., Heggors, J.P., 1990. Wound healing alterations caused by infection. *Clin. Plast. Surg.* 17, 485–492.
- Rouhana, L.L., Jaber, J.A., Schlenoff, J.B., 2007. Aggregation-resistant water-soluble gold nanoparticles. *Langmuir* 23, 12799–12801. <https://doi.org/10.1021/la702151q>
- Saha, K., Agasti, S.S., Kim, C., Li, X., Rotello, V.M., 2012. Gold nanoparticles in chemical and biological sensing. *Chem. Rev.* 112, 2739–2779. <https://doi.org/10.1021/cr2001178>
- Sansone, P., Storci, G., Tavolari, S., Guarnieri, T., Giovannini, C., Taffurelli, M., Ceccarelli, C., Santini, D., Paterini, P., Marcu, K.B., Chieco, P., Bonafè, M., 2007. IL-6 triggers malignant features in mammospheres from human ductal breast carcinoma and normal mammary gland. *J. Clin. Invest.* 117, 3988–4002. <https://doi.org/10.1172/JCI32533>
- Santhoshkumar, J., Rajeshkumar, S., Venkat Kumar, S., 2017. Phyto-assisted synthesis, characterization and applications of gold nanoparticles – A review. *Biochem. Biophys. Reports* 11, 46–57. <https://doi.org/10.1016/j.bbrep.2017.06.004>
- Schweizer, A., Feige, U., Fontana, A., Müller, K., Dinarello, C.A., 1988. Interleukin-1 enhances pain reflexes. Mediation through increased prostaglandin E2 levels. *Agents Actions* 25, 246–251.
- Shah, M., Fawcett, D., Sharma, S., Tripathy, S.K., Poinern, G.E.J., 2015. Green synthesis of metallic nanoparticles via biological entities, *Materials*.
<https://doi.org/10.3390/ma8115377>
- Shamaila, S., Zafar, N., Riaz, S., Sharif, R., Nazir, J., Naseem, S., 2016. Gold Nanoparticles: An Efficient Antimicrobial Agent against Enteric Bacterial Human Pathogen. *Nanomaterials* 6. <https://doi.org/10.3390/nano6040071>
- Shankar, P.D., Shobana, S., Karuppusamy, I., Pugazhendhi, A., Ramkumar, V.S., Arvindnarayan, S., Kumar, G., 2016. A review on the biosynthesis of metallic nanoparticles (gold and silver) using bio-components of microalgae: Formation mechanism and applications. *Enzyme Microb. Technol.* 95, 28–44.
<https://doi.org/10.1016/j.enzmictec.2016.10.015>
- Sharon, M., Sharon, M., Pandey, S., Oza, G., 2012. *Bio-nanotechnology: concepts and applications*. CRC press, Boca Raton, FL, USA.
- Sheth, A.N., 2013. Can Anti-Inflammatory Drugs Fight Infection? *Sci. Transl. Med.* 5,

192ec110. <https://doi.org/10.1126/scitranslmed.3006879>

- Shukla, R., Bansal, V., Chaudhary, M., Basu, A., Bhonde, R.R., Sastry, M., 2005. Biocompatibility of Gold Nanoparticles and Their Endocytotic Fate Inside the Cellular Compartment: A Microscopic Overview. *Langmuir* 21, 10644–10654. <https://doi.org/10.1021/LA0513712>
- Siddiqi, K.S., Husen, A., 2017. Recent advances in plant-mediated engineered gold nanoparticles and their application in biological system. *J. Trace Elem. Med. Biol.* 40, 10–23. <https://doi.org/10.1016/J.JTEMB.2016.11.012>
- Siddiqi, K.S., Husen, A., 2016. Green Synthesis, Characterization and Uses of Palladium/Platinum Nanoparticles. *Nanoscale Res. Lett.* 11, 482. <https://doi.org/10.1186/s11671-016-1695-z>
- Sieweke, M.H., Allen, J.E., 2013. Beyond Stem Cells: Self-Renewal of Differentiated Macrophages. *Science* (80-.). 342.
- Singh, A.K., Talat, M., Singh, D.P., Srivastava, O.N., 2010. Biosynthesis of gold and silver nanoparticles by natural precursor clove and their functionalization with amine group. *J. Nanoparticle Res.* 12, 1667–1675. <https://doi.org/10.1007/s11051-009-9835-3>
- Singh, N., Armstrong, D.G., Lipsky, B.A., 2005. Preventing Foot Ulcers in Patients With Diabetes. *JAMA* 293, 217–228. <https://doi.org/10.1001/jama.293.2.217>
- Singh, S., Young, A., McNaught, C.E., 2017. The physiology of wound healing. *Surgery* 35, 473–477. <https://doi.org/10.1016/j.mpsur.2017.06.004>
- Singh, Y., 2009. Systematics of Hypoxis (Hypoxidaceae) in Southern Africa. University of Pretoria.
- Sjöström, T., Nobbs, A.H., Su, B., 2016. Bactericidal nanospikes via thermal oxidation of Ti alloy substrates. *Mater. Lett.* 167, 22–26. <https://doi.org/10.1016/J.MATLET.2015.12.140>
- Slavin, Y.N., Asnis, J., Häfeli, U.O., Bach, H., 2017. Metal nanoparticles: understanding the mechanisms behind antibacterial activity. *J. Nanobiotechnology* 15, 65. <https://doi.org/10.1186/s12951-017-0308-z>
- Smyth, M.J., Cretney, E., Kelly, J.M., Westwood, J.A., Street, S.E.A., Yagita, H., Takeda, K., Dommelen, S.L.H. van, Degli-Esposti, M.A., Hayakawa, Y., 2005. Activation of NK cell cytotoxicity. *Mol. Immunol.* 42, 501–510. <https://doi.org/10.1016/J.MOLIMM.2004.07.034>
- Sonohara, R., Muramatsu, N., Ohshima, H., Kondo, T., 1995. Difference in surface properties between *Escherichia coli* and *Staphylococcus aureus* as revealed by electrophoretic mobility measurements. *Biophys. Chem.* 55, 273–277. [https://doi.org/10.1016/0301-4622\(95\)00004-H](https://doi.org/10.1016/0301-4622(95)00004-H)
- Sperling, R.A., Pellegrino, T., Li, J.K., Chang, W.H., Parak, W.J., 2006. Electrophoretic Separation of Nanoparticles with a Discrete Number of Functional Groups. *Adv. Funct. Mater.* 16, 943–948. <https://doi.org/10.1002/adfm.200500589>
- Steenkamp, V., Gouws, M.C., 2006. Cytotoxicity of six South African medicinal plant

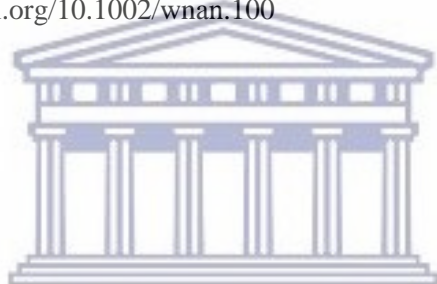
- extracts used in the treatment of cancer. *South African J. Bot.* 72, 630–633.
<https://doi.org/10.1016/J.SAJB.2006.02.004>
- Su, X., Liu, X., Wang, S., Li, B., Pan, T., Liu, D., Wang, F., Diao, Y., Li, K., 2017. Wound-healing promoting effect of total tannins from *Entada phaseoloides* (L.) Merr. in rats. *Burns* 43, 830–838. <https://doi.org/10.1016/j.burns.2016.10.010>
- Sumbayev, V. V., Yasinska, I.M., Garcia, C.P., Gilliland, D., Lall, G.S., Gibbs, B.F., Bonsall, D.R., Varani, L., Rossi, F., Calzolari, L., 2013. Gold Nanoparticles Downregulate Interleukin-1 β -Induced Pro-Inflammatory Responses. *Small* 9, 472–477.
<https://doi.org/10.1002/sml.201201528>
- Suresh, S., 2013. Semiconductor Nanomaterials, Methods and Applications: A Review. *Nanosci. Nanotechnol.* 3, 62–74. <https://doi.org/10.5923/j.nn.20130303.06>
- Sýkora, D., Kašička, V., Mikšík, I., Řezanka, P., Záruba, K., Matějka, P., Král, V., 2010. Application of gold nanoparticles in separation sciences. *J. Sep. Sci.* 33, 372–387.
<https://doi.org/10.1002/jssc.200900677>
- Tanaka, T., Narazaki, M., Kishimoto, T., 2014. IL-6 in inflammation, immunity, and disease. *Cold Spring Harb. Perspect. Biol.* 6, a016295.
<https://doi.org/10.1101/cshperspect.a016295>
- Thakral, S., Mehta, R.M., 2006. Fullerenes: An introduction and overview of their biological properties. *Indian J. Pharm. Sci.* 68, 13. <https://doi.org/10.4103/0250-474X.22957>
- Thomas, S., Harshita, B.S.P., Mishra, P., Talegaonkar, S., 2015. Ceramic Nanoparticles: Fabrication Methods and Applications in Drug Delivery. *Curr. Pharm. Des.* 21, 6165–6188. <https://doi.org/10.2174/1381612821666151027153246>
- Toy, L.W., 2005. Matrix metalloproteinases: their function in tissue repair. *J. Wound Care* 14, 20–22. <https://doi.org/10.12968/jowc.2005.14.1.26720>
- Tran, M., DePenning, R., Turner, M., Padalkar, S., 2016. Effect of citrate ratio and temperature on gold nanoparticle size and morphology. *Mater. Res. Express* 3, 105027.
<https://doi.org/10.1088/2053-1591/3/10/105027>
- Trautwein, C., Rakemann, T., Niehof, M., Rose-John, S., Manns, M.P., 1996. Acute-phase response factor, increased binding, and target gene transcription during liver regeneration. *Gastroenterology* 110, 1854–1862.
- Trinchieri, G., 1989. Biology of Natural Killer Cells. *Adv. Immunol.* 47, 187–376.
[https://doi.org/10.1016/S0065-2776\(08\)60664-1](https://doi.org/10.1016/S0065-2776(08)60664-1)
- Truong, L., Tilton, S.C., Zaikova, T., Richman, E., Waters, K.M., Hutchison, J.E., Tanguay, R.L., 2013. Surface functionalities of gold nanoparticles impact embryonic gene expression responses. *Nanotoxicology* 7, 192–201.
<https://doi.org/10.3109/17435390.2011.648225>
- Tsi Ndeh, N., Maensiri, S., Maensiri, D., 2017. The effect of green synthesized gold nanoparticles on rice germination and roots. *Adv. Nat. Sci. Nanosci. Nanotechnol.* 8, 35008. <https://doi.org/10.1088/2043-6254/aa724a>
- Tsuji, T., Kakita, T., Tsuji, M., 2003. Preparation of nano-size particle of silver with

- femtosecond laser ablation in water. *Appl. Surf. Sci.* 206, 314–320.
- Turkevich, J., Stevenson, P.C., Hillier, J., 1951. A study of the nucleation and growth processes in the synthesis of colloidal gold. *Discuss. Faraday Soc.* 11, 55.
<https://doi.org/10.1039/df9511100055>
- Ueno, C., Hunt, T.K., Hopf, H.W., 2006. Using Physiology to Improve Surgical Wound Outcomes. *Plast. Reconstr. Surg.* 117, 59S–71S.
<https://doi.org/10.1097/01.prs.0000225438.86758.21>
- Umer, A., Naveed, S., Ramzan, N., Rafique, M.S., Imran, M., Umer, A., Naveed, S., Ramzan, N., Rafique, M.S., Imran, M., 2014. A green method for the synthesis of Copper Nanoparticles using L-ascorbic acid. *Matéria (Rio Janeiro)* 19, 197–203.
<https://doi.org/10.1590/S1517-70762014000300002>
- Van Der Lugt, J.J., Schultz, R.A., Fourie, N., Hon, L.J., Jordaan, P., Labuschagne, L., 1992. *Galenia africana* L. poisoning in sheep and goats: hepatic and cardiac changes. *Onderstepoort J. Vet. Res.* 59, 323–33.
- Veerasamy, R., Xin, T.Z., Gunasagaran, S., Xiang, T.F.W., Yang, E.F.C., Jeyakumar, N., Dhanaraj, S.A., 2011. Biosynthesis of silver nanoparticles using mangosteen leaf extract and evaluation of their antimicrobial activities. *J. Saudi Chem. Soc.* 15, 113–120.
<https://doi.org/10.1016/J.JSCS.2010.06.004>
- Velnar, T., Bailey, T., Smrkolj, V., 2009. The Wound Healing Process: An Overview of the Cellular and Molecular Mechanisms. *J. Int. Med. Res.* 37, 1528–1542.
<https://doi.org/10.1177/147323000903700531>
- Ventola, C.L., 2015. The antibiotic resistance crisis: part 1: causes and threats. *Pharm. Ther.* 40, 277–283.
- Vesaratchanon, S., Nikolov, A., Wasan, D.T., 2007. Sedimentation in nano-colloidal dispersions: Effects of collective interactions and particle charge. *Adv. Colloid Interface Sci.* 134–135, 268–278. <https://doi.org/10.1016/J.CIS.2007.04.026>
- Vijayakumar, S., Ganesan, S., 2012. *In Vitro* Cytotoxicity Assay on Gold Nanoparticles with Different Stabilizing Agents. *J. Nanomater.* 2012, 1–9.
<https://doi.org/10.1155/2012/734398>
- Vivier, E., Tomasello, E., Baratin, M., Walzer, T., Ugolini, S., 2008. Functions of natural killer cells. *Nat. Immunol.* 9, 503–510. <https://doi.org/10.1038/ni1582>
- Vo-Dinh, T., 2006. Nanotechnology in Biology and Medicine: The New Frontier, in: Vo-Dinh, T. (Ed.), *Nanotechnology in Biology and Medicine: Methods, Devices, and Applications*. CRC Press, New York, pp. 23–31.
- Vries, F.A., El Bitar, H., Green, I.R., Klaasen, J.A., Bodo, B., Johnson, Q., Mabusela, W.T., 2005. An antifungal active extract from the aerial parts of *Galenia africana*, in: 11th Napreca Symposium Book of Proceedings. Antananarivo, Madagascar, pp. 123–131.
- Wagers, K., Chui, T., Adem, S., 2014. Effect of pH on the Stability of Gold Nanoparticles and Their Application for Melamine Detection in Infant Formula. *IOSR J. Appl. Chem.* 7, 15–20.

- Walzer, T., Dalod, M., Robbins, S.H., Zitvogel, L., Vivier, E., 2005. Natural-killer cells and dendritic cells: "l'union fait la force" Blood 106, 2252–2258. <https://doi.org/10.1182/blood-2005-03-1154>
- Wang, F., Li, D., Mao, C., 2008. Genetically Modifiable Flagella as Templates for Silica Fibers: From Hybrid Nanotubes to 1D Periodic Nanohole Arrays. *Adv. Funct. Mater.* 18, 4007–4013. <https://doi.org/10.1002/adfm.200800889>
- Wang, F., Nimmo, S.L., Cao, B., Mao, C., 2012. Oxide formation on biological nanostructures via a structure-directing agent: towards an understanding of precise structural transcription. *Chem. Sci.* 3, 2639. <https://doi.org/10.1039/c2sc00583b>
- Wang, G., Lu, Y., Yan, C., Lu, Y., 2015. DNA-functionalization gold nanoparticles based fluorescence sensor for sensitive detection of Hg²⁺ in aqueous solution. *Sensors Actuators B Chem.* 211, 1–6. <https://doi.org/10.1016/J.SNB.2015.01.051>
- Wang, L., Hu, C., Shao, L., 2017. The antimicrobial activity of nanoparticles: present situation and prospects for the future. *Int. J. Nanomedicine* 12, 1227–1249. <https://doi.org/10.2147/IJN.S121956>
- Wang, X., Chang, J., Wu, C., 2018. Bioactive inorganic/organic nanocomposites for wound healing. *Appl. Mater. Today* 11, 308–319. <https://doi.org/10.1016/J.APMT.2018.03.001>
- Watkins, L.R., Wiertelak, E.P., Goehler, L.E., Smith, K.P., Martin, D., Maier, S.F., 1994. Characterization of cytokine-induced hyperalgesia. *Brain Res.* 654, 15–26.
- Wei, M., Chen, N., Li, J., Yin, M., Liang, L., He, Y., Song, H., Fan, C., Huang, Q., 2012. Polyvalent Immunostimulatory Nanoagents with Self-Assembled CpG Oligonucleotide-Conjugated Gold Nanoparticles. *Angew. Chemie Int. Ed.* 51, 1202–1206. <https://doi.org/10.1002/anie.201105187>
- Wieder, M.E., Hone, D.C., Cook, M.J., Handsley, M.M., Gavrilovic, J., Russell, D.A., 2006. Intracellular photodynamic therapy with photosensitizer-nanoparticle conjugates: cancer therapy using a "Trojan horse". *Photochem. Photobiol. Sci.* 5, 727–734. <https://doi.org/10.1039/b602830f>
- Wong, H.L., Bendayan, R., Rauth, A.M., Li, Y., Wu, X.Y., 2007. Chemotherapy with anticancer drugs encapsulated in solid lipid nanoparticles. *Adv. Drug Deliv. Rev.* 59, 491–504. <https://doi.org/10.1016/J.ADDR.2007.04.008>
- Woolf, C.J., Allchorne, A., Safieh-Garabedian, B., Poole, S., 1997. Cytokines, nerve growth factor and inflammatory hyperalgesia: the contribution of tumour necrosis factor α . *Br. J. Pharmacol.* 121, 417–424. <https://doi.org/10.1038/sj.bjp.0701148>
- Wu, J., Shen, Y., Jiang, W., Jiang, W., Shen, Y., 2016. Magnetic targeted drug delivery carriers encapsulated with pH-sensitive polymer: synthesis, characterization and *in vitro* doxorubicin release studies. *J. Biomater. Sci. Polym. Ed.* 27, 1303–1316. <https://doi.org/10.1080/09205063.2016.1195159>
- Xie, X., Liao, J., Shao, X., Li, Q., Lin, Y., 2017. The Effect of shape on Cellular Uptake of Gold Nanoparticles in the forms of Stars, Rods, and Triangles. *Sci. Rep.* 7, 3827. <https://doi.org/10.1038/s41598-017-04229-z>

- Xing, T., Sunarso, J., Yang, W., Yin, Y., Glushenkov, A.M., Li, L.H., Howlett, P.C., Chen, Y., 2013. Ball milling: a green mechanochemical approach for synthesis of nitrogen doped carbon nanoparticles. *Nanoscale* 5, 7970–7976. <https://doi.org/10.1039/c3nr02328a>
- Xue, C., Xue, Y., Dai, L., Urbas, A., Li, Q., 2013. Size- and Shape-Dependent Fluorescence Quenching of Gold Nanoparticles on Perylene Dye. *Adv. Opt. Mater.* 1, 581–587. <https://doi.org/10.1002/adom.201300175>
- Yadav, V.S., Mishra, K.P., Singh, D.P., Mehrotra, S., Singh, V.K., 2005. Immunomodulatory Effects of Curcumin. *Immunopharmacol. Immunotoxicol.* 27, 485–497. <https://doi.org/10.1080/08923970500242244>
- Yager, D.R., Nwomeh, B.C., 1999. The proteolytic environment of chronic wounds. *Wound Repair Regen.* 7, 433–441.
- Yang, J., Weinberg, R.A., 2008. Epithelial-Mesenchymal Transition: At the Crossroads of Development and Tumor Metastasis. *Dev. Cell* 14, 818–829. <https://doi.org/10.1016/j.devcel.2008.05.009>
- Yeh, Y.-C., Czeran, B., Rotello, V.M., 2012. Gold nanoparticles: preparation, properties, and applications in bionanotechnology. *Nanoscale* 4, 1871–1880. <https://doi.org/10.1039/c1nr11188d>
- Yen, H.-J., Hsu, S., Tsai, C.-L., 2009. Cytotoxicity and Immunological Response of Gold and Silver Nanoparticles of Different Sizes. *Small* 5, 1553–1561. <https://doi.org/10.1002/smll.200900126>
- Yingchoncharoen, P., Kalinowski, D.S., Richardson, D.R., 2016. Lipid-Based Drug Delivery Systems in Cancer Therapy: What Is Available and What Is Yet to Come. *Pharmacol. Rev.* 68, 701–787. <https://doi.org/10.1124/pr.115.012070>
- Yu, D.G., 2007. Formation of colloidal silver nanoparticles stabilized by Na⁺-poly(γ -glutamic acid)-silver nitrate complex via chemical reduction process. *Colloids Surfaces B Biointerfaces* 59, 171–178. <https://doi.org/10.1016/j.colsurfb.2007.05.007>
- Yu, J., Xu, D., Guan, H.N., Wang, C., Huang, L.K., Chi, D.F., 2016. Facile one-step green synthesis of gold nanoparticles using *Citrus maxima* aqueous extracts and its catalytic activity. *Mater. Lett.* 166, 110–112. <https://doi.org/10.1016/J.MATLET.2015.12.031>
- Yuan, C.G., Huo, C., Yu, S., Gui, B., 2017. Biosynthesis of gold nanoparticles using *Capsicum annum* var. *grossum* pulp extract and its catalytic activity. *Phys. E Low-Dimensional Syst. Nanostructures* 85, 19–26. <https://doi.org/10.1016/j.physe.2016.08.010>
- Yuan, F., Dellian, M., Fukumura, D., Leunig, M., Berk, D.A., Torchilin, V.P., Jain, R.K., 1995. Vascular permeability in a human tumor xenograft: molecular size dependence and cutoff size. *Cancer Res.* 55, 3752–3756.
- Zeng, S., Yong, K.-T., Roy, I., Dinh, X.-Q., Yu, X., Luan, F., 2011. A Review on Functionalized Gold Nanoparticles for Biosensing Applications. *Plasmonics* 6, 491–506. <https://doi.org/10.1007/s11468-011-9228-1>

- Zhang, J.-M., An, J., 2007. Cytokines, inflammation, and pain. *Int. Anesthesiol. Clin.* 45, 27–37. <https://doi.org/10.1097/AIA.0b013e318034194e>
- Zhang, Q., Lambert, G., Liao, D., Kim, H., Robin, K., Tung, C. -k., Pourmand, N., Austin, R.H., 2011. Acceleration of Emergence of Bacterial Antibiotic Resistance in Connected Microenvironments. *Science* (80-.). 333, 1764–1767. <https://doi.org/10.1126/science.1208747>
- Zhang, X., 2015. Gold Nanoparticles: Recent Advances in the Biomedical Applications. *Cell Biochem. Biophys.* 72, 771–775. <https://doi.org/10.1007/s12013-015-0529-4>
- Zhang, X.-D., Guo, M.-L., Wu, H.-Y., Sun, Y.-M., Ding, Y.-Q., Feng, X., Zhang, L.-A., 2009. Irradiation stability and cytotoxicity of gold nanoparticles for radiotherapy. *Int. J. Nanomedicine* 4, 165–173.
- Zhao, P., Li, N., Astruc, D., 2013. State of the art in gold nanoparticle synthesis. *Coord. Chem. Rev.* 257, 638–665. <https://doi.org/10.1016/j.ccr.2012.09.002>
- Zhong, S.P., Zhang, Y.Z., Lim, C.T., 2010. Tissue scaffolds for skin wound healing and dermal reconstruction. *Wiley Interdiscip. Rev. Nanomedicine Nanobiotechnology* 2, 510–525. <https://doi.org/10.1002/wnan.100>



UNIVERSITY *of the*
WESTERN CAPE

**CHAPTER THREE: MANUSCRIPT “LARGE SCALE
SCREENING OF SOUTHERN AFRICAN PLANT EXTRACTS
FOR THE GREEN SYNTHESIS OF GOLD
NANOPARTICLES USING MICROTITRE-PLATE
METHOD”**

UNIVERSITY *of the*
WESTERN CAPE

Article

Large Scale Screening of Southern African Plant Extracts for the Green Synthesis of Gold Nanoparticles Using Microtitre-Plate Method

Abdulrahman M. Elbagory¹, Christopher N. Cupido^{2,3}, Mervin Meyer¹ and Ahmed A. Hussein^{4,*},[†]

¹ DST/Mintek Nanotechnology Innovation Centre, Department of Biotechnology, University of the Western Cape, Private Bag X17, Bellville 7530, South Africa; 3376881@myuwc.ac.za (A.M.E.); memeyer@uwc.ac.za (M.M.)

² South African National Biodiversity Institute, Compton Herbarium, Private bag X7, Claremont 7735, South Africa; C.Cupido@sanbi.org.za

³ Department of Biodiversity and Conservation Biology, University of the Western Cape, Private Bag X17, Bellville 7535, South Africa

⁴ Department of Chemistry, University of the Western Cape, Private Bag X17, Bellville 7530, South Africa

* Correspondence: ahmohammed@uwc.ac.za; Tel.: +27-21-959-2262; Fax: +27-21-959-3055

† Present address: Chemistry Department, Cape Peninsula University of Technology, P.O. BOX 1906, Bellville 7535, South Africa.

Academic Editors: Wei Zhang and Derek J. McPhee

Received: 10 August 2016; Accepted: 1 November 2016; Published: 8 November 2016

Abstract: The preparation of gold nanoparticles (AuNPs) involves a variety of chemical and physical methods. These methods use toxic and environmentally harmful chemicals. Consequently, the synthesis of AuNPs using green chemistry has been under investigation to develop eco-friendly nanoparticles. One approach to achieve this is the use of plant-derived phytochemicals that are capable of reducing gold ions to produce AuNPs. The aim of this study was to implement a facile microtitre-plate method to screen a large number of aqueous plant extracts to determine the optimum concentration (OC) for the bio-synthesis of the AuNPs. Several AuNPs of different sizes and shapes were successfully synthesized and characterized from 17 South African plants. The characterization was done using Ultra Violet-Visible Spectroscopy, Dynamic Light Scattering, High Resolution Transmission Electron Microscopy and Energy-Dispersive X-ray Spectroscopy. We also studied the effects of temperature on the synthesis of the AuNPs and showed that changes in temperatures affect the size and dispersity of the generated AuNPs. We also evaluated the stability of the synthesized AuNPs and showed that some of them are stable in biological buffer solutions.

Keywords: green nanotechnology; gold nanoparticles; biosynthesis; high resolution transmission electron microscopy; Cape flora

1. Introduction

Metallic nanoparticles have potential applications in chemistry, physics and biology due to their unequalled optical, electrical and photothermal properties [1]. These metal nanoparticles have drawn researchers' attention because of the ease of their synthesis and modification [2]. Among the metal nanoparticles, gold nanoparticles (AuNPs) have received much attention for their unique and adjustable Surface Plasmon Resonance (SPR) [3]. AuNPs have been utilized in several biomedical applications such as drug delivery, disease diagnosis, treatment of cancer, photothermal therapy and immunochromatographic identification of pathogens in clinical specimens [4–7].

In general, the preparation of metal nanoparticles involves a variety of chemical and physical methods, such as chemical reduction [8], photochemical reduction [9], electrochemical reduction [10], laser ablation [11] and lithography [12]. These methods are expensive and involve the use of several toxic, environmentally harmful inorganic chemicals, such as sodium/potassium borohydrate, hydrazine and salts of tartrate, or organic chemicals, such as sodium citrate, ascorbic acid and amino acids, which are used for their reducing capabilities [13]. The employment of these harmful chemicals can limit the use of nanoparticles in biomedical applications [14].

Consequently, the green synthesis of AuNPs has been under investigation owing to the rising need to develop biocompatible, less-toxic and eco-friendly nanoparticles. One method to achieve this is the utilization of biological systems such as bacteria, fungi and plant extracts. For example, Kalishwaralal and co-workers synthesized gold nanocubes, ranging from 10 to 100 nm, from the bacterium *Bacillus licheniformis* after incubation with gold salt for 48 h [15]. Shankar et al., synthesized spherical AuNPs from an endophytic fungus (*Colletotrichum* sp.) after 96 h of incubation [16]. Several studies reported the synthesis of AuNPs using extracts from plants such as, *Aloe vera* [17], *Terminalia catappa* [18], *Suaeda monoica* [19], *Trianthema decandra* [1] and *Memecylon umbellatum* [20]. These synthesis methods are not only eco-friendly, but also cost-effective and can be easily modified for large-scale synthesis [1].

The use of plants is more attractive, compared to the other biological systems, as they are readily available, safer and contain wide variety of reducing phytochemicals. Compared to microbial-derived chemicals, the plant-derived phytochemicals require shorter incubation periods with gold salt in order to synthesize AuNPs [2]. These phytochemicals are not only responsible for the synthesis of metal nanoparticles, but also they act as capping agents to prevent the coalescence of colloidal particles, which are kept apart in solution by electrostatic forces [13]. It is thought that different-shaped polyol and water-soluble heterocyclic components of plant phytochemicals are mainly responsible for the reduction and coating the gold ions [20].

The flora of the South Western Cape, which is commonly referred to as the Cape Flora or the Core Cape Sub-region of the Greater Cape Floristic Region, is the smallest and richest floral kingdom in the world. It has over 9300 species occupying a land area of approximately 90,000 km² with about 70% of the species occurring nowhere else in the world [21].

Herein we report the synthesis of AuNPs from aqueous extracts prepared from 17 plants collected from the South Western Cape area of South Africa. The synthesis process was monitored under two different temperature conditions to measure the effect of temperature on the geometric properties of the synthesized AuNPs. The stability of the AuNPs was measured in different biological buffer solutions. Several physical and optical measurement techniques including, Ultraviolet-Visible Spectroscopy (UV-Vis), Dynamic Light Scattering (DLS), High Resolution Transmission Electron Microscopy (HR-TEM) and Energy-dispersive X-ray spectroscopy (EDS) were used to characterize the AuNPs.

2. Results and Discussion

Previous studies reported the green synthesis of the plant-extract mediated AuNPs by mixing fixed concentrations of gold salt solutions with the plant extracts solutions [1,17–20]. In this study, we sought to improve current methods used to biosynthesize AuNPs from plant extracts by developing micro-scale method to screen a large number of plants simultaneously. Using this method, we can also determine the optimum concentrations (OC) at which the plant extracts can reduce gold salts to form AuNPs.

2.1. Synthesis of AuNPs and Their UV-Vis Analysis

The formation of the AuNPs was visually observed by the development of red/wine-red colour in the 96 well plates. The measurement of the UV-Vis spectra also confirmed the formation of the AuNPs. A maxima absorbance between 500 and 600 nm (Table 1), is attributed to the excitation of AuNPs' SPR [22] and considered as a distinct feature for the presence of AuNPs. Synthesis with three

plant extracts namely; *Aspalathus hispida*, *Asparagus rubicundus*, and *Dicerotheramnus rhinocertis*, did not produce any colour change at 25 °C. This may indicate the absence of strong reducing phytochemicals in their aqueous extracts, which may require higher temperatures to initiate the reduction process. However, since in this study the extracts were incubated with gold salt for 1 h, the synthesis of AuNPs with these plant extracts may also require longer periods to initiate the reduction of the gold ions at low temperature. Epigallocatechin gallate (EGCG), a phytochemical present in tea, was previously reported by Nune et al. to reduce gold salt [23] and used as a control to monitor the synthesized AuNPs. The λ_{\max} of EGCG was 532 nm, which is within the same range of 530 nm the λ_{\max} reported by Nune et al. [23].

The SPR of the AuNPs can be affected by factors such as particle shape and size, the refractive index of the dispersion medium and the average distance between neighbouring AuNPs [24]. From the UV-Vis spectra of the AuNPs shown in Figure 1, it is evident that no major shifts were observed for AuNPs synthesized at 25 °C or at 70 °C. The notable difference observed, however, was the dissimilarity in the peaks' height, which may relate to the number of the nanoparticles produced, as the OD-value correlates linearly with the concentration of the AuNPs in a solution [25]. Further, the bands generated by AuNPs synthesized at 70 °C were generally sharper and more symmetrical, which can be an indication of the increased uniformity in size distribution of AuNPs [26]. It was also observed that the plasmon bands of most of AuNPs are broad with an absorption tail in the longer wavelength attributing the excitation of the in-plane SPR and indicates significant anisotropy in the shape of gold nanoparticles [27] or the formation of aggregated spherical nanostructures [28]. For example, samples 1, 3, 16 and 18 (Figure 1) showed absorbance at higher wavelength, whereas green tea and EGCG (at both temperatures) showed a minimum absorption tail towards the near infrared region, which may indicate their stability and/or the lack of anisotropic nanoparticles compared to the previously mentioned samples. The relationship between the UV-Vis spectra and the polydispersity is also discussed later in Section 2.2.2. Table 1 summarizes the maxima absorbance data recorded from all the plant extracts tested.

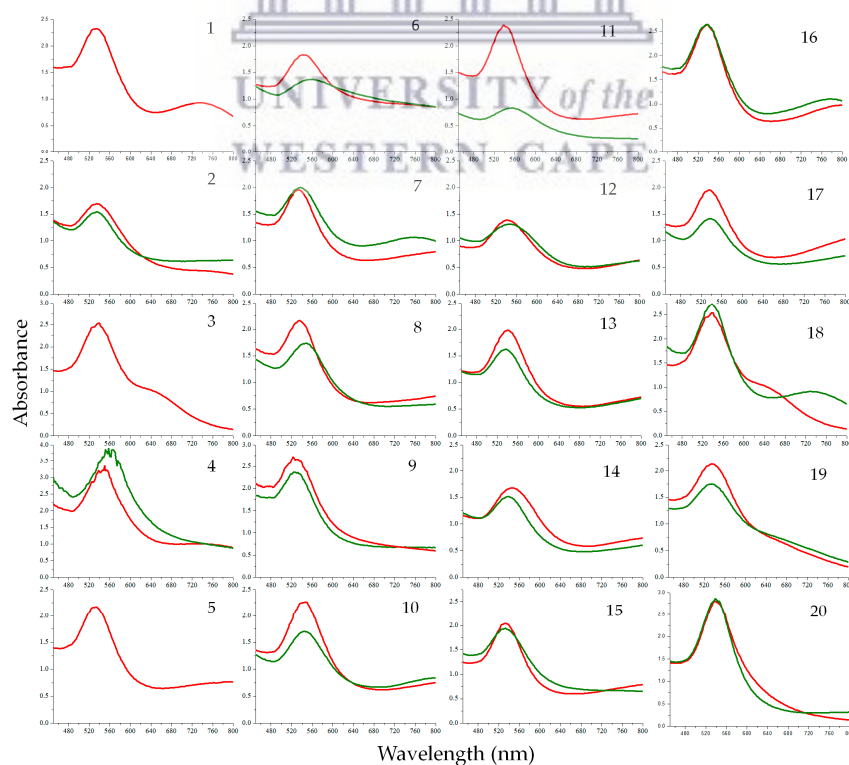


Figure 1. Comparison of the Ultraviolet-Visible Spectroscopy (UV-Vis) spectra for the AuNPs produced at 25 °C (green line graph) and at 70 °C (red line graph). The numbers on the spectra correspond to the numbers given to each plant in Table 1. *Camellia sinensis* (black tea) (18), *Camellia sinensis* (green tea) (19) and Epigallocatechin gallate (EGCG) (20) represent positive controls.

Table 1. The optimum concentration (OC), particle diameter (PD), the polydispersity index (Pdi), λ_{\max} and average zeta potential values (ZP) of the AuNPs synthesized from the plant extracts at 25 °C and 70 °C.

Plant name	25 °C					70 °C				
	OC (mg/mL)	λ_{\max} (nm)	PD (nm)	Pdi	ZP (mV)	OC (mg/mL)	λ_{\max} (nm)	PD (nm)	Pdi	ZP (mV)
1 <i>Aspalathus hispida</i>	*	*	*	*	*	0.5	534	34	0.564	−13
2 <i>Aspalathus linearis</i>	0.5	536	99	0.343	−23	0.5	536	61	0.315	−20
3 <i>Asparagus rubicundus</i>	*	*	*	*	*	1	538	28	0.66	−22
4 <i>Cynanchum africanum</i>	2	558	110	0.396	−14	0.5	546	99	0.407	−21
5 <i>Dicerotheramnus rhinocertis</i>	*	*	*	*	*	0.5	534	63	0.551	−41
6 <i>Eriocephalus africanus</i>	1	554	67	0.565	−23	0.5	542	102	0.326	−23
7 <i>Hermannia alnifolia</i>	1	536	78	0.398	−21	0.5	536	66	0.42	−27
8 <i>Indigofera brachystachya</i>	1	548	87	0.371	−16	1	534	100	0.477	−41
9 <i>Lobostemon glaber</i>	0.5	552	218	0.76	−23	0.5	540	136	0.217	−26
10 <i>Metalasia muricata</i>	1	546	65	0.469	−16	0.25	544	61	0.352	−14
11 <i>Nidorella foetida</i>	0.5	564	124	0.231	−24	0.5	548	97	0.243	−28
12 <i>Otholobium bracteolatum</i>	4	546	47	0.525	−20	1	542	53	0.423	−25
13 <i>Podocarpus falcatus</i>	1	538	141	0.6	−15	0.5	540	102	0.577	−15
14 <i>Podocarpus latifolius</i>	2	540	76	0.46	−16	1	540	54	0.513	−18
15 <i>Salvia africana-lutea</i>	1	534	148	0.466	−25	0.5	534	69	0.202	−23
16 <i>Searsia dissecta</i>	0.5	538	62	0.405	−12	0.5	538	68	0.299	−14
17 <i>Senecio pubigerus</i>	1	538	75	0.519	−18	0.5	536	49	0.469	−15
18 <i>Camellia sinensis</i> (Black tea)	2	538	63	0.535	−0.2	1	540	23	0.67	−19
19 <i>Camellia sinensis</i> (Green tea)	1	535	104	0.61	−12	1	534	47	0.376	−12
20 EGCG	0.125	532	45	0.324	−26	0.125	534	52	0.311	−22

* No nanoparticles were synthesized at this condition.

2.2. Particle Size Diameter, Distribution and Shape Analysis

2.2.1. DLS Analysis

Synthesis at 25 °C produced nanoparticles with larger sizes for most of the plant extracts (Table 1). This is in agreement with previous studies, which also showed that the green synthesis of AuNPs at lower temperatures yielded larger AuNPs and that the synthesis of smaller nanoparticles can be optimised by increasing the temperature at which the synthesis is performed [29–31]. However, three of plant extracts (*E. africanus*, *H. alnifolia* and *I. brachystachya*) investigated in this study produced smaller AuNPs at 25 °C than at 70 °C. This may be due to the destruction of the capping agents in these plant extracts at high temperature which allowed the growth of larger particles. The smallest (47 nm) AuNPs produced at 25 °C was generated by the extract of *O. bracteolatum*, while the smallest (23 nm) AuNPs produced at 70 °C was obtained from green tea extract. The extract of *L. glaber* produced the largest AuNPs diameters of 218 nm and 136 nm at 25 °C and 70 °C, respectively.

The polydispersity index (Pdi) values in Table 1 also shows that the AuNPs are often more monodispersed when synthesized at 70 °C. The Pdi represents the ratio of particles of different size to total number of particles. A sample with low Pdi value more monodispersed. A study by Rajathi and co-workers, which reported the synthesis of AuNPs from the leaves of *S. monoica*, considered a sample with a Pdi value of 0.286 to be monodispersed particles [19]. AuNPs from *N. foetida* gave the lowest Pdi values both at 25 °C and 70 °C.

2.2.2. HRTEM and EDX Analysis

The TEM images of the AuNPs, produced from plant extracts (Figure 2), show variable geometrical shapes and sizes. However, AuNPs produced from some extracts show a dominance of specific shapes over others. The presence of the anisotropic particles in the samples is indicated by the presence of absorbance towards the near infrared region in their spectra as discussed in Section 2.1. For instance, AuNPs produced with EGCG showed minimum absorbance in the near infrared region in the UV-Vis spectrum (Section 2.1) and TEM analysis (Figure 2) confirmed that these AuNPs were mostly uniform in shape. In contrast AuNPs synthesized from extracts produced from *S. dissecta* exhibited higher absorbance in the near infrared region in the UV-Vis spectrum (Sample 16 in Figure 1) and the TEM analysis shows that these AuNPs are more polydispersed (Figure 2).

Overall, larger particles, from ~150 nm in size, were mostly triangular, truncated triangular, and hexagonal in shape. On the other hand, smaller nanoparticles were mostly, spherical, pentagonal and hexagonal, although a few small triangles could also be observed. This mixture of geometrical shapes is a common feature of AuNPs as reported before [32,33]. This is presumably due to the presence of cocktail of reducing phytochemicals in the extracts acting together to form the AuNPs. The fact that a singular phytochemical, EGCG, produced uniform AuNPs is supporting this assumption. Moreover, there was no apparent difference in the shapes between AuNPs synthesized at 25 °C and 70 °C (for the same plant extract) as seen for AuNPs synthesized from *P. latifolius* (Figure 2). One interesting observation from the TEM images is the presence of a halo surrounding most of the nanoparticles (Figure 3). This halo was also observed by Zeiri et al., which has a width of 2 to 3 nm, and was proposed that this halo the AuNPs from aggregation [34]. TEM images show only a few particles in each frame, hence statistically reliable distributions of these shapes and sizes cannot be evaluated using TEM analysis [34].

To illustrate the crystalline nature of the AuNPs, Figure 4A shows the fringe lattice of the AuNPs synthesized from *A. linearis* (rooibos tea). The fringe spacing was measured to be 0.23 nm, which closely matches the spacing between (111) plane of the face centred cubic (fcc) of gold (0.235 nm) [35]. Figure 4B shows the selected electron diffraction (SAED) pattern, which confirmed the crystalline nature of the AuNPs. The rings were indexed and was found to correspond to the (111), (200), (220), (311) and (222) reflections of fcc gold.

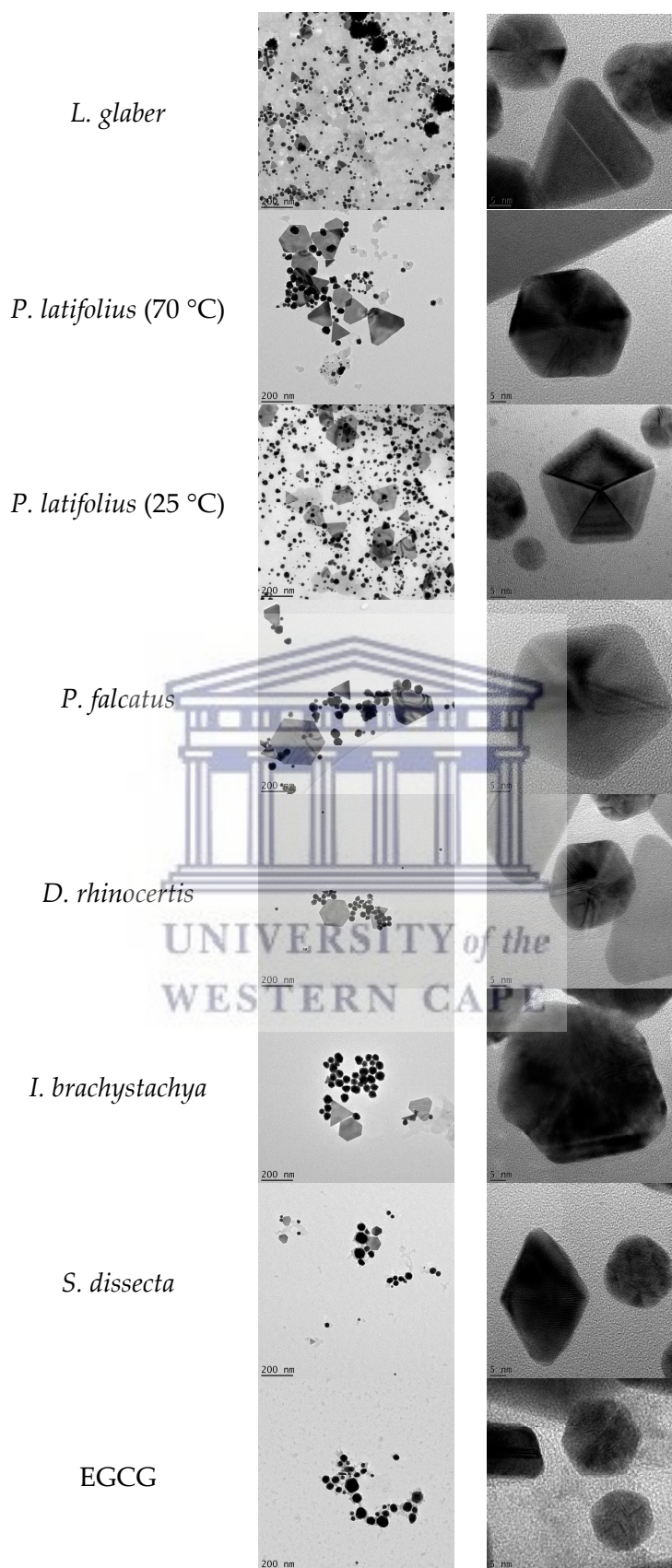


Figure 2. Transmission Electron Microscopy (TEM) images of the synthesized AuNPs.

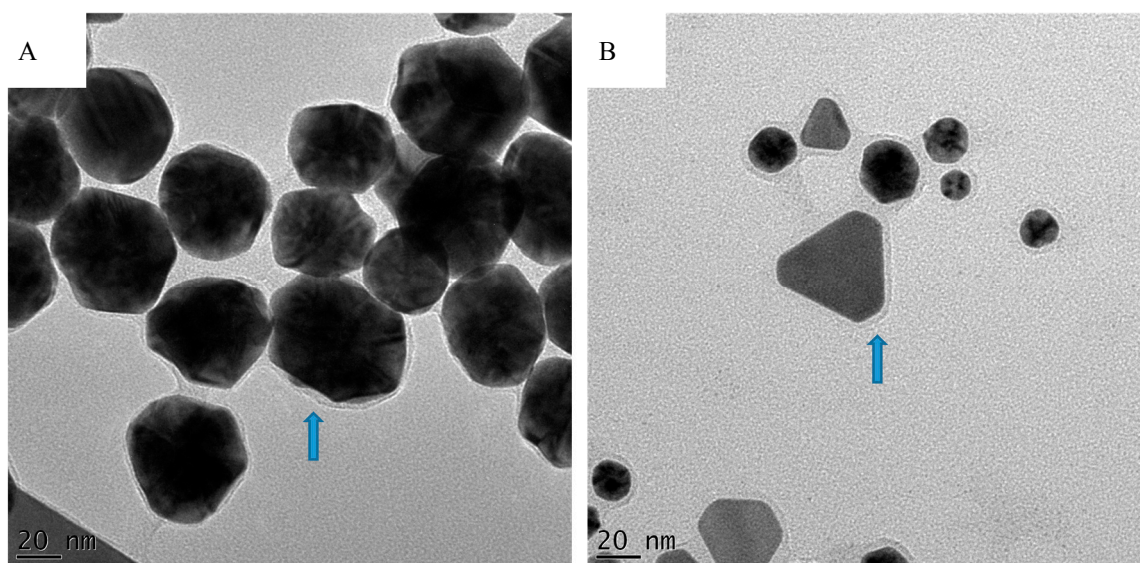


Figure 3. TEM images of AuNPs produced from (A) *I. brachystachya* and (B) *A. rubicundus*. The arrows point towards the halo surrounding the nanoparticles.

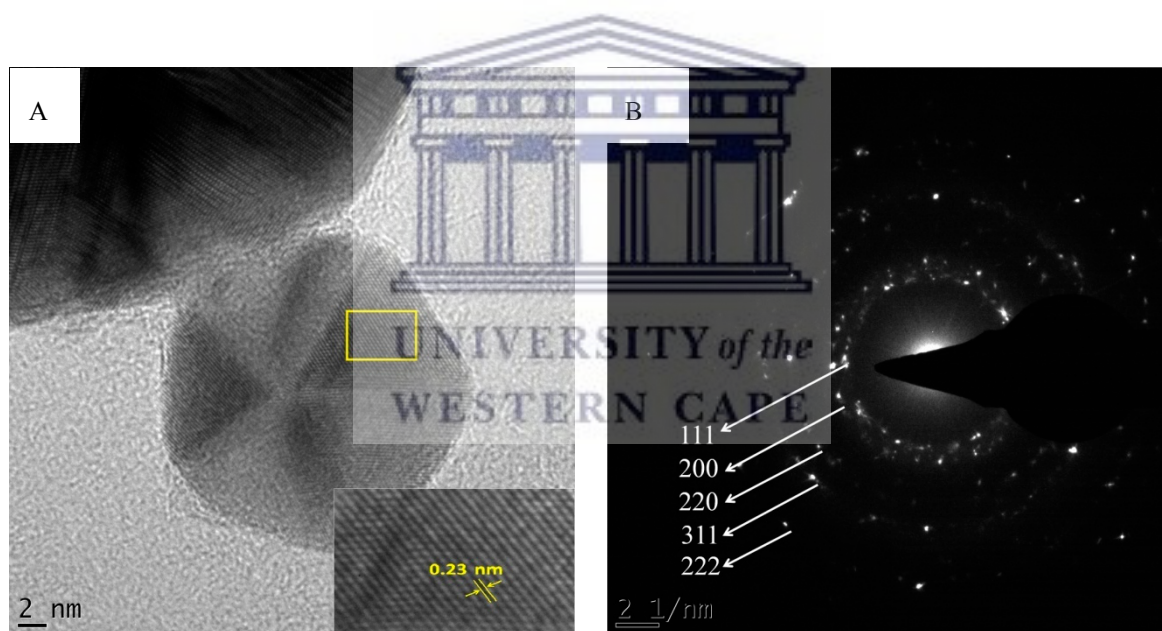


Figure 4. TEM images of *A. linearis* (rooibos tea) AuNPs showing (A) decahedron nanocrystal demonstrating the lattice fringes with spacing of 0.23 nm; (B) selected electron diffraction (SAED) pattern.

The EDX spectroscopy analysis of the AuNPs confirmed the presence of gold ions in the samples selected for TEM analysis. Strong optical adsorption peaks were observed at around 2.3, 9.7 and 11.3 KeV (Figure 5), which are consistent with a previous study [20]. The presence of strong peaks of carbon, copper and silicon in some samples is attributed to the TEM grid and the detector window [36], whereas the presence of oxygen, potassium and chloride is suggested due to traces of the phytochemicals of the extracts and the gold salt [19,34].

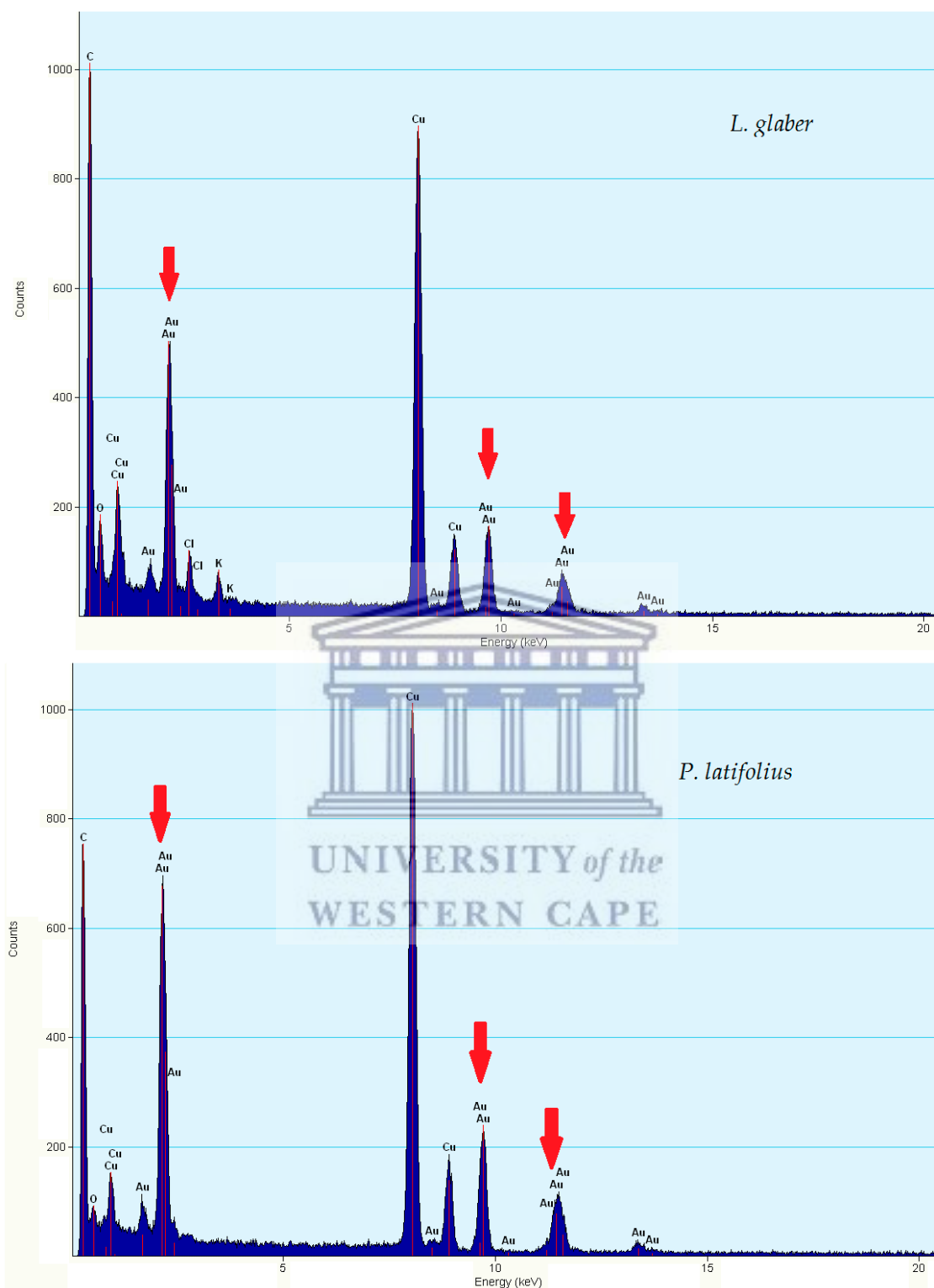


Figure 5. Energy Dispersive X-ray Spectroscopy (EDX) spectra of AuNPs from the extracts of *L. glaber* and *P. latifolius*. The red arrows show Au peaks.

2.3. Stability of the AuNPs

The zeta potential values of the synthesized AuNPs were measured in order to evaluate their stability. All measurements were done immediately after synthesis. Generally, the zeta potential measurements can be used to predict the long term stability of the AuNPs in a solution, as the

magnitude of the charge is a reflection of the repulsion forces between the particles [37]. All of the plant extracts demonstrated negative zeta potential as shown in Table 1. A negative zeta potential value commonly suggests that the particles will be stable in solutions [37].

It is important that AuNPs, used in biological applications, retain their stability in biological environments. Biologically stable AuNPs are not expected to aggregate (manifested by minimal changes in their UV-Vis spectra) when placed, for extended periods, in buffers that simulate various biological conditions (e.g., salts and biological additives) [37]. In this study, the AuNPs were incubated with three different buffers solutions (10% NaCl, 0.5% cysteine and 0.5% Bovine Serum Albumin (BSA)). The stability of AuNPs was monitored by recording changes in UV-Vis spectra over time. Only AuNPs synthesized from *P. latifolius* and *A. rubicundus* demonstrated excellent stability by retaining their SPR (Figure 6). This indicates that these nanoparticles are highly stable at different environmental conditions and can therefore potentially be used in different biomedical applications. On the other hand, none of the other AuNPs synthesized from the other plant extracts showed a similar stability upon incubation with the same buffer solutions. For instance, the AuNPs generated from *O. bracteolatum* and *A. linearis* exhibited significant changes in their respective UV-Vis spectra as shown in Figure 6. It is suggested that the flattening in their SPR is due to the formation of larger particles. Also, the decrease of the intensities of the absorbance maxima may be due to the reduction of the AuNPs in terms of their number especially when incubated with 0.5% BSA.

2.4. Effect of Temperature on AuNPs Characteristics

In order to view the effect of elevated temperature on the overall synthesis of the AuNPs, the average values of the PD, λ_{\max} , and Pdi values were calculated (Table 2). It was previously reported that high temperatures could produce AuNPs of better size distribution [31]. The measurement of the particle size distribution of some AuNPs synthesized in this study, produced data that support that report. For example, Figure 7 shows that at a higher temperature the AuNPs synthesized from *E. africanus* exhibited better size distribution in contrast to the AuNPs synthesized at a lower temperature. Overall, particles synthesized at 70 °C were smaller and better defined, which is also correlated with the blue shift of the λ_{\max} . This is in agreement with the study conducted by Mountrichas and co-workers [31]. Another study reported by Song et al. explained that the formation of smaller AuNPs at higher reaction temperatures are due to the fact that gold ions are consumed in the formation of the nuclei with the increase of reaction temperature as a result of an increased reaction rate, which prevents the secondary reduction process of the formed nuclei and hence stops the formation of larger AuNPs [38].

Table 2. The average PD, λ_{\max} , and polydispersity index (Pdi) values obtained from all the plant extracts at 25 °C and 70 °C.

Nanoparticles Characteristics	25 °C	70 °C
λ_{\max} (nm)	543 ± 9	539 ± 4
particle diameter (nm)	97 ± 44	68 ± 29
Pdi	0.465 ± 0.127	0.419 ± 0.14

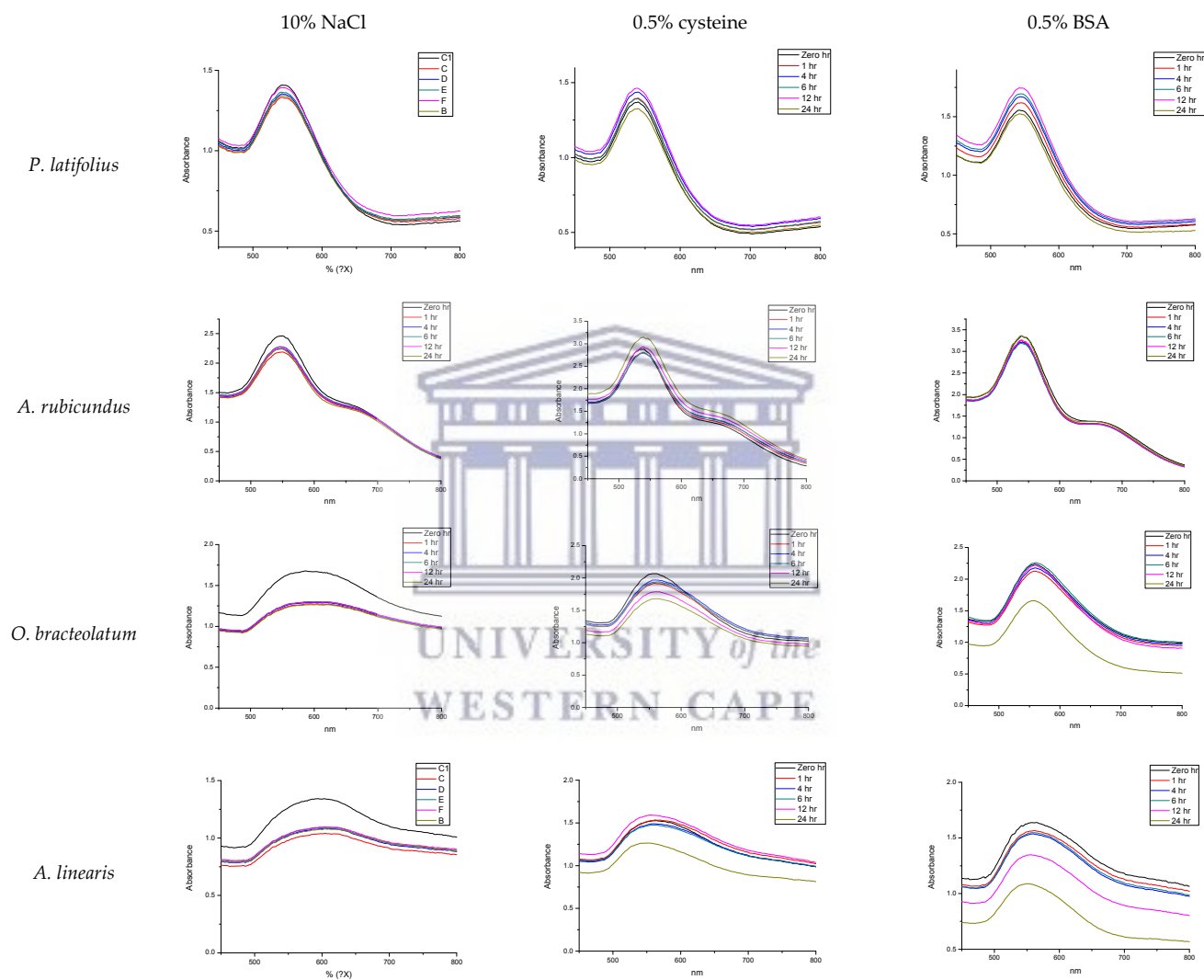


Figure 6. Changes in UV-Vis spectra of AuNPs over a 24-h period in buffers containing 10% NaCl, 0.5% cysteine and 0.5% Bovine Serum Albumin (BSA).

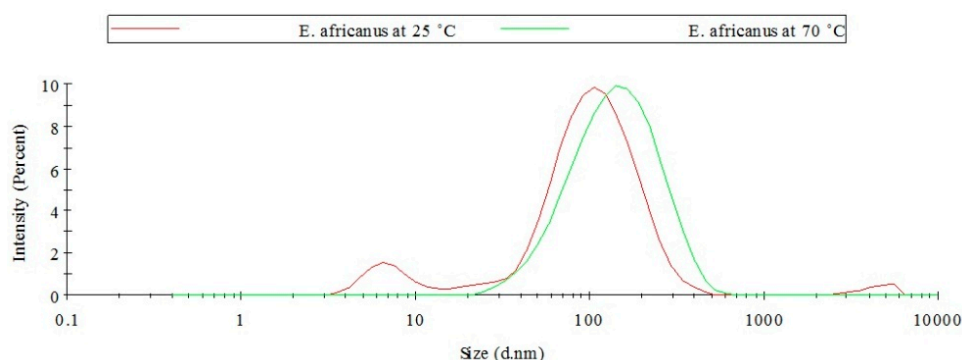


Figure 7. Particle size distribution for AuNPs produced from *E. africanus*.

2.5. Effect of Concentration and Determination of OC for Each Plant Extract

In our study, the OC is considered the concentration of the plant extract at which the smallest and most uniform AuNPs are produced. To investigate the effect of plant extract concentration, fixed concentration of gold salt was incubated with different concentrations (16–0.007 mg/ml) of the plant extracts. The determination of the OC was firstly based on the SPR (λ_{\max}) and the uniformity of the UV-Vis curve, and secondly on the PD and Pdi values, which give an indication of the uniformity of the AuNPs produced. Synthesis to identify the OC was performed at a micro-scale in microtitre plates and thereafter the identified OCs were used to scale up the synthesis of the AuNPs to larger quantities. It was observed that higher temperatures yielded smaller particle sizes at lower concentrations of the plant extracts. Figure 8 shows that the OC at 25 °C is 1 mg/mL, while at 70 °C it is 0.5 mg/mL. No uniform AuNPs were synthesized at concentrations higher than 4 mg/mL.

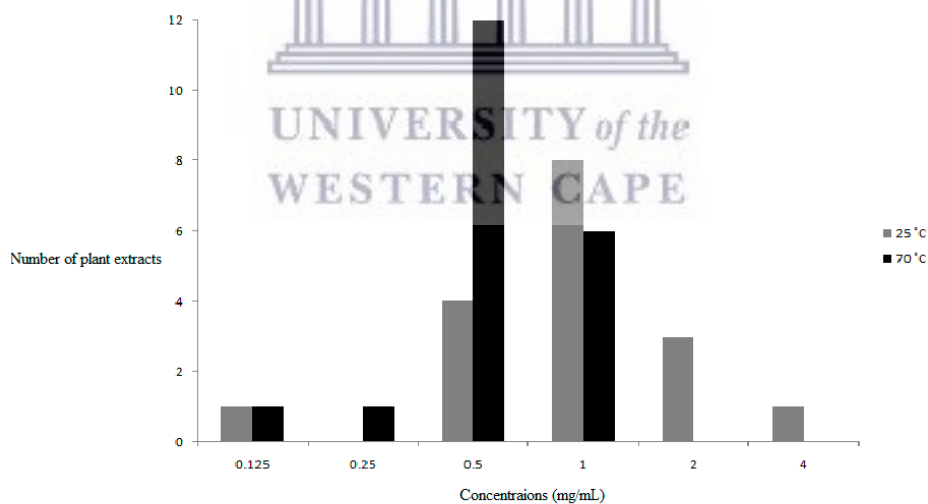


Figure 8. Optimum concentrations for AuNPs synthesis for all plant extracts at 25 °C and 70 °C.

In Figure 9, we show as an example, the changes in UV-Vis spectra as the concentrations of EGCG (one of the controls) and *P. latifolius* (one of the plant extracts) increase to demonstrate the growth pattern of the AuNPs at different concentrations. At low concentrations the SPR of both EGCG and *P. latifolius* exhibited red shifts, indicating the formation of AuNPs with a large particle size (at 0.0625 mg/mL EGCG produced λ_{\max} of 550 nm with particles of an average diameter of 393 nm, while at 1 mg/mL *P. latifolius* produced λ_{\max} of 554 nm with particles of an average diameter of 79 nm). By increasing the concentration of the reducing material (EGCG or the plant extracts) particles with smaller diameter was obtained and the OCs were reached. The SPR of the OCs exhibited the maximum blue shift compared to the SPR of the lower concentrations. At this point, the growth pattern for AuNPs

of both EGCG and *P. latifolius* comes in agreement with the nucleation-growth mechanism of the citrate AuNPs proposed by Frens [39]. Frens showed that smaller citrate AuNPs can be obtained by increasing the sodium citrate (reducing agent) concentration while using fixed gold salt concentration. It was suggested that the citrate AuNPs were grown through a fast nucleation process followed by controlled diffusion growth at which average sizes can be reduced as sodium citrate concentrations increased. However, as we increase the concentration of the reducing material beyond the OC (0.125 mg/mL for EGCG and 2 mg/mL for *P. latifolius*) smaller AuNPs could not be obtained as expected. On the contrary, the SPR curves became more flat and/or red shifted as the concentrations increase, which is a clear indication of the increased average size of the AuNPs as discussed in Section 2.1. For instance, at a concentration of 0.25 mg/mL EGCG produced AuNPs with a diameter of 55 nm and a λ_{\max} of 536 nm, while at a concentration of 0.125 mg/mL EGCG produced AuNPs with a diameter 45 nm and a λ_{\max} 532 nm. In the case of *P. latifolius* no shifts were observed compared to the OC curve, but instead the SPR curves became more flat and showed absorbance above 600 nm, which are indications of the formation of larger particles (particle diameter of 83 nm at 4 mg/mL and 207 nm at 16 mg/mL).

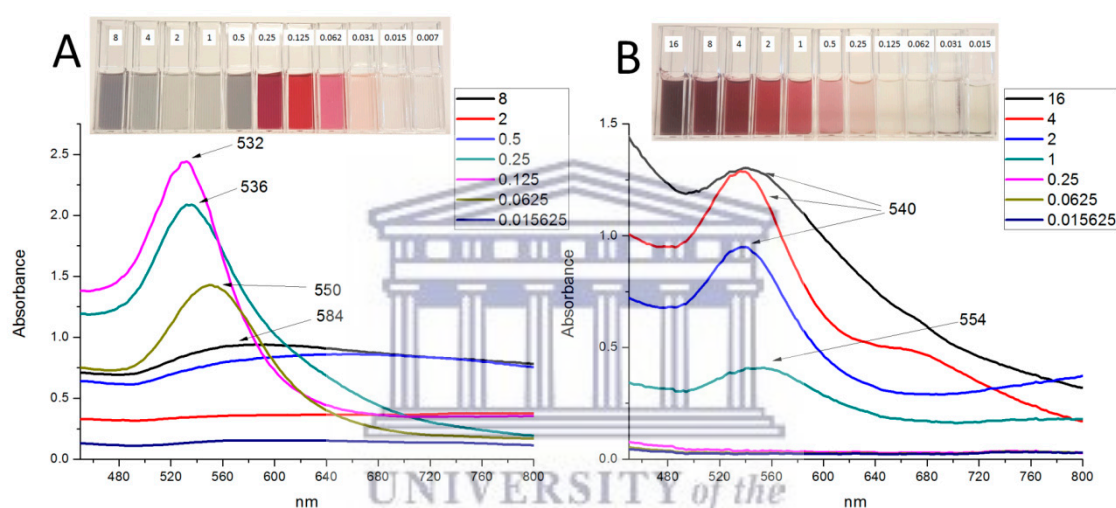


Figure 9. UV-Vis spectra for the AuNPs produced from (A) EGCG and (B) *P. latifolius* using different concentrations (mg/mL) at 25 °C. The insets show photos of the reaction mixture of different concentrations (mg/mL) of EGCG and *P. latifolius* after 1 h of reaction with gold salt.

Ji and co-workers [40], observed that citrate AuNPs were produced, with larger diameter, when increasing the sodium citrate concentration above a certain limit. They showed that two different pathways can produce AuNPs resulting in AuNPs with different sizes. These pathways were dependent on the pH of the reaction medium. They established that above a certain critical pH value, the AuNPs grow differently via Ostwald ripening, which leads to the formation of larger AuNPs. In their study, the pH of the reaction mixture was dependent on the initial sodium citrate/gold salt ratio. In another study, Guo and co-workers [41] also reported that the pH of the reaction medium affects the synthesis of AuNPs from *Eucommia ulmoides* bark aqueous extract. They showed that at pH values above a certain optimum value the reaction mixture turned blue due to the formation of larger and aggregated AuNPs according to the authors. This was also observed in our study with EGCG at 8 mg/mL (see inset Figure 9A). While the *P. latifolius* extract at the highest concentration tested (16 mg/mL) started to give blue/red colour compared to the rosy red colour obtained at the OC (see inset Figure 9B). We presume a similar mechanism occurs in our study as a change in pH was detected between the smallest and highest concentrations, even if it was small changes.

We are also proposing other factor(s) that may as well be responsible for the non-linear relationship between the concentration of plant extracts and the formation of AuNPs. It is likely that, at concentrations above the OC the crowded reaction mixture causes a certain degree of impedance

that prevent the reducing and/or capping agents to function effectively to produce AuNPs. The plant extracts generally contain a large number of phytochemicals. Some of these phytochemicals are present at high concentration and may insulate or even reverse the action of the reducing and/or capping agents. Therefore, the determination of OC at which the interaction of the plant extract with gold salt reach the optimum level is highly important and considered to be the optimal concentration for the synthesis of AuNPs, above the OC the growth pattern of the AuNPs change and produce larger particles.

2.6. Plant Phytochemicals Role in Bio-Reduction of Gold Salt

The bio-reduction of gold salt using plant extracts is mediated through the phytochemicals occluded within their aqueous extracts. These phytochemicals can mainly include free sugars (polysaccharides) and/or glycosidic containing derivatives (e.g., saponins), proteins, alkaloids and polyphenolic compounds (e.g., tannins and flavonoid derivatives), in addition to low percentage of lipophilic compounds coming to the solution by cosolvation. These phytochemicals provide polyfunctional matrix that has the ability to initiate the reduction of the gold ions and is also capable of providing stability to the AuNPs. Moreover, it appears that it is not just one type of phytochemical is responsible for the reducing actions of the plant extracts, but it can differ from one plant to another depending on the major phytochemical constituents in each plant. For instance, polyphenols and flavonoids were shown to be responsible for the formation of AuNPs from black tea [42]. AuNPs synthesized from *M. umbellatum* was attributed to the saponin content of the plant [20]. Organosulphur compounds were suggested to be the reducing agents in the synthesis of AuNPs from garlic (*Allium sativum*) [43]. AuNPs were also successfully synthesized from the aldehyde containing cinnamon essential oils [37]. The formation of AuNPs from *Cinnamomum camphora* was associated with the presence of terpenoids [44]. Dzimitrowicz and co-workers concluded that phenolic compounds play essential roles in the synthesis of AuNPs from some of *Lamiaceae* plants [45]. On the other hand, pure phytochemicals such as EGCG [23], apiin (apigenin-7-*O*-apioglucoside) [46], and guavanoic acid [47] were reported to have dual actions (as reducer and stabilizer).

Little is known about the chemistry of the tested plants in this study, yet some studies reported the isolation of various compounds that could possibly play a role in the formation of the AuNPs (Figure 10). For instance, several caffeic acid derivatives, e.g., 3-caffeoylquinic acid (1), 3,5-dicaffeoylquinic acid (2) were major phenolic compounds identified from the hydroethanolic extract of the aerial parts of *E. africanus* [48]. Additionally, a mixture of sesquiterpene lactones of the eudesmanolide type, e.g., 4 α ,11-dihydroxy-eudesmane (3) and 5 α -hydroperoxy-eudesmane (4) were also reported [49]. Phenolic diterpenes namely; carnosol (5), rosmadial (6), and the 12-*O*-methyl-20-methyl ester derivative of carnosic acid (7) were identified from *S. africana-lutea* [50]. High phenolic contents were also observed in the aerial parts of *P. latifolius* and *P. falcatus*, with total flavonoid content ranging from 49.76 to 27.18 μ g catechin/g dry sample [51]. A study of the chemical profile of the root extract of *P. falcatus* led to the isolation of several nagilactones viz; 16-hydroxynagilactone F (8), 2 β ,16-dihydroxynagilactone F (9), 2 β -hydroxynagilactone F (10), nagilactone D (11), 15-hydroxynagilactone D (12) and nagilactone I (13), along with the bisditerpenoid; 7 β -hydroxymacrophyllic acid (14), the totarol dimer macrophyllic acid (15) and the totarane-type diterpenoid inumakiol D (16) [52]. The flavone glycoside, Aspalathin (17), is a unique constituent of rooibos tea, which constitutes up to 9.3% of the dried leaves [53]. The chemical investigation of *C. africanum* led to the isolation of several pregnane glycosides named cynafoside C–H [54]. The aerial parts of *M. muricata* gave a mixture of unidentified triterpenes when studied chemically, while other *Metalisia* species afforded various chalcone derivatives [55]. Phytochemical investigation of several species of genus *Asparagus* led to isolation of several steroidal saponins [56–58].

The presence of certain part of structure like glucose unit(s) in some compound(s) in addition to phenolic or primary hydroxyls, peroxy, and aldehydic groups can play an important role in reducing gold salt. Also, the presence of carboxyl or hydroxyls groups in addition to the aromatic rings in different structural units can contribute to the stability of the AuNPs.

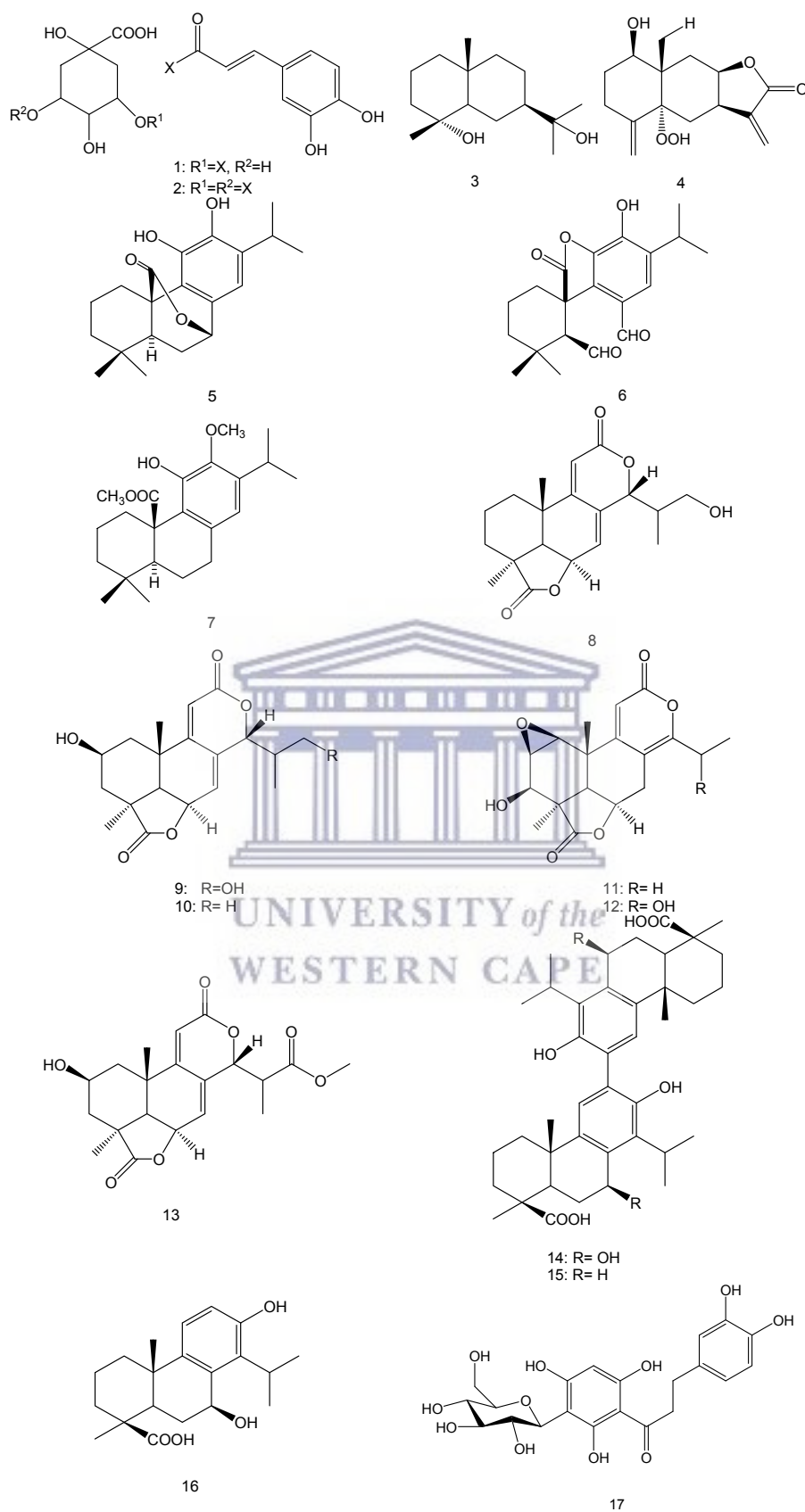


Figure 10. Chemical structures of compounds previously isolated from some of the plants used in this study.

3. Materials and Methodology

3.1. Materials

C. sinensis (black and green tea) and *A. linearis* (rooibos tea) were purchased from local vendors in South Africa, EGCG from Zhejiang Yixin Pharmaceutical Co., Ltd. (Lanxi City, China), 96 well polystyrene microplates from Greiner bio-one GmbH (Frickenhausen, Germany), gold salt (sodium tetrachloroaurate (III) dehydrate) from Sigma-Aldrich (Cape Town, South Africa), Bovine Serum Albumin (BSA) from Miles Laboratories (Pittsburgh, Pa, USA), *N*-Acetyl-L-cysteine from Boehringer Mannheim GmbH (Mannheim, Germany) and sodium chloride (NaCl) from Merck (Cape Town, South Africa).

3.2. Instruments

Centrifugation for the extracts was done using Allegra[®] X-12R (Beckman Coulter, Cape Town, South Africa). The AuNPs were centrifuged using Centrifuge 5417R (Eppendorf AG, Hamburg, Germany). The extracts were freeze dried using FreeZone 2.5 L (Labconco, Kansas City, MO, USA). UV-Vis spectra were recorded using POLARstar Omega microplate reader (BMG Labtech, Cape Town, South Africa). The particle size, size distribution and zeta potential measurements of the freshly synthesized AuNPs in solution were analysed using Zeta sizer (Malvern Instruments Ltd., Malvern, UK). TEM analysis was done using FEI Tecnai G² 20 field-emission gun (FEG).

3.3. Plant Collection

Aerial plant samples (Table 3) were collected during May 2015 from two sites in the Western Cape Province of South Africa. The first site is situated in Malmesbury (GPS coordinates: 33°27'33.44"S, 18°44'39.87"E) approximately 60 km north of the University of the Western Cape. The vegetation on this site is classified as the critically endangered Swartland Granite Renosterveld. The second collection site is situated approximated 20 km south of the University of the Western Cape in Mfuleni (GPS coordinates: 34°00'18.54"S, 18°41'8.19"E) that supports an endangered vegetation unit known as Cape Flats Dune Strandveld. On both sites the sampling strategy was random and all the specimens collected were identified and deposited at the Compton Herbarium (NBG), Kirstenbosch, Cape Town, South Africa. The collection and identification process was performed by C.N. Cupido the co-author of this paper.

Table 3. The collected plants and their accession numbers.

Plant Name	Family Name	Accession Number
<i>Aspalathus hispida</i>	Fabaceae	1463158/NBG
<i>Asparagus rubicundus</i>	Asparagaceae	1463146/NBG
<i>Cynanchum africanum</i>	Apocynaceae	1463157/NBG
<i>Dicrothamnus rhinocertis</i>	Asteraceae	1463148/NBG
<i>Eriocephalus africanus</i>	Asteraceae	1463147/NBG
<i>Hermannia alnifolia</i>	Malvaceae	1463145/NBG
<i>Indigofera brachystachya</i>	Fabaceae	1463156/NBG
<i>Lobostemon glaber</i>	Boraginaceae	1463149/NBG
<i>Metalasia muricata</i>	Asteraceae	1463150/NBG
<i>Nidorella foetida</i>	Asteraceae	1463153/NBG
<i>Otholobium bracteolatum</i>	Fabaceae	1463155/NBG
<i>Podocarpus falcatus</i>	Podocarpaceae	*
<i>Podocarpus latifolius</i>	Podocarpaceae	*
<i>Salvia africana-lutea</i>	Lamiaceae	1463154/NBG
<i>Searsia dissecta</i>	Anacardiaceae	1463151/NBG
<i>Senecio pubigerus</i>	Asteraceae	1463152/NBG

* *P. falcatus* and *P. latifolius* were purchased from Kirstenbosch national botanical garden, Cape Town, South Africa.

3.4. Preparation of the Plant Extracts

Fresh plant materials were dried in the shade for two weeks. After drying, the plant materials were grinded and extracted using boiled distilled water (50 mL of distilled water added to 5 g of each plant powder). The plant decoctions were then centrifuged at 3750 rpm for 2 h. The supernatants were then freeze dried. A stock solution of 32 mg/mL was freshly prepared for each extract before the screening step.

3.5. Screening of Gold Nanoparticles Synthesis

In a 96 well plate, 250 μ L of 1 mM [20] gold salt were added to 50 μ L of plant extracts stock solutions with increasing concentrations (0.007 to 16 mg/mL). The plates were incubated at 25 $^{\circ}$ C and 70 $^{\circ}$ C with shaking (40 rpm). After 1 h of shaking, the SPR of the AuNPs was measured by recording the UV-Vis spectrum ranging from 300 nm to 800 nm. For further characterization and stability evaluations, the synthesis of the AuNPs from the tested plant extracts was scaled up using the OC of the plant extracts.

3.6. High Resolution Transmission Electron Microscopy (HRTEM) and Energy Dispersive X-ray Spectroscopy (EDX) Analysis

To study the surface morphology of the AuNPs, samples were prepared by drop-coating one drop of each sample solution onto a holey carbon coated copper grid. This was then dried under a Xenon lamp for 10 min, where after the sample coated grids were analysed under the microscope. Transmission electron micrographs were operated in bright field mode at an accelerating voltage of 200 kV. Energy dispersive X-ray spectra were collected using an EDAX liquid nitrogen cooled Lithium doped Silicon detector.

3.7. Stability Testing of the Synthesized AuNPs

The in vitro stability of the synthesized AuNPs was measured by incubating the AuNPs with three aqueous buffer solutions (NaCl, cysteine and BSA). First, the synthesized AuNPs were centrifuged at 10,000 rpm for 5 min. The pellets were washed three times with distilled water to remove phytochemicals that are not capping the AuNPs. The nanoparticles were re-suspended in 1 mL autoclaved distilled water. Thereafter, 100 μ L of the tested AuNPs solutions was incubated with equal volume of the buffer solutions in a 96 well plate. The final concentrations of the biological media in the final mixture were as follow; 10% NaCl, 0.5% cysteine and 0.5% BSA. The stability of the AuNPs was evaluated by measuring the changes in UV-Vis spectra after 1, 4, 6, 12 and 24 h.

4. Conclusions

It is well known that plants contain countless numbers of primary and secondary metabolites and we therefore expected that characteristically different AuNPs can be synthesized using aqueous extracts of different plants. Since the phytochemical constituent in one plant extract is different from another, the use of different plant extracts can lead to dissimilar degree of bio-reduction of gold salt to synthesize AuNPs of variable shape, size, dispersity and bio-stability. This variability may also extend their potential in biological activities and other applications. This study shows for the first time a quick and easy screening method of a large number of aqueous plant extracts for the bio-synthesis of AuNPs on micro-scale level. Considering the number of plant species that can potentially be screened, this approach has several advantages since it reduces cost and time of the synthesis. In this study we also investigated the effect of the concentration of different plant extracts on the formation of AuNPs. The results showed a non-linear relationship between the concentrations of the plant extracts and the formation of AuNPs. We determined an optimum concentration for each plant extract at which the smallest and most uniform AuNPs were obtained. The synthesized AuNPs were thoroughly characterised, and their shapes, size and in vitro stability were examined. The formation of the AuNPs

was confirmed by the presence of characteristic SPR in the UV-Vis spectra. We applied different reaction conditions to study the effect of temperature on the synthesis and showed that smaller particle size and more defined AuNPs can be synthesized at a higher temperature. The particle sizes were studied by DLS analysis, which also gave an indication about the stability of AuNPs in aqueous solutions. In agreement with the UV-Vis data, TEM analysis showed that AuNPs of various geometrical shapes were produced. EDX analysis also confirmed the presence of gold ions in the samples. By monitoring changes in the SPR bands of the synthesized AuNPs when incubated with different buffer solutions, we were able to determine that AuNPs produced from two plant extracts namely, *P. latifolius* and *A. rubicundus* are highly stable in these buffers which suggested that these AuNPs will be very stable in biological environments. These AuNPs may be suitable for various biomedical applications such as drug delivery.

Acknowledgments: We would like to thank the DST/Mintek Nanotechnology Innovation Centre (NIC) and the National Research Foundation (NRF) for funding this study.

Author Contributions: A.M. Elbagory, M. Meyer and A.A. Hussein conceived and designed the experiments and analysed the data; C.N. Cupido collected and identified the plants; A.M. Elbagory performed the experiments and drafted the paper; A.A. Hussein coordinated writing the paper to which all co-authors contributed.

Conflicts of Interest: The authors declare no conflict of interest.

References

1. Geethalakshmi, R.; Sarada, D.V.L. Gold and silver nanoparticles from *Trianthema decandra*: synthesis, characterization, and antimicrobial properties. *Int. J. Nanomed.* **2012**, *5*, 375. [[CrossRef](#)]
2. Nath, D.; Banerjee, P. Green nanotechnology—A new hope for medical biology. *Environ. Toxicol. Pharmacol.* **2013**, *36*, 997–1014. [[CrossRef](#)] [[PubMed](#)]
3. El-Sayed, M. Some interesting properties of metals confined in time and nanometer space of different shapes. *Acc. Chem. Res.* **2001**, *34*, 257–264. [[CrossRef](#)] [[PubMed](#)]
4. Huang, X.; El-Sayed, I.; Qian, W.; El-Sayed, M. Cancer cell imaging and photothermal therapy in the near-infrared region by using gold nanorods. *J. Am. Chem. Soc.* **2006**, *128*, 2115–2120. [[CrossRef](#)] [[PubMed](#)]
5. Dykman, L.; Khlebtsov, N. Gold nanoparticles in biomedical applications: Recent advances and perspectives. *Chem. Soc. Rev.* **2012**, *41*, 2256–2282. [[CrossRef](#)] [[PubMed](#)]
6. Qiu, P.; Yang, M.; Qu, X.; Huai, Y.; Zhu, Y.; Mao, C. Tuning photothermal properties of gold nanodendrites for in vivo cancer therapy within a wide near infrared range by simply controlling their degree of branching. *Biomaterials* **2016**, *104*, 138–144. [[CrossRef](#)] [[PubMed](#)]
7. Abadeer, N.; Murphy, C. Recent Progress in Cancer Thermal Therapy Using Gold Nanoparticles. *J. Phys. Chem. C* **2016**, *120*, 4691–4716. [[CrossRef](#)]
8. Yu, D. Formation of colloidal silver nanoparticles stabilized by Na⁺-poly(γ -glutamic acid)-silver nitrate complex via chemical reduction process. *Colloids Surf. B* **2007**, *59*, 171–178. [[CrossRef](#)] [[PubMed](#)]
9. Mallick, K.; Witcomb, M.; Scurrill, M. Self-assembly of silver nanoparticles in a polymer solvent: Formation of a nanochain through nanoscale soldering. *Mater. Chem. Phys.* **2005**, *90*, 221–224. [[CrossRef](#)]
10. Liu, Y.; Lin, L. New pathway for the synthesis of ultrafine silver nanoparticles from bulk silver substrates in aqueous solutions by sonoelectrochemical methods. *Electrochem. Commun.* **2004**, *6*, 1163–1168. [[CrossRef](#)]
11. Tsuji, T.; Kakita, T.; Tsuji, M. Preparation of nano-size particles of silver with femto second laser ablation in water. *Appl. Surf. Sci.* **2003**, *206*, 314–320. [[CrossRef](#)]
12. Jensen, T.; Malinsky, M.; Haynes, C.; Van Duyne, R. Nanosphere lithography: Tunable localized surface plasmon resonance spectra of silver nanoparticles. *J. Phys. Chem. B* **2000**, *104*, 10549–10556. [[CrossRef](#)]
13. Lukman, A.; Gong, B.; Marjo, C.; Roessner, U.; Harris, A. Facile synthesis, stabilization, and anti-bacterial performance of discrete Ag nanoparticles using *Medicago sativa* seed exudates. *J. Colloid Interface Sci.* **2011**, *353*, 433–444. [[CrossRef](#)] [[PubMed](#)]
14. Shankar, S.; Rai, A.; Ahmad, A.; Sastry, M. Rapid synthesis of Au, Ag, and bimetallic Au core—Ag shell nanoparticles using Neem (*Azadirachta indica*) leaf broth. *J. Colloid Interface Sci.* **2004**, *275*, 496–502. [[CrossRef](#)] [[PubMed](#)]

15. Kalishwaralal, K.; Deepak, V.; Ram Kumar Pandian, S.; Gurunathan, S. Biological synthesis of gold nanocubes from *Bacillus licheniformis*. *Bioresour. Technol.* **2009**, *100*, 5356–5358. [[CrossRef](#)] [[PubMed](#)]
16. Shankar, S.; Ahmad, A.; Pasricha, R.; Sastry, M. Bioreduction of chloroaurate ions by geranium leaves and its endophytic fungus yields gold nanoparticles of different shapes. *J. Mater. Chem.* **2003**, *13*, 1822. [[CrossRef](#)]
17. Kumar, V.; Yadav, S. Plant-mediated synthesis of silver and gold nanoparticles and their applications. *J. Chem. Technol. Biotechnol.* **2009**, *84*, 151–157. [[CrossRef](#)]
18. Ankamwar, B. Biosynthesis of gold nanoparticles (green-gold) using leaf extract of *Terminalia catappa*. *Eur. J. Chem.* **2010**, *7*, 1334–1339.
19. Arockiya Aarathi Rajathi, F.; Arumugam, R.; Saravanan, S.; Anantharaman, P. Phyto fabrication of gold nanoparticles assisted by leaves of *Suaeda monoica* and its free radical scavenging property. *J. Photochem. Photobiol. B* **2014**, *135*, 75–80. [[CrossRef](#)] [[PubMed](#)]
20. Arunachalam, K.; Annamalai, S.; Shanmugasundaram, H. One-step green synthesis and characterization of leaf extract-mediated biocompatible silver and gold nanoparticles from *Memecylon umbellatum*. *Int. J. Nanomed.* **2013**, *8*, 1307–1315. [[CrossRef](#)] [[PubMed](#)]
21. Manning, J.; Goldblatt, P. *Plants of the Greater Cape Floristic Region 1: The Core Cape flora, Strelitzia29*; South African National Biodiversity Institute: Pretoria, South Africa, 2012.
22. Rastogi, L.; Arunachalam, J. Microwave-assisted green synthesis of small gold nanoparticles using aqueous garlic (*Allium sativum*) extract: Their application as antibiotic carriers. *Int. J. Green Nanotechnol.* **2012**, *4*, 163–173. [[CrossRef](#)]
23. Nune, S.; Chanda, N.; Shukla, R.; Katti, K.; Kulkarni, R.; Thilakavathi, S.; Mekapothula, S.; Kannan, R.; Katti, K.V. Green nanotechnology from tea: Phytochemicals in tea as building blocks for production of biocompatible gold nanoparticles. *J. Mater. Chem.* **2009**, *19*, 2912–2920. [[CrossRef](#)] [[PubMed](#)]
24. Guo, L.; Jackman, J.; Yang, H.; Chen, P.; Cho, N.; Kim, D. Strategies for enhancing the sensitivity of plasmonic nanosensors. *Nano Today* **2015**, *10*, 213–239. [[CrossRef](#)]
25. Abdelhalim, M.; Mady, M.; Ghannam, M. Physical properties of different gold nanoparticles: Ultraviolet-visible and fluorescence measurements. *J. Nanomed. Nanotechnol.* **2012**, *3*. [[CrossRef](#)]
26. Saifuddin, N.; Wong, C.; Yasumira, A. Rapid biosynthesis of silver nanoparticles using culture supernatant of bacteria with microwave irradiation. *Eur. J. Chem.* **2009**, *6*, 61–70. [[CrossRef](#)]
27. Narayanan, K.; Sakthivel, N. Coriander leaf mediated biosynthesis of gold nanoparticles. *Mater. Lett.* **2008**, *62*, 4588–4590. [[CrossRef](#)]
28. Shipway, A.; Lahav, M.; Gabai, R.; Willner, I. Investigations into the electrostatically induced aggregation of Au nanoparticles. *Langmuir* **2000**, *16*, 8789–8795. [[CrossRef](#)]
29. Zhu, J.; Kónya, Z.; Puntès, V.; Kiricsi, I.; Miao, C.X.; Ager, J.; Alivisatos, A.; Somorjai, G. Encapsulation of metal (Au, Ag, Pt) nanoparticles into the mesoporous SBA-15 structure. *Langmuir* **2003**, *19*, 4396–4401. [[CrossRef](#)]
30. Pandey, S.; Oza, G.; Mewada, A.; Sharon, M. Green synthesis of highly stable gold nanoparticles using *Momordica charantia* as nano fabricator. *Arch. Appl. Sci. Res.* **2012**, *4*, 1135–1141.
31. Mountrichas, G.; Pispas, S.; Kamitsos, E. Effect of temperature on the direct synthesis of gold nanoparticles mediated by poly (dimethylaminoethyl methacrylate) Homopolymer. *J. Phys. Chem. C* **2014**, *118*, 22754–22759. [[CrossRef](#)]
32. Chen, R.; Wu, J.; Li, H.; Cheng, G.; Lu, Z.; Che, C. Fabrication of gold nanoparticles with different morphologies in HEPES buffer. *Rare Metals* **2010**, *29*, 180–186. [[CrossRef](#)]
33. Foss, C.; Hornyak, G.; Stockert, J.; Martin, C. Template-synthesized nanoscopic gold particles: Optical spectra and the effects of particle size and shape. *J. Phys. Chem.* **1994**, *98*, 2963–2971. [[CrossRef](#)]
34. Zeiri, Y.; Elia, P.; Zach, R.; Hazan, S.; Kolusheva, S.; Porat, Z. Green synthesis of gold nanoparticles using plant extracts as reducing agents. *Int. J. Nanomed.* **2014**, *9*, 4007–4021. [[CrossRef](#)] [[PubMed](#)]
35. Yin, X.; Chen, S.; Wu, A. Green chemistry synthesis of gold nanoparticles using lactic acid as a reducing agent. *Micro Nano Lett.* **2010**, *5*, 270–273. [[CrossRef](#)]
36. Rodríguez-León, E.; Iñiguez-Palomares, R.; Navarro, R.; Herrera-Urbina, R.; Tánori, J.; Iñiguez-Palomares, C.; Maldonado, A. Synthesis of silver nanoparticles using reducing agents obtained from natural sources (*Rumex hymenosepalus* extracts). *Nanoscale Res. Lett.* **2013**, *8*, 318. [[CrossRef](#)] [[PubMed](#)]

37. Chanda, N.; Shukla, R.; Zambre, A.; Mekapothula, S.; Kulkarni, R.; Katti, K.; Bhattacharyya, K.; Fent, G.; Casteel, S.; Boote, E.; et al. An effective strategy for the synthesis of biocompatible gold nanoparticles using cinnamon phytochemicals for phantom CT imaging and photoacoustic detection of cancerous cells. *Pharm. Res.* **2010**, *28*, 279–291. [[CrossRef](#)] [[PubMed](#)]
38. Song, J.; Jang, H.; Kim, B. Biological synthesis of gold nanoparticles using *Magnolia kobus* and *Diopyros kaki* leaf extracts. *Process Biochem.* **2009**, *44*, 1133–1138. [[CrossRef](#)]
39. Frens, G. Controlled nucleation for the regulation of the particle size in monodisperse gold suspensions. *Nat. Phys. Sci.* **1973**, *241*, 20–22. [[CrossRef](#)]
40. Ji, X.; Song, X.; Li, J.; Bai, Y.; Yang, W.; Peng, X. Size control of gold nanocrystals in citrate reduction: The third role of citrate. *J. Am. Chem. Soc.* **2007**, *129*, 13939–13948. [[CrossRef](#)] [[PubMed](#)]
41. Guo, M.; Li, W.; Yang, F.; Liu, H. Controllable biosynthesis of gold nanoparticles from a *Eucommia ulmoides* bark aqueous extract. *Spectrochim. Acta Mol. Biomol. Spectrosc.* **2015**, *142*, 73–79. [[CrossRef](#)] [[PubMed](#)]
42. Begum, N.; Mondal, S.; Basu, S.; Laskar, R.; Mandal, D. Biogenic synthesis of Au and Ag nanoparticles using aqueous solutions of Black Tea leaf extracts. *Colloids Surf. B.* **2009**, *71*, 113–118. [[CrossRef](#)] [[PubMed](#)]
43. Rastogi, L.; Arunachalam, J. Green synthetic route for the size controlled synthesis of biocompatible gold nanoparticles using aqueous extract of garlic (*Allium Sativum*). *Adv. Mater. Lett.* **2013**, *4*, 548–555. [[CrossRef](#)]
44. Huang, J.; Li, Q.; Sun, D.; Lu, Y.; Su, Y.; Yang, X.; Wang, H.; Wang, Y.; Shao, W.; He, N.; Hong, J.; Chen, C. Biosynthesis of silver and gold nanoparticles by novel sundried *Cinnamomum camphora* leaf. *Nanotechnology* **2007**, *18*, 105104. [[CrossRef](#)]
45. Dzimitrowicz, A.; Jamróz, P.; di Cenzo, G.; Sergiel, I.; Kozlecki, T.; Pohl, P. Preparation and characterization of gold nanoparticles prepared with aqueous extracts of *Lamiaceae* plants and the effect of follow-up treatment with atmospheric pressure glow micro discharge. *Arabian J. Chem.* **2016**. [[CrossRef](#)]
46. Kasthuri, J.; Veerapandian, S.; Rajendiran, N. Biological synthesis of silver and gold nanoparticles using apiin as reducing agent. *Colloids Surf. B* **2009**, *68*, 55–60. [[CrossRef](#)] [[PubMed](#)]
47. Khaleel Basha, S.; Govindaraju, K.; Manikandan, R.; Ahn, J.; Bae, E.; Singaravelu, G. Phytochemical mediated gold nanoparticles and their PTP 1B inhibitory activity. *Colloids Surf. B* **2010**, *75*, 405–409. [[CrossRef](#)] [[PubMed](#)]
48. Catarino, M.; Silva, A.; Saraiva, S.; Sobral, A.; Cardoso, S. Characterization of phenolic constituents and evaluation of antioxidant properties of leaves and stems of *Eriocephalus africanus*. *Arabian J. Chem.* **2015**. [[CrossRef](#)]
49. Zdero, C.; Bohlmann, F.; Müller, M. Sesquiterpene lactones and other constituents from *Eriocephalus* species. *Phytochemistry* **1987**, *26*, 2763–2775. [[CrossRef](#)]
50. Hussein, A.; Meyer, J.; Jimeno, M.; Rodríguez, B. Bioactive Diterpenes from *Orthosiphon labiatus* and *Salvia africana-lutea*. *J. Nat. Prod.* **2007**, *70*, 293–295. [[CrossRef](#)] [[PubMed](#)]
51. Abdillahi, H.; Finnie, J.; Van Staden, J. Anti-inflammatory, antioxidant, anti-tyrosinase and phenolic contents of four *Podocarpus* species used in traditional medicine in South Africa. *J. Ethnopharmacol.* **2011**, *136*, 496–503. [[CrossRef](#)] [[PubMed](#)]
52. Addo, E.; Chai, H.; Hymete, A.; Yeshak, M.; Slebodnick, C.; Kingston, D.; Rakotondraibe, L. Antiproliferative constituents of the roots of Ethiopian *Podocarpus falcatus* and structure revision of 2 α -hydroxynagilactone F and nagilactone I. *J. Nat. Prod.* **2015**, *78*, 827–835. [[CrossRef](#)] [[PubMed](#)]
53. Snijman, P.; Joubert, E.; Ferreira, D.; Li, X.; Ding, Y.; Green, I.; Gelderblom, W. Antioxidant activity of the dihydrochalcones aspalathin and nothofagin and their corresponding flavones in relation to other rooibos (*Aspalathus linearis*) flavonoids, epigallocatechin gallate, and trolox. *J. Agric. Food Chem.* **2009**, *57*, 6678–6684. [[CrossRef](#)] [[PubMed](#)]
54. Steyn, P.; van Heerden, F.; Vleggaart, R. Toxic constituents of the *Asclepiadaceae*. Structure elucidation of the cynafosides, toxic pregnane glycosides of *Cynanchum africanum* R. Br. *S. Afr. J. Chem.* **1989**, *42*, 29–37.
55. Zdero, C.; Bohlmann, F. Glycerol derivatives and other constituents from *Metalasia* species. *Phytochemistry* **1990**, *29*, 2179–2180. [[CrossRef](#)]
56. Shao, Y.; Poobrasert, O.; Kennelly, E.; Chin, C.; Ho, C.; Huang, M.; Garrison, S.A.; Cordell, G.A. Cytotoxic activity of steroidal saponins from *Asparagus officinalis*. *Acta Hort.* **1999**, *479*, 277–282. [[CrossRef](#)]
57. Kim, G.; Kim, H.; Seong, J.; Oh, S.; Lee, C.; Bang, J.; Seong, N.; Song, K. Cytotoxic steroidal saponins from the rhizomes of *Asparagus oligoclonos*. *J. Nat. Prod.* **2005**, *68*, 766–768. [[CrossRef](#)] [[PubMed](#)]

58. Zhou, L.; Chen, T.; Bastow, K.; Shibano, M.; Lee, K.; Chen, D. Filiasparosides A–D, cytotoxic steroidal saponins from the roots of *Asparagus filicinus*. *J. Nat. Prod.* **2007**, *70*, 1263–1267. [[CrossRef](#)] [[PubMed](#)]

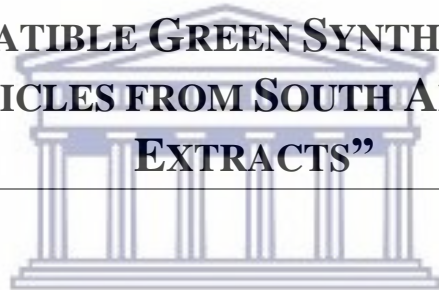
Sample Availability: Some samples of the AuNPs are available from the authors.



© 2016 by the authors; licensee MDPI, Basel, Switzerland. This article is an open access article distributed under the terms and conditions of the Creative Commons Attribution (CC-BY) license (<http://creativecommons.org/licenses/by/4.0/>).



**CHAPTER FOUR: MANUSCRIPT “INHIBITION OF
BACTERIA ASSOCIATED WITH WOUND INFECTION BY
BIOCOMPATIBLE GREEN SYNTHESIZED GOLD
NANOPARTICLES FROM SOUTH AFRICAN PLANT
EXTRACTS”**



UNIVERSITY *of the*
WESTERN CAPE



Article

Inhibition of Bacteria Associated with Wound Infection by Biocompatible Green Synthesized Gold Nanoparticles from South African Plant Extracts

Abdulrahman M. Elbagory ¹, Mervin Meyer ¹, Christopher N. Cupido ²
and Ahmed A. Hussein ^{3,*} 

¹ DST/Mintek Nanotechnology Innovation Centre, Department of Biotechnology, University of the Western Cape, Private Bag X17, Bellville 7535, South Africa; 3376881@myuwc.ac.za (A.M.E.); memeyer@uwc.ac.za (M.M.)

² Botany Department, University of Forte Hare, Private Bag X1314, Alice 5700, South Africa; ccupido@ufh.ac.za

³ Chemistry Department, Cape Peninsula University of Technology, P.O. Box 1906, Bellville 7535, South Africa

* Correspondence: mohammedam@cput.ac.za; Tel.: +27-21-9596193

Received: 11 October 2017; Accepted: 10 November 2017; Published: 26 November 2017

Abstract: Unlike conventional physical and chemical methods, the biogenic synthesis of gold nanoparticles (GNPs) is considered a green and non-toxic approach to produce biocompatible GNPs that can be utilized in various biomedical applications. This can be achieved by using plant-derived phytochemicals to reduce gold salt into GNPs. Several green synthesized GNPs have been shown to have antibacterial effects, which can be applied in wound dressings to prevent wound infections. Therefore, the aim of this study is to synthesize biogenic GNPs from the South African *Galenia africana* and *Hypoxis hemerocallidea* plants extracts and evaluate their antibacterial activity, using the Alamar blue assay, against bacterial strains that are known to cause wound infections. Additionally, we investigated the toxicity of the biogenic GNPs to non-cancerous human fibroblast cells (KMST-6) using 3-[4,5-dimethylthiazol-2-yl]-2,5-diphenyl tetrazolium bromide (MTT) assay. In this paper, spherical GNPs, with particle sizes ranging from 9 to 27 nm, were synthesized and fully characterized. The GNPs from *H. hemerocallidea* exhibited antibacterial activity against all the tested bacterial strains, whereas GNPs produced from *G. africana* only exhibited antibacterial activity against *Pseudomonas aeruginosa*. The GNPs did not show any significant toxicity towards KMST-6 cells, which may suggest that these nanoparticles can be safely applied in wound dressings.

Keywords: gold nanoparticles; green nanotechnology; *Galenia africana*; *Hypoxis hemerocallidea*; antibacterial activity; Alamar blue; MTT; HRTEM

1. Introduction

The antibacterial potential of the metallic nanoparticles (NPs) have been under investigation to counter the increase of microbial resistance against the current antimicrobial agents [1]. Additionally, the potential application of the NPs in wound dressings to fight infections makes these NPs extremely useful in wound care. Different metals such as gold, silver, platinum, palladium, copper, aluminum, iron, and titanium have been used to synthesize NPs [2]. Gold nanoparticles (GNPs) in particular have attracted huge attention for their unique optical properties as well as their biocompatibility [1]. GNPs are included in a variety of applications such as separation science [3], optical sensors, food industry as well as space and environmental sciences [4]. GNPs have also shown potential in several biomedical applications. GNPs have been shown to destroy tumors by photothermal therapy [5]. Other biomedical applications of GNPs include gene therapy, drug delivery, DNA and RNA analysis and as antibacterial agents, etc. [6].

The use of environmentally toxic reagents, the production of harmful by-products and the use of expensive apparatus during conventional physical and chemical synthesis of metallic NPs hinder their exploitation in biomedical applications. Conversely, the green synthesis of metallic NPs involves the use of safe biological reagents that produce biocompatible NPs using cost effective methods [7]. GNPs have been successfully synthesized from different biological sources such as proteins, flagella, bacteria and fungi [8–11]. Among these biological entities, plant extracts are extensively used in the synthesis of GNPs, because they are easier to handle, more readily available, cheaper and safer compared to the other aforementioned biological sources [7,12–16]. The synthesis of metal NPs using plant extracts is mediated through the presence of numerous reducing phytochemicals such as proteins, amines, phenols, carboxylic acids, ketones, aldehydes, etc. [17].

Several studies have reported the antimicrobial activities of biogenic GNPs. GNPs synthesized from natural honey exhibited significant antibacterial activity against pathogenic bacteria including multi-drug resistant bacterial strains [18]. Ayaz Ahmed et al. (2014) reported a potent antibacterial activity against several pathogenic bacteria such as *Pseudomonas aeruginosa* and *Escherichia coli* for the GNPs synthesized from the Indian plant, *Salicornia brachiata* [19]. *E. coli* and *Staphylococcus aureus* were also found to be sensitive to GNPs synthesized from *Mentha piperita* [20]. The synthesis of GNPs using extracts produced from plants with known antibacterial activities can potentially produce NPs with significant antibacterial activities.

Galenia africana L. var. *africana*, locally known as “kraalbos” or “geelbos”, is a common plant found throughout Namaqualand, South Africa [21]. This plant is used to treat venereal sores, asthma, coughs and eye infections. Indigenous tribes use the leaves from this plant to relieve toothache [22]. *Hypoxis hemerocallidea* is also an important medicinal plant that is indigenous to South Africa. Its corms are used in traditional medicine to treat psychiatric disturbances and as a diuretic. It is also used to kill small vermin and to treat gall sickness in cattle [23]. The infusion of this plant is widely exploited by the Zulu tribe to cure impotency [24]. Moreover, the extracts of *H. hemerocallidea* are used to treat many diseases including diabetes, urinary infections, cancer and in the management of Human Immunodeficiency Virus infection and Acquired Immune Deficiency Syndrome HIV/AIDS [25]. In addition to these medicinal uses, both *G. africana* and *H. hemerocallidea* plants are also known for their wound healing properties. A lotion from *G. africana* decoction is used to alleviate inflammation and to treat skin diseases [26]. *H. hemerocallidea* extracts can be applied topically to relieve skin wounds and rashes [27].

Microbial infections can deter the wound healing process as microbial pathogens can reduce the number of fibroblasts and collagen regeneration via activation of inflammatory mediators as a result of the production of microbial toxins [28]. Therefore, an ideal wound-healing agent should demonstrate antimicrobial activity. Both *G. africana* and *H. hemerocallidea* exhibited antibacterial activity, which could be potentially beneficial for wound healing. The 5,7,2-trihydroxyflavone isolated from *G. africana* has been found to have antibacterial activity against *Mycobacterium smegmatis* and *Mycobacterium tuberculosis* [29]. The acetone and the ethanolic extracts of *H. hemerocallidea* have been shown antibacterial activities against *S. aureus*. Also, different extracts of *H. hemerocallidea* exhibited efficient antibacterial activity against several bacterial strains. This activity was enhanced when the extracts of *H. hemerocallidea* were combined with other medicinal plant extracts [30]. All these studies demonstrate that the extracts of *G. africana* and *H. hemerocallidea* plants contain phytochemicals with antibacterial activity that could aid in the wound healing process.

In this paper, GNPs were synthesized from the aqueous extracts of *G. africana* and *H. hemerocallidea*. The synthesis of GNPs was monitored using Ultraviolet-Visible Spectroscopy (UV-Vis). The hydrodynamic size measurement of the GNPs was done using Dynamic Light Scattering (DLS). The GNPs' morphology and their crystalline nature were inspected using High Resolution Transmission Electron Microscopy (HRTEM). Energy-Dispersive X-ray spectroscopy (EDX) was utilized to confirm the presence of the elemental gold in the GNPs. Additionally, the possible chemical functional groups involved in the biosynthesis of the GNPs were identified using Fourier Transform Infrared spectroscopy (FTIR).

Thermogravimetric analysis (TGA) was also done to get an estimation of the amount of organic layer that surrounds the GNPs. The growth kinetics of the GNPs was also studied. The stability of the GNPs was measured in different biological buffer solutions. The in vitro toxicity of the synthesized GNPs was evaluated on non-cancerous human fibroblast cell line (KMST-6). The antibacterial evaluation of the GNPs and the extracts against several gram-positive and gram-negative bacteria was performed.

2. Results and Discussion

In order to produce GNPs chemically, a reducing agent is normally added to the gold salt to reduce gold atoms and allowing them to grow into GNPs. The addition of other organic molecules can be done to surround the GNPs in order to control their growth, prevent their aggregation and increase their stability [31].

The ability of *G. africana* and *H. hemerocallidea* plant extracts to provide secondary metabolites, not only capable of reducing the gold salt but also able to provide stabilization (capping) properties, was examined. The shape, distribution, morphology and surface charges of the GNPs were studied. The study also evaluated the biocompatibility and antibacterial activity of the GNPs.

This study follows on from a previous report in which extracts from several indigenous South African plants were screened for the biosynthesis of GNPs using a quick and easy microtitre plate method [32]. The previously reported methodology was applied here in order to obtain the optimum concentration for each plant extract (as mentioned in Section 3) that can produce the smallest and most defined GNPs. In the previous report, it was also concluded that the use of high temperature facilitates the synthesis of smaller GNPs. Hence, the synthesis of the GNPs in the current study was done at 70 °C.

2.1. UV-Vis Analysis

The visual observation of the color change from light yellow to red for the gold salt/plant extract mixtures after the 1 h incubation (Figure 1) is an indication that GNPs were formed. This confirmed that the extracts were able to reduce the Au^{+3} ions to Au^0 by the secondary metabolites/phytochemicals present in the extracts [15]. The cause of this red color in the GNPs' colloidal solution, which is not observable in the bulk material or the individual atoms, is a result of the oscillation of free conduction electrons known as Surface Plasmon Resonance (SPR) [33]. A UV-Vis spectrum with a maxima absorbance between 500 and 600 nm is indicative of GNPs formation [34]. Figure 2 shows the UV-Vis spectra of GNPs from Galenia-GNPs (GNPs produced from *G. africana*) and Hypoxis-GNPs (GNPs produced from *H. hemerocallidea*). Galenia-GNPs and Hypoxis-GNPs exhibited a maximum absorbance (λ_{max}) of 534 ± 2 nm and 530 ± 1 nm, respectively. Several factors such as the size and the shape of the NPs, the refractive index of the medium and the inter-particle distances affect the shape and position of the GNPs' SPR in the UV-Vis spectrum [35]. In Figure 2, the band generated by Hypoxis-GNPs was sharper and more symmetrical with small absorption after 600 nm as opposed to Galenia-GNPs' band, which can be a sign of better uniformity in size distribution of Hypoxis-GNPs compared to Galenia-GNPs [36]. Further, the absorption tail in the Near Infrared (NIR) wavelength observed for Galenia-GNPs could be caused by the excitation of the in-plane SPR and can be a result of anisotropic GNPs [37] or the deviation from spherical geometry of the GNPs [38]. These results may indicate the presence of more effective capping agents in *H. hemerocallidea* plant extract compared to *G. africana* that prevented the aggregation of the GNPs and enhanced their uniformity. However, the GNPs with absorption in the NIR region have been found to be useful in several biomedical applications and in the fabrication of photonic devices such as optical sensors [39].

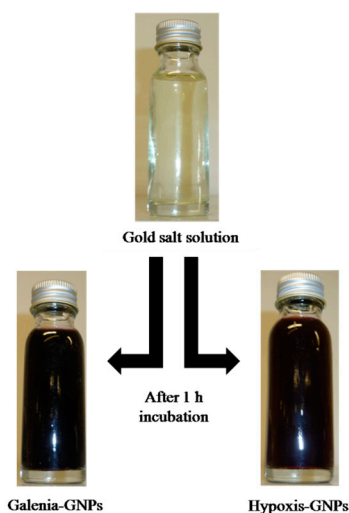


Figure 1. Digital photographs of the aqueous solutions of gold salt before the addition of the extracts, and Galenia-GNPs and Hypoxis-GNPs after 1 h incubation of the gold salt with the respective extracts.

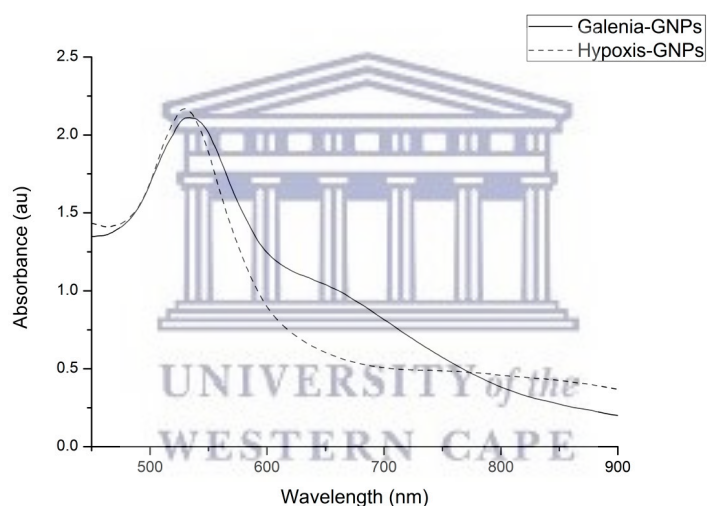


Figure 2. UV-Vis spectra of GNPs synthesized from *G. africana* (Galenia-GNPs) and *H. hemerocallidea* (Hypoxis-GNPs) plant extracts.

We also studied the kinetics of GNPs formation by examining the changes in the λ_{\max} of the plant extract/gold salt mixtures over time. Hypoxis-GNPs started to form and show λ_{\max} above 1 Absorbance unit (au) after 5 min (Figure 3A). This increase in λ_{\max} is the result of the increasing number of GNPs as Au^{+3} ions are reduced to Au^0 [40]. The Hypoxis-GNPs reached a maximum value after 40 min and thereafter remained unchanged suggesting the reaction was complete at 40 min (Figure 3C). On the other hand, the reaction with the *G. africana* plant extract started to change color and the λ_{\max} increased above 1 au only after 20 min (Figure 3B) indicating the presence of lower reduction power phytochemicals in *G. africana* extract compared to *H. hemerocallidea*'s. Both GNPs exhibited constant λ_{\max} from 60 min (Figure 3C), which show that 1 h of incubation was sufficient to complete the reaction for both plant extracts.

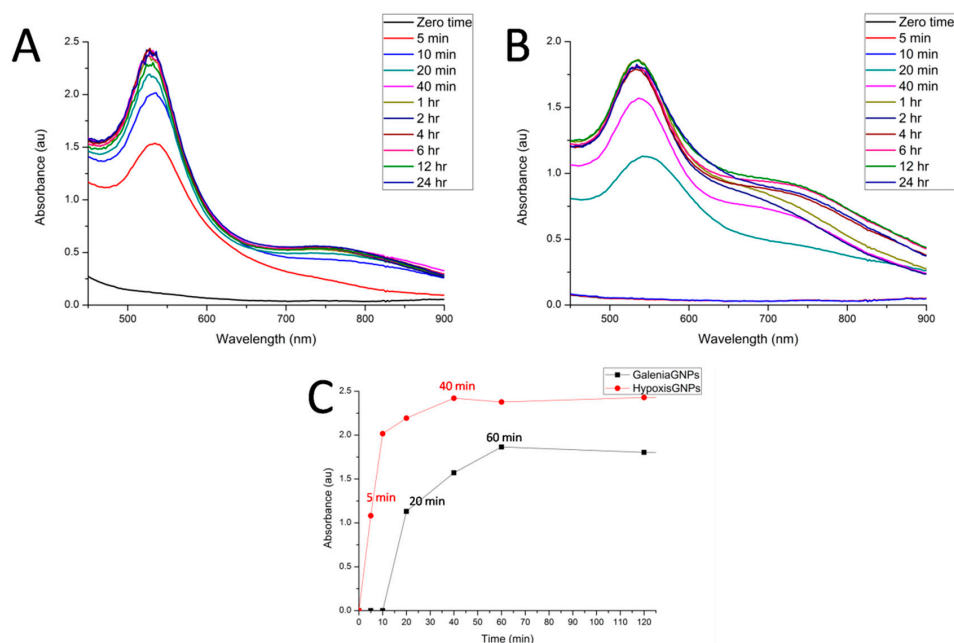


Figure 3. The UV-Vis spectra recorded as a function of time of GNPs synthesized from (A) *H. hemerocallidea* and (B) *G. africana*; (C) shows the λ_{\max} values of the two GNPs as a function of time.

2.2. Particle Diameter and Particle Size Distribution Analysis

The distribution of the hydrodynamic diameters of the GNPs was measured by two different DLS-based techniques (based on size by intensity and by the number of GNPs) using the Zetasizer (Malvern Instruments Ltd., Malvern, UK). The size distribution based on intensity is depicted in Figure 4A, in which the scattering intensity is plotted against the logarithms of the particle diameter. Hypoxis-GNPs showed bimodal distribution, whereas Galenia-GNPs showed multimodal distribution that indicates the anisometric nature of Galenia-GNPs compared to Hypoxis-GNPs (Figure 4A). This may also explain the presence of NIR absorption peak in the UV-Vis spectrum of the Galenia-GNPs (Figure 2). In both GNPs, the peak intensity of the large particles was higher than the peak intensity of the small particles, which was expected since the particle size distribution based on the light-scattering intensity is greatly influenced by larger particles [41]. Conversely, the peaks for small particles showed higher intensity in the number-weight based size distribution (Figure 4B), with no intensity observed for larger particles. It should be taken into consideration that the error in the data obtained from number-weight size distribution is large due to its sixth power dependence on the original scattering intensity data. Yet, it can be a useful tool to compare the distribution of the two plant extracts' GNPs of small size. From Figure 4B it can be observed that the two plant extracts were able to synthesize very small GNPs (1–2 nm) in which a higher number of small size GNPs could be synthesized with *G. africana* extract as opposed to *H. hemerocallidea* as can be deduced from the intensity of the peaks.

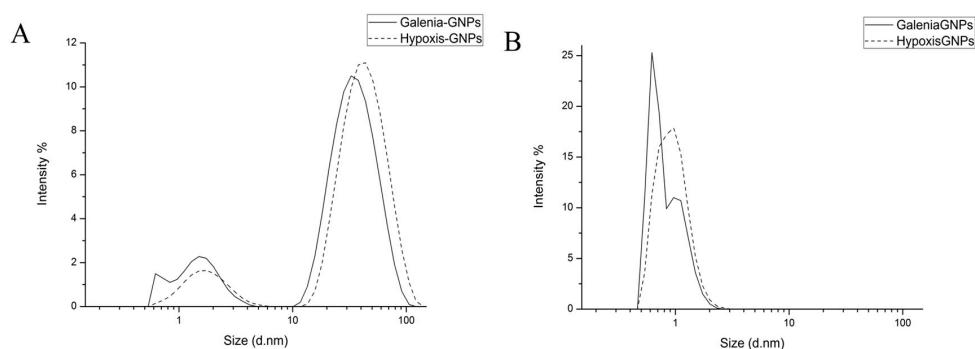


Figure 4. DLS distribution curves of GNPs' hydrodynamic diameter by (A) intensity and (B) number of GNPs.

Table 1 shows the average diameters of light-scattering intensity peaks shown in Figure 4A as well as the Z-average diameter, which is derived from the light-scattering intensity data. In agreement to the distribution curves, the Z-average diameter of the Galenia-GNPs have smaller average diameter in comparison to Hypoxis-GNPs.

Table 1. Average diameter of Galenia-GNPs and Hypoxis-GNPs obtained from DLS analysis.

GNPs	Small-Particle Peaks Average Diameter (nm)	Large-Particle Peaks Average Diameter (nm)	Z-Average Diameter (nm)
Galenia-GNPs	1.9 ± 1.1	44 ± 29	11 ± 1
Hypoxis-GNPs	2.3 ± 1.6	51 ± 34	26 ± 6

2.3. FTIR Analysis

The FTIR analysis was done for the plant extracts and the GNPs to identify the possible functional groups involved in the biosynthesis of GNPs. This information can aid in identifying the phytochemicals involved in the reduction of the gold salt and may also provide useful information on how to conjugate other chemical entities (e.g., small molecule drugs, peptides, nucleic acids, etc.) onto the GNPs for biomedical applications. The bio-reduction mechanism of gold ions using plants extracts continues to be elucidated, despite the increasing attention being given to the biogenic synthesis of the GNPs [42]. Several studies suggest that various phytochemicals may play a role in the synthesis of GNPs [42,43]. Generally, different chemical classes were found to influence the production of the GNPs based on the major constituent of each plant extract [32].

Figure 5 shows the FTIR spectra of both the plant extracts and the GNPs. Both GNPs showed similarities with their respective extracts, which may be due to the presence of similar compounds in both the extracts and the GNPs. Additionally, some bands of the FTIR spectra of the GNPs appeared to be shifted when compared to the FTIR spectra of the extracts. These shifts were expected and are believed to be caused by the influence of the nearby metal and possibly suggest the involvement of the corresponding functional groups in the GNPs synthesis [41]. These observed shifts are highlighted in Table 2, which also shows the possible functional groups involved in the synthesis of the GNPs from both extracts. Interestingly, some major peaks were generated in the FTIR spectra of both GNPs indicating that similar functional groups are key players in the synthesis of the GNPs. For instance, the FTIR spectra of Galenia-GNPs and Hypoxis-GNPs revealed similar broad bands at 3428 and 3420, respectively, which represents the O–H group of alcohols [12]. The intense band at $\sim 2924 \text{ cm}^{-1}$ can be a result of asymmetric stretching of the C–H group [12]. Also, the peak centered at 1384 cm^{-1} , which indicates the presence of the $-\text{CH}_3$ group of alkanes, was also recorded in Galenia-GNPs. Galenia-GNPs also demonstrated a peak at 1329 cm^{-1} that corresponds to an alcoholic or phenolic O–H group [41]. The transmittance of O–H and C–O bands in the FTIR spectra indicates the presence of hydroxyl and carbonyl groups on the GNPs possibly as a result of the involvement

of flavonoids, terpenoids, phenolic compounds and/or carbohydrates in the GNPs biosynthesis (Table 2). Several studies reported the role of these hydroxyl and carbonyl containing compounds in the reduction, capping and stabilization of the GNPs [12,44]. Amino acids and proteins were also suggested to act as stabilizers of GNPs after the reduction step [13]. Yet, a quick phytochemical screening, using the Biuret and Ninhydrin tests, showed that both aqueous extracts were negative for the presence of proteins and amino acids, and hence we postulate that proteins and amino acids do not play a role in the stabilization of the GNPs in this study.

The chemical study of *G. africana* revealed that this plant is rich in flavonoids [21,22]. Indeed, the FTIR spectrum of *G. africana* aqueous extract showed a strong band at 1384 cm^{-1} that corresponds to the phenolic O–H group and hence we speculate that the flavonoids of this plant are responsible for the reduction of the gold salt to produce Galenia-GNPs. Further, *H. hemerocallidea* is well known for producing a variety of hydroxyl-rich phytoglycosides [27]. A study by Jung et al. (2014) reported the synthesis of GNPs from several glycosides and concluded that the GNPs can be reduced as a result of the oxidation of C-6-OH in the sugar unit into carboxylic acid [45]. The presence of the shifted band at 1267 cm^{-1} , in the FTIR spectrum of Hypoxis-GNPs, which can be attributed to the C–O group of carboxylic acids, may be a result of the oxidation of the aforementioned oxidation site (Table 2). One of the major secondary metabolites of *H. hemerocallidea* is Hypoxoside, which is a phytoglycoside compound containing the same oxidation site reported by Jung et al. (2014). Hence, we also speculate that Hypoxoside may play a major role in the synthesis of the GNPs. Clearly, these major compounds should be isolated and tested for the synthesis of the GNPs in order to identify, with certainty, the actual functional groups responsible for the synthesis of the GNPs from each plant. This investigation is ongoing.

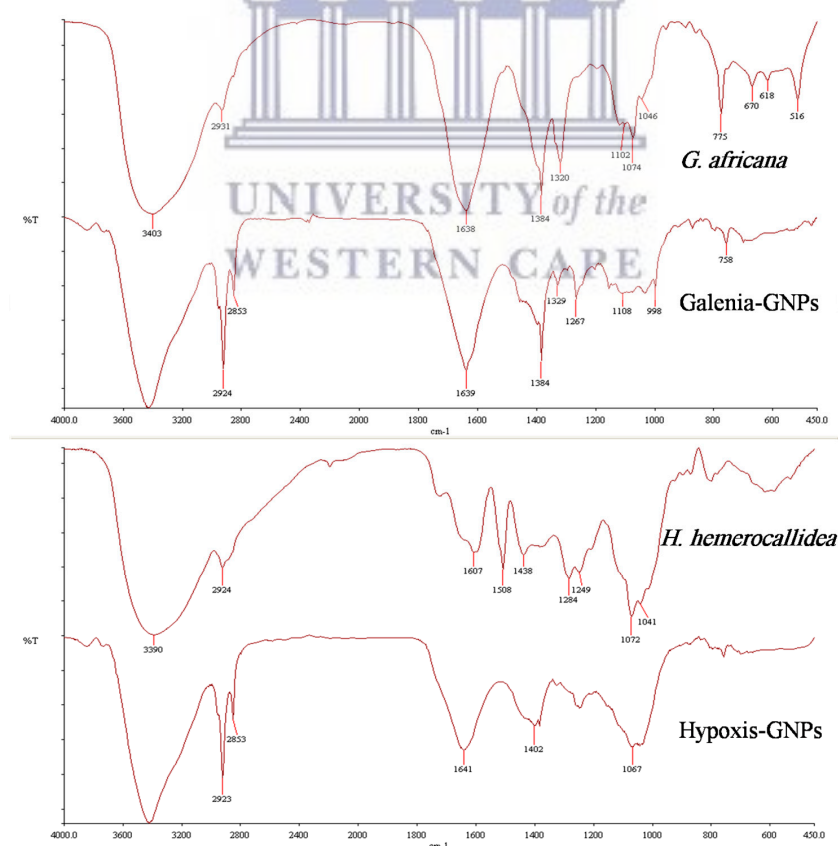


Figure 5. FTIR spectra of *H. hemerocallidea* and *G. africana* and their respective GNPs.

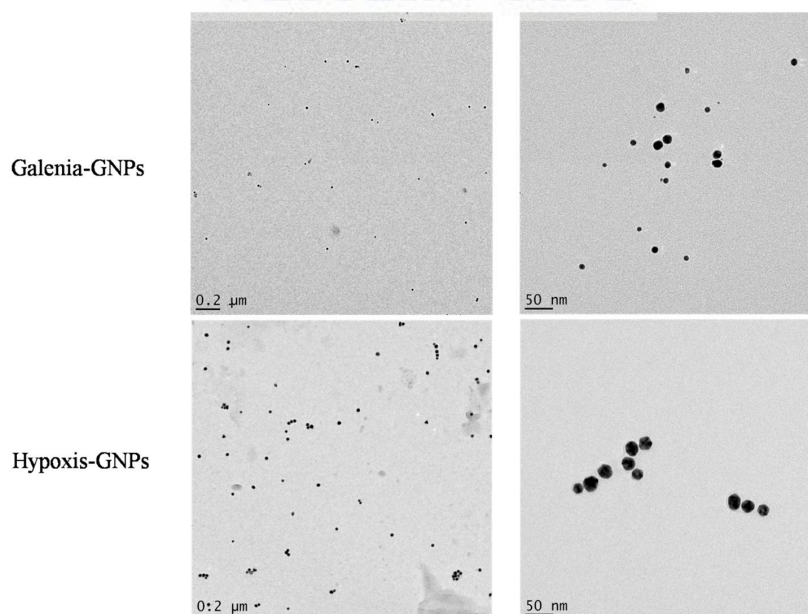
Table 2. Shifts of the FTIR spectra bands (cm^{-1}) of the major peaks of *H. hemerocallidea* and *G. africana* aqueous extracts and their respective GNPs.

<i>G. africana</i>				<i>H. hemerocallidea</i>			
Aqueous Extract	Galenia-GNPs	Shift Value *	Possible Functional Groups	Aqueous Extract	Hypoxis-GNPs	Shift Value *	Possible Functional Groups
3403	3428	−25	O–H Alcohols	3390	3420	−30	O–H Alcohols
2931	2924	+7	C–H Alkanes	2924	2923	+1	C–H Alkanes
1384	1384	0	−CH ₃ Alkanes	1438	1402	+36	C=C Aromatics
1320	1329	−9	O–H Alcohols, Phenols	1249	1267	−18	C–O Aromatic esters, Ethers, Carboxylic acids
775	758	+17	C–Cl Alkanes C–H Benzenes	1072	1067	−5	C–O–C

* The shift values were calculated by subtracting the peak transmittance of GNPs from the peak transmittance of the extract.

2.4. HRTEM and EDX Analysis

The HRTEM analysis of the GNPs was done to study their morphologies, crystalline nature and their particle size distribution. Interestingly, the HRTEM images show predominance of spherical GNPs from the two plant extracts (Figure 6). Due to the presence of numerous phytochemicals in the extracts that are capable of reducing the gold salt, it is common that plant phytochemicals produce GNPs with a mixture of geometrical shapes [32]. It is suggested that the presence of strong interaction forces between the capping bio-molecules and the surfaces of GNPs could keep the nascent GNPs from sintering, resulting in small sized spherical GNPs [33]. Therefore, the synthesis of spherical shapes in this study may imply that the capping agents, present in *H. hemerocallidea* and *G. africana*, exhibit strong interaction with the newly grown GNPs and prevent them from developing into other shapes. Yet, some deviations from the spherical shapes were observed in the HRTEM images of the two GNPs (Figure 7). These deviations, which were more common in Galenia-GNPs, may explain the absorbance peak beyond 600 nm in the UV-Vis spectra of Galenia-GNPs in Figure 2.

**Figure 6.** HRTEM images of Galenia-GNPs and Hypoxis-GNPs.

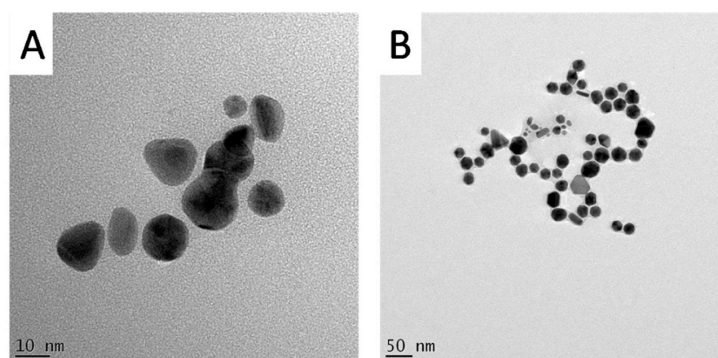


Figure 7. HRTEM images showing spherical deviations observed in (A) Galenia-GNPs and (B) Hypoxis-GNPs.

The HRTEM analysis also revealed the crystalline nature of the GNPs. Figure 8A,C show the lattice fringes of the two GNPs. The shortest lattice distances were 0.234 and 0.227 nm for Hypoxis-GNPs and Galenia-GNPs, respectively (Figure 8A,C). These values correspond approximately to the interplanar spacing between (111) planes of gold [46]. The crystalline nature of the GNPs was also confirmed by the selected area electron diffraction (SAED). The bright rings were found to correspond to the (111), (200), (220), (311) and (222) planes of the gold (Figure 8B,D).

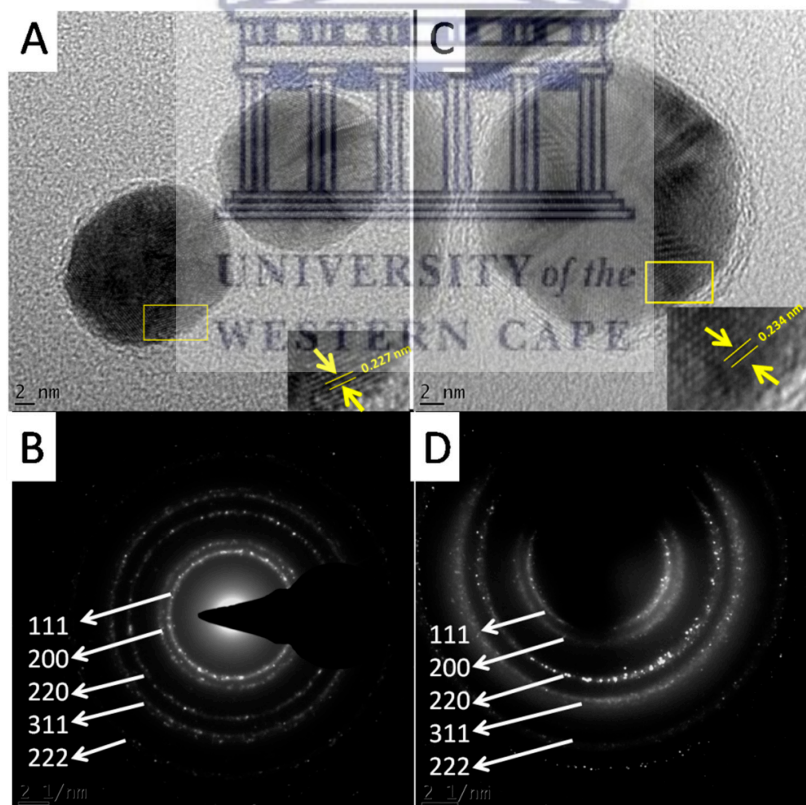


Figure 8. HRTEM images showing fringe lattices observed in (A) Galenia-GNPs and (C) Hypoxis-GNPs, and SAED pattern of (B) Galenia-GNPs and (D) Hypoxis-GNPs.

The particle size distributions obtained from the HRTEM images were similar to the DLS data (Figure 9). The particle size range of Galenia-GNPs was between 2 and 16 nm with the largest number of the particles being between 8 and 10 nm in diameter (Figure 9A). On the other hand, the particle size of Hypoxis-GNPs ranged from 10 to 45 nm with the majority of the NPs being between 25 and

30 nm in diameter (Figure 9B). Also, the average particle size of Galenia-GNPs (9 ± 2 nm) was smaller than those of Hypoxis-GNPs (27 ± 6 nm) as obtained by HRTEM analysis. It must be noted that the hydrodynamic particle size data obtained from the DLS analysis is usually larger than the particle size determined by HRTEM [12]. Indeed, the average size of Galenia-GNPs obtained by HRTEM was smaller than the average size determined by Zetasizer. Conversely, the average size of Hypoxis-GNPs as determined by HRTEM was slightly larger than the size obtained using the Zetasizer. Yet, it must be taken into consideration that only a few NPs are shown in each frame of the HRTEM images, so any shape and size distributions determinations of the GNPs using HRTEM images will not be completely statistically reliable [41].

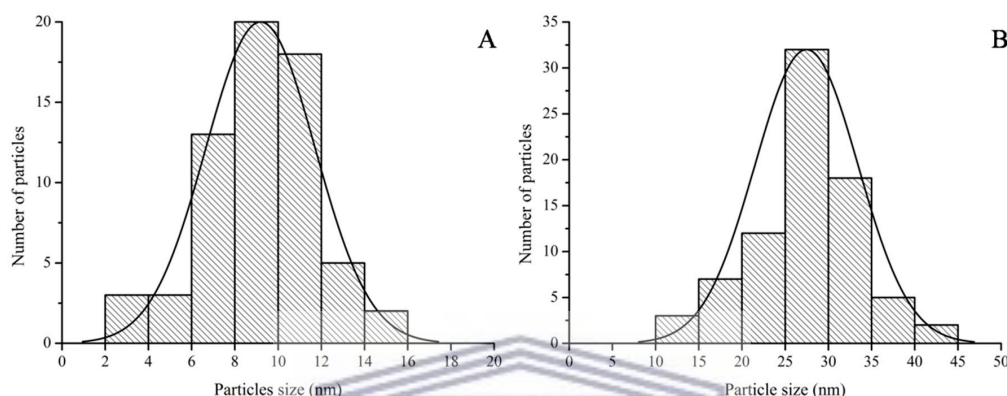


Figure 9. Particle size distributions of (A) Galenia-GNPs and (B) Hypoxis-GNPs as obtained from the HRTEM images.

The concentration of GNPs in this study was determined using their UV-Vis data as reported [47]. Using multipole scattering theory, Haiss and co-workers (2007) showed that the optical properties of the spherical GNPs are dependent on the particle size. As a result, the authors showed that the molar concentration and particle size of the GNPs could be deduced from their UV-Vis spectra. Hence, it was useful to measure the difference in the particle size data obtained using the three methods applied in this study, i.e., Zetasizer, HRTEM and UV-Vis spectra (Table 3). The results in Table 3 confirmed that three techniques showed that Galenia-GNPs were smaller in size when compared to Hypoxis-GNPs. The difference in size between Galenia-GNPs and Hypoxis-GNPs as determined by the Zetasizer and HRTEM was 15 nm and 18 nm, respectively, while the size determined using the UV-Vis spectra was 8 nm.

Table 3. Average particle size of Galenia-GNPs and Hypoxis-GNPs as obtained from the Zetasizer, HRTEM and UV-Vis spectra.

Type of GNPs	Average Size (nm)		
	Zetasizer	HRTEM	UV-Vis
Galenia-GNPs	11 ± 1	9 ± 2	10
Hypoxis-GNPs	26 ± 6	27 ± 6	18
Difference in size *	+15	+18	+8

* Difference was calculated as follow: (average size of Hypoxis-GNPs) – (average size of Galenia-GNPs).

The presence of the elemental gold was confirmed in the graphs obtained from the EDX spectroscopy analysis of the GNPs. The EDX data showed adsorption of gold peaks at around 2.3, 9.7 and 11.3 keV (Figure 10). These values are in agreement with a previous study [48]. The presence of carbon, copper and silicon peaks in the samples is attributed to the HRTEM grid and/or the detector window [49]. On the other hand, traces of the phytochemicals of the extracts present around the GNPs or in the medium may have caused the presence of oxygen peaks [13].

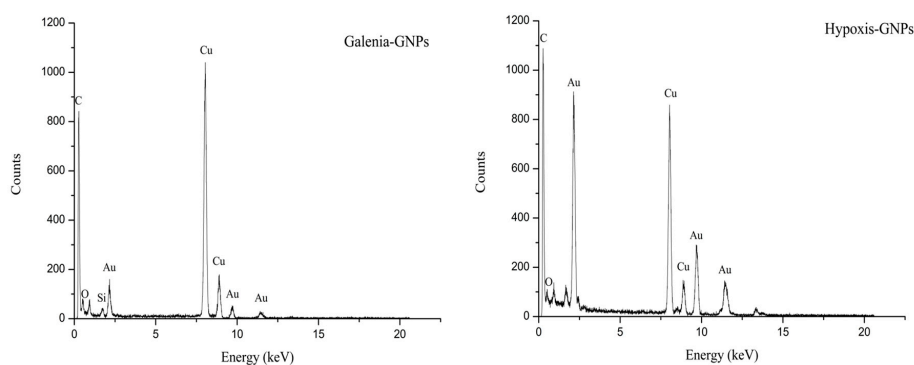


Figure 10. EDX spectra of Galenia-GNPs and Hypoxis-GNPs.

2.5. Thermal Study

The TGA was done in order to determine the percentage of the organic matter (phytochemicals involved in the synthesis) present in the GNPs. The weight loss of 5 mg of the GNPs and the extracts was measured between 20 and 800 °C (Figure 11). Table 4 summarizes the weight loss percentage of the extracts and the GNPs at different temperatures. Unlike the extracts, both GNPs did not show weight loss at 100 °C. Any weight loss at this temperature is believed to be a result of the loss of evaporation of adsorbed water [50]. It is expected that most organic compounds and functional groups will be completely burned off at 400 °C [51,52]. Table 4 shows that Hypoxis-GNPs and Galenia-GNPs, respectively, only lost 2.5% and 3.4% of their weight at 400 °C. Both of the extracts showed nearly 50% weight loss at the same temperature. The thermal decomposition of resistant aromatic compounds and biogenic salts is expected to occur at temperatures beyond 400 °C [50]. Thus, the lower weight loss in the case of *G. africana* may be as a result of the presence of higher content of these heat resistant compounds. At 800 °C Galenia-GNPs showed more weight loss (4%) when compared to Hypoxis-GNPs. It should be noted that the amount of the *G. africana* extract used in the synthesis of Galenia-GNPs was twice the amount of *H. hemerocallidea* extract used to synthesize the Hypoxis-GNPs (as mentioned in Section 3) and it was therefore expected that the weight loss value of Galenia-GNPs would be higher compared to Hypoxis-GNPs.

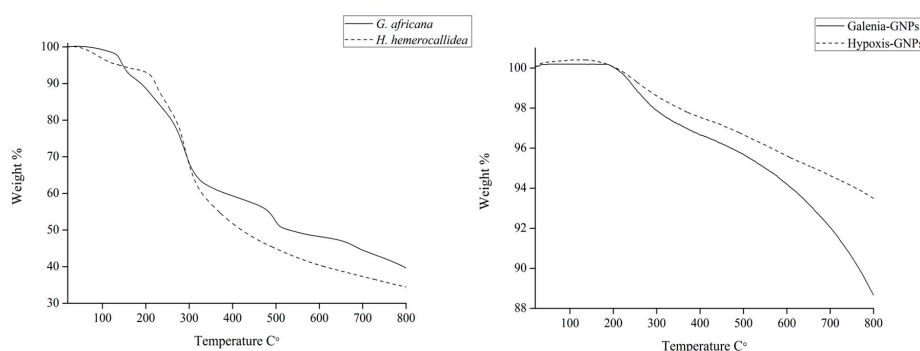


Figure 11. TGA data for *H. hemerocallidea* and *G. africana* and their respective GNPs.

Table 4. Weight (expressed as percentage) of *H. hemerocallidea* and *G. africana* extracts and their respective GNPs at different temperatures as obtained from TGA.

Sample	Weight % at 100 °C	Weight % at 400 °C	Weight % at 800 °C
Hypoxis-GNPs	100%	97.5%	91.8%
Galenia-GNPs	100%	96.6%	87.7%
<i>H. hemerocallidea</i> extract	96.8%	52%	34%
<i>G. africana</i> extract	99.2%	60%	39%

2.6. Stability of the GNPs

To understand the stability of the GNPs, the zeta potential values, measured immediately after the synthesis, were obtained using the Zetasizer. Hypoxis-GNPs and Galenia-GNPs demonstrated negative zeta potential values of -22 and -20 , respectively. These negative values can estimate the long-term stability of the GNPs in a solution, as they can provide enough repulsion forces between the particles and prevent their agglomeration [53].

If these GNPs are to be considered for biomedical applications, they must maintain their stability in different buffer solutions (e.g., Sodium Chloride (NaCl), cysteine and Bovine Serum Albumin (BSA)). The stability of the GNPs was measured after incubation with the aforementioned buffer solutions as well as the growth media used in the biological assays in this study (Dulbecco's Modified Eagle's Medium (DMEM) supplemented with 10% Fetal Bovine Serum (FBS) and Nutrient broth). The GNPs were incubated at $37\text{ }^{\circ}\text{C}$ with DMEM and Nutrient broth in order to determine the effect of the media on the stability of the GNPs under experimental conditions. A minimal change in the UV-Vis spectra of the GNPs is an indication of the GNPs stability. When the GNPs lose stability they may precipitate, which can be observed by the significant red shifts and broadening of the UV-Vis bands [54]. After measuring the UV-Vis of the two GNPs incubated with different buffers and the biological media over a 24 h period, it was observed that these GNPs were generally stable in most of the buffer conditions tested with no changes in the UV-Vis bands (Figure 12). One exception was the effect of 0.5% cysteine on Galenia-GNPs, which caused the UV-Vis bands to become broader at all the time-points. Nonetheless, Galenia-GNPs showed excellent stability in DMEM that usually contains cysteine and other amino acids but at lower concentrations.

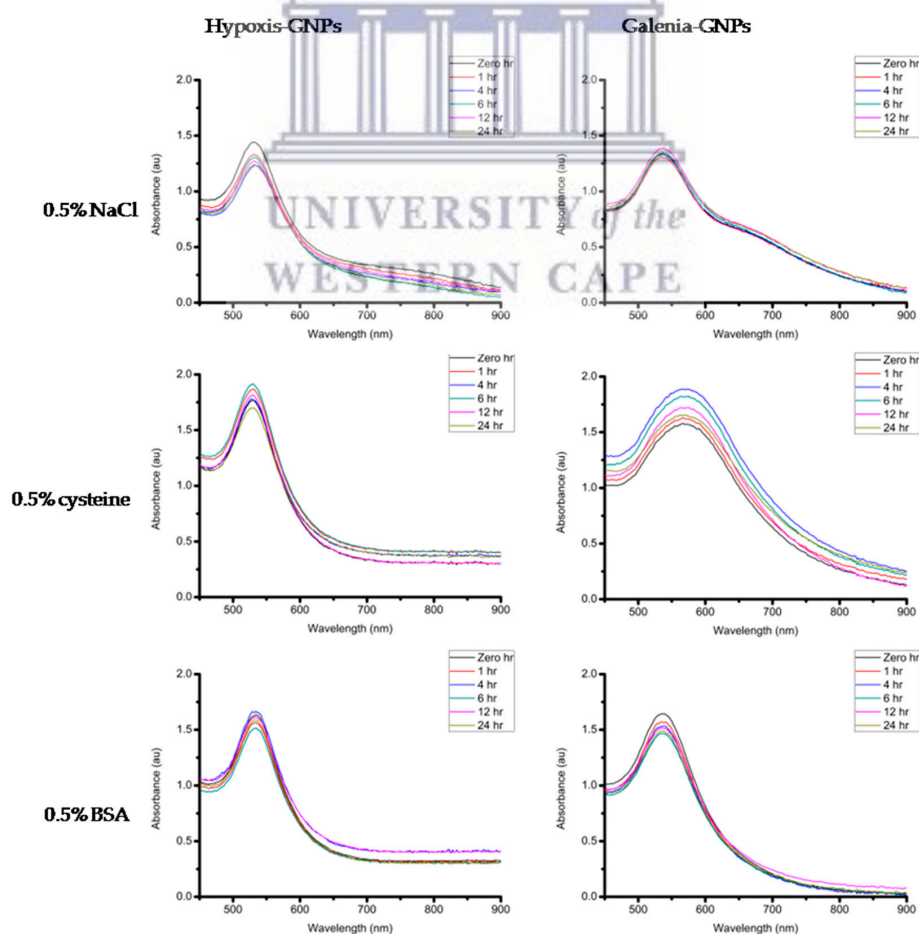


Figure 12. Cont.

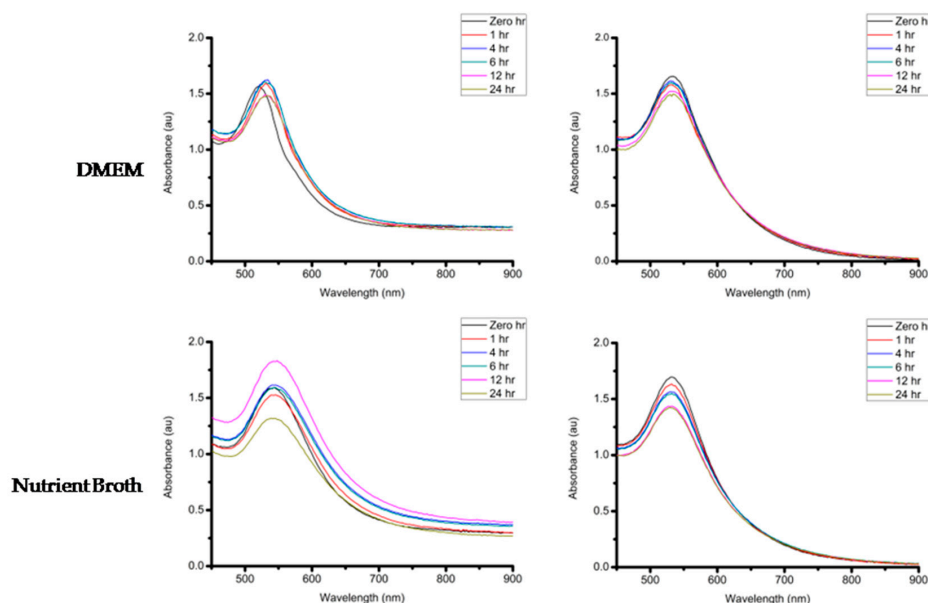


Figure 12. UV-Vis spectra of the GNPs taken over a 24-h period in buffers containing 0.5% NaCl, 0.5% cysteine and 0.5% BSA, Nutrient broth and in DMEM supplemented with 10% FBS.

2.7. Antibacterial Effects and Toxicity of the GNPs

Generally, the antibacterial effect of different plant extracts is well documented and recognized. However, the antibacterial effect of the biogenic metal NPs produced from such plant extracts still remains largely unexplored and can prove useful in the search for new antibacterial agents [12]. For this reason, the antibacterial activities of Hypoxis-GNPs, Galenia-GNPs along with the tested plant extracts were investigated. The Alamar blue assay was used to measure the bacterial growth after treatment. Resazurin (Alamar blue dye) undergoes colorimetric change in response to cellular metabolic reduction to give the highly fluorescent compound resorufin that can be quantified by measuring its fluorescence [55]. The Minimum Inhibitory Concentration (MIC) in this study was defined as the lowest concentration of the tested samples that significantly ($p < 0.05$) inhibits the growth of the tested bacterial strains as compared to the negative control value. The antibacterial evaluation was done against a panel of gram-positive and gram-negative bacterial strains that are known to cause wound infections.

The MIC values for the GNPs and the plant extracts are summarized in Table 5. The antibiotic Ampicillin was included as a positive control. The antibacterial effect of citrate-capped GNPs was also tested. Hypoxis-GNPs demonstrated significant antibacterial activity against the tested bacterial strains when compared to Galenia-GNPs. Interestingly, the MIC value of the Hypoxis-GNPs (32 nM) was the same for the bacterial strains. However, the viability of the bacteria at this MIC value varied between the different bacterial strains. For instance, *P. aeruginosa* was the most susceptible by Hypoxis-GNPs and showed the lowest viability with $10 \pm 1\%$ compared to $16 \pm 1\%$, $20 \pm 1\%$ and $43 \pm 5\%$ for *E. coli*, *Staphylococcus epidermidis* and *S. aureus*, respectively. Galenia-GNPs only showed an antibacterial effect on *P. aeruginosa* with a MIC value of 32 nM and viability of $35 \pm 5\%$. Further, none of the aqueous plant extracts induced any growth inhibition in this study. However, Ncube et al. (2012) reported that the *H. hemerocallidea* aqueous extract have an MIC value of 12.5 mg/mL against *S. aureus* and *E. coli*, which is significantly higher than the highest concentration tested in this study [30]. Katerere and Eloff (2008) also reported that the acetone corm extract of this plant had a low MIC value of 0.31 mg/mL against *S. aureus* [56]. This difference is likely to be attributed to the difference in the chemical nature of phytochemicals present in the acetone and water extracts. The citrate-capped GNPs failed to induce similar antibacterial activity as observed with the biogenic GNPs. Also, the MIC

values obtained for Ampicillin were within the ranges reported in previous studies [57–59]. The MIC for Ampicillin was significantly higher for *P. aeruginosa* (2 mg/mL) compared to the other bacterial strains tested. The increased resistance of *P. aeruginosa* to Ampicillin is possibly due to changes in the penicillin-binding proteins, membrane impermeability and the production of beta-lactamases [60].

Table 5. The MIC values of the GNPs, the aqueous extracts and Ampicillin on the tested bacterial strains. The viability recorded at each MIC of the GNPs are written in brackets.

Sample Tested	Bacterial Strains			
	<i>S. aureus</i>	<i>E. coli</i>	<i>S. epidermidis</i>	<i>P. aeruginosa</i>
Hypoxis-GNPs (nM)	32 (43 ± 5%) *	32 (16 ± 1%) ***	32 (20 ± 1%) ***	32 (10 ± 1%) ***
Galenia-GNPs (nM)	>32	>32	>32	32 (35 ± 5%) **
Citrate GNPs (nM)	>32	>32	>32	>32
<i>H. hemerocallidea</i> extract (mg/mL)	>0.48	>0.48	>0.48	>0.48
<i>G. africana</i> extract (mg/mL)	>0.48	>0.48	>0.48	>0.48
Ampicillin (mg/mL)	0.004	0.002	0.0005	2.0

*** Statistical significance ($p < 0.001$) compared to negative control, ** Statistical significance ($p < 0.01$) compared to negative control, * Statistical significance ($p < 0.05$) compared to negative control.

It is thought that the smaller size of the GNPs compared to the size of the bacterium enables the GNPs to exert bacterium cell death by adhering to its cell wall [61]. The GNPs can then penetrate the cell wall of the bacterium and induce death by affecting respiratory mechanisms and cell division by binding to protein- or phosphorus-containing compounds, such as DNA [62]. It is believed that the variation in activity against the bacterial strains is dictated by the nature of the bacterial cell wall. The cell wall of the gram-positive bacterial strains, for example, has a thicker peptidoglycan layer compared to the cell wall of the gram-negative bacteria [63]. As a result, GNPs can penetrate the cell wall of the gram-negative bacteria and exert their antibacterial action more easily than in gram-positive bacteria [64]. Accordingly, the variation in the viability of the bacterial strains after treatment with the MIC value of Hypoxis-GNPs could be attributed to the nature of the cell wall composition. In fact, growth inhibition caused by the Hypoxis-GNPs was more significant in the two gram-negative bacterial strains (*E. coli* and *P. aeruginosa*).

Furthermore, the results show that the aqueous plant extracts lacked any bacterial activity at the highest concentration tested in this study in contrast to the biogenic GNPs. It is, however, possible that a higher concentration of the extracts can be active against these bacterial strains as demonstrated previously [30]. The lower antibacterial activity of the extracts compared to the GNPs may be due to the fact that either the bacteria are adopting resistance mechanisms against the free phytochemicals or there is some synergistic activity between the GNPs and the capping phytochemicals [65]. The higher antibacterial activity of the biogenic GNPs may also be associated with the increase in the concentration of the active phytochemicals capping the GNPs. Consequently, when bacteria are exposed to the GNPs an augmented antibacterial effect is obtained. It is also possible that the GNPs have more targeting effect or higher affinity towards the bacterial cells in comparison to the free phytochemicals. The fact that the non-phytochemical capped GNPs (Citrate NPs) was not as active as Hypoxis- or Galenia-GNPs further supports the role of the phytochemicals in inhibiting the bacterial growth. In addition, it is known that the antibacterial activity of the NPs is inversely proportional on their particle size [66], yet the bigger size Hypoxis-GNPs were more active against the bacteria than the smaller particle size Galenia-GNPs. Hence, it could be speculated that the properties of the phytochemicals capping the NPs are an important factor in determining the antibacterial activity regardless of the size of the GNPs.

In view of the fact that biogenic GNPs such as Hypoxis-GNPs and Galenia-GNPs can potentially be applied in wound dressings to protect the exposed tissue against bacterial infections, we also investigated the potential toxicity of these GNPs to the human fibroblast cells. The toxicity of the GNPs towards the KMST-6 cell line therefore was established using in vitro cell culture testing. Figure 13 shows that there was no significant reduction in the viability of KMST-6 cells after a 24 h treatment with different concentrations (up to 32 nM) of the GNPs, which is equivalent to the MIC values obtained for

the GNPs against some of the bacterial strains. This preliminary data suggests that these GNPs are safe for therapeutic use.

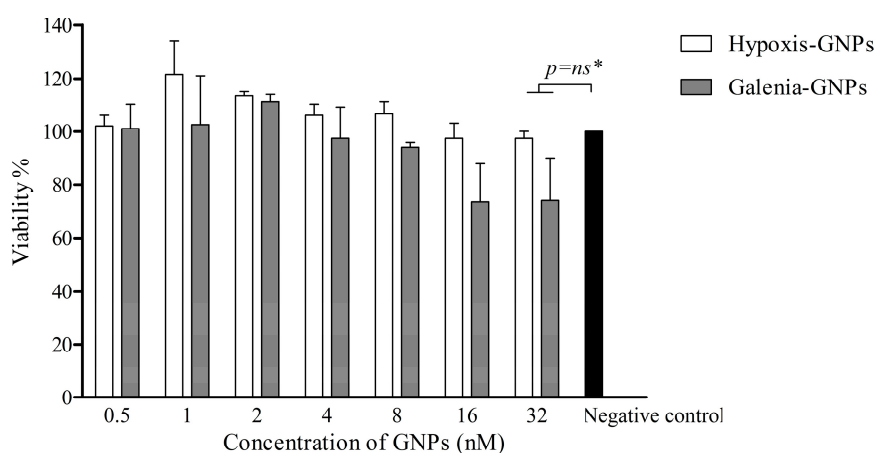


Figure 13. The effect of the GNPs on the cell viability of KMST-6 as determined by the MTT assay.
* No statistically significant difference ($p > 0.05$) compared to the negative control.

3. Materials and Methods

3.1. Materials

The aqueous extract of *H. hemerocallidea* was purchased from Afriplex (Cape Town, South Africa). Polystyrene 96-well microtitre plates were obtained from Greiner bio-one GmbH (Frickenhausen, Germany). Ampicillin, 3-[4,5-dimethylthiazol-2-yl]-2,5-diphenyl tetrazolium bromide (MTT) and gold salt (sodium tetrachloroaurate (III) dihydrate) were purchased from Sigma-Aldrich (Cape Town, South Africa). *N*-Acetyl-L-cystein and Alanin were purchased from Boehringer Mannheim GmbH (Mannheim, Germany). DMEM, penstrep (penicillin–streptomycin) and Phosphate buffered saline (PBS) were purchased from Lonza (Cape Town, South Africa). BSA was procured from Miles Laboratories (Pittsburgh, PA, USA). FBS was bought from Thermo Scientific (Ansfre, South Africa). Nutrient broth and Miller Hinton agar were purchased from Biolab (supplied by Merck, Modderfontein, South Africa). Alamar blue dye was obtained from Invitrogen Corporation (San Diego, CA, USA). NaCl, Sodium Hydroxide (NaOH) and Ninhydrin reagent were brought from Merck (Cape Town, South Africa). Citrate-capped GNPs (14 nm) were obtained from DST/Mintek Nanotechnology Innovation Centre (Gauteng, South Africa).

3.2. Preparation of *G. africana* Aqueous Extract

G. africana was collected during the month of May 2015 from the Western Cape Province, South Africa. The plant was identified by Dr. Chris N. Cupido, the co-author of this paper, and a specimen was deposited in Kirstenbosch National Botanical Garden (Cape Town, South Africa) under accession number 1468255/NBG. The fresh aerial parts of *G. africana* were dried in the shade. To obtain the aqueous extract, 50.0 mL of boiled distilled water were added to 5.0 g of the dried plant powder. Afterwards, the plant decoction was centrifuged for 2 h at 3750 rpm using an Allegra® X-12R centrifuge (Beckman Coulter, Cape Town, South Africa). The supernatant was then filtered through 0.45 µm filters and freeze-dried using FreeZone 2.5 L freeze-dryer (Labconco, Kansas City, MO, USA).

3.3. Biogenic Synthesis of the GNPs and Their Characterization

The *H. hemerocallidea* and *G. africana* plant extracts were first screened for the production of GNPs in 96-well microtitre plates using the method reported in a previous study [32]. In short, 250 µL of 1.0 mM sodium tetrachloroaurate (III) dihydrate were mixed with 50.0 µL of each plant extract in

a 96-well microtitre plate (the concentrations of the extracts varied from 8.0 to 0.125 mg/300 μ L). The plate was incubated for 1 h at 70 °C with shaking at 40.0 rpm. The production of the GNPs was monitored by measuring the UV-Vis spectra (450–900 nm) using a POLARstar Omega microtitre plate reader (BMG Labtech, Cape Town, South Africa). For further evaluations of the GNPs, the volume of the gold salt and plant extracts mixtures was up-scaled after determining the optimum concentrations of the plant extracts that produce desirable GNPs (0.5 mg/300 μ L for *G. africana* and 0.25 mg/300 μ L for *H. hemerocallidea*). The GNPs were then centrifuged and the pellets were washed three times with distilled water and ultimately re-suspended in distilled water.

3.4. DLS Analysis

The zeta potential and hydrodynamic size values of the freshly synthesized GNPs were measured using a Zetasizer (Malvern Instruments Ltd., Malvern, UK) at 25 °C and a 90° angle. Zetasizer software version 7.11 was used to analyze the data.

3.5. FTIR Spectroscopy

The FTIR analysis was done using PerkinElmer spectrum one FTIR spectrophotometer (Waltham, MA, USA) according to the method reported previously [7]. The freeze-dried GNPs and the extracts were added to KBr powder and pressed into a round disk. A pure KBr round disk was used for background correction.

3.6. HRTEM and EDX Analysis

One drop of the GNPs solution was added onto a carbon coated copper grid. The grids were allowed to dry for a few minutes under a Xenon lamp. The HRTEM images were obtained using FEI Tecnai G² 20 field-emission gun (FEG) HRTEM operated in bright field mode at an accelerating voltage of 200 kV. The elemental composition of the GNPs was identified using EDX liquid nitrogen cooled Lithium doped Silicon detector.

3.7. Image Processing

The image analysis software ImageJ 1.50b version 1.8.0_60 (<http://imagej.nih.gov/ij>) was used to analyze the HRTEM images.

3.8. TGA

The TGA was done using PerkinElmer TGA 4000 (Waltham, MA, USA). The freeze-dried GNPs (5.0 mg) or plant extracts (5.0 mg) were heated from 20 to 800 °C in nitrogen atmosphere (flow rate was 20.0 mL/min) [67]. The temperature was increased at a rate of 10 °C/min.

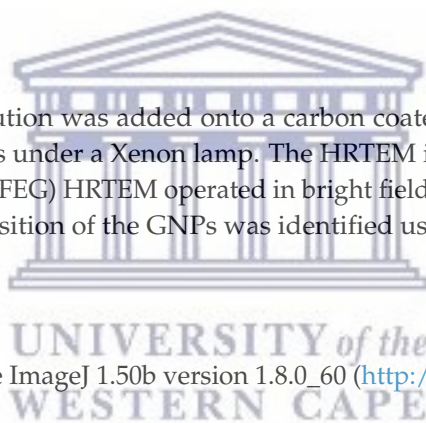
3.9. Stability Evaluation of the GNPs

To measure the effect of different aqueous buffer solutions (e.g., 0.5% NaCl, 0.5% cysteine and 0.5% BSA) on the stability of the biogenic GNPs, 100 μ L of the GNPs solutions were mixed with 100 μ L of the buffer solutions in a 96-well microtitre plate. The stability of the GNPs was also evaluated in DMEM (supplemented with 10% FBS) and Nutrient broth. The stability of the GNPs was monitored by measuring the UV-Vis spectrum (between 450 and 900 nm) of the samples at 1, 4, 6, 12 and 24 h after mixing the GNPs with the buffer solutions or the media.

3.10. Phytochemical Screening

3.10.1. Test for Proteins (Biuret Test)

The phytochemical assays were done as described previously with minor modifications [68]. To test the aqueous extracts for the presence of proteins, a few drops of 5.0% NaOH and a few drops



of 1.0% Cu(SO₄)₂ were added to 2.0 mL of each aqueous extract. BSA was used as a positive control. A violet color change indicated the presence of proteins.

3.10.2. Test for Amino Acids (Ninhydrin Test)

Few drops of Ninhydrin reagent were added to 2.0 mL of the aqueous extracts. The mixtures were heated in water bath for 10 min. Alanin was used as a positive control. The formation of purple color indicated the presence of amino acids.

3.11. Cytotoxicity Evaluation of the GNPs

The toxicity of the GNPs was tested on the non-cancerous human fibroblast cell line (KMST-6). The cells were maintained in DMEM containing 10% FBS and 1% penstrep in a 37 °C humidified incubator with 5% CO₂ saturation. The viability of the KMST-6 cells was evaluated using the MTT assay as described by Mmola and co-workers with some modifications [65]. The cells were seeded in a 96-well microtitre plates at a density of 2.0 × 10⁴ cells/100 μL/well. The plates were incubated at 37 °C in a humidified CO₂ incubator. After 24 h, the culture medium was replaced with fresh medium containing the GNPs at increasing concentrations of 0.5 to 32 nM. The concentrations of the GNPs were calculated from their UV-Vis spectra as described previously [47]. As a positive control, cells were treated with 50.0 μM C₂-Ceramide, which is a known inducer of apoptotic cell death [69]. Untreated cells were used as a negative control. All treatments were done in triplicate. After 24 h, the GNPs were removed and the wells were washed with PBS to ensure complete removal of GNPs. Thereafter, 100 μL of MTT reagent (prepared from 5.0 mg/mL stock solution and diluted with DMEM medium using a dilution factor of 1:10) were added to each well. The plates were incubated again at 37 °C for 4 h. The MTT reagent was then removed and replaced with 100 μL alkaline DMSO to dissolve the purple formazan crystals as recommended by Wang and colleagues [70]. After a 15 min incubation period at 37 °C, the absorbance of the samples was measured at 540 nm using the microtitre plate reader. The absorbance at 630 nm was used as a reference wavelength. The percentage of cell viability was calculated using the following equation:

$$\% \text{ cell viability} = \frac{\text{sample absorbance} - \text{cell free sample blank}}{\text{negative control absorbance}} \quad (1)$$

3.12. Antibacterial Evaluation of the GNPs

Table 6 lists the bacterial strains selected for testing the antibacterial activity of the GNPs in this study. The Alamar blue assay was used to evaluate the inhibition of bacterial growth by both the GNPs and the plant extracts. The test was done according to the manufacturer's instructions. The bacterial strains were first cultured and maintained on Miller Hinton agar plates. Single colonies were then inoculated into Nutrient broth and incubated at 37 °C with shaking for overnight. The number of bacterial cells was determined and adjusted to 0.5 McFarland using OD₄₅₀ to give final cell concentration of 1–2 × 10⁸ CFU/mL [71]. The cell cultures were further diluted in order to give a final concentration of 5.0 × 10⁵ CFU/mL as recommended by the European committee for Antimicrobial Susceptibility Testing (EUCAST). To determine the MIC values of the tested samples, 50.0 μL of the bacterial broth were mixed, in a 96 microtitre plate, with 50.0 μL of the GNPs (the concentrations of the GNPs varied between 0.5 and 32 nM) or 50.0 μL of the plant extracts (the concentrations of the plant extracts varied between 30.0 and 480 μg/mL). Ampicillin was used as a positive control. Negative controls were also prepared by mixing 50.0 μL of the bacterial culture with 50.0 μL of Nutrient broth. The plates were incubated at 37 °C for 24 h, after which 10.0 μL of the Alamar blue dye were added to each well. The plates were further incubated for a 3 h and then the fluorescence of resorufin was measured using a microtitre plate reader at 544 nm (excitation wavelength) and 590 nm (emission wavelength). To evaluate whether the GNPs and plant extracts interfere with the Alamar blue assay, a sample control was also prepared by mixing 50.0 μL of the GNPs and the plant extracts (all the

different concentrations were tested) with 50.0 μ L of nutrient broth. The fluorescence of the sample control was subtracted from the sample fluorescence as illustrated in the equation below, which was used to calculate the percentage bacterial growth.

$$\% \text{ bacterial growth} = \frac{(\text{sample fluorescence} - \text{sample control}) - \text{cell free sample blank}}{\text{negative control fluorescence}} \times 100 \quad (2)$$

Table 6. List of bacterial strains used in the antibacterial assay.

Bacterial Strains	ATCC Number	Gram Reaction
<i>E. coli</i>	25,922	Gram-negative
<i>P. aeruginosa</i>	27,853	Gram-negative
<i>S. aureus</i>	29,213	Gram-positive
<i>S. epidermidis</i>	12,228	Gram-positive

3.13. Statistical Analysis

The data presented are means \pm SD obtained from at least three independent experiments. Differences between the means were considered to be significant if $p < 0.05$ according to Prism's two-way ANOVA.

4. Conclusions

The study demonstrated an effective and easy methodology for the green synthesis of GNPs from two South African plant extracts, *G. africana* and *H. hemerocallidea*. To the best of our knowledge, this is the first report on GNPs synthesis from these two plants. The GNPs were characterized using different spectroscopic and microscopic techniques such as UV-Vis, DLS analysis, HRTEM, EDX, TGA and FTIR. *G. africana* and *H. hemerocallidea* produced spherical GNPs with an average particle size of 11 ± 1 and 26 ± 6 nm, respectively, as determined by DLS analysis. The FTIR data suggested that the flavonoids of *G. africana* and the glycosides contents of *H. hemerocallidea* might be responsible for the biogenic synthesis of the GNPs. In vitro stability investigation showed that both GNPs, in particular Hypoxis-GNPs, are stable when incubated with different biological buffers and the culture media. Hypoxis-GNPs showed a higher antibacterial effect compared to Galenia-GNPs against the bacterial strains tested in this study. Both GNPs were found to be non-toxic against a non-cancerous human fibroblast cell line suggesting that it may be safe to use these GNPs in wound dressings for the prevention of wound infections. However, more cytotoxic assays should be carried out to fully determine their toxicity. Additionally, a wider panel of bacterial strains that are known to cause skin infections should be investigated.

Acknowledgments: The authors would like to thank the South African National Research Foundation (NRF) and the DST/Mintek Nanotechnology Innovation Centre (NIC) for funding this research.

Author Contributions: Abdulrahman M. Elbagory, Mervin Meyer and Ahmed A. Hussein conceived and designed the experiments and analyzed the data; Christopher N. Cupido collected and identified *G. africana*; Abdulrahman M. Elbagory performed the experiments and drafted the paper; Mervin Meyer and Ahmed A. Hussein coordinated writing the paper to which all co-authors contributed.

Conflicts of Interest: The authors report no conflicts of interest in this work.

References

1. Ahmed, S.; Annu, Ikram, S.; Yudha, S. Biosynthesis of gold nanoparticles: A green approach. *J. Photochem. Photobiol. B Biol.* **2016**, *161*, 141–153. [[CrossRef](#)] [[PubMed](#)]
2. Sekhon, B.S. Nanotechnology in agri-food production: An overview. *Nanotechnol. Sci. Appl.* **2014**, *7*, 31–53. [[CrossRef](#)] [[PubMed](#)]

3. Sýkora, D.; Kašička, V.; Mikšík, I.; Řezanka, P.; Záruba, K.; Matějka, P.; Král, V. Application of gold nanoparticles in separation sciences. *J. Sep. Sci.* **2010**, *33*, 372–387. [[CrossRef](#)] [[PubMed](#)]
4. Santhoshkumar, J.; Rajeshkumar, S.; Venkat Kumar, S. Phyto-assisted synthesis, characterization and applications of gold nanoparticles—A review. *Biochem. Biophys. Rep.* **2017**, *11*, 46–57. [[CrossRef](#)] [[PubMed](#)]
5. Qiu, P.; Yang, M.; Qu, X.; Huai, Y.; Zhu, Y.; Mao, C. Tuning photothermal properties of gold nanodendrites for in vivo cancer therapy within a wide near infrared range by simply controlling their degree of branching. *Biomaterials* **2016**, *104*, 138–144. [[CrossRef](#)] [[PubMed](#)]
6. Santra, T.S.; Tseng, F.-G.; Barik, T.K. Green biosynthesis of gold nanoparticles and biomedical applications. *Am. J. Nano Res. Appl.* **2014**, *2*, 5–12. [[CrossRef](#)]
7. Khan, M.; Khan, M.; Adil, S.F.; Tahir, N.M.; Tremel, W.; Alkathlan, H.Z.; Al-Warthan, A.; Siddiqui, M.R.H. Green synthesis of silver nanoparticles mediated by *Pulicaria glutinosa* extract. *Int. J. Nanomed.* **2013**, *8*, 1507–1516. [[CrossRef](#)]
8. Wang, F.; Nimmo, S.L.; Cao, B.; Mao, C. Oxide formation on biological nanostructures via a structure-directing agent: Towards an understanding of precise structural transcription. *Chem. Sci.* **2012**, *3*, 2639–2645. [[CrossRef](#)] [[PubMed](#)]
9. Wang, F.; Li, D.; Mao, C. Genetically Modifiable Flagella as Templates for Silica Fibers: From Hybrid Nanotubes to 1D Periodic Nanohole Arrays. *Adv. Funct. Mater.* **2008**, *18*, 4007–4013. [[CrossRef](#)]
10. Kitching, M.; Ramani, M.; Marsili, E. Fungal biosynthesis of gold nanoparticles: Mechanism and scale up. *Microb. Biotechnol.* **2015**, *8*, 904–917. [[CrossRef](#)] [[PubMed](#)]
11. He, S.; Guo, Z.; Zhang, Y.; Zhang, S.; Wang, J.; Gu, N. Biosynthesis of gold nanoparticles using the bacteria *Rhodospseudomonas capsulata*. *Mater. Lett.* **2007**, *61*, 3984–3987. [[CrossRef](#)]
12. Dorosti, N.; Jamshidi, F. Plant-mediated gold nanoparticles by *Dracocephalum kotschy* as anticholinesterase agent: Synthesis, characterization, and evaluation of anticancer and antibacterial activity. *J. Appl. Biomed.* **2016**, *14*, 235–245. [[CrossRef](#)]
13. Balashanmugam, P.; Durai, P.; Balakumaran, M.D.; Kalaichelvan, P.T. Phytosynthesized gold nanoparticles from *C. roxburghii* DC. leaf and their toxic effects on normal and cancer cell lines. *J. Photochem. Photobiol. B Biol.* **2016**, *165*, 163–173. [[CrossRef](#)] [[PubMed](#)]
14. Rajan, A.; Rajan, A.R.; Philip, D. *Elettaria cardamomum* seed mediated rapid synthesis of gold nanoparticles and its biological activities. *OpenNano* **2017**, *2*, 1–8. [[CrossRef](#)]
15. Yuan, C.G.; Huo, C.; Yu, S.; Gui, B. Biosynthesis of gold nanoparticles using *Capsicum annum* var. *grossum* pulp extract and its catalytic activity. *Phys. E Low-Dimens. Syst. Nanostruct.* **2017**, *85*, 19–26. [[CrossRef](#)]
16. Song, J.-Y.; Byun, T.-G.; Kim, B.-S. Synthesis of Magnetic Nanoparticles Using *Magnolia kobus* Leaf Extract. *Process Biochem. J.* **2012**, *27*, 157–160. [[CrossRef](#)]
17. Siddiqi, K.S.; Husen, A. Recent advances in plant-mediated engineered gold nanoparticles and their application in biological system. *J. Trace Elem. Med. Biol.* **2017**, *40*, 10–23. [[CrossRef](#)] [[PubMed](#)]
18. Sreelakshmi, C.; Datta, K.K.R.; Yadav, J.S.; Reddy, B.V.S. Honey derivatized Au and Ag nanoparticles and evaluation of its antimicrobial activity. *J. Nanosci. Nanotechnol.* **2011**, *11*, 6995–7000. [[CrossRef](#)] [[PubMed](#)]
19. Ayaz Ahmed, K.B.; Subramanian, S.; Sivasubramanian, A.; Veerappan, G.; Veerappan, A. Preparation of gold nanoparticles using *Salicornia brachiata* plant extract and evaluation of catalytic and antibacterial activity. *Spectrochim. Acta Part A Mol. Biomol. Spectrosc.* **2014**, *130*, 54–58. [[CrossRef](#)] [[PubMed](#)]
20. MubarakAli, D.; Thajuddin, N.; Jeganathan, K.; Gunasekaran, M. Plant extract mediated synthesis of silver and gold nanoparticles and its antibacterial activity against clinically isolated pathogens. *Colloids Surf. B Biointerfaces* **2011**, *85*, 360–365. [[CrossRef](#)] [[PubMed](#)]
21. Vries, F.A.; El Bitar, H.; Green, I.R.; Klaasen, J.A.; Bodo, B.; Johnson, Q.; Mabusela, W.T. An antifungal active extract from the aerial parts of *Galenia africana*. In Proceedings of the 11th Napreca Symposium Book of Proceedings, Antananarivo, Madagascar, 9–12 August 2005; pp. 123–131.
22. Mativandlela, S.P.N.; Muthivhi, T.; Kikuchi, H.; Oshima, Y.; Hamilton, C.; Hussein, A.A.; van der Walt, M.L.; Houghton, P.J.; Lall, N. Antimycobacterial flavonoids from the leaf extract of *Galenia africana*. *J. Nat. Prod.* **2009**, *72*, 2169–2171. [[CrossRef](#)] [[PubMed](#)]
23. Hutchings, A.; Scott, A.; Lewis, G.; Cunningham, A. *Zulu Medicinal Plants: An Inventory*; Illustrate; Hutchings, A., Ed.; University of Natal Press: Pietermaritzburg, South Africa, 1996; ISBN 0869808931, 9780869808931.

24. Bryant, A.T. Zulu Medicine and Medicine-Men. In *Annals of the Natal Museum*; Warren, E., Ed.; Adlard & Son and West Newman: London, UK, 1916; Volume 2, pp. 1–103.
25. Drewes, S.E.; Elliot, E.; Khan, F.; Dhlamini, J.T.B.; Gcumisa, M.S.S. Hypoxis hemerocallidea—Not merely a cure for benign prostate hyperplasia. *J. Ethnopharmacol.* **2008**, *119*, 593–598. [[CrossRef](#)] [[PubMed](#)]
26. Lall, N.; Kishore, N. Are plants used for skin care in South Africa fully explored? *J. Ethnopharmacol.* **2014**, *153*, 61–84. [[CrossRef](#)] [[PubMed](#)]
27. Bassey, K.; Viljoen, A.; Combrinck, S.; Choi, Y.H. New phytochemicals from the corms of medicinally important South African Hypoxis species. *Phytochem. Lett.* **2015**, *10*, lxix–lxxv. [[CrossRef](#)]
28. Su, X.; Liu, X.; Wang, S.; Li, B.; Pan, T.; Liu, D.; Wang, F.; Diao, Y.; Li, K. Wound-healing promoting effect of total tannins from *Entada phaseoloides* (L.) Merr. in rats. *Burns* **2017**, *43*, 830–838. [[CrossRef](#)] [[PubMed](#)]
29. McGaw, L.J.; Lall, N.; Meyer, J.J.M.; Eloff, J.N. The potential of South African plants against Mycobacterium infections. *J. Ethnopharmacol.* **2008**, *119*, 482–500. [[CrossRef](#)] [[PubMed](#)]
30. Ncube, B.; Finnie, J.F.; Van Staden, J. In vitro antimicrobial synergism within plant extract combinations from three South African medicinal bulbs. *J. Ethnopharmacol.* **2012**, *139*, 81–89. [[CrossRef](#)] [[PubMed](#)]
31. Virkutyte, J.; Varma, R.S. Green synthesis of metal nanoparticles: Biodegradable polymers and enzymes in stabilization and surface functionalization. *Chem. Sci.* **2011**, *2*, 837–846. [[CrossRef](#)]
32. Elbagory, A.M.; Cupido, C.N.; Meyer, M.; Hussein, A.A. Large Scale Screening of Southern African Plant Extracts for the Green Synthesis of Gold Nanoparticles Using Microtitre-Plate Method. *Molecules* **2016**, *21*, 1498. [[CrossRef](#)] [[PubMed](#)]
33. Sujitha, M.V.; Kannan, S. Green synthesis of gold nanoparticles using Citrus fruits (*Citrus limon*, *Citrus reticulata* and *Citrus sinensis*) aqueous extract and its characterization. *Spectrochim. Acta Part A Mol. Biomol. Spectrosc.* **2013**, *102*, 15–23. [[CrossRef](#)] [[PubMed](#)]
34. Rastogi, L.; Arunachalam, J. Microwave-Assisted Green Synthesis of Small Gold Nanoparticles Using Aqueous Garlic (*Allium sativum*) Extract: Their Application as Antibiotic Carriers. *Int. J. Green Nanotechnol.* **2012**, *4*, 163–173. [[CrossRef](#)]
35. Guo, L.; Jackman, J.A.; Yang, H.H.; Chen, P.; Cho, N.J.; Kim, D.H. Strategies for enhancing the sensitivity of plasmonic nanosensors. *Nano Today* **2015**, *10*, 213–239. [[CrossRef](#)]
36. Saifuddin, N.; Wong, C.W.; Nur Yasumira, A.A. Rapid Biosynthesis of Silver Nanoparticles Using Culture Supernatant of Bacteria with Microwave Irradiation. *E-J. Chem.* **2009**, *6*, 61–70. [[CrossRef](#)]
37. Narayanan, K.B.; Sakthivel, N. Coriander leaf mediated biosynthesis of gold nanoparticles. *Mater. Lett.* **2008**, *62*, 4588–4590. [[CrossRef](#)]
38. Shipway, A.N.; Lahav, M.; Gabai, R.; Willner, I. Investigations into the electrostatically induced aggregation of Au nanoparticles. *Langmuir* **2000**, *16*, 8789–8795. [[CrossRef](#)]
39. Smitha, S.L.; Philip, D.; Gopchandran, K.G. Green synthesis of gold nanoparticles using *Cinnamomum zeylanicum* leaf broth. *Spectrochim. Acta Part A Mol. Biomol. Spectrosc.* **2009**, *74*, 735–739. [[CrossRef](#)] [[PubMed](#)]
40. Mishra, A.; Tripathy, S.K.; Yun, S.I. Fungus mediated synthesis of gold nanoparticles and their conjugation with genomic DNA isolated from *Escherichia coli* and *Staphylococcus aureus*. *Process Biochem.* **2012**, *47*, 701–711. [[CrossRef](#)]
41. Elia, P.; Zach, R.; Hazan, S.; Kolusheva, S.; Porat, Z.; Zeiri, Y. Green synthesis of gold nanoparticles using plant extracts as reducing agents. *Int. J. Nanomed.* **2014**, *9*, 4007–4021. [[CrossRef](#)]
42. Singh, P.; Kim, Y.J.; Zhang, D.; Yang, D.C. Biological Synthesis of Nanoparticles from Plants and Microorganisms. *Trends Biotechnol.* **2016**, *34*, 588–599. [[CrossRef](#)] [[PubMed](#)]
43. Baker, S.; Rakshith, D.; Kavitha, K.S.; Santosh, P.; Kavitha, H.U.; Rao, Y.; Satish, S. Plants: Emerging as nanofactories towards facile route in synthesis of nanoparticles. *BiolImpacts* **2013**, *3*, 111–117. [[CrossRef](#)] [[PubMed](#)]
44. Ajitha, B.; Ashok Kumar Reddy, Y.; Sreedhara Reddy, P. Green synthesis and characterization of silver nanoparticles using *Lantana camara* leaf extract. *Mater. Sci. Eng. C* **2015**, *49*, 373–381. [[CrossRef](#)] [[PubMed](#)]
45. Jung, J.; Park, S.; Hong, S.; Ha, M.W.; Park, H.G.; Park, Y.; Lee, H.J.; Park, Y. Synthesis of gold nanoparticles with glycosides: Synthetic trends based on the structures of glycones and aglycones. *Carbohydr. Res.* **2014**, *386*, 57–61. [[CrossRef](#)] [[PubMed](#)]

46. Gardea-Torresdey, J.L.; Parson, J.G.; Gomez, E.; Peralta-Videa, J.; Troiani, H.E.; Santiago, P.; Yacarman, M.J. Formation and Growth of Au Nanoparticles in live side Live Alfalfa Plants. *Nano Lett.* **2002**, *2*, 397–401. [[CrossRef](#)]
47. Haiss, W.; Thanh, N.T.K.; Aveyard, J.; Fernig, D.G. Determination of size and concentration of gold nanoparticles from UV-Vis spectra. *Anal. Chem.* **2007**, *79*, 4215–4221. [[CrossRef](#)] [[PubMed](#)]
48. Arunachalam, K.D.; Annamalai, S.K.; Hari, S. One-step green synthesis and characterization of leaf extract-mediated biocompatible silver and gold nanoparticles from Memecylon umbellatum. *Int. J. Nanomed.* **2013**, *8*, 1307–1315. [[CrossRef](#)] [[PubMed](#)]
49. Rodríguez-León, E.; Iñiguez-Palomares, R.; Navarro, R.; Herrera-Urbina, R.; Tánori, J.; Iñiguez-Palomares, C.; Maldonado, A. Synthesis of silver nanoparticles using reducing agents obtained from natural sources (Rumex hymenosepalus extracts). *Nanoscale Res. Lett.* **2013**, *8*, 318. [[CrossRef](#)] [[PubMed](#)]
50. Sun, Q.; Cai, X.; Li, J.; Zheng, M.; Chen, Z.; Yu, C.-P. Green synthesis of silver nanoparticles using tea leaf extract and evaluation of their stability and antibacterial activity. *Colloids Surf. A Physicochem. Eng. Asp.* **2014**, *444*, 226–231. [[CrossRef](#)]
51. Gaabour, L.H. Results in Physics Spectroscopic and thermal analysis of polyacrylamide/chitosan (PAM/CS) blend loaded by gold nanoparticles. *Results Phys.* **2017**, *7*, 2153–2158. [[CrossRef](#)]
52. Sebby, K.B.; Mansfield, E. Determination of the surface density of polyethylene glycol on gold nanoparticles by use of microscale thermogravimetric analysis. *Anal. Bioanal. Chem.* **2015**, *407*, 2913–2922. [[CrossRef](#)] [[PubMed](#)]
53. Chanda, N.; Shukla, R.; Zambre, A.; Mekapothula, S.; Kulkarni, R.R.; Katti, K.; Bhattacharyya, K.; Fent, G.M.; Casteel, S.W.; Boote, E.J.; et al. An effective strategy for the synthesis of biocompatible gold nanoparticles using cinnamon phytochemicals for phantom CT imaging and photoacoustic detection of cancerous cells. *Pharm. Res.* **2011**, *28*, 279–291. [[CrossRef](#)] [[PubMed](#)]
54. Rouhana, L.L.; Jaber, J.A.; Schlenoff, J.B. Aggregation-resistant water-soluble gold nanoparticles. *Langmuir* **2007**, *23*, 12799–12801. [[CrossRef](#)] [[PubMed](#)]
55. Huang, T.H.; Chen, C.L.; Hung, C.J.; Kao, C.T. Comparison of antibacterial activities of root-end filling materials by an agar diffusion assay and Alamar blue assay. *J. Dent. Sci.* **2012**, *7*, 336–341. [[CrossRef](#)]
56. Katerere, D.R.; Eloff, J.N. Anti-bacterial and anti-oxidant activity of Hypoxis hemerocallidea (Hypoxidaceae): Can leaves be substituted for corms as a conservation strategy? *S. Afr. J. Bot.* **2008**, *74*, 613–616. [[CrossRef](#)]
57. Nhung, N.; Thuy, C.; Trung, N.; Campbell, J.; Baker, S.; Thwaites, G.; Hoa, N.; Carrique-Mas, J. Induction of Antimicrobial Resistance in Escherichia coli and Non-Typhoidal Salmonella Strains after Adaptation to Disinfectant Commonly Used on Farms in Vietnam. *Antibiotics* **2015**, *4*, 480–494. [[CrossRef](#)] [[PubMed](#)]
58. Manosalva, L.; Mutis, A.; Urzúa, A.; Fajardo, V.; Quiroz, A. Antibacterial activity of alkaloid fractions from berberis microphylla G. Forst and study of synergism with ampicillin and cephalothin. *Molecules* **2016**, *21*, 76. [[CrossRef](#)] [[PubMed](#)]
59. Hakanen, A.; Huovinen, P.; Kotilainen, P.; Siitonen, A.; Jousimies-Somer, H. Quality control strains used in susceptibility testing of Campylobacter spp. *J. Clin. Microbiol.* **2002**, *40*, 2705–2706. [[CrossRef](#)] [[PubMed](#)]
60. Nasreen, M.; Sarker, A.; Malek, M.A. Prevalence and Resistance Pattern of Pseudomonas aeruginosa Isolated from Surface Water. *Adv. Microbiol.* **2015**, *5*, 74–81. [[CrossRef](#)]
61. Chwalibog, A.; Sawosz, E.; Hotowy, A.; Szeliga, J.; Mitura, S.; Mitura, K.; Grodzik, M.; Orłowski, P.; Sokolowska, A. Visualization of interaction between inorganic nanoparticles and bacteria or fungi. *Int. J. Nanomed.* **2010**, *5*, 1085–1094. [[CrossRef](#)] [[PubMed](#)]
62. Rai, M.; Yadav, A.; Gade, A. Silver nanoparticles as a new generation of antimicrobials. *Biotechnol. Adv.* **2009**, *27*, 76–83. [[CrossRef](#)] [[PubMed](#)]
63. Piruthiviraj, P.; Margret, A.; Priyadharsani, P. Gold nanoparticles synthesized by Brassica oleracea (Broccoli) acting as antimicrobial agents against human pathogenic bacteria and fungi. *Appl. Nanosci.* **2016**, *6*, 467–473. [[CrossRef](#)]
64. Ahmad, B.; Hafeez, N.; Bashir, S.; Rauf, A. Mujeeb-ur-Rehman Phytofabricated gold nanoparticles and their biomedical applications. *Biomed. Pharmacother.* **2017**, *89*, 414–425. [[CrossRef](#)] [[PubMed](#)]
65. Mmola, M.; Le Roes-Hill, M.; Durrell, K.; Bolton, J.J.; Sibuyi, N.; Meyer, M.E.; Beukes, D.R.; Antunes, E. Enhanced antimicrobial and anticancer activity of silver and gold nanoparticles synthesised using Sargassum incisifolium aqueous extracts. *Molecules* **2016**, *21*, 1633. [[CrossRef](#)] [[PubMed](#)]

66. Raza, M.; Kanwal, Z.; Rauf, A.; Sabri, A.; Riaz, S.; Naseem, S. Size- and Shape-Dependent Antibacterial Studies of Silver Nanoparticles Synthesized by Wet Chemical Routes. *Nanomaterials* **2016**, *6*, 74. [[CrossRef](#)] [[PubMed](#)]
67. Khalil, M.M.H.; Ismail, E.H.; El-Baghdady, K.Z.; Mohamed, D. Green synthesis of silver nanoparticles using olive leaf extract and its antibacterial activity. *Arab. J. Chem.* **2014**, *7*, 1131–1139. [[CrossRef](#)]
68. Samejo, M.Q.; Sumbul, A.; Shah, S.; Memon, S.B.; Chundrigar, S. Phytochemical screening of Tamarix dioica Roxb. ex Roch. *J. Pharm. Res.* **2013**, *7*, 181–183. [[CrossRef](#)]
69. Obeid, L.; Lincardic, C.; Karolak, L.; Hannun, Y. Programmed cell death induced by ceramide. *Science* **1993**, *259*, 1769–1771. [[CrossRef](#)] [[PubMed](#)]
70. Wang, H.; Wang, F.; Tao, X.; Cheng, H. Ammonia-containing dimethyl sulfoxide: An improved solvent for the dissolution of formazan crystals in the 3-(4,5-dimethylthiazol-2-yl)-2,5-diphenyl tetrazolium bromide (MTT) assay. *Anal. Biochem.* **2012**, *421*, 324–326. [[CrossRef](#)] [[PubMed](#)]
71. Naimi, M.; Khaled, M.B. Exploratory Tests of Crude Bacteriocins from Autochthonous Lactic Acid Bacteria against Food-Borne Pathogens and Spoilage Bacteria Exploratory Tests of Crude Bacteriocins from Autochthonous Lactic Acid Bacteria against Food-Borne Pathogens and Spoilage Bact. *World Acad. Sci. Eng. Technol.* **2014**, *8*, 113–119.



© 2017 by the authors. Licensee MDPI, Basel, Switzerland. This article is an open access article distributed under the terms and conditions of the Creative Commons Attribution (CC BY) license (<http://creativecommons.org/licenses/by/4.0/>).



**CHAPTER FIVE: MANUSCRIPT DRAFT “PLANT-
DERIVED GOLD NANOPARTICLES AS CARRIERS OF
AMPICILLIN”**

UNIVERSITY *of the*
WESTERN CAPE

Plant-derived gold nanoparticles as carriers of ampicillin

Abdulrahman M. Elbagory¹, Ahmed A. Hussein² and Mervin Meyer^{1*}

¹DST/Mintek Nanotechnology Innovation Centre, Department of Biotechnology, University of the Western Cape, Private Bag X17, Bellville 7535, South Africa.

²Chemistry Department, Cape Peninsula University of Technology, P.O. Box 1906, Bellville 7535, South Africa.

*Correspondence: memeyer@uwc.ac.za; Tel.: +27 21 959 2032

Abstract

AuNPs continue to capture researchers' attention due to their unique physicochemical properties, which can be exploited for numerous applications in biomedicine. AuNPs are excellent drug carriers, which can improve the therapeutic efficacy of drugs. Bioinspired or biogenic AuNPs are particularly interesting since these nanomaterials can overcome the toxicity associated with AuNPs synthesized using conventional methods. It was previously shown that AuNPs (Hypoxis-AuNPs) produced from the *Hypoxis hemerocallidea*, a medicinal plant that is indigenous to South Africa, has significant antibacterial activity and that it is not toxic to human fibroblast cells. Herein we explore the use of Hypoxis-AuNPs as drug carriers, more specifically ampicillin. We demonstrate the successful conjugation of ampicillin to Hypoxis-AuNPs to produce Amp-AuNPs. Spectroscopic and microscopic analytical techniques have been used to demonstrate successful conjugation of ampicillin onto Hypoxis-AuNPs. We show that the antibacterial activity of Amp-AuNPs against some microorganisms is significantly higher, when compared to Hypoxis-AuNPs. This study demonstrates the potential of biogenic AuNP as drug carriers.

27 **1. Introduction**

28

29 The unique physicochemical properties of nanoparticles (NPs) can determine their
30 application. It is in particularly their small size that have captured widespread interest for
31 applications in biomedical research. The fact that their sizes are in the same range as some
32 biomolecules, render them compatible in hybrid systems for biological application [1].
33 Gold nanoparticles (AuNPs) have been used extensively as delivery systems because they
34 can carry different active groups on their surface [2]. In addition to their enhanced
35 absorption and scattering properties, AuNPs offer biocompatibility, ease of synthesis, and
36 can be conjugated to targeting moieties such as antibodies and biomolecular ligands [3].
37 This can facilitate the production of multimodal systems that can be used for the targeted
38 delivery drugs to disease sites. AuNPs have also been conjugated to several drugs, which
39 include antitubercular drugs [2], anticancer drugs [4] and several antibiotics, which include
40 gentamycin [5], amoxicillin [6], ciprofloxacin [1] and ampicillin [7].

41 The emergence of multidrug-resistant (MDR) bacterial strains is a global problem which
42 impacts on health care costs [8]. This has motivated researchers to explore the development
43 of new antibacterial agents. AuNPs have been shown to have antibacterial properties,
44 which are exerted through several modes of action [9]. AuNPs have also been used as
45 carriers of antibiotics which can increase the antibacterial effect as it can offer improved
46 delivery mechanisms to the infection site, enhanced antibiotic efficiency and reduce
47 toxicity caused by the antibiotic [10, 11]. The conjugation of antibiotics to AuNPs is mostly
48 done using chemical linkers such as glutathione [12] and polyethylene glycol [13].
49 Antibiotics have also been attached directly onto the surface of citrate capped AuNPs [1]

50 and biogenic AuNPs [14], while antibiotics such kanamycin have been used as reducing or
51 capping agents to synthesize AuNPs [15].

52 Aqueous extracts of several plants have been used to synthesize AuNPs [16]. Plants contain
53 a plethora of phytochemicals that can be involved in the synthesis and stabilisation of
54 AuNPs [17]. Such biogenic AuNPs are believed be more biocompatible and
55 environmentally friendly than AuNP produced using traditional methods [18]. In a
56 previous study, we reported on the synthesis and characterisation of biogenic AuNPs
57 (Hypoxis-AuNP) synthesised using a water extract of *Hypoxis hemerocallidea* [19]. *H.*
58 *hemerocallidea* is a famous South African medicinal plant that is commonly used by local
59 traditional healers for the management of several diseases. A summary of the medicinal
60 uses and the reported biological activities of *H. hemerocallidea*, including its antibacterial
61 actions, was reported in a review by Owira and Oewole [20]. Hypoxis-AuNPs also
62 demonstrated antibacterial activity against bacterial strains associated with wound
63 infections, in which the Hypoxis-AuNPs exhibited minimum inhibitory concentrations
64 (MIC) lower than other biogenic AuNPs and citrate-AuNPs, citing the antibacterial
65 properties of the phytochemicals of *H. hemerocallidea* [19].

66 Herein, we investigate the conjugation of ampicillin to Hypoxis-AuNP to produce Amp-
67 AuNPs. We also evaluated the antimicrobial activity of Amp-AuNPs. We report on the
68 successful conjugation of ampicillin to Hypoxis-AuNP and demonstrate that the
69 antimicrobial activity of Amp-AuNP is significantly higher compared to Hypoxis-AuNP.
70 To the best of our knowledge, this is the first report of successful conjugation of an
71 antibiotic to a biogenic AuNPs produced from a plant extract.

72

73 2. Materials and methodology

74

75

2.1. Materials

76 The aqueous extract of *H. hemerocallidea* was purchased from Afriplex (Cape Town,
77 South Africa). Polystyrene 96-well microtitre plates were purchased from Greiner bio-one
78 GmbH (Frickenhausen, Germany). Ampicillin, 3-[4,5-dimethylthiazol-2-yl]-2,5-diphenyl
79 tetrazolium bromide (MTT) and gold salt (sodium tetrachloroaurate (III) dihydrate) were
80 purchased from Sigma-Aldrich (Cape Town, South Africa). Dulbecco's Modified Eagle's
81 Medium (DMEM), penicillin–streptomycin (penstrep) and Phosphate buffered saline
82 (PBS) were purchased from Lonza (Cape Town, South Africa). Foetal Bovine Serum
83 (FBS) was bought from Thermo Scientific (Ansofrere, South Africa). Nutrient broth was
84 purchased from Biolab (supplied by Merck, Modderfontein, South Africa). Alamar blue
85 dye was obtained from Invitrogen Corporation (San Diego, CA, USA).

86

2.2. Biosynthesis of Hypoxis-AuNPs and their characterization

87

88 Hypoxis-AuNPs were biosynthesized according to the methodology reported previously
89 [19]. A POLARstar Omega microtitre plate reader (BMG Labtech, Cape Town, South
90 Africa) was used to monitor the Ultraviolet-Visible (UV-Vis) spectra (450–900 nm) of the
91 AuNPs.

92

2.3. Functionalization of Hypoxis-AuNPs

93

94 Upon the biosynthesis of Hypoxis-AuNPs, 12 mM of Ampicillin solution was added to the
95 Hypoxis-AuNPs solution with dilution factor of (2:3). The mixture was left at room
96 temperature for 24 hr with stirring. The mixture was then centrifuged trice. The pellet of

97 the ampicillin conjugated AuNPs (Amp-AuNPs) was resuspended in d.H₂O for further
98 characterization and antibacterial evaluation.

99 **2.4. Dynamic Light Scattering (DLS) analysis**

100

101 A Zetasizer (Malvern Instruments Ltd., Malvern, UK) was used to measure the zeta
102 potential and hydrodynamic size values of the freshly biosynthesized AuNPs at 25 °C and
103 a 90° angle. The data were analysed using Zetasizer software version 7.11.

104 **2.5. Fourier-Transform Infrared (FTIR) Spectroscopy**

105

106 The FTIR spectra of ampicillin and the AuNPs were obtained using PerkinElmer spectrum
107 two FTIR spectrophotometer (Waltham, MA, USA) according to the method reported
108 previously [21]. Ampicillin and the freeze-dried AuNPs were mixed with KBr powder and
109 pressed into a round disk. A pure KBr was used for background correction.

110 **2.6. High Resolution Transmission Electron Microscope** 111 **(HRTEM) and Energy-Dispersive X-ray (EDX) analysis**

112

113 A drop of Amp-AuNPs solution was loaded and dried onto a carbon coated copper grid.
114 FEI Tecnai G² 20 field-emission gun (FEG) HRTEM, operated in bright field mode at an
115 accelerating voltage of 200 kV, was used to capture the HRTEM images. EDX liquid
116 nitrogen cooled Lithium doped Silicon detector was used to identify the elemental
117 composition of the Amp-AuNPs.

118 **2.7. Image processing**

119

120 The image analysis software ImageJ 1.50b version 1.8.0_60 (<http://imagej.nih.gov/ij>) was
121 used to analyse the HRTEM images.

122 **2.8. Stability evaluation of the AuNPs**

123

124 The stability of Amp-AuNPs was determined by incubating 100 μ L of the AuNPs with 100
125 μ L of nutrient broth in a 96-well microtitre plate at 37 °C and measure the UV-Vis
126 spectrum of the AuNPs at zero h and 24 h.

127 **2.9. Cytotoxicity evaluation of the AuNPs on KMST-6**

128

129 The toxicity of the AuNPs was tested on the non-cancerous human fibroblast cell line
130 (KMST-6) according the previously reported methodology [19]. The cells were maintained
131 in DMEM containing 10% FBS and 1% penstrep in a 37 °C humidified incubator with 5%
132 CO₂ saturation. In short, the cells (2.0×10^4 cells/100 μ L/well) were incubated for 24 h
133 with increasing concentrations (0.5 to 32 nM) of Amp-AuNPs. Untreated cells were used
134 as a negative control. PBS was then used to wash the wells after removing the AuNPs.
135 Next, 100 μ L of MTT reagent were added to each well and plates were incubated at 37 °C
136 for 4 h. The wells were afterwards washed and alkaline DMSO was used to dissolve the
137 formazan crystals. The plates were incubated for 15 min and the microtitre plate reader was
138 used to measure the absorbance of the wells 540 nm and 630 nm as a reference wavelength.
139 The cell viability percentage was determined using the following equation:

$$\% \text{ cell viability} = \frac{\text{sample absorbance} - \text{cell free sample blank}}{\text{negative control absorbance}}$$

140

141 **2.10. Antibacterial evaluation of the AuNPs**

142

143 The Alamar blue assay was used to evaluate the inhibition of bacterial growth by the
 144 Hypoxis-AuNPs, Amp-AuNPs and free ampicillin on the bacterial strains listed in Table
 145 1. Detailed description the methodology adapted herein was previously reported [19]. The
 146 Minimum Inhibition Concentration (MIC) was identified as the lowest concentration of the
 147 samples to significantly inhibit the bacterial growth compared to the negative control. In
 148 short, 50.0 μL of the bacterial broth (5.0×10^5 CFU/mL) were mixed with 50.0 μL of the
 149 tested samples with increasing concentrations (0.5 and 32 nM) in a 96 well plate. Similar
 150 volumes of bacterial broth and nutrient broth were mixed as negative control. AuNPs
 151 controls were prepared to omit the interference of the AuNPs with the assay measurement.
 152 After 24 h incubation at 37 °C, 10.0 μL of the Alamar blue dye were added to each well.
 153 This was followed by incubation for another 3 h and the fluorescence of resorufin was then
 154 measured using a microtitre plate reader at 544 nm (excitation wavelength) and 590 nm
 155 (emission wavelength). The percentage bacterial growth was calculated using the equation
 156 below:

$$\% \text{ bacterial growth} = \frac{(\text{sample fluorescence} - \text{sample control}) - \text{cell free sample blank}}{\text{negative control fluorescence}} \times 100$$

157

158 Table 1 List of the bacterial strains selected in this study.

Bacterial Strains	ATCC Number	Gram Reaction
<i>Escherichia coli</i>	25922	Gram-negative
<i>Klebsiella pneumonia</i>	13883	Gram-negative
Methicillin-resistant <i>Staphylococcus aureus</i> (MRSA)	33591	Gram-positive
<i>Pseudomonas aeruginosa</i>	27853	Gram-negative
<i>Staphylococcus aureus</i>	29213	Gram-positive
<i>Staphylococcus epidermidis</i>	12228	Gram-positive

159

160 **2.11. Statistical analysis**

161

162 The data presented are means \pm SD obtained from at least three independent experiments.
163 Differences between the means were significant if $p < 0.05$ according to Prism's two-way
164 ANOVA.

165 **3. Results and discussion**

166

167 Conventional synthesis methods of the AuNPs make use of reducing agents such as sodium
168 citrate, ascorbate, sodium borohydride, hydrazine, hydroquinone, etc. to reduce gold ions
169 to neutral gold ions, which aggregate to form AuNPs. Additional capping agents are
170 occasionally added to optimize the final shape and size of the AuNPs [22]. These methods
171 involve the use of toxic chemicals that can hinder the biomedical application of the AuNPs
172 [23]. The use of biocompatible chemicals found in biological organisms such as bacteria
173 or plants, i.e. green synthesis methods can produce AuNPs that are more biocompatible
174 [24]. Hypoxis-AuNPs are biogenic AuNPs that were synthesised from *H. hemerocallidea*
175 plant extract [19]. This study also reported on the antibacterial activity of Hypoxis-AuNPs
176 and proposed the application of these nanoparticles in the treatment of wound infections.
177 The current study investigated the potential of enhancing the antibacterial activity of
178 Hypoxis-AuNPs by conjugating ampicillin onto the Hypoxis-AuNPs.

179 **3.1. UV-Vis analysis**

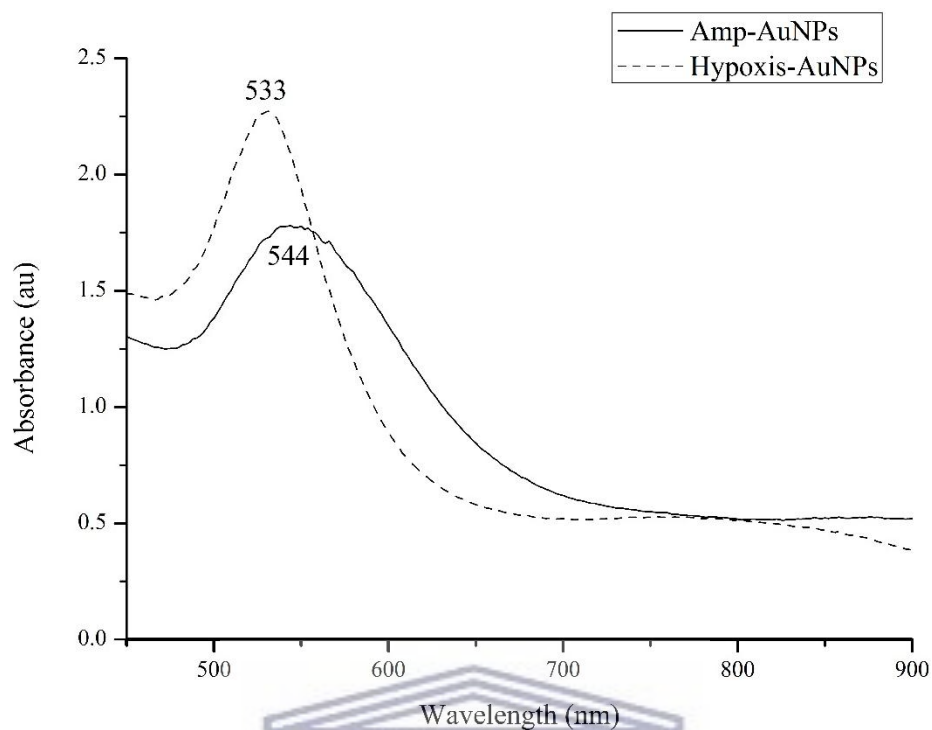
180

181 Hypoxis-AuNPs were synthesised using the method described previously (denoted
182 Hypoxis-GNPs) [19]. Ampicillin was conjugated to Hypoxis-AuNPs to produce Amp-
183 AuNPs by adding 12 mM of ampicillin solution to a solution of freshly synthesized
184 Hypoxis-AuNPs and stirring the mixture for 24 h at room temperature. The ampicillin and

185 Hypoxis-AuNPs' solutions were mixed in 2:3 ratio (V:V). This functionalization method
186 by chemisorption is based on the procedures described by different studies with
187 modifications [1, 7, 14]. The concentration of ampicillin and the ratio of ampicillin:
188 Hypoxis-AuNPs' solutions were established by optimisation (data not shown).

189 UV-Vis analysis of Hypoxis-AuNPs and Amp-AuNPs was done using a POLARstar
190 Omega microtitre plate reader (BMG Labtech, Cape Town, South Africa). The absorption
191 peak value (λ_{\max}) of the characteristic localized surface plasmon resonance (LSPR) for
192 Hypoxis-AuNPs was determined to be to be 533 ± 1 nm. This is very similar to the λ_{\max}
193 value (530 ± 1 nm) reported previously for Hypoxis-AuNPs [19]. The λ_{\max} values for the
194 LSPR peaks that lie in the visible region of the electromagnetic spectrum (between 500
195 and 600 nm) are the result of the coherent electron motion of the AuNPs. These LSPR
196 bands are characteristic to the AuNPs and provide information about the particle size,
197 particle size distribution and the potential of the AuNPs to aggregate [25].

198 The λ_{\max} value for the AuNP formed by the addition of the ampicillin to a solution of
199 Hypoxis-AuNPs was 544 nm (Figure 1). This was also accompanied by a colour change
200 from wine red (which was the colour of the Hypoxis-AuNPs solution) to blue. This colour
201 change is an indication of successful conjugation [1]. The λ_{\max} values of the AuNPs are
202 directly proportional to their size [26] and the conjugation of any molecule onto the AuNPs
203 surface will result in an increase in size of AuNPs [11]. The UV-Vis results therefore
204 suggest that ampicillin was successfully conjugated to Hypoxis-AuNPs to produce Amp-
205 AuNPs.



206

207 Figure 1 The UV-Vis data of Hypoxis-AuNPs and Amp-AuNPs.

208

209 To eliminate the possibility of generation of AuNPs by ampicillin alone, 12 mM ampicillin
 210 was added to gold salt using the same dilution factor with distilled water instead of
 211 Hypoxis-AuNPs for 24 h. The solution remained colourless with no absorption peaks
 212 observed in the UV-Vis spectrum (data not shown). Some studies reported the synthesis of
 213 AuNPs using antibiotics alone without the use of other reducing agents. Ampicillin alone
 214 was reported to be a poor reducing agent for the synthesis of AuNPs [2]. Hur and co-
 215 workers on the other hand reported the synthesis of AuNPs from ampicillin alone [27].
 216 Nonetheless, in their report the ampicillin-AuNPs were synthesised at high temperature (80
 217 °C) for 15 h, which were not followed in the methodology herein.

218

219

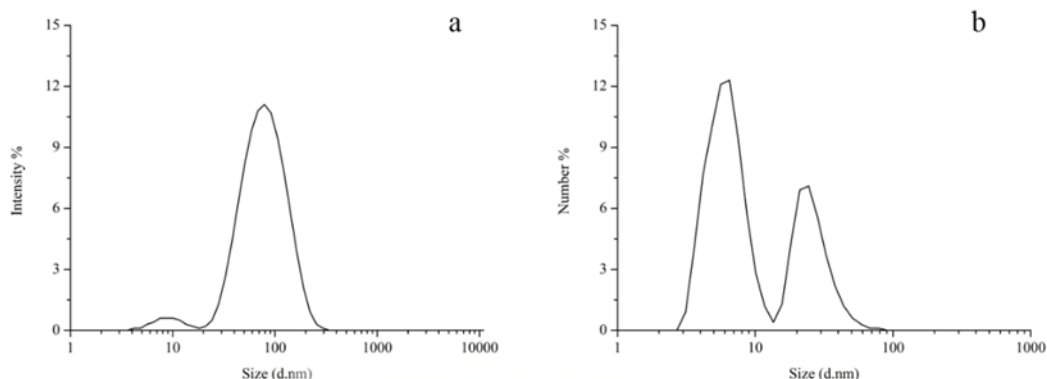
220 **3.2. DLS analysis**

221

222 The measurement of the particle size and surface charge are key physical characterization
223 methods that can be used to demonstrate that AuNPs were successfully conjugated with a
224 ligand since conjugation with ligands are expected to increase size and possibly also affect
225 the charge of the AuNPs [28]. The distribution of the hydrodynamic diameters of the Amp-
226 AuNPs was measured by two different DLS techniques (based on size by intensity and by
227 the number of AuNPs) using the Zetasizer (Malvern Instruments Ltd., Malvern, UK) as
228 previously described for Hypoxis-AuNPs [19]. It was previously shown that the synthesis
229 of Hypoxis-AuNPs produce AuNPs of bimodal size distribution. Two AuNP populations,
230 one with an average size distribution of 51 ± 34 nm and one with an average size
231 distribution of 2.3 ± 1.6 nm was produced [19]. The Z-average size of Hypoxis-AuNPs was
232 26 ± 6 nm. DLS analysis of Amp-AuNPs showed also show the presence of two AuNP
233 populations, one with an average size distribution of 77 ± 25 nm and one with an average
234 size distribution of 6.5 ± 2.0 nm (Figure 2). The Z-average size of Amp-AuNPs was $77 \pm$
235 30 nm. This suggests that the average size of the larger Hypoxis-AuNPs increased from 26
236 nm to 77 nm and the smaller Hypoxis-AuNPs increased from 2.3 nm to 6.5 nm. This
237 increase in the NPs size further affirms the assumption that ampicillin was successfully
238 conjugated to Hypoxis-AuNPs to produce Amp-AuNPs. The zeta-potential of Hypoxis-
239 AuNPs was reported to be -22 mV, while the zeta-potential of Amp-AuNPs was
240 determined to be -13 mV. This increase in zeta-potential also confirms that the surface of
241 Hypoxis-AuNPs was changed, possibly due to the attachment of ampicillin [29]. AuNPs
242 with a zeta-potential between +30 mV and -30 mV are stable in solution [30] and since the

243 zeta-potential of Amp-AuNPs is -13 mV, these nanoparticles are expected to be well
 244 dispersed in solution.

245



246

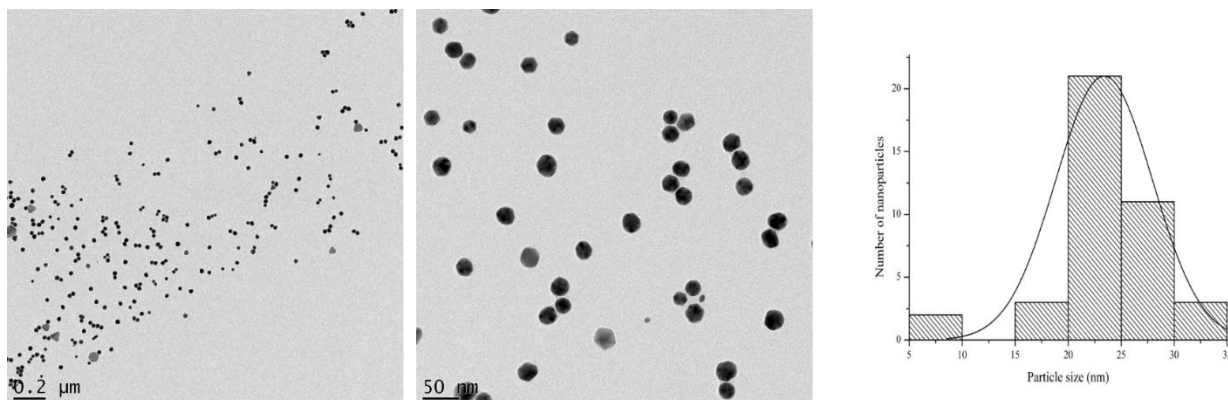
247 Figure 2 The particle size distribution of Amp-AuNPs by (a) intensity and (b) by number as shown by the DLS
 248 analysis.

249

250 3.3. HRTEM and Selected Area Electron Diffraction (SAED) 251 analysis

252

253 The HRTEM analysis of the Amp-AuNPs was performed to investigate the morphology of
 254 the AuNPs after the conjugation with Ampicillin. Hypoxis-AuNPs were previously found
 255 to be mostly spherical in shape with most of the particles being between 25-30 nm as
 256 determined by the HRTEM images [19]. The HRTEM images of the Amp-AuNPs also
 257 showed spherical formations with a similar particle size distribution (20-25 nm) (Figure 3)
 258 as calculated manually using ImageJ software. HRTEM analysis therefore did not show an
 259 increase in size due to the conjugation ampicillin. Yet it should be taken into consideration
 260 that HRTEM analysis can only visualize high-Z matter and the size determinations by
 261 HRTEM does not include the ligand shell in contrary to the DLS analysis [31].



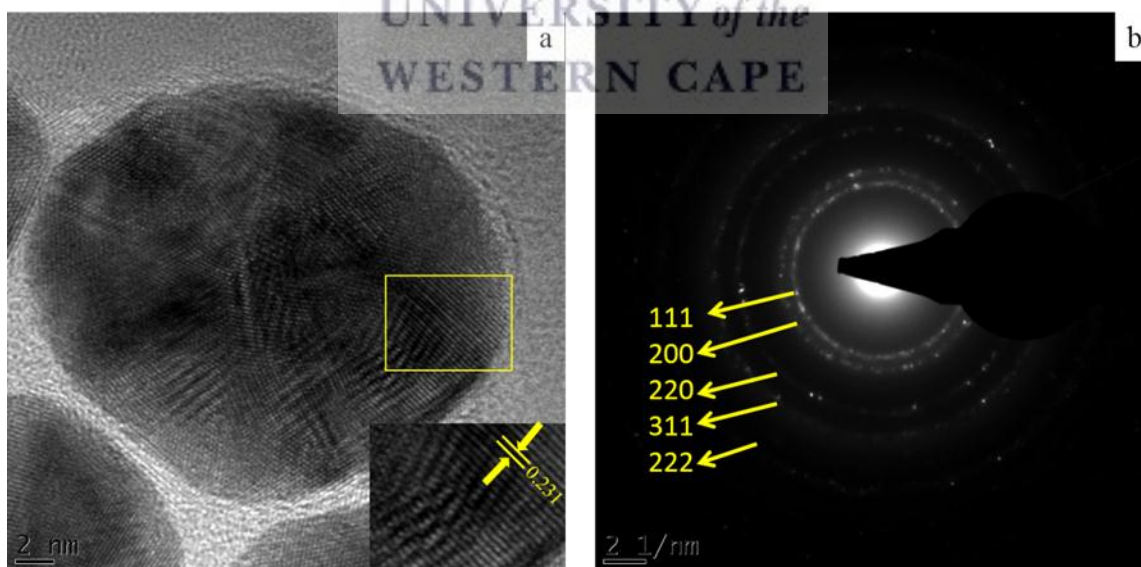
262

263 Figure 3 HRTEM images and particle size distribution of Amp-AuNPs calculated using ImageJ software.

264

265 The crystallinity of the Amp-AuNPs was also determined from the HRTEM. AuNPs
 266 showed lattice fringes with distance of 0.231 nm (Figure 4a) corresponding to the
 267 interplanar spacing between (111) plane of gold [32]. The SAED patterns also confirmed
 268 the crystallinity of the AuNPs with indexed bright rings were shown to correspond to the
 269 (111), (200), (220), (311) and (222) planes of the gold (Figure 4b).

270

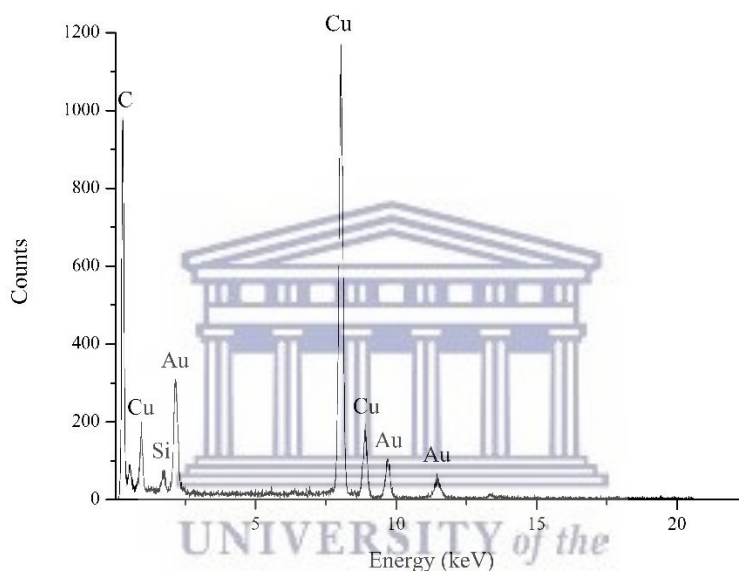


271

272 Figure 4 HRTEM images showing the (a) lattice fringe and (b) SAED pattern of Amp-AuNPs.

273

274 Adsorption peaks representing the gold element was detected in the EDX spectra (Figure
 275 5) around 2.3, 9.7 and 11.3 keV. These values are similar to the values of gold's adsorption
 276 peaks reported previously [33]. The presence of other adsorption peaks for elements such
 277 as carbon, copper and silicon are also present. Rodríguez-León et al. suggested that the
 278 presence of these elements in the spectra of AuNPs is due to the HRTEM loading grid
 279 and/or the detector window [34].



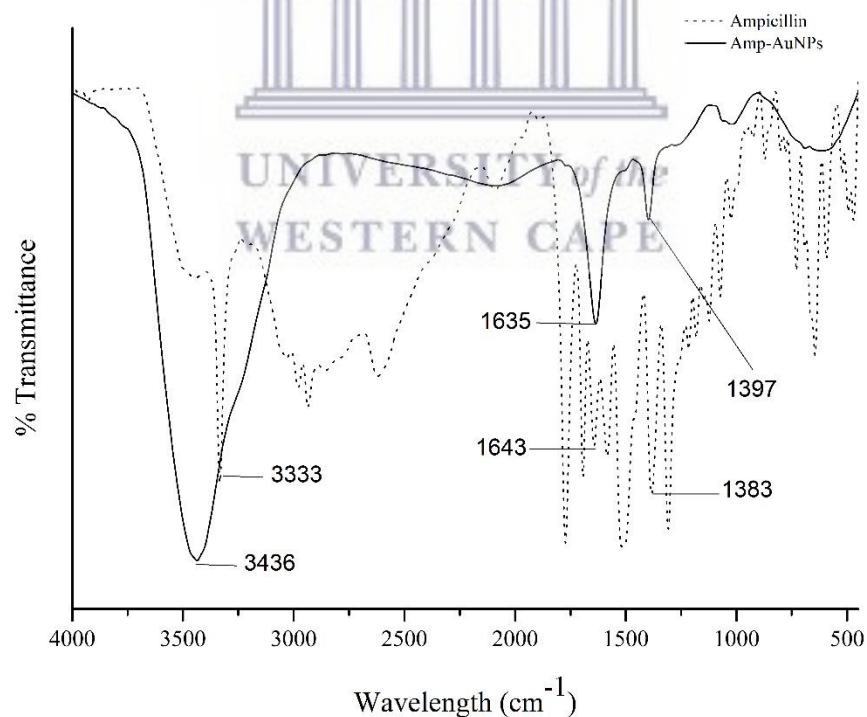
280
 281 Figure 5 EDX spectra of Amp-AuNPs. The adsorption peaks are labelled on top with the elements that were detected.
 282

283 3.4. FTIR analysis

284

285 FTIR spectroscopy was carried out to investigate the functional groups on the surface of
 286 the Hypoxis-AuNPs. Previous studies suggested that the attachment of ampicillin on the
 287 surface of the AuNPs is most likely to be physical in nature [7, 11], however the exact
 288 mechanism of attachment is still not known. Leff et al. suggested that AuNPs can bind
 289 more readily to amine groups. Several other reports suggested that the nitrogen of the amine
 290 functional group of ampicillin is responsible for adsorption of ampicillin onto the AuNPs

291 surface [10, 27]. Figure 6 shows the FTIR spectra of Amp-AuNPs and the free Ampicillin.
 292 The FTIR spectrum of ampicillin displayed bands pertaining to the functional groups of
 293 the anhydrous ampicillin as reported previously [35]. The FTIR spectrum of the Amp-
 294 AuNPs showed three major bands. Two of these bands were centred at 1635 and 1397
 295 cm^{-1} , which were transmitting at almost the same wavelength of two similar peaks of
 296 ampicillin (1643 and 1383 cm^{-1}) that correspond to amide I and COO^- groups, respectively.
 297 One the other hand, the N-H stretching frequency of the amine group of the ampicillin at
 298 3333 cm^{-1} underwent broadening and shifted to a higher wavelength (3436 cm^{-1}) in the
 299 FTIR spectrum of Amp-AuNPs. These data suggest that the nitrogen atoms of the amine
 300 groups of the ampicillin are responsible for binding on the surface of the AuNPs [10, 27].



301

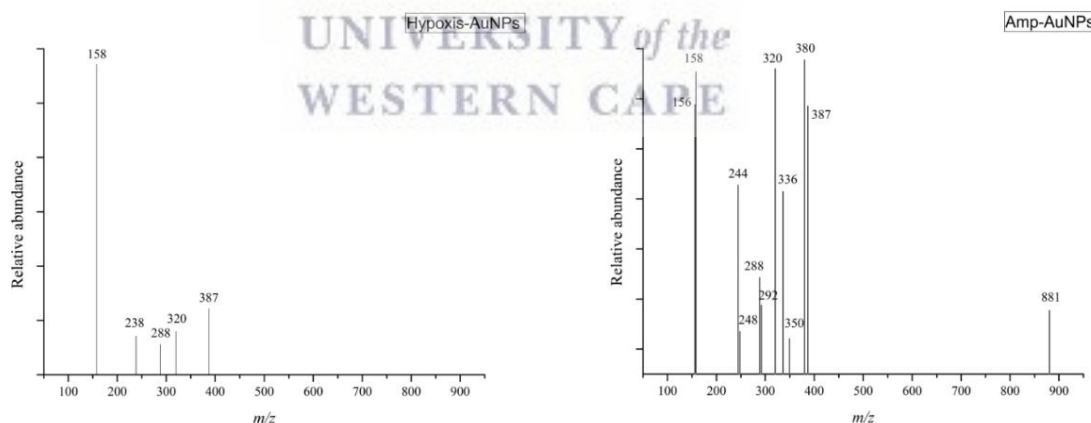
302 Figure 6 FTIR spectra of ampicillin and Amp-AuNPs.

303

304 **3.5. FAB-MS analysis**

305

306 FAB-MS is a useful technique to determine the of the mass of ligands conjugated onto
 307 functionalized AuNPs [36]. The ionization of the AuNPs samples using FAB-MS
 308 technique has been reported before [37, 38]. The MS analysis of ampicillin has been
 309 reported in several studies [39, 40]. Even though the identity of the phytochemical ligands
 310 attached on the Hypoxis-AuNPs surface is still unknown, FAB-MS can still provide
 311 information with regards to the presence of ampicillin on Amp-AuNPs. Figure 7 shows the
 312 FAB-MS data of Hypoxis-AuNPs and Amp-AuNPs. Interestingly, Amp-AuNPs showed
 313 the presence of a fragmented ion at m/z 350, which corresponds to the protonated ampicillin
 314 as previously reported (Suwanrumpha and Freast, 1989). Hypoxis-AuNPs, on the other
 315 hand, lacked this ion at m/z 350, which confirms the successful conjugation of ampicillin
 316 to Hypoxis-AuNP to produce Amp-AuNP.



317

318 Figure 7 The FAB-MS data of Hypoxis-AuNPs and Amp-AuNPs.

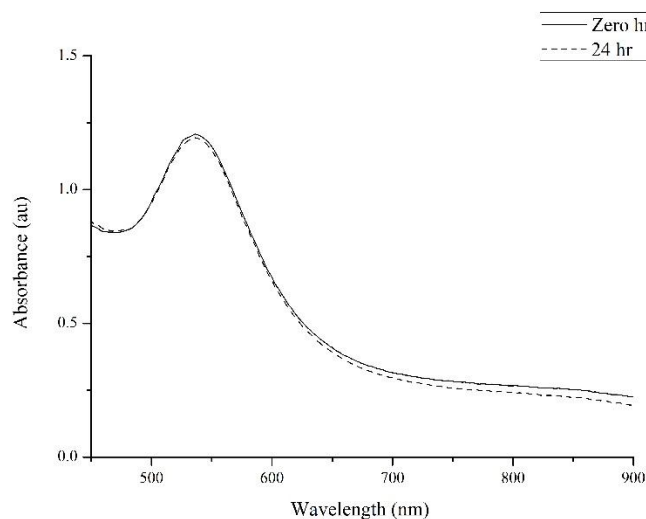
319

320 **3.6. Antibacterial testing**

321

322 The antimicrobial activity of Amp-AuNPs was evaluated against several Gram-positive
323 (e.g. *K. pneumoniae*, *P. aeruginosa* and *E. coli*) and Gram-negative (e.g. *S. aureus* and *S.*
324 *epidermidis*) bacterial strains using the Alamar blue assay. This required that the stability
325 of the Amp-AuNPs be tested in nutrient broth, since the exposure of the bacteria to the
326 Amp-AuNPs would be done in this growth medium. It is expected that these AuNPs will
327 interact with the biological components of any growth medium, which can lead to changes
328 in their physicochemical properties such as hydrodynamic size, surface charge and
329 colloidal stability, and thus it is imperative to measure the chemical and physical changes
330 that occur to the AuNPs after introducing them to such biological media [41].

331 The stability of Amp-AuNPs was investigated by incubating the Amp-AuNPs in nutrient
332 broth for a period of 24 hr, after which the NPs were subjected to UV-Vis analysis as
333 described previously for the stability testing of Hypoxis-AuNP [19]. An overlay of the UV-
334 Vis spectra of Amp-AuNPs in the presence of nutrient broth (Figure 8) shows that there
335 are minimal changes in the UV-Vis spectrum of Amp-AuNPs after incubation in nutrient
336 broth. This suggest that the Amp-AuNPs did not aggregate or increase in size due to the
337 binding of other molecules, which may be present in the nutrient broth, to the surface of
338 the Amp-AuNPs. The Amp-AuNPs therefore remained stable in nutrient broth for 24 hr
339 and can be used in antimicrobial assays.



340

341 Figure 8 UV-Vis spectra of Amp-AuNPs mixed with nutrient broth at zero h and after 24 h incubation.

342

343 It was previously reported that Hypoxis-AuNPs demonstrated significant antibacterial
 344 activity against *P. aeruginosa*, *E. coli*, *S. epidermidis* and *S. aureus* [19]. An MIC value
 345 of 32 nM was reported for Hypoxis-AuNPs against these four bacterial strains. With an
 346 MIC value of 32 nM, the antibacterial activity of Amp-AuNP against *P. aeruginosa*, *E.*
 347 *coli*, and *S. aureus* was similar to that of Hypoxis-AuNPs (Table 1). However, the
 348 antibacterial activity of Amp-AuNP against *S. epidermidis* was significantly higher than
 349 that of Hypoxis-AuNPs. The MIC value for Amp-AuNPs against *S. epidermidis* was 16
 350 nM compared to 32 nM for Hypoxis-AuNPs. It is also important to note that although the
 351 MIC values for Hypoxis-AuNPs and Amp-AuNPs against *S. aureus* was the same (32 nM),
 352 the percentage viability of the bacteria after treatment was 0% for Amp-AuNPs compared
 353 to 43% for Hypoxis-AuNPs. In this study, the antibacterial activity of both Hypoxis-AuNPs
 354 and Amp-AuNPs were also tested against *Salmonella sp.*, MRSA and *K. pneumoniae*. The
 355 MIC values for Hypoxis-AuNPs against *Salmonella sp.*, MRSA and *K. pneumoniae* was
 356 >32, 32 and 16 nM, respectively. However, while the MIC values for Hypoxis-AuNPs

357 against *Salmonella sp.*, was >32 nM, the MIC values for Amp-AuNPs was 16 nM.
358 Importantly the viability of *Salmonella sp.* treated with Amp-AuNPs was 0%. The similar
359 MIC values for Amp-AuNPs and Hypoxis-AuNPs against MRSA and *K. pneumoniae* and
360 *P. pneumoniae* may be due to the natural resistance of these bacterial strains against
361 Ampicillin [42–44], which may have led to the exclusion of Ampicillin effect on these
362 strains. It is worth noting that free ampicillin did not show any growth inhibition against all
363 the bacterial strains at concentration up to 32 nM. This study demonstrates that the
364 antibacterial activities of ampicillin and Hypoxis-AuNPs is significantly enhanced when
365 ampicillin is conjugated to Hypoxis-AuNPs to form Amp-AuNPs. This enhanced
366 antibacterial activity was not observed in all the bacterial strains tested. This points to a
367 very specific mechanism of action which is probably dependent on the interaction of Amp-
368 AuNPs with the specific microorganism.

369 Several studies reported the enhanced effect of antibiotics conjugated AuNPs in
370 comparison to either AuNPs or free antibiotics [7, 14, 45]. Since the AuNPs are used as
371 carriers of the antibiotic and since a single AuNP can carry several molecules of the
372 antibiotic, Bhattacharya et al. suggested that it is possible that the increased activity may
373 be due to higher concentrations of the antibiotic inside the bacterial cells [11]. Hayden
374 et al. also suggested that the electrostatic attraction between the AuNPs and the negatively
375 charged bacterial cells may enhance the delivery of the antibiotic. The shift of the zeta
376 potential to less negative values might have increased the electrostatic attraction between
377 the AuNPs and the negatively charged bacterial cells, which in turn could have facilitated
378 the deposition of Amp-AuNPs on the bacterial cell wall [46].

379

380 Table 1 MIC values (nM) of Hypoxis-AuNPs and Amp-AuNPs against the tested bacterial strains as obtained by the Alamar blue assay (calculated viability is shown in
 381 parentheses)

Sample Tested	Bacterial Strains						
	<i>S. aureus</i>	<i>E. coli</i>	<i>S. epidermidis</i>	<i>Salmonella sp.</i>	MRSA	<i>P. aeruginosa</i>	<i>K. pneumoniae</i>
Hypoxis-AuNPs	32 (43±5 %)*	32 (16±1 %)*	32 (20±1 %)*	> 32	32 (21±3 %)*	32 (10±1 %)*	16 (22±5 %)*
Amp-AuNPs	32 (0 %)	32 (10±2 %)*	16 (35±4 %)*	16 (0 %)*	32 (23±1 %)*	32 (23±6 %)*	16 (24±2 %)*
Ampicillin (free form)	> 32	> 32	> 32	> 32	> 32	> 32	> 32

382 * Statistical significance ($p < 0.05$) compared to the negative control.

383

384

385

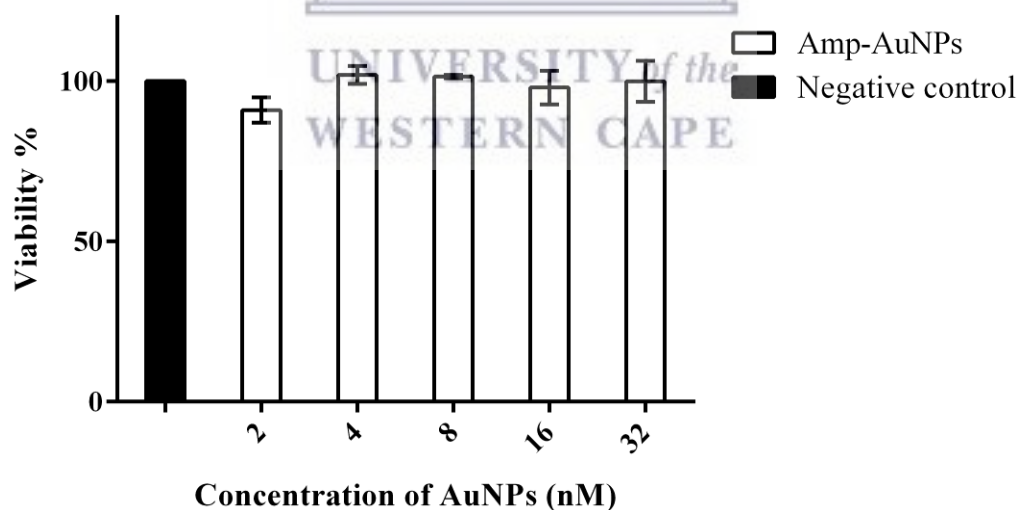
386



387 3.7. Toxicity of Amp-AuNPs

388

389 The toxicity of Hypoxis-AuNPs against human fibroblast cells were previously
390 investigated to evaluate the safety of these AuNPs for application biomedical products [19].
391 KMST-6 cells were treated for 24 h with increasing concentrations (up to 32 nM) of
392 Hypoxis-AuNPs and the viability of the cells were assessed using the MTT assay. It was
393 shown that Hypoxis-AuNPs does not affect the viability of these cells. Amp-AuNPs were
394 also subjected to the same testing to evaluate whether the toxicity of Hypoxis-AuNPs upon
395 functionalization with ampicillin altered the toxicity of these AuNPs. Figure 9 shows that
396 Amp-AuNPs did not induce cell death at any of the concentrations tested against KMST-6
397 cells. Although further toxicity testing is required, these preliminary results suggest that
398 Amp-AuNPs can be safely applied in the production of biomedical products.



399

400 Figure 9 The effect of Amp-AuNPs on the viability of KMST-6 cells as determined by the MTT assay.

401

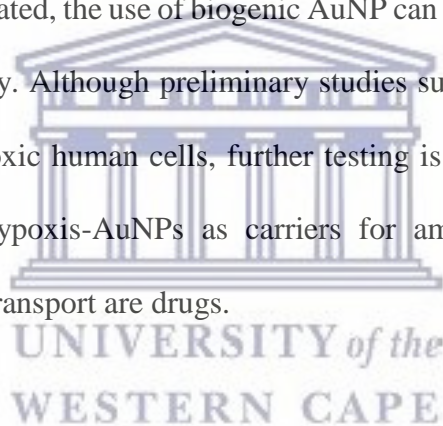
402

403

404 **Conclusion**

405

406 In the present work, the drug ampicillin was successfully conjugated to the plant-derived
407 AuNPs, Hypoxis-AuNPs. These AuNPs were synthesised from the plant *H.*
408 *hemerocallidea*. The conjugation of ampicillin to Hypoxis-AuNPs was demonstrated by
409 UV-Vis, DLS analysis, HRTEM, FTIR and FAB-MS analysis. The ampicillin conjugated
410 Hypoxis-AuNPs, denoted as Amp-AuNPs showed enhanced antibacterial activity against
411 several Gram-positive and Gram-negative bacteria. This study demonstrates the use on
412 these plant-derived AuNPs as drug carriers. While the application of nanomaterials as drug
413 carriers have been demonstrated, the use of biogenic AuNP can be even more advantageous
414 due to their biocompatibility. Although preliminary studies suggest that Hypoxis-AuNPs
415 and Amp-AuNPs are not toxic human cells, further testing is required. While this study
416 investigated the use of Hypoxis-AuNPs as carriers for ampicillin, these AuNP can
417 potentially also be used to transport are drugs.



418

419

420

421

422

423

424

425

426

427 **References**

428

- 429 1. Renjis TT, Suryanarayanan V, Ganapati Reddy P, et al (2004) Ciprofloxacin-Protected
430 Gold Nanoparticles. *Langmuir* 20:1909–1914. <https://doi.org/10.1021/LA0358567>
- 431 2. Saha B, Bhattacharya J, Mukherjee A, et al (2007) In Vitro Structural and Functional
432 Evaluation of Gold Nanoparticles Conjugated Antibiotics. *Nanoscale Res Lett* 2:614–622.
433 <https://doi.org/10.1007/s11671-007-9104-2>
- 434 3. Jain PK, Lee KS, El-Sayed IH, El-Sayed MA (2006) Calculated Absorption and Scattering
435 Properties of Gold Nanoparticles of Different Size, Shape, and Composition: Applications
436 in Biological Imaging and Biomedicine. *J Phys Chem B* 110:7238–7248.
437 <https://doi.org/10.1021/JP057170O>
- 438 4. Moghimi SM (2006) Recent developments in polymeric nanoparticle engineering and
439 their applications in experimental and clinical oncology. *Anticancer Agents Med Chem*
440 6:553–561
- 441 5. Lecaroz C, Gamazo C, Blanco-Prieto MJ (2006) Nanocarriers with gentamicin to treat
442 intracellular pathogens. *J Nanosci Nanotechnol* 6:3296–3302
- 443 6. Umamaheshwari RB, Ramteke S, Jain NK (2004) Anti-Helicobacter pylori effect of
444 mucoadhesive nanoparticles bearing amoxicillin in experimental gerbils model. *AAPS*
445 *PharmSciTech* 5:60–68. <https://doi.org/10.1208/pt050232>
- 446 7. Brown AN, Smith K, Samuels TA, et al (2012) Nanoparticles functionalized with
447 ampicillin destroy multiple-antibiotic-resistant isolates of *Pseudomonas aeruginosa* and
448 *Enterobacter aerogenes* and methicillin-resistant *Staphylococcus aureus*. *Appl Environ*
449 *Microbiol* 78:2768–2774. <https://doi.org/10.1128/AEM.06513-11>
- 450 8. Fair RJ, Tor Y (2014) Antibiotics and bacterial resistance in the 21st century. *Perspect*
451 *Medicin Chem* 6:25–64. <https://doi.org/10.4137/PMC.S14459>
- 452 9. Rajchakit U, Sarojini V (2017) Recent Developments in Antimicrobial-Peptide-
453 Conjugated Gold Nanoparticles. *Bioconj Chem* 28:2673–2686.
454 <https://doi.org/10.1021/acs.bioconjchem.7b00368>
- 455 10. Nirmala Grace A, Pandian K (2007) Antibacterial efficacy of aminoglycosidic antibiotics
456 protected gold nanoparticles-A brief study. *Colloids Surfaces A Physicochem Eng Asp*
457 297:63–70. <https://doi.org/10.1016/j.colsurfa.2006.10.024>
- 458 11. Bhattacharya D, Saha B, Mukherjee A, et al (2012) Gold Nanoparticles Conjugated
459 Antibiotics: Stability and Functional Evaluation. *Nanosci Nanotechnol* 2:14–21.
460 <https://doi.org/10.5923/j.nn.20120202.04>
- 461 12. Perni S, Prokopovich P (2014) Continuous release of gentamicin from gold nanocarriers.
462 *RSC Adv* 4:51904–51910. <https://doi.org/10.1039/c4ra10023a>
- 463 13. Gu Y-J, Cheng J, Man CW-Y, et al (2012) Gold-doxorubicin nanoconjugates for
464 overcoming multidrug resistance. *Nanomedicine Nanotechnology, Biol Med* 8:204–211.
465 <https://doi.org/10.1016/J.NANO.2011.06.005>
- 466 14. Mohammed Fayaz A, Girilal M, Mahdy SA, et al (2011) Vancomycin bound biogenic
467 gold nanoparticles: A different perspective for development of anti VRSA agents. *Process*

- 468 Biochem 46:636–641. <https://doi.org/10.1016/J.PROCBIO.2010.11.001>
- 469 15. Payne JN, Waghwani HK, Connor MG, et al (2016) Novel synthesis of kanamycin
470 conjugated gold nanoparticles with potent antibacterial activity. *Front Microbiol* 7:.
471 <https://doi.org/10.3389/fmicb.2016.00607>
- 472 16. Elbagory AM, Cupido CN, Meyer M, Hussein AA (2016) Large Scale Screening of
473 Southern African Plant Extracts for the Green Synthesis of Gold Nanoparticles Using
474 Microtitre-Plate Method. *Molecules* 21:1498. <https://doi.org/10.3390/molecules21111498>
- 475 17. Yulizar Y, Utari T, Ariyanta HA, Maulina D (2017) Green Method for Synthesis of Gold
476 Nanoparticles Using *Polyscias scutellaria* Leaf Extract under UV Light and Their
477 Catalytic Activity to Reduce Methylene Blue. *J Nanomater* 2017:.
478 <https://doi.org/10.1155/2017/3079636>
- 479 18. Menon S, S. R, S. VK (2017) A review on biogenic synthesis of gold nanoparticles,
480 characterization, and its applications. *Resour Technol* 3:516–527.
481 <https://doi.org/10.1016/J.REFFIT.2017.08.002>
- 482 19. Elbagory A, Meyer M, Cupido C, Hussein A (2017) Inhibition of Bacteria Associated with
483 Wound Infection by Biocompatible Green Synthesized Gold Nanoparticles from South
484 African Plant Extracts. *Nanomaterials* 7:417. <https://doi.org/10.3390/nano7120417>
- 485 20. Owira PMO, Ojewole JAO (2009) “African potato” (*Hypoxis hemerocallidea* corm): a
486 plant-medicine for modern and 21st century diseases of mankind? - a review. *Phyther Res*
487 23:147–152. <https://doi.org/10.1002/ptr.2595>
- 488 21. Khan M, Khan M, Adil SF, et al (2013) Green synthesis of silver nanoparticles mediated
489 by *Pulicaria glutinosa* extract. *Int J Nanomedicine* 8:1507.
490 <https://doi.org/10.2147/IJN.S43309>
- 491 22. Shah M, Badwaik V, Kherde Y, et al (2014) Gold nanoparticles: various methods of
492 synthesis and antibacterial applications. *Front Biosci (Landmark Ed)* 19:1320–1344
- 493 23. Kunoh T, Takeda M, Matsumoto S, et al (2018) Green Synthesis of Gold Nanoparticles
494 Coupled with Nucleic Acid Oxidation. *ACS Sustain Chem Eng* 6:364–373.
495 <https://doi.org/10.1021/acssuschemeng.7b02610>
- 496 24. Sujitha M V., Kannan S (2013) Green synthesis of gold nanoparticles using Citrus fruits
497 (*Citrus limon*, *Citrus reticulata* and *Citrus sinensis*) aqueous extract and its
498 characterization. *Spectrochim Acta - Part A Mol Biomol Spectrosc* 102:15–23.
499 <https://doi.org/10.1016/j.saa.2012.09.042>
- 500 25. Rastogi L, Kora AJ, J A (2012) Highly stable, protein capped gold nanoparticles as
501 effective drug delivery vehicles for amino-glycosidic antibiotics. *Mater Sci Eng C Mater*
502 *Biol Appl* 32:1571–7. <https://doi.org/10.1016/j.msec.2012.04.044>
- 503 26. Penders J, Stolzoff M, Hickey DJ, et al (2017) Shape-dependent antibacterial effects of
504 non-cytotoxic gold nanoparticles. *Int J Nanomedicine* 12:2457–2468.
505 <https://doi.org/10.2147/IJN.S124442>
- 506 27. Hur YE, Kim S, Kim J-H, et al (2014) One-step functionalization of gold and silver
507 nanoparticles by ampicillin. *Mater Lett* 129:185–190.
508 <https://doi.org/10.1016/J.MATLET.2014.05.032>
- 509 28. Tsai D-H, Davila-Morris M, DelRio FW, et al (2011) Quantitative Determination of

- 510 Competitive Molecular Adsorption on Gold Nanoparticles Using Attenuated Total
511 Reflectance–Fourier Transform Infrared Spectroscopy. *Langmuir* 27:9302–9313.
512 <https://doi.org/10.1021/la2005425>
- 513 29. Rogowska A, Rafińska K, Pomastowski P, et al (2017) Silver nanoparticles functionalized
514 with ampicillin. *Electrophoresis* 38:2757–2764. <https://doi.org/10.1002/elps.201700093>
- 515 30. Xin Lee K, Shameli K, Miyake M, et al (2016) Green Synthesis of Gold Nanoparticles
516 Using Aqueous Extract of *Garcinia mangostana* Fruit Peels. *J Nanomater* 2016:.
517 <https://doi.org/10.1155/2016/8489094>
- 518 31. Richman EK, Hutchison JE (2009) The Nanomaterial Characterization Bottleneck. *ACS*
519 *Nano* 3:2441–2446. <https://doi.org/10.1021/nn901112p>
- 520 32. Gardea-Torresdey JL, Parson JG, Gomez E, et al (2002) Formation and Growth of Au
521 Nanoparticles in live side Live Alfalfa Plants. *Nano Lett* 2:397–401.
522 <https://doi.org/10.1021/nl015673+>
- 523 33. Arunachalam KD, Annamalai SK, Hari S (2013) One-step green synthesis and
524 characterization of leaf extract-mediated biocompatible silver and gold nanoparticles from
525 *Memecylon umbellatum*. *Int J Nanomedicine* 8:1307–1315.
526 <https://doi.org/10.2147/IJN.S36670>
- 527 34. Rodríguez-León E, Iñiguez-Palomares R, Navarro R, et al (2013) Synthesis of silver
528 nanoparticles using reducing agents obtained from natural sources (*Rumex hymenosepalus*
529 extracts). *Nanoscale Res Lett* 8:318. <https://doi.org/10.1186/1556-276X-8-318>
- 530 35. Baraldi C, Tinti A, Ottani S, Gamberini MC (2014) Characterization of polymorphic
531 ampicillin forms. *J Pharm Biomed Anal* 100:329–340.
532 <https://doi.org/10.1016/J.JPBA.2014.08.021>
- 533 36. Unnikrishnan B, Chang C-Y, Chu H-W, et al (2016) Functional gold nanoparticles
534 coupled with laser desorption ionization mass spectrometry for bioanalysis. *Anal Methods*
535 8:8123–8133. <https://doi.org/10.1039/C6AY02378A>
- 536 37. Dass A, Dubay GR, Fields-Zinna CA, Murray RW (2008) FAB Mass Spectrometry of Au
537 ₂₅ (SR) ₁₈ Nanoparticles. *Anal Chem* 80:6845–6849. <https://doi.org/10.1021/ac801259j>
- 538 38. Siddiqui MRH (2013) Protected Gold Nanoparticles with Thioethers and Amines As
539 Surrogate Ligands. *J Chem* 2013:780939. <https://doi.org/10.1155/2013/780939>
- 540 39. Suwanrumpha S, Freast RB (1989) Identification of metabolites of ampicillin using liquid
541 chromatography/thermospray mass spectrometry and fast atom bombardment tandem
542 mass spectrometry. *Biol Mass Spectrom* 18:983–994.
543 <https://doi.org/10.1002/bms.1200181106>
- 544 40. Casy AF, Cryer C, Ominde EMA (1989) Mass spectrometry of β -lactam antibiotics with
545 special reference to ionization by fast atom bombardment (FAB). *J Pharm Biomed Anal*
546 7:1121–1157. [https://doi.org/10.1016/0731-7085\(89\)80050-0](https://doi.org/10.1016/0731-7085(89)80050-0)
- 547 41. Alkilany AM, Murphy CJ (2010) Toxicity and cellular uptake of gold nanoparticles: What
548 we have learned so far? *J Nanoparticle Res* 12:2313–2333.
549 <https://doi.org/10.1007/s11051-010-9911-8>
- 550 42. Findlay J, Hamouda A, Dancer SJ, Amyes SGB (2012) Rapid acquisition of decreased
551 carbapenem susceptibility in a strain of *Klebsiella pneumoniae* arising during meropenem

- 552 therapy. *Clin Microbiol Infect* 18:140–146. <https://doi.org/10.1111/J.1469->
553 0691.2011.03515.X
- 554 43. Foxley MA, Friedline AW, Jensen JM, et al (2016) Efficacy of ampicillin against
555 methicillin-resistant *Staphylococcus aureus* restored through synergy with branched
556 poly(ethylenimine). *J Antibiot (Tokyo)* 69:871–878. <https://doi.org/10.1038/ja.2016.44>
- 557 44. Fass RJ, Barnishan J (1979) Minimal inhibitory concentrations of 34 antimicrobial agents
558 for control strains *Escherichia coli* ATCC 25922 and *Pseudomonas aeruginosa* ATCC
559 27853. *Antimicrob Agents Chemother* 16:622–624
- 560 45. Gu H, Ho PL, Tong E, et al (2003) Presenting Vancomycin on Nanoparticles to Enhance
561 Antimicrobial Activities. *Nano Lett* 3:1261–1263. <https://doi.org/10.1021/NL034396Z>
- 562 46. Hayden SC, Zhao G, Saha K, et al (2012) Aggregation and Interaction of Cationic
563 Nanoparticles on Bacterial Surfaces. *J Am Chem Soc* 134:6920–6923.
564 <https://doi.org/10.1021/ja301167y>

565

566

567

568

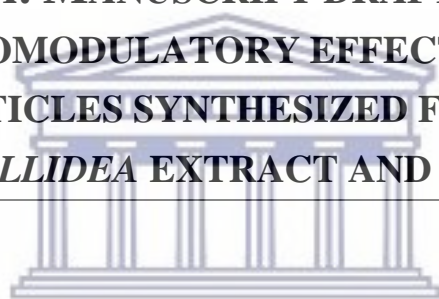
569

570



UNIVERSITY of the
WESTERN CAPE

**CHAPTER SIX: MANUSCRIPT DRAFT “THE IN VITRO
IMMUNOMODULATORY EFFECTS OF GOLD
NANOPARTICLES SYNTHESIZED FROM *HYPOXIS
HEMEROCALLIDEA* EXTRACT AND HYPOXOSIDE”**



UNIVERSITY *of the*
WESTERN CAPE

ORIGINAL RESEARCH

Elbagory et al

The in vitro immunomodulatory effects of gold nanoparticles synthesized from *Hypoxis hemerocallidea* extract and Hypoxoside

Abdulrahman M. Elbagory¹

Ahmed A. Hussein²

Mervin Meyer¹



¹DST/Mintek Nanotechnology Innovation Centre, Department of Biotechnology, University of the Western Cape, Private Bag X17, Bellville 7535, South Africa.

²Chemistry Department, Cape Peninsula University of Technology, P.O. Box 1906, Bellville 7535, South Africa.

Correspondence: Mervin Meyer

Department of Biotechnology, University of the Western Cape, Private Bag X17, Bellville 7535, South Africa.

Tel [+27 21 959 2032]

Fax [+27 21 959 3505]

Email memeyer@uwc.ac.za

Abstract:

Macrophages and Natural Killer (NK) cells are phagocytic cells and are an integral part of the innate immune system. These cells produce pro-inflammatory cytokines in response to bacterial infections. However, prolonged inflammation can be a contributing factor in the etiology of several diseases such as rheumatoid arthritis, inflammatory bowel disease, multiple sclerosis, psoriasis and eczema. Reducing the secretion of pro-inflammatory cytokines is an effective treatment strategy for these conditions. Gold nanoparticles (AuNPs) have been shown to have immunosuppressive effects by lowering the production of the pro-inflammatory cytokines. This study reports the synthesis of AuNPs from hypoxoside, a major secondary metabolite in the *Hypoxis hemerocallidea* plant. *H. hemerocallidea* is used in traditional medicine as an immunophytotherapy. This study also describes the immunomodulatory effects of extracts prepared from the *H. hemerocallidea* plant, hypoxoside, as well as AuNPs produced from the extract and hypoxoside. The results show that these treatments can lower the pro-inflammatory cytokine levels in macrophages (IL-1 β , IL-6 and TNF- α) and NK (IFN- γ) cells, and could thus be explored for the development of anti-inflammatory therapies.

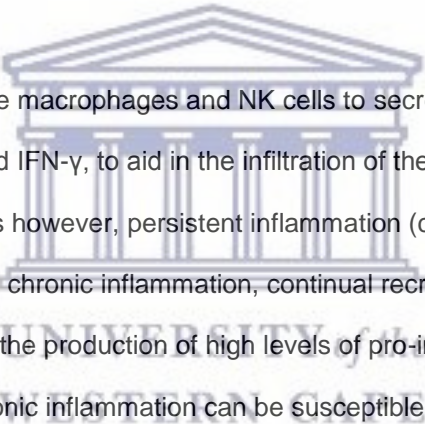
Keywords: Green nanotechnology, Gold nanoparticles, *Hypoxis hemerocallidea*, Hypoxoside, Anti-inflammatory, Innate immune cells, Cytokines, ELISA

Introduction

The function of the immune system is to provide protection against the invasion of foreign substances such as pathogens.¹ In humans, the immune system also prevents the proliferation of tissues that can potentially be harmful, such as tumors and damaged tissues.² The immune system can be separated into the innate and adaptive immune system. Macrophages and natural killer (NK) cells are part of the innate immune system, which is considered as the first line of defense. The function of macrophage and NK cells, which is mainly to phagocytose pathogens, is orchestrated by cytokines or interleukins (ILs).³ The modulation of the immune system, by altering

the secretion of ILs, is considered an integral part of new immunotherapies for the treatment of cancer, as well as bacterial and viral infections.⁴⁻⁹

Immune responses are carefully controlled by the collective action of molecular pathways that either suppress or activate immune activation. A disturbance in this balance can result in increased susceptibility to infections, chronic inflammation or autoimmune diseases depending on whether the immune system is overly active or suppressed.¹⁰ Immunomodulatory drugs that can stimulate or suppress immune responses can be used for the treatment of such immune disorders. For instance, drugs that suppress the immune system can be useful in the treatment of inflammatory disorders, such as rheumatoid arthritis, inflammatory bowel disease, multiple sclerosis, psoriasis and eczema.¹¹



Bacterial infections stimulate the macrophages and NK cells to secrete pro-inflammatory cytokines, e.g. IL-1 β , TNF- α and IFN- γ , to aid in the infiltration of the immune cells into the infected tissue.¹² In some cases however, persistent inflammation (chronic inflammation) can lead to undesired complications.¹³ In chronic inflammation, continual recruitment of innate and adaptive immune cells leads to the production of high levels of pro-inflammatory modulators.¹⁴ Patients with chronic inflammation can be susceptible to several diseases such as diabetes, cancer, inflammatory bowel syndrome and rheumatoid arthritis.¹⁵ Anti-inflammatory agents, therefore, can prove useful in the management of bacterial infections.¹⁶ Several nanomaterials are emerging as promising agents for application immune modulation.¹⁷ Gene expression analysis showed that the expression levels of several cytokines including IL-1 β , IL-6 and TNF- α was affected in rats after the animals were injected with Gold nanoparticles (AuNPs).¹⁸ Citrate-AuNPs, on the other hand, exhibited anti-inflammatory responses by downregulating the cellular response induced by IL-1 β both *in vivo* and *in vitro*.¹⁹

Nanoparticles can be formulated using several physical and chemical techniques.²⁰ However, the green synthesis of nanoparticles using plants is gaining interest to avoid using toxic materials.²¹

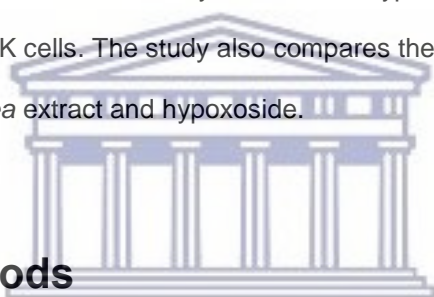
The synthesis of biogenic gold nanoparticles (Hypoxis-AuNPs) from *Hypoxis hemerocallidea* extracts was previously described.²² These AuNPs were found to inhibit the growth of several bacterial strains known to cause chronic wound infections. It is likely that nanoparticles synthesized from the plant extract could have similar bioactivities to the extract. This depends on whether phytochemicals responsible for the bioactivities of the plant extract are also involved in the synthesis of the NPs. Plant-derived NPs can enhance the bioavailability and biological activity of the phytochemicals responsible for the bioactivity.^{23–25}

H. hemerocallidea, commonly known as African Potato, is a wild tuberous plant that is native to the southern parts of Africa.²⁶ The plant has several medicinal uses and is considered the best-known medicinal plant among South Africans.²⁷ It is claimed that *H. hemerocallidea* can be used as an immune modulation phytotherapy in the management of immune related diseases such as the common cold, flu, rheumatic arthritis, cancer and HIV/AIDS.²⁸ *H. hemerocallidea* is also used by traditional healers to treat hypertension, diabetes, psoriasis, ulcers, urinary infections, tuberculosis, asthma and central nervous system disorders.^{29,30} Researchers reported that *H. hemerocallidea* showed antibacterial, antioxidant and anticancer activities.^{31,32} Animal studies have shown that the aqueous extract of *H. hemerocallidea* have anti-inflammatory activities. This was demonstrated by the ability of *H. hemerocallidea* to inhibit the acute inflammation in rats induced by egg albumin.²⁹ The anti-inflammatory activity of *H. hemerocallidea* was attributed to the ability of extracts from this plant to inhibit the synthesis of inflammatory mediators.³³

Hypoxoside is an important and well-studied phytochemical that is found in the corms of *H. hemerocallidea*.³⁴ This unique norlignan diglucoside can be found abundantly in several *Hypoxis* spp. and was used as an analytical marker to investigate the authenticity of the *Hypoxis* spp. and their products.³⁵ Hypoxoside is a prodrug, which, upon its hydrolysis by the gastric lysosomal enzyme, β -glucosidase, is converted to the biologically active aglycon form, rooperol.³³ This conversion of hypoxoside to rooperol can also occur in tumor tissues and inflammatory sites, where lysosomal enzymes including β -glucosidase can be released by cancer cells or the

activation of macrophages.³⁶ Studies have shown that rooperol exhibits strong antioxidant, anticancer and antibacterial activities.^{37–40} Rooperol was also shown to have potent anti-inflammatory action. It has been suggested that the increased production of reactive oxygen species (ROS) and nitric oxide (NO) in response to rooperol treatment is responsible for its anti-inflammatory activity.⁴¹ Derivatives of rooperol have been shown to inhibit the production of several pro-inflammatory ILs in stimulated human macrophages.⁴²

Since extracts of *H. hemerocallidea* has been shown to have immune modulatory activities, it is possible that the NPs produced from this plant may also have immune modulatory activities. This study reports for the first time the synthesis of AuNPs from hypoxoside (Hy-AuNPs) as well as the immune modulatory activities of the extract of Hy-AuNPs and Hypoxis-AuNPs using cell culture models of macrophages and NK cells. The study also compares the immune modulatory activities the AuNPs to *H. hemerocallidea* extract and hypoxoside.



Material and methods

Isolation of hypoxoside

An ethanolic extract of the *H. hemerocallidea* was acquired from Afriplex Pty Ltd. (Paarl, South Africa). This extract was concentrated and partitioned with ethyl acetate. The ethyl acetate fraction (5.0 g) was separated by chromatography on a Sephadex LH-20 column using a Methanol:H₂O mixture 1:1 (v/v) to isolate the fraction containing hypoxoside. The fraction containing hypoxoside was further purified using Prep-HPLC (Waters model, Milford, MA, USA) equipped with Waters 2535 Quaternary Gradient Module pump, a manual injector and variable wavelength detector (Waters 2489 UV-Vis detector). A C18 YMC column (5 μM, 250 × 30 mm) was used and separation was monitored at 254 nm. The elution was performed using Methanol:H₂O (1:1, v/v) solvent mixture at a flow rate of 5 mL/min. The ¹H and ¹³C NMR spectra of the isolated hypoxoside correlated with the spectra described by Nair and Kanfer.³⁵

Biosynthesis and characterization of AuNPs

The synthesis of Hypoxis-AuNPs (AuNPs synthesized from *H. hemerocallidea* extract) was done using a method previously described.²² A similar protocol was followed for the synthesis of Hy-AuNPs (AuNPs synthesized using hypoxoside) with slight modification. Sodium tetrachloroaurate (III) dihydrate (Sigma Aldrich, St. Louis, MO, USA) was mixed with hypoxoside (1.0 mg/mL) in a ratio of 5:1 (v/v). The mixture was stirred (40 rpm) for 2 h, centrifuged and the AuNPs were obtained in the pellet. The AuNPs were washed thrice with distilled water. A POLARstar Omega microtitre plate reader (BMG Labtech, Ortenberg, Germany) was used to monitor the characteristic Localized Surface Plasmon Resonance (LSPR) peaks of the AuNPs. The morphology and the elemental composition of the AuNPs were investigated by High Resolution Transmission Electron Microscope (HRTEM) using the FEI Tecnai G² 20 field-emission gun (FEG) equipped with an Electron Diffraction X-ray (EDX) liquid nitrogen cooled Lithium doped Silicon detector. A suspension of AuNPs' was deposited onto copper grids, which was then air-dried. The images obtained were analyzed using ImageJ 1.50b version 1.8.0_60 (<http://imagej.nih.gov/ij>). Dynamic Light Scattering (DLS) analysis was done using a Malvern Zetasizer Instrument (Malvern Ltd., UK) at 25 °C and a 90° angle. The chemical functional groups of hypoxoside and Hy-AuNPs were studied using a PerkinElmer spectrum two Fourier-Transform Infrared (FTIR) spectrophotometer (Waltham, MA, USA) as described previously.⁴³

Evaluating the stability of the AuNPs

The stability of Hypoxis-AuNPs and Hy-AuNPs in RPMI 1640 and α -MEM (Gibco, UK) cell culture media were tested as described previously.²² The stability of the AuNPs was evaluated by mixing the AuNPs and the cell culture medium at 1:1 ratio and incubating the mixture at 37 °C for 24 h. The mixtures of the AuNPs and the cell culture medium were subjected to UV-Vis analysis after the 24 h period.

Cell culture

The human leukemic monocyte cell line (THP1) (kindly provided by Prof. Samantha Sampson, from the Host-Pathogen Mycobacteriomics group at Stellenbosch University) was maintained in RPMI 1640 containing 50% Fetal Bovine Serum (FBS) (Lonza, Walkersville, MD, USA) and 1% penicillin–streptomycin (Lonza, Walkersville, MD, USA). The human Natural Killer cell line, NK92, was obtained from American Type Culture Collection (ATCC) and maintained in α -MEM supplemented with 12.5% FBS, 12.5% horse serum (Sigma-Aldrich, Cape Town, South Africa), 200 U/mL recombinant IL-2 (R&D systems, MN, USA), 0.1 mM 2-mercaptoethanol and 1% penicillin–streptomycin. The cells were cultured in a 37°C humidified incubator at 5% CO₂ saturation.

Differentiation of THP1 cells

Differentiation of THP1 cells into macrophage-like cells was done using 25 nM phorbol 12-myristate 13-acetate (PMA) (Sigma Aldrich, St. Louis, MO, USA) as previously described.⁴⁴ The cells were seeded in a 96-well plate (Greiner Bio-one GmbH, Frickenhausen, Germany) at a density of 2×10^5 cells/100 μ L/well. The cells were treated for 2 days with 25 nM PMA to induce cell differentiation. PMA induced macrophage-like phenotypic changes were confirmed by optical microscopy.

Determining the toxicity of extracts and AuNP in THP1 and NK92 cells

The effects of the *H. hemerocallidea* aqueous extract, hypoxoside, Hypoxis-AuNPs and Hy-AuNPs on the cell viability of NK92 and PMA differentiated THP1 cells were determined using the WST-1 Cell Proliferation Assay as recommended by the manufacturer (Roche Diagnostics GmbH, Mannheim, Germany). The cells were treated for 24 h with increasing concentrations of *H. hemerocallidea* extract, hypoxoside and the AuNPs. The concentrations of the *H. hemerocallidea* extract and hypoxoside were 30, 60, 120, 240 and 480 μ g/mL, while the

concentrations of Hypoxis-AuNPs and Hy-AuNPs were 1, 2, 4, 8, 16, 32 nM. To compensate for any interference from the AuNPs on the assay, background controls were included as previously described.²²

Measurement of cytokine responses in THP1 and NK92 cells

NK92 and PMA differentiated THP1 cells were seeded at a density of 2×10^5 cells/100 μ L/well in 24-well cell culture plates. After 24 h, the THP1 cells were exposed for 6 h to cell culture medium containing 10 μ g/mL Lipopolysaccharide (LPS). Based on the results of the WST-1 Cell Proliferation Assay, concentrations of *H. hemerocallidea* aqueous plant extract (240 μ g/mL), hypoxoside (240 μ g/mL), Hypoxis-AuNPs (16 nM) and Hy-AuNPs (16 nM) that were not toxic to the cells were identified. The NK92 and LPS activated THP1 cells were subjected to these treatments for 18 h after removing the LPS containing medium. The negative controls were cells that were not treated any way, while the positive controls for THP1 cells were cells that were treated for 6 h with LPS, which was replaced afterwards with cell culture medium for 18 h. After 24 h, the supernatants were collected from all wells. The samples were centrifuged at 10000 rpm for 15 min using an Eppendorf 5417 R Centrifuge equipped with F-45-30-11 rotor (Eppendorf, Hamburg, Germany) to remove any cells and the AuNPs. The presence of IL-1 β , IL-6 and TNF- α in the supernatants collected from THP1 cells were assessed using MaxDiscovery™ ELISA kits (Bioo Scientific, TX, USA). The cytokines concentrations were measured according to the manufacturer's protocol. Supernatants from NK92 cells were analyzed for the presence of IFN- γ .

Statistical analysis

Data were expressed as the mean \pm standard deviation of the three replicates. Statistical analysis was conducted using the GraphPad Prism 6 and two-tailed Student's *t*-test. Differences among three or more groups were analyzed by one- or two-way analysis of variance. Differences with *p* < 0.05 were considered to be statistically significant.

Results and discussion

Biosynthesis of AuNP using hypoxoside

The synthesis and characterization of Hypoxis-AuNPs using the water extract of *H. hemerocallidea* to reduce gold(III) chloride was previously reported.²² Hypoxoside is a unique glycoside and a major phytochemical component of *H. hemerocallidea* extracts. It was reported that glycosides can reduce gold(III) chloride to AuNPs,⁴⁵ and it is therefore possible that hypoxoside was involved in the synthesis of Hypoxis-AuNPs. Here the study investigated whether hypoxoside can reduce gold(III) chloride and found that hypoxoside was able to reduce gold(III) chloride resulting in the formation of Hy-AuNPs. The optimal synthesis conditions (temperature, concentration of hypoxoside and the time of synthesis) was established using the same methods described previously for the synthesis of AuNPs from plant extracts.⁴⁶ The UV-Vis spectrum for Hy-AuNP showed absorption maximum (λ_{\max}) at around 534 nm (Figure 1), which is within the range of the visible spectrum (500 - 600 nm) and the characteristic λ_{\max} for spherical AuNPs.⁴⁷ The optimal synthesis time was established by measuring changes in λ_{\max} over time (Figure 1A). A sharp increase in absorbance (up to about 1.1 absorbance units) was detected between 0 and 20 min, however the increase in absorbance from 20 to 120 min was moderate since the absorbance units only increased from 1.1 to 1.25 over this time period (Figure 1B). Yulizar et al suggested that an increase in absorbance reflect an increase in AuNP number.⁴⁸ This implies that the number of Hy-AuNPs increased over the 120 min time period, but that the formation of new seeds (nucleation) of Hy-AuNPs occurs mainly within 20 min from the start of the reaction. While λ_{\max} at 60 and 120 min is around 534 nm, the λ_{\max} at earlier time points 10, 20 and 40 min appears to be red-shifted. Moreover, the absorbance peaks produced at 10, 20 and 40 min also appeared to be much broader. Yulizar et al also suggested that the shape of absorbance peaks is mainly determined by the morphological characteristics of the AuNPs.⁴⁸ It can therefore be postulated that the growth of Hy-AuNPs, which follows the nucleation step, occurs after 20 min, reaching the final energetically stable form at 120 min.

The Z-average size of Hy-NPs was 26 ± 2 nm as determined by the DLS analysis. The size distribution by intensity was bimodal. Small nanoparticles with an average diameter of 1.5 ± 0.5 nm and larger nanoparticles with an average diameter of 56 ± 33 nm can be observed in Figure 2. The zeta potential of Hy-NPs was -23 . Such low zeta potential value has been shown to indicate colloidal stability of AuNPs due to the repulsive force between the particles.⁴⁹ It can thus be concluded that the Hy-NPs are stable in solution.

The HRTEM images in Figure 3 show the quasi-spherical shape of Hy-AuNPs (Figure 3A and 3B). The particle size distribution of Hy-AuNPs determined from the HRTEM images (using ImageJ software) showed that most of the particles are between 24 to 28 nm in diameter (Figure 3C), which is in accordance with the DLS analysis. Moreover, the SAED pattern of Hy-AuNPs confirmed their polycrystalline nature as indicated by the presence of the bright rings corresponding to (111), (200), (210), (311) and (222) of the face centered cubic structure of gold (Figure 3D), as previously reported.⁵⁰ The lattice fringes of the Hy-AuNPs had a distance of 0.271 nm, which corresponds to the (111) orientation of gold (Figure 3E).⁵¹ Additional confirmation about the bio-reduction of gold(III) chloride to form AuNPs was presented by the appearance of elemental Au peaks in the EDX profile of Hy-AuNPs (Figure 3F).

FTIR analysis was applied to investigate the possible functional groups in the structure of hypoxoside that is involved in the synthesis of Hy-AuNPs. Figure 4 shows the FTIR spectra of both hypoxoside and Hy-AuNPs. The FTIR spectrum of hypoxoside is similar to the spectrum reported previously.³⁵ The C–H rocking vibration is shown by the absorption bands at 801 and 890 cm^{-1} and the C–H bending at 2884 cm^{-1} . The absorption bands at 1246 and 3280 cm^{-1} represent the bending and stretching alcoholic O–H, respectively. The peaks at 890 and 1070 cm^{-1} denote the out of plane C–H attached to a carbon through a double bond (C=C–H). The sharp absorption bands at 1510 and 1586 cm^{-1} indicate the C=C in aromatic ring. It is expected that hypoxoside will undergo oxidation to reduce gold(III) chloride, which should be manifested in the FTIR spectrum of Hy-AuNPs. It was reported that C–6–OH in the sugar unit of glycosides is

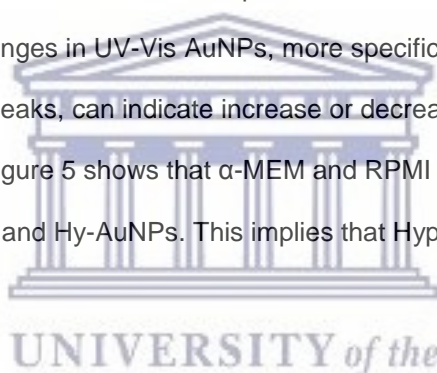
readily oxidized into carboxylic acid upon reaction with gold(III) chloride.⁴⁵ Interestingly, the FTIR spectrum of Hy-AuNPs showed a very broad band starting from 3000 to 1750 cm^{-1} , which may be a result of the stretching the O–H group of carboxylic acid, which is a characteristic band of carboxylic acids that overlap other peaks of other functional groups.⁵² Moreover, Hy-AuNPs showed two bands at 3770 and 3703 cm^{-1} , which may be the result of the shift of both the alcoholic O–H and the bending C–H groups (from 3280 and 2884 cm^{-1} , respectively, as shown in the FTIR spectrum of hypoxoside). This huge shift is caused by strong hydrogen bonding of the functional groups involved and is sometimes detectable in systems that are in a complex.⁵³ From the above, it can be hypothesized that the reduction of gold(III) chloride by hypoxoside was mainly mediated through the oxidation site at C–6–OH, which is converted into carboxylic acid. Secondly, the alcoholic O–H groups of hypoxoside were responsible for the stabilization of Hy-AuNPs by means of chemisorption with the growing Au seeds.

Furthermore, the results indicate that hypoxoside might have contributed largely to the synthesis of AuNPs from the *H. hemerocallidea* water extract. This is evident from the similar physicochemical characteristics reported here for Hy-AuNPs and those reported previously for Hypoxis-AuNPs.²² However, because of the longer incubation time needed for the synthesis of Hy-AuNPs and for the difference in the average size, hypoxoside may not be the sole contributor in the synthesis of Hypoxis-AuNPs.

The immunomodulation activity of H. hemerocallidea, hypoxoside and AuNPs

H. hemerocallidea is used in traditional medicine for the treatment of immune related diseases and it has been shown that extracts of *H. hemerocallidea* have anti-inflammatory activity (Ojewole, 2006). It has been suggested that the immunomodulatory effects of *H. hemerocallidea* can be ascribed to the bioactivity of rooperol, which is formed when hypoxoside, a major constituent of the *H. hemerocallidea* plant, is hydrolyzed (Owira and Ojewole, 2009). It is

demonstrated here for the first time that hypoxoside can reduce gold(III) chloride to form Hy-AuNPs. It has also been demonstrated that metal-based nanoparticles have immune modulatory effects.¹⁷ Herein, the immunomodulatory effects the AuNP that has been synthesized from *H. hemerocallidea* (i.e. Hypoxis-AuNPs) and Hy-AuNPs are investigated using macrophage and NK cell cultures. *In vitro* immunomodulatory assays require that the treatments with the AuNPs be done in cell culture medium. Cell culture media contain proteins, peptides, amino-acids, carbohydrates, minerals and buffering agents. If any of these media constituents react with the AuNPs, the biophysical properties of the AuNPs will be altered. This can also cause the AuNPs to aggregate. For this reason, the stability of the AuNPs was investigated in α -MEM and RPMI cell culture media. This involved placing Hypoxis-AuNPs and Hy-AuNPs in α -MEM and RPMI medium for a period of 24 h and to determine if the UV-vis spectra of the AuNPs change over this period as described previously.⁵⁴ Changes in UV-Vis AuNPs, more specifically the red shift or broadening of the adsorption peaks, can indicate increase or decrease in the size of AuNPs or the aggregation of AuNPs.⁵⁵ Figure 5 shows that α -MEM and RPMI media did not affect the UV-Vis spectra of Hypoxis-AuNPs and Hy-AuNPs. This implies that Hypoxis-AuNPs and Hy-AuNPs were stable in these media.



The immunomodulatory effects of the *H. hemerocallidea* plant extract, hypoxoside, Hypoxis-AuNPs and Hy-AuNPs were evaluated in THP1 and NK92 cell lines. Monocytes and NK cells are an integral part of the innate immune system, in part by producing several ILs that exert their functions on other cells and thus control immune responses to infections.⁵⁶ The toxicity of the *H. hemerocallidea* plant extract, hypoxoside, Hypoxis-AuNPs and Hy-AuNPs to THP1 and NK92 cells was determined using the WST-1 viability assay (Figure 6). This was done to determine if the AuNPs, extract and hypoxoside were toxic to these cells. The concentrations of Hypoxis-AuNPs and Hy-AuNPs ranged from 1 to 32 nM, while the concentrations of *H. hemerocallidea* plant extract and hypoxoside, ranged from 30 to 480 μ g/mL. The viability of THP1 cells were unaffected by Hypoxis-AuNPs and Hy-AuNPs, while the viability of NK92 cells were only significantly affected by Hypoxis-AuNPs and Hy-AuNPs at the highest dose, 32 nM. The viability

of NK92 cells was reduced to around 15% when treated with 32 nM Hypoxis-AuNPs or Hy-AuNPs. NK92 cells were unaffected by *H. hemerocallidea* plant extract and hypoxoside, while THP1 cells were only significantly affected by hypoxoside at the highest dose, 480 nM. Based on this data 16 nM of Hypoxis-AuNPs or Hy-AuNPs and 240 µg/mL of hypoxoside or *H. hemerocallidea* plant extract were selected to investigate the immunomodulatory effects of the extracts and AuNPs on THP1 and NK92 cells. This is the first time that the immune modulatory effects of the *H. hemerocallidea* plant extract and hypoxoside has been studied in this way using in vitro culture of macrophages and NK cells.

Prior to treatment with the extract, hypoxoside and AuNPs, THP1 cells were induced to differentiate into macrophage-like cells using PMA. After exposure to PMA, the differentiated THP1 cells were treated with LPS, a bacterial endotoxin that has been used to trigger pro-inflammatory response in macrophage-like THP1 cells.⁵⁷ It has been shown that LPS can activate the secretion of pro-inflammatory cytokines, which includes IL-1 β , IL-6, TNF- α and IFN- γ .⁵⁸ IL-1 β is considered a key mediator between the innate and the adaptive immune cells as it activates the antigen-presenting cells, which in turn leads to the production of aggressive adaptive immune cells against infections.⁵⁹ TNF- α is one of the early cytokines released from macrophages after infections and is considered a “master regulator” of other pro-inflammatory cytokines.⁶⁰ IL-6 is another important immune system regulator, but with both pro- and anti-inflammatory actions.⁶¹ It was shown that the pleiotropic effect of IL-6 depends on the activation of either one of its two signaling pathways.⁶¹ The relationship between IL-6 and bacterial infections is well established. Indeed, increased IL-6 levels are considered a diagnostic marker for early bacterial infections.⁶² Differentiated THP1 cells treated with LPS for 6 h, showed a significant increase in IL-1 β , IL-6 and TNF- α levels, when compared to THP1 cells that were not treated with LPS (negative control) (Figure 7). Differentiated THP1 cells that were also stimulated with LPS for 6 h and then treated for 18 h with Hypoxis-AuNPs, Hy-AuNPs, hypoxoside or *H. hemerocallidea* plant extract showed a significant decrease in IL-1 β and TNF- α levels when compared to THP1 cells that were treated with LPS only (LPS control). It was shown that at these doses of Hypoxis-AuNPs, Hy-

AuNPs, hypoxoside and *H. hemerocallidea* plant extract are not toxic to the cells, which suggests that these treatments exert an anti-inflammatory response in THP1 macrophage-like cells. IL-6 responses in THP1 cells were also significantly reduced when the cells were treated with the *H. hemerocallidea* plant extract. However, treatments with Hypoxis-AuNPs, Hy-AuNPs and hypoxoside did not significantly affect IL-6 responses in THP1 cells. In fact, treatment of THP1 cells with Hy-AuNPs and hypoxoside resulted in a moderate increase in IL-6 level when compared to cells that were treated with LPS only for 6 h. However, this increase was not significant. Higher doses of Hy-AuNPs and hypoxoside or a longer treatment may result in significant increase of the IL-6 response.

The immunomodulation effect of H. hemerocallidea, Hypoxoside and their AuNPs on NK92

The effects of Hypoxis-AuNPs, Hy-AuNPs, hypoxoside and *H. hemerocallidea* plant extract on cytokine responses in NK92 cells, more specifically IFN- γ , were also investigated. IFN- γ is a major effector cytokine that is mainly produced by NK cells in response to viral and bacterial infections.⁶³ The treatment of NK92 cells with Hypoxis-AuNPs, hypoxoside and *H. hemerocallidea* plant extract did not alter the production of IFN- γ levels when compared to the untreated negative control cells (Figure 7). However, IFN- γ production was significantly reduced in NK92 cells treated with Hy-AuNPs. The IFN- γ levels in Hy-AuNPs-treated cells were 13 ± 7 pg/mL, compared to 84 ± 17 pg/mL for the untreated cells. It has been reported that IFN- γ increase the production of pro-inflammatory cytokines, including IL-1 β and TNF- α .⁶⁴ In this context, the effects of Hy-AuNPs on NK92 cells can be viewed as an anti-inflammatory response. Interestingly, the free hypoxoside or any of the other AuNPs did not downregulate the production IFN- γ compared to the Hy-AuNPs. It can be postulated that hypoxoside might have undergone chemical modification upon oxidation with the gold(III) chloride, which might have converted it to a more active form. It is known from the literature for example that hypoxoside can be converted to rooperol upon hydrolysis. The FTIR data in this study also suggest major modification in the

chemistry of hypoxoside after AuNPs synthesis. This can only be confirmed by performing more sophisticated spectroscopic analysis of the hypoxoside and the Hy-AuNPs. It is also worth noting that IL-2, used in culturing the NK92 cells, can cause elevated IFN- γ production, and that might be the reason for the moderately elevated levels of this cytokine in the negative controls in our study.^{65,66}

Inflammation is considered an essential mechanism of the innate immune system to control pathogens and bacterial infections.⁶⁷ The increased production of pro-inflammatory cytokines during infections triggers a cascade of events that result in the infiltration of infected tissues by innate immune cells.¹³ However, the overproduction of the pro-inflammatory cytokines in response to infections may also have severe adverse health effects. Irreversible damage to the inflamed tissue can occur due to the release of lytic enzymes or through oxidative stress.¹³ Elevated IL-1 β levels are associated with several inflammatory disorders including rheumatoid arthritis and psoriasis.¹⁹ Lowering TNF- α production is also a key therapy for rheumatoid arthritis.⁶⁸ Inflammatory disorders, such as rheumatoid arthritis, inflammatory bowel disease, multiple sclerosis, psoriasis and eczema can benefit from anti-inflammatory therapies. This study demonstrated the anti-inflammatory responses of Hypoxis-AuNPs, Hy-AuNPs, hypoxoside and *H. hemerocallidea* plant extract in THP1 cells. It also found that Hy-AuNPs has an anti-inflammatory response in NK92 cells.

Conclusion

This study demonstrates for the first time the biosynthesis of AuNPs using hypoxoside, which was isolated from *H. hemerocallidea*. The physicochemical properties of Hy-AuNPs were similar to that of Hypoxis-AuNPs, which was synthesized from the water extracts of *H. hemerocallidea*. This may suggest that hypoxoside is involved in the synthesis of Hypoxis-AuNPs. Water extracts of *H. hemerocallidea* and hypoxoside reduced the secretion of pro-inflammatory cytokines in the macrophage cell line THP1. This finding lends support to the traditional use of the plant in the

treatment of inflammation. Hypoxis-AuNP and Hy-AuNP also reduced the secretion of pro-inflammatory cytokines in THP1 cells. Hy-AuNP was the only treatment that affected cytokine responses in NK92 cells by significantly reducing IFN- γ secretion. These AuNPs can be explored further as anti-inflammatory treatments. Metallic nanoparticles are commonly used for skin care and dermatological treatments. Considering that this study shows that Hypoxis-AuNP and Hy-AuNP have anti-inflammatory properties, these nanoparticles can potentially be used in the development of topical treatments for the autoimmune skin conditions such as psoriasis and eczema. To fully understand their activities on the immune system, it is recommended to evaluate the immunomodulatory effects of *H. hemerocallidea*, hypoxoside and their AuNPs on immune cells isolated from blood and in animal models.

Disclosure

The author reports no conflicts of interest in this work.

References

1. Mogensen TH. Pathogen Recognition and Inflammatory Signaling in Innate Immune Defenses. *Clin Microbiol Rev.* 2009;22(2):240-273. doi:10.1128/CMR.00046-08.
2. Candeias SM, Gaipi US. The Immune System in Cancer Prevention, Development and Therapy. *Anticancer Agents Med Chem.* 2016;16(1):101-107.
3. Jiao Q, Li L, Mu Q, Zhang Q. Immunomodulation of nanoparticles in nanomedicine applications. *Biomed Res Int.* 2014;2014:426028. doi:10.1155/2014/426028.
4. Péchiné S, Bruxelles JF, Janoir C, Collignon A. Targeting Clostridium difficile Surface Components to Develop Immunotherapeutic Strategies Against Clostridium difficile Infection. *Front Microbiol.* 2018;9:1009. doi:10.3389/fmicb.2018.01009.
5. Barthelemy A, Sencio V, Soulard D, et al. Interleukin-22 Immunotherapy during Severe Influenza Enhances Lung Tissue Integrity and Reduces Secondary Bacterial Systemic Invasion. *Infect Immun.* 2018;86(7):e00706-17. doi:10.1128/IAI.00706-17.
6. Manglani M, McGavern DB. New advances in CNS immunity against viral infection. *Curr*

- Opin Virol.* 2018;28:116-126. doi:10.1016/J.COVIRO.2017.12.003.
7. Walker LM, Burton DR. Passive immunotherapy of viral infections: “super-antibodies” enter the fray. *Nat Rev Immunol.* 2018;18(5):297-308. doi:10.1038/nri.2017.148.
 8. Waldmann TA. Cytokines in Cancer Immunotherapy. *Cold Spring Harb Perspect Biol.* 2018;10(12):a028472. doi:10.1101/cshperspect.a028472.
 9. Ripley RT, Ayabe RI. Immunotherapy: The power of perseverance. *J Thorac Cardiovasc Surg.* 2018;155(4):1775-1776. doi:10.1016/j.jtcvs.2017.12.002.
 10. Haase D, Starke M, Puan KJ, Lai TS, Rotzschke O. Immune modulation of inflammatory conditions: regulatory T cells for treatment of GvHD. *Immunol Res.* 2012;53(1-3):200-212. doi:10.1007/s12026-012-8267-9.
 11. Coutinho AE, Chapman KE. The anti-inflammatory and immunosuppressive effects of glucocorticoids, recent developments and mechanistic insights. *Mol Cell Endocrinol.* 2011;335(1):2-13. doi:10.1016/j.mce.2010.04.005.
 12. Arango Duque G, Descoteaux A. Macrophage Cytokines: Involvement in Immunity and Infectious Diseases. *Front Immunol.* 2014;5:491. doi:10.3389/fimmu.2014.00491.
 13. Rauch I, Müller M, Decker T. The regulation of inflammation by interferons and their STATs. *JAK-STAT.* 2013;2(1):e23820. doi:10.4161/jkst.23820.
 14. Meirow Y, Baniyash M. Immune biomarkers for chronic inflammation related complications in non-cancerous and cancerous diseases. *Cancer Immunol Immunother.* 2017;66(8):1089-1101. doi:10.1007/s00262-017-2035-6.
 15. Pahwa R, Jialal I. *Chronic Inflammation.* StatPearls Publishing; 2018.
 16. Sheth AN. Can Anti-Inflammatory Drugs Fight Infection? *Sci Transl Med.* 2013;5(192):192ec110. doi:10.1126/scitranslmed.3006879.
 17. Luo YH, Chang LW, Lin P. Metal-Based Nanoparticles and the Immune System: Activation, Inflammation, and Potential Applications. *Biomed Res Int.* 2015;2015:143720. doi:10.1155/2015/143720.
 18. Khan HA, Abdelhalim MAK, Alhomida AS, Al Ayed MS. Transient increase in IL-1 β , IL-6 and TNF- α gene expression in rat liver exposed to gold nanoparticles. *Genet Mol Res.*

- 2013;12(4):5851-5857. doi:10.4238/2013.November.22.12.
19. Sumbayev V V., Yasinska IM, Garcia CP, et al. Gold Nanoparticles Downregulate Interleukin-1 β -Induced Pro-Inflammatory Responses. *Small*. 2013;9(3):472-477. doi:10.1002/sml.201201528.
 20. Ghosh Chaudhuri R, Paria S. Core/shell nanoparticles: Classes, properties, synthesis mechanisms, characterization, and applications. *Chem Rev*. 2012;112(4):2373-33. doi:10.1021/cr100449n.
 21. Souri M, Hoseinpour V, Shakeri A, Ghaemi N. Optimisation of green synthesis of MnO nanoparticles via utilising response surface methodology. *IET Nanobiotechnology*. 2018;12(6):822-827. doi:10.1049/iet-nbt.2017.0145.
 22. Elbagory A, Meyer M, Cupido C, Hussein A. Inhibition of Bacteria Associated with Wound Infection by Biocompatible Green Synthesized Gold Nanoparticles from South African Plant Extracts. *Nanomaterials*. 2017;7(12):417. doi:10.3390/nano7120417.
 23. Rao PV, Nallappan D, Madhavi K, Rahman S, Jun Wei L, Gan SH. Phytochemicals and Biogenic Metallic Nanoparticles as Anticancer Agents. *Oxid Med Cell Longev*. 2016;2016:3685671. doi:10.1155/2016/3685671.
 24. Park Y, Hong YN, Weyers A, Kim YS, Linhardt RJ. Polysaccharides and phytochemicals: a natural reservoir for the green synthesis of gold and silver nanoparticles. *IET Nanobiotechnology*. 2011;5(3):69-78. doi:10.1049/iet-nbt.2010.0033.
 25. Lee J, Park EY, Lee J. Non-toxic nanoparticles from phytochemicals: Preparation and biomedical application. *Bioprocess Biosyst Eng*. 2014;37(6):983-989. doi:10.1007/s00449-013-1091-3.
 26. Drewes SE, Elliot E, Khan F, Dhlamini JTB, Gcumisa MSS. Hypoxis hemerocallidea—Not merely a cure for benign prostate hyperplasia. *J Ethnopharmacol*. 2008;119(3):593-598. doi:10.1016/j.jep.2008.05.027.
 27. Nair VDP, Kanfer I. *South African Journal of Science*. Vol 104. Academy of Science of South Africa; 2008.
 28. Mills E, Cooper C, Seely D, Kanfer I. African herbal medicines in the treatment of HIV:

- Hypoxis and Sutherlandia. An overview of evidence and pharmacology. *Nutr J.* 2005;4(19). doi:10.1186/1475-2891-4-19.
29. Ojewole JAO. Antinociceptive, anti-inflammatory and antidiabetic properties of Hypoxis hemerocallidea Fisch. & C.A. Mey. (Hypoxidaceae) corm ["African Potato"] aqueous extract in mice and rats. *J Ethnopharmacol.* 2006;103(1):126-134. doi:10.1016/J.JEP.2005.07.012.
 30. Steenkamp V, Gouws MC, Gulumian M, Elgorashi EE, van Staden J. Studies on antibacterial, anti-inflammatory and antioxidant activity of herbal remedies used in the treatment of benign prostatic hyperplasia and prostatitis. *J Ethnopharmacol.* 2006;103(1):71-75. doi:10.1016/J.JEP.2005.07.007.
 31. Oguntibeju OO, Meyer S, Aboua YG, Goboza M. Hypoxis hemerocallidea Significantly Reduced Hyperglycaemia and Hyperglycaemic-Induced Oxidative Stress in the Liver and Kidney Tissues of Streptozotocin-Induced Diabetic Male Wistar Rats. *Evidence-based Complement Altern Med.* 2016;2016:8934362. doi:10.1155/2016/8934362.
 32. Katerere DR. Hypoxis hemerocallidea (African potato): A Botanical Whose Time Has Come? In: Juliani HR, Simon JE, Ho C-T, eds. *African Natural Plant Products Volume II: New Discoveries and Challenges in Chemistry and Quality.* Washington: American Chemical Society; 2013:51-61. doi:10.1021/bk-2013-1127.ch004.
 33. Owira PMO, Ojewole JAO. "African potato" (*Hypoxis hemerocallidea* corm): a plant-medicine for modern and 21st century diseases of mankind? - a review. *Phyther Res.* 2009;23(2):147-152. doi:10.1002/ptr.2595.
 34. Nsibandé BE, Gustavsson K-E, Zhu L-H. Analysis of Health-Associated Phytochemical Compounds in Seven *Hypoxis* Species. *Am J Plant Sci.* 2018;9(4):571-583. doi:10.4236/ajps.2018.94044.
 35. Nair VDP, Kanfer I. High-performance liquid chromatographic method for the quantitative determination of hypoxoside in African potato (*Hypoxis hemerocallidea*) and in commercial products containing the plant material and/or its extracts. *J Agric Food Chem.* 2006;54(8):2816-2821. doi:10.1021/jf052418s.

36. Albrecht C. Hypoxoside: a putative, non-toxic prodrug for the possible treatment of certain malignancies, HIV-infection and inflammatory conditions. Hypoxoside: a putative, non-toxic prodrug for the possible treatment of certain malignancies, HIV-infection and inflam. In: *Proceedings of the First International IOCD-Symposium*. Victoria Falls, Zimbabwe. Harare: UZ Publications; 1996:303-309.
37. Nair VDP, Dairam A, Agbonon A, Arnason JT, Foster BC, Kanfer I. Investigation of the antioxidant activity of African potato (*Hypoxis hemerocallidea*). *J Agric Food Chem*. 2007;55(5):1707-1711. doi:10.1021/jf0619838.
38. Laporta O, Funes L, Garzón MT, Villalaín J, Micol V. Role of membranes on the antibacterial and anti-inflammatory activities of the bioactive compounds from *Hypoxis rooperi* corm extract. *Arch Biochem Biophys*. 2007;467(1):119-131. doi:10.1016/j.abb.2007.08.013.
39. Kabanda MM. Antioxidant Activity of Rooperol Investigated through Cu (I and II) Chelation Ability and the Hydrogen Transfer Mechanism: A DFT Study. *Chem Res Toxicol*. 2012;25(10):2153-2166. doi:10.1021/tx300244z.
40. Ali Azouaou S, Emhemmed F, Idris-Khodja N, et al. Selective ROS-dependent p53-associated anticancer effects of the hypoxoside derivative rooperol on human teratocarcinoma cancer stem-like cells. *Invest New Drugs*. 2015;33(1):64-74. doi:10.1007/s10637-014-0182-6.
41. Boukes GJ, van de Venter M. Rooperol as an antioxidant and its role in the innate immune system: An in vitro study. *J Ethnopharmacol*. 2012;144(3):692-699. doi:10.1016/J.JEP.2012.10.014.
42. Guzdek A, Niżankowska E, Allison AC, Kruger PB, Koj A. Cytokine production in human and rat macrophages and dicatechol rooperol and esters. *Biochem Pharmacol*. 1996;52(7):991-998. doi:10.1016/0006-2952(96)00386-3.
43. Khan M, Khan M, Adil SF, et al. Green synthesis of silver nanoparticles mediated by *Pulicaria glutinosa* extract. *Int J Nanomedicine*. 2013;8:1507. doi:10.2147/IJN.S43309.
44. Lund ME, To J, O'Brien BA, Donnelly S. The choice of phorbol 12-myristate 13-acetate

differentiation protocol influences the response of THP-1 macrophages to a pro-inflammatory stimulus. *J Immunol Methods*. 2016;430:64-70.

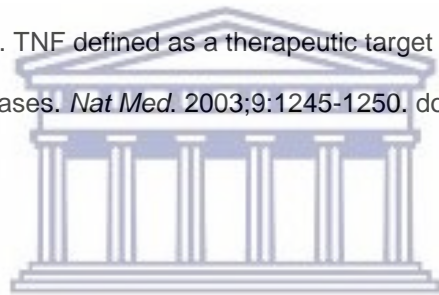
doi:10.1016/J.JIM.2016.01.012.

45. Jung J, Park S, Hong S, et al. Synthesis of gold nanoparticles with glycosides: Synthetic trends based on the structures of glycones and aglycones. *Carbohydr Res*. 2014;386(1):57-61. doi:10.1016/j.carres.2013.12.012.
46. Elbagory AM, Cupido CN, Meyer M, Hussein AA. Large Scale Screening of Southern African Plant Extracts for the Green Synthesis of Gold Nanoparticles Using Microtitre-Plate Method. *Molecules*. 2016;21(11):1498. doi:10.3390/molecules21111498.
47. Prevo BG, Esakoff SA, Mikhailovsky A, Zasadzinski JA. Scalable routes to gold nanoshells with tunable sizes and response to near-infrared pulsed-laser irradiation. *Small*. 2008;4(8):1183-1195. doi:10.1002/smll.200701290.
48. Yulizar Y, Utari T, Ariyanta HA, Maulina D. Green Method for Synthesis of Gold Nanoparticles Using Polyscias scutellaria Leaf Extract under UV Light and Their Catalytic Activity to Reduce Methylene Blue. *J Nanomater*. 2017;2017. doi:10.1155/2017/3079636.
49. Noruzi M. Biosynthesis of gold nanoparticles using plant extracts. *Bioprocess Biosyst Eng*. 2015;38(1):1-14. doi:10.1007/s00449-014-1251-0.
50. Ndeh NT, Maensiri S, Maensiri D. The effect of green synthesized gold nanoparticles on rice germination and roots. *Adv Nat Sci Nanosci Nanotechnol*. 2017;8. doi:10.1088/2043-6254/aa724a.
51. Gardea-Torresdey JL, Parson JG, Gomez E, et al. Formation and Growth of Au Nanoparticles in live side Live Alfalfa Plants. *Nano Lett*. 2002;2:397-401. doi:10.1021/nl015673+.
52. Max J-J, Chapados C. Infrared Spectroscopy of Aqueous Carboxylic Acids: Comparison between Different Acids and Their Salts. *J Phys Chem A*. 2004;108(16):3324–3337. doi:10.1021/JP036401T.
53. Fornaro T, Burini D, Biczysko M, Barone V. Hydrogen-Bonding Effects on Infrared Spectra from Anharmonic Computations: Uracil–Water Complexes and Uracil Dimers. *J Phys*

- Chem A.* 2015;119(18):4224-4236. doi:10.1021/acs.jpca.5b01561.
54. Bano S, Nazir S, Nazir A, et al. Microwave-assisted green synthesis of superparamagnetic nanoparticles using fruit peel extracts: surface engineering, T₂ relaxometry, and photodynamic treatment potential. *Int J Nanomedicine.* 2016;11:3833-3848. doi:10.2147/IJN.S106553.
55. Rouhana LL, Jaber JA, Schlenoff JB. Aggregation-resistant water-soluble gold nanoparticles. *Langmuir.* 2007;23(26):12799-12801. doi:10.1021/la702151q.
56. Lacy P, Stow JL. Cytokine release from innate immune cells: association with diverse membrane trafficking pathways. *Blood.* 2011;118(1):9-18. doi:10.1182/blood-2010-08-265892.
57. Juskewitch JE, Platt JL, Knudsen BE, Knutson KL, Brunn GJ, Grande JP. Disparate roles of marrow- and parenchymal cell-derived TLR4 signaling in murine LPS-induced systemic inflammation. *Sci Rep.* 2012;2:918. doi:10.1038/srep00918.
58. Rossol M, Heine H, Meusch U, et al. LPS-induced Cytokine Production in Human Monocytes and Macrophages. *Crit Rev Immunol.* 2011;31(5):379-446. doi:10.1615/CritRevImmunol.v31.i5.20.
59. Loiarro M, Ruggiero V, Sette C. Targeting TLR/IL-1R Signalling in Human Diseases. *Mediators Inflamm.* 2010;2010. doi:10.1155/2010/674363.
60. Parameswaran N, Patial S. Tumor necrosis factor- α signaling in macrophages. *Crit Rev Eukaryot Gene Expr.* 2010;20(2):87-103.
61. Scheller J, Chalaris A, Schmidt-Arras D, Rose-John S. The pro- and anti-inflammatory properties of the cytokine interleukin-6. *Biochim Biophys Acta - Mol Cell Res.* 2011;1813(5):878-888. doi:10.1016/J.BBAMCR.2011.01.034.
62. Le Moine O, Devière J, Devaster JM, et al. Interleukin-6: an early marker of bacterial infection in decompensated cirrhosis. *J Hepatol.* 1994;20(6):819-824.
63. González-Navajas JM, Lee J, David M, Raz E. Immunomodulatory functions of type I interferons. *Nat Rev Immunol.* 2012;12(2):125-135. doi:10.1038/nri3133.
64. Gessani S, Belardelli F. IFN- γ Expression in Macrophages and Its Possible Biological

Significance. *Cytokine Growth Factor Rev.* 1998;9(2):117-123. doi:10.1016/S1359-6101(98)00007-0.

65. Ye J, Ortaldo JR, Conlon K, Winkler-Pickett R, Young HA. Cellular and molecular mechanisms of IFN-gamma production induced by IL-2 and IL-12 in a human NK cell line. *J Leukoc Biol.* 1995;58(2):225-233. doi:10.1002/jlb.58.2.225.
66. Bream JH, Curiel RE, Yu CR, et al. IL-4 synergistically enhances both IL-2- and IL-12-induced IFN- γ expression in murine NK cells. *Blood.* 2003;102:207-214. doi:10.1182/blood-2002-08-2602.
67. Ohkusa T, Nomura T, Sato N. The Role of Bacterial Infection in the Pathogenesis of Inflammatory Bowel Disease. *Intern Med.* 2004;43(7):534-539. doi:10.2169/internalmedicine.43.534.
68. Feldmann M, Maini RN. TNF defined as a therapeutic target for rheumatoid arthritis and other autoimmune diseases. *Nat Med.* 2003;9:1245-1250. doi:10.1038/nm939.



UNIVERSITY of the
WESTERN CAPE

List of figures

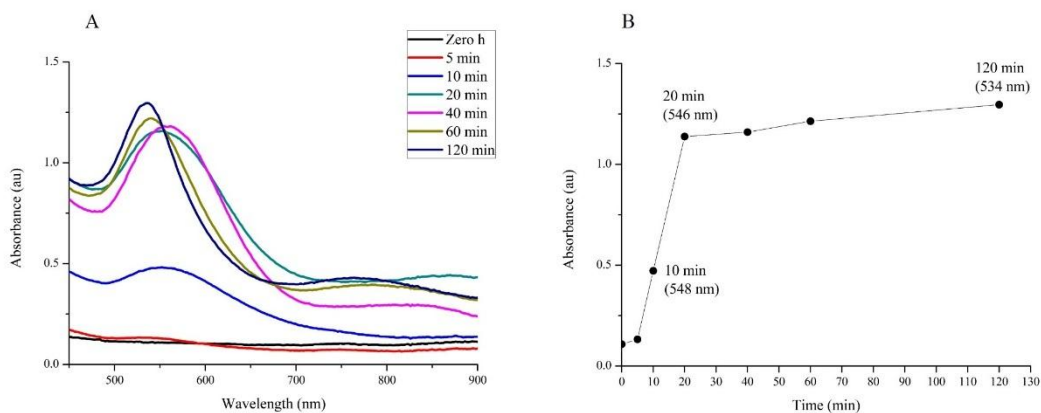


Figure 1 Optimization of reaction time for the synthesis of AuNPs using hypoxoside (i.e. Hy-AuNPs). (A) shows the UV-Vis spectra recorded as a function of time (0 -120 min) of Hy-AuNPs; (B) shows the λ_{max} values of Hy-AuNPs as a function of time.

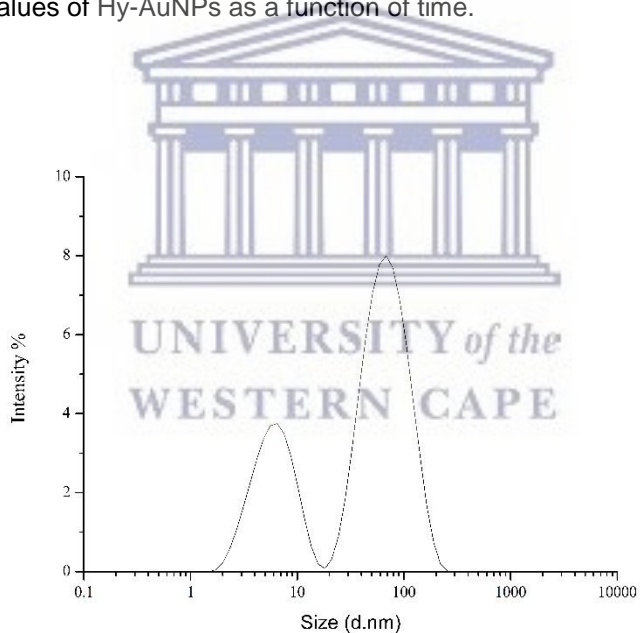


Figure 2 The hydrodynamic diameter of Hy-AuNPs displayed by intensity as determined by the DLS analysis.

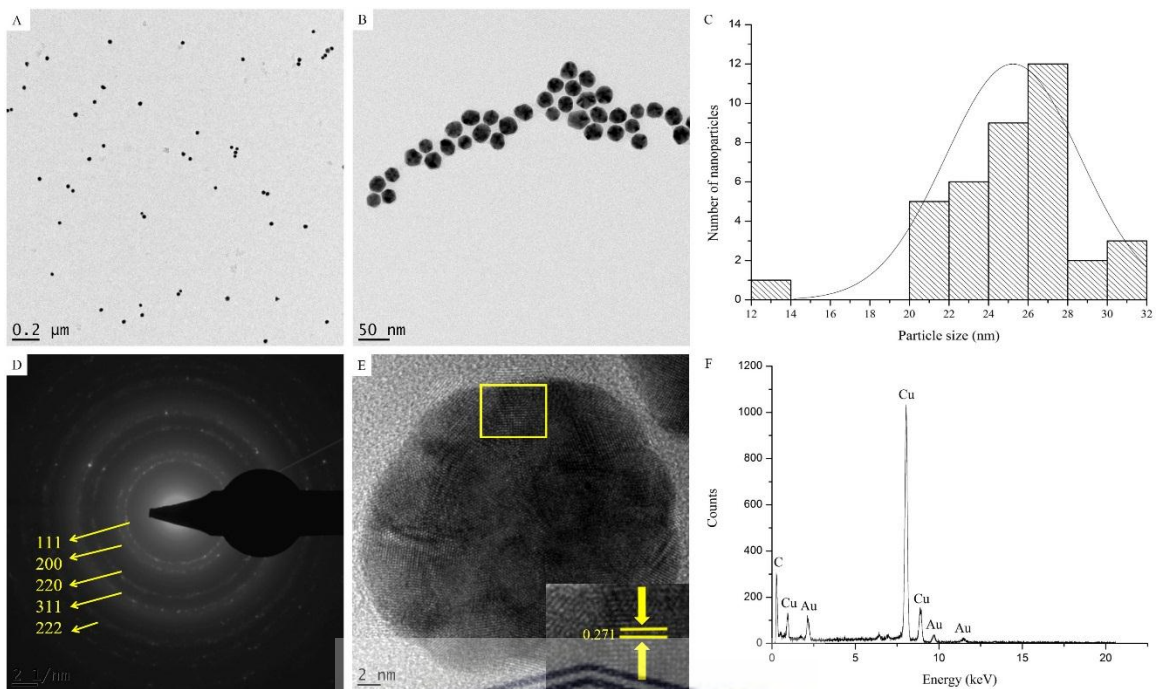


Figure 3 HRTEM analysis of Hy-AuNPs. (A) and (B) show HRTEM images at a magnification of 0.2 μm and 50 nm, respectively. (C) shows particle size distribution determined from the HRTEM images using ImageJ software, (D) shows SAED pattern, (E) shows lattice fringes and (F) shows EDX spectra.

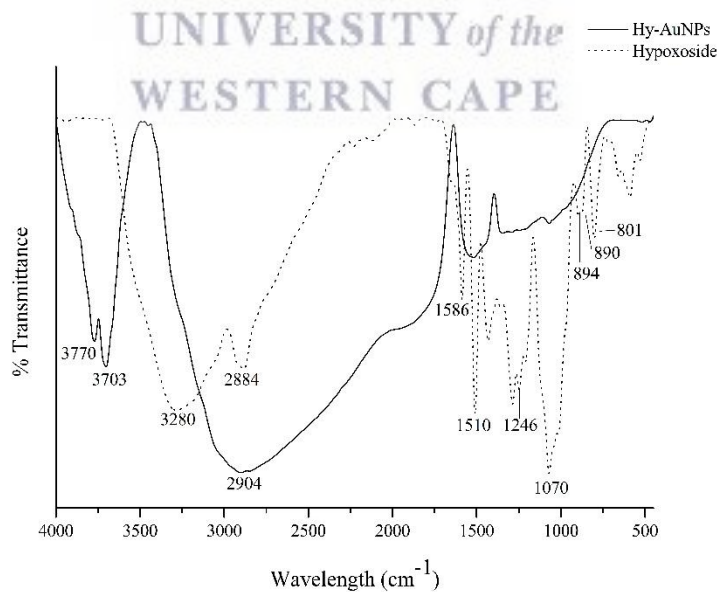


Figure 4 FTIR spectra of hypoxiside and Hy-AuNPs.

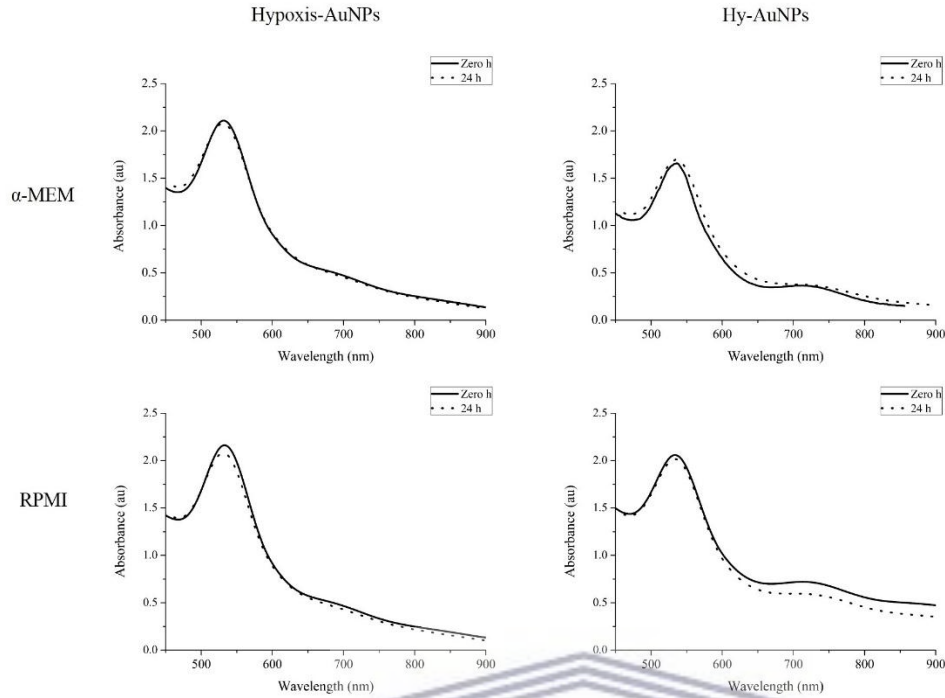


Figure 5 UV-Vis spectra of Hypoxis-AuNPs and Hy-AuNPs before and after 24 h incubation in the presence of α -MEM and RPMI cell growth media.

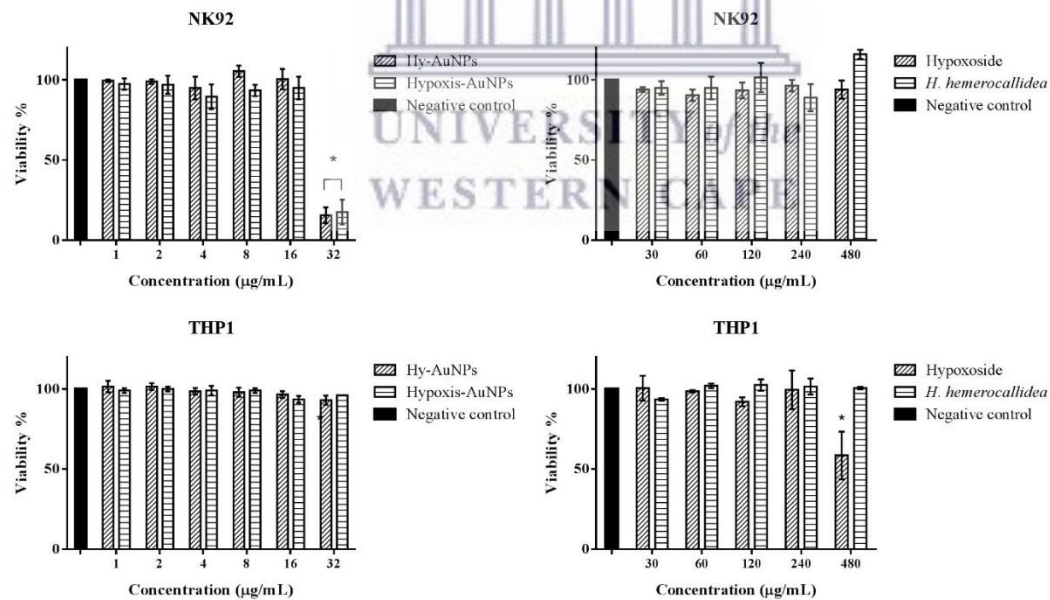


Figure 6 The effect of *H. hemerocallidea*, hypoxoside, Hypoxis-AuNPs and Hy-AuNPs on the viability of NK92 cells and PMA differentiated THP1 cells as determined by WST-1 assay.

*Statistically significant ($p < 0.05$) compared to the negative control.

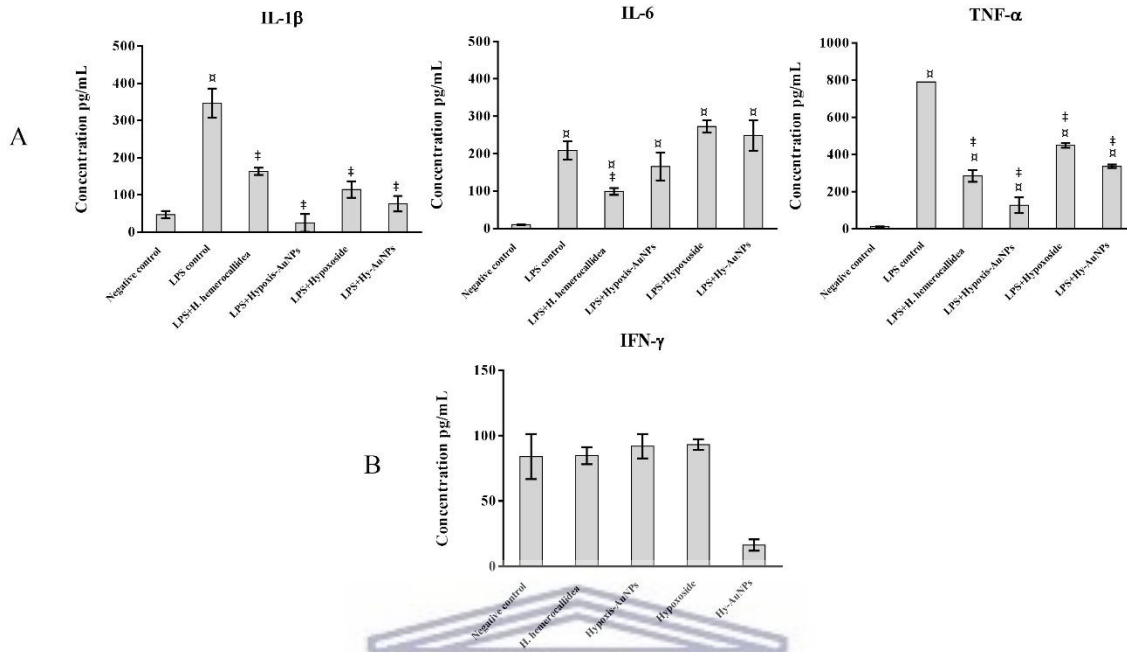


Figure 7 Quantification of cytokines release from THP1 and NK92 cells following treatment with *H. hemerocallidea* extract, Hypoxoside, Hypoxis-AuNPs and Hy-AuNPs. (A) THP1 cells were stimulated with LPS for 6 h. The LPS containing medium was then replaced by the respective treatments and the cells were incubated for another 18 h, after which the cytokine production (IL-1 β , IL-6 and TNF- α) were quantified by ELISA. (B) NK92 cells were exposed to the respective treatments for 24 h, after which IFN- γ production was quantified by ELISA.

α Statistical significance ($p < 0.05$) compared to the negative control.

‡ Statistical significance ($p < 0.05$) compared to the 6 h treatment with LPS (LPS control).

CHAPTER SEVEN: GENERAL CONCLUSIONS AND RECOMMENDATIONS

7.1 General Conclusions

This study investigated the ability of several South African plants to biosynthesize AuNPs. The study described a facile and quick microtitre plate method to screen several plants for the AuNPs production. The reduction of the gold(III) chloride by the plant extracts was confirmed by the presence of the LSPR absorption peaks in the visible light region as shown by the UV-Vis analysis. It was shown also that only certain concentration of the plant extract (optimum concentration (OC)) can produce AuNPs with favourable sizes. This effect may be caused by the changes in the pH of the reaction medium, influenced by the concentration of the plant extract. The biosynthesis was optimized by changing the reaction conditions. The results showed that high temperature lead to the production of more monodispersed AuNPs. This was confirmed by the measurement of the particle sizes using the DLS technique and observing the morphology of the AuNPs using electron microscopy.

The study also investigated the synthesis of biogenic AuNPs from two important South African medicinal plants, *H. hemerocallidea* and *G. africana*. The AuNPs from these two plants we mostly spherical in contrast to the AuNPs biosynthesized from the other studied plants. The FTIR spectra showed that the flavonoids and glycosides contents of *G. africana* and *H. hemerocallidea*, respectively, might be responsible for the biosynthesis of the AuNPs.

The antibacterial investigation of *H. hemerocallidea* and *G. africana* against bacterial strains known to cause wound infection was done using *in vitro* cell viability colorimetric assay. The AuNPs from *H. hemerocallidea* (Hypoxis-AuNPs) showed antibacterial actions with MIC values lower than those of the AuNPs from *G. africana*

(Galenia-AuNPs) and the spherical citrate-AuNPs. These results indicate that the capping material (phytochemicals) play important part in the antibacterial activity of Hypoxis-AuNPs. Moreover, Hypoxis-AuNPs showed stronger antibacterial activity against Gram-negative bacterial strains selected in this study. This might indicate that the activity of Hypoxis-AuNPs is dependent on the cell wall composition of the bacterial strain.

Furthermore, the study reported the functionalization of Hypoxis-AuNPs with ampicillin. Unlike Hypoxis-AuNPs, the LSPR peaks of Amp-AuNPs were red-shifted and the particle diameters were larger than Hypoxis-AuNPs. The FAB-MS data of Amp-AuNPs showed the fragmented ion of ampicillin. These results confirmed the conjugation of ampicillin on the surface of Hypoxis-AuNPs. The conjugated AuNPs (Amp-AuNPs) also demonstrated higher antibacterial activity than the free AuNPs (Hypoxis-AuNPs). These data suggest that Hypoxis-AuNPs can be effectively used as a drug carrier.

The chemical study of *H. hemerocallidea* led to the isolation of the glycoside hypoxoside, a major metabolite of the *Hypoxis* species. Hypoxoside was able to generate AuNPs (Hy-AuNPs) with similar physicochemical characters to the Hypoxis-AuNPs. Hence, it might be possible that this compound play a role in the synthesis of AuNPs from *H. hemerocallidea* as suggested by the FTIR data of Hypoxis-AuNPs. Also, the FTIR data of Hy-AuNPs showed that the reduction of gold(III) chloride by hypoxoside might be mediated by the oxidation of C-6-OH of its glucose unit.

Furthermore, the immunomodulatory effects of Hypoxis-AuNPs and Hy-AuNPs was investigated by measuring the expression of several pro- and anti-inflammatory cytokines from LPS-induced macrophages and NK cells. The immunomodulatory evaluation of *H. hemerocallidea* and hypoxoside was also included in this study. The results showed that the plant extract, hypoxoside and their biogenic AuNPs reduced or had no effect on the production of several pro-inflammatory cytokines such as TNF- α , IFN- γ and IL-1 β . This anti-inflammatory activity combined with the antibacterial

activity of the AuNPs can be useful in the management of chronic wounds infections and the persistent inflammation caused by the bacterial toxins.

The AuNPs exhibited high stability when incubated with biological buffers and media, as shown by the minimum changes in their UV-Vis spectra over 24 h incubation period. Galenia-AuNPs, Hypoxis-AuNPs and Hy-AuNPs also showed no *in vitro* cytotoxicity on the normal human fibroblasts at the highest concentration tested (32 nM). Hypoxis-AuNPs and Hy-AuNPs also did not induce cell death on macrophages at the same concentration. Hypoxis-AuNPs and Hy-AuNPs affected only the viability of NK cells at 32 nM. Still, the viability of NK was not affected at lower concentrations of the AuNPs. These results, therefore, confirmed the safety of the green synthesized AuNPs *in vitro*, which make them useful for possible biomedical application.



7.2 Recommendations

This study showed the effect of temperature and changing the plant extract concentration on the synthesis. However, the study can be also expanded to include the effect of the pH of the reaction medium on the synthesis by using suitable buffers. Moreover, it can be also useful to study the chemical synthesis of Hy-AuNPs using other spectroscopic characterization techniques such as nuclear magnetic resonance (NMR) to confirm the possible functional groups involved in the synthesis with greater accuracy. This can be done by comparing the NMR spectra of the free compound, Hy-AuNPs and the reaction medium after centrifugation. This chemical information can be useful to understand the functional groups present on the surface of the Hy-AuNPs for any possible future conjugation studies.

Further, it is known that other MNPs, especially silver NPs, can have potent antibacterial activity. It is therefore recommended to evaluate the possibility of *H. hemerocallidea* to synthesize silver NPs and to evaluate their antibacterial activity. Further antibacterial evaluations, such as biology TEM, can be used to investigate the

possible mechanisms of action (specifically on the cell wall) of the produced NPs. Moreover, it is postulated that AuNPs and other MNPs can exert their antibacterial activity by inducing the formation of ROS. Hence, studying the possibility of ROS production by the green synthesized AuNPs can further provide answers on their antibacterial mechanism of action.

The wound healing properties of Hypoxis-AuNPs can be further expanded to include other biological assays to evaluate their role on the different stages of wound healing such as, collagen synthesis and cell migration. This evaluation can be expanded to include animal models.

Animal models can also be used to investigate the toxicity of the biogenic *in vivo*. This can include the study of the biogenic AuNPs bio-distribution and accumulation and their mode of excretion.

Finally, it was reported that the hydrolysed form of hypoxoside (rooperol) is more biological active. It is therefore advised to investigate the production of MNPs from rooperol and evaluate the biological activities of the produced NPs.

